

---

Theses and Dissertations

---

2013

# The role of organic cation transporters in the nasal uptake and brain distribution of organic cation substrates

Maya George  
*University of Iowa*

Copyright 2013 Maya George

This dissertation is available at Iowa Research Online: <http://ir.uiowa.edu/etd/1605>

---

## Recommended Citation

George, Maya. "The role of organic cation transporters in the nasal uptake and brain distribution of organic cation substrates." PhD (Doctor of Philosophy) thesis, University of Iowa, 2013.  
<http://ir.uiowa.edu/etd/1605>.

---

Follow this and additional works at: <http://ir.uiowa.edu/etd>



Part of the [Pharmacy and Pharmaceutical Sciences Commons](#)

THE ROLE OF ORGANIC CATION TRANSPORTERS IN THE NASAL UPTAKE  
AND BRAIN DISTRIBUTION OF ORGANIC CATION SUBSTRATES

by  
Maya George

An Abstract

Of a thesis submitted in partial fulfillment  
of the requirements for the Doctor of  
Philosophy degree in Pharmacy (Pharmaceutics)  
in the Graduate College of  
The University of Iowa

May 2013

Thesis Supervisor: Professor Maureen D. Donovan

## ABSTRACT

The objective of this study was to investigate the role of organic cation transporters (OCTs) in the uptake of hydrophilic drugs into the olfactory bulb and subsequently to the brain. Two OCT2 substrates, amantadine and cimetidine were used as model drugs for this purpose.

Bovine nasal explants (olfactory and respiratory tissue) were used as an *in vitro* model for preliminary screening to identify the role of transporters involved in the uptake of drug across these tissues. It was observed from both PCR and immunohistochemistry that OCTs, OCT2, OCTN1 and OCTN2 were present in the bovine respiratory and olfactory mucosa. Transport studies of amantadine in the presence and absence of OCT2 and OCTN2 inhibitors indicated that both these transporters play a role in the transport of amantadine across the bovine respiratory mucosa, whereas transport across the olfactory mucosa was predominantly via OCT2.

This was followed by *in vivo* studies in rats where the blood, striatum and olfactory bulb concentrations of amantadine were determined following intranasal and intra-arterial administration. Shortly after nasal administration, the olfactory bulb concentrations exceeded the concentrations in the striatum suggesting the olfactory pathway to be the major route of uptake. Co-administration of the drug with an OCT2 inhibitor intranasally showed statistically significant reductions in the brain uptake of amantadine. A synergistic inhibitory effect on amantadine uptake was observed with the combined inhibition OCT2 and OCTN2. Additionally, the CNS exposure of these drugs following intranasal administration in the presence and absence of the OCT inhibitors was evaluated using the ratio of the free drug concentrations in the brain compared to

plasma. While the plasma concentration profiles were similar both in the presence and absence of inhibition, the free drug ratios were highest when no inhibitor was included. Additionally similar *in vivo* studies were also carried out for a second model drug, cimetidine, where cimetidine uptake into the rat brain was found to be significantly reduced in the presence of the OCT2 inhibitor, pentamidine.

This demonstrates that there was a greater CNS exposure to each drug when OCT transporters were active, confirming their role in their direct CNS distribution from the nasal cavity to the brain. The results of this study suggest that OCT substrates might be good candidates for the delivery to the brain via the olfactory route.

Abstract Approved: \_\_\_\_\_  
Thesis Supervisor  
\_\_\_\_\_  
Title and Department  
\_\_\_\_\_  
Date

THE ROLE OF ORGANIC CATION TRANSPORTERS IN THE NASAL  
UPTAKE AND BRAIN DISTRIBUTION OF ORGANIC CATION  
SUBSTRATES

by  
Maya George

A thesis submitted in partial fulfillment  
of the requirements for the Doctor of  
Philosophy degree in Pharmacy (Pharmaceutics)  
in the Graduate College of  
The University of Iowa

May 2013

Thesis Supervisor: Professor Maureen D. Donovan

Copyright by  
MAYA GEORGE  
2013  
All Rights Reserved

Graduate College  
The University of Iowa  
Iowa City, Iowa

CERTIFICATE OF APPROVAL

---

PH.D. THESIS

---

This is to certify that the Ph.D. thesis of

Maya George

has been approved by the Examining Committee  
for the thesis requirement for the Doctor of Philosophy  
degree in Pharmacy (Pharmaceutics) at the May 2013 graduation.

Thesis Committee: \_\_\_\_\_  
Maureen D. Donovan, Thesis Supervisor

\_\_\_\_\_  
Daryl J. Murry

\_\_\_\_\_  
Aliasger K.Salem

\_\_\_\_\_  
Mahfoud Assem

\_\_\_\_\_  
Jennifer Fiegel

*To all my fellow wayfarers who have been a part of this journey.*



An investment in knowledge pays the best interest.

-Benjamin Franklin

## ACKNOWLEDGMENTS

I would like to express my deepest appreciation and sincere gratitude for the support, encouragement and guidance I received from my advisor, Professor Maureen Donovan throughout my graduate education. I would like to thank my committee members Aliasger Salem, Daryl Murry, Jennifer Fiegel and Mahfoud Assem for their helpful suggestions and comments towards my research. I would like to add a special note of thanks to Dr. Vijay Kumar for his valuable inputs to my thesis proposal. I also take this opportunity to express my gratitude to all the other faculty members in the Division of Pharmaceutics who have been an unlimited source of knowledge and expertise and have had a major role in shaping my scientific perspective.

I thank Professor Daryl Murry in the method development of amantadine and cimetidine and also for his patience during trouble shooting with LCMS. I would also like to thank Dr. Mahfoud Assem for his assistance in PCR studies and allowing the use of his lab facility. I take this opportunity to thank Kathy Walters of the Central Microscopy Research Facility at the University of Iowa for her guidance in the immunohistochemistry work. I would also like to acknowledge the significant contribution of Dr. Jiangeng Huang, in the animal studies of amantadine. This work could not have been completed without his efforts. I also would like to recognize the help of Bryan L Gonzalez Rivera with the *in vitro* transport studies of cimetidine. I am also grateful for the inputs given to me by Dr. Aliasger Salem's students in carrying out ELISA assays. I also hereby acknowledge the financial support for this project from NIH RO1 00837 grant.

I take this opportunity to extend my heartfelt gratitude to my labmates, Heifei, Joanne, Nan, Varsha, Ana, Manar, Krupal, Bhanu, Rakesh, Namita and also my fellow

colleagues for their friendship and moral support throughout my time here. I would also like to mention the divisional secretaries, Joasanna Birtcher, Kate Kopriva and Rita Schneider for just being there to help us through any difficulty. I am deeply grateful to my sisters, Henna and Ann for their unconditional love that kept me motivated. Above all, I would like to thank my parents, who instilled in me the value of education. Last but not the least, I would like to thank my husband, Amit for his faith in me, without whose constant support, I would have never made it this far.

## ABSTRACT

The objective of this study was to investigate the role of organic cation transporters (OCTs) in the uptake of hydrophilic drugs into the olfactory bulb and subsequently to the brain. Two OCT2 substrates, amantadine and cimetidine were used as model drugs for this purpose.

Bovine nasal explants (olfactory and respiratory tissue) were used as an *in vitro* model for preliminary screening to identify the role of transporters involved in the uptake of drug across these tissues. It was observed from both PCR and immunohistochemistry that OCTs, OCT2, OCTN1 and OCTN2 were present in the bovine respiratory and olfactory mucosa. Transport studies of amantadine in the presence and absence of OCT2 and OCTN2 inhibitors indicated that both these transporters play a role in the transport of amantadine across the bovine respiratory mucosa, whereas transport across the olfactory mucosa was predominantly via OCT2.

This was followed by *in vivo* studies in rats where the blood, striatum and olfactory bulb concentrations of amantadine were determined following intranasal and intra-arterial administration. Shortly after nasal administration, the olfactory bulb concentrations exceeded the concentrations in the striatum suggesting the olfactory pathway to be the major route of uptake. Co-administration of the drug with an OCT2 inhibitor intranasally showed statistically significant reductions in the brain uptake of amantadine. A synergistic inhibitory effect on amantadine uptake was observed with the combined inhibition OCT2 and OCTN2. Additionally, the CNS exposure of these drugs following intranasal administration in the presence and absence of the OCT inhibitors was evaluated using the ratio of the free drug concentrations in the brain compared to

plasma. While the plasma concentration profiles were similar both in the presence and absence of inhibition, the free drug ratios were highest when no inhibitor was included. Additionally similar *in vivo* studies were also carried out for a second model drug, cimetidine, where cimetidine uptake into the rat brain was found to be significantly reduced in the presence of the OCT2 inhibitor, pentamidine.

This demonstrates that there was a greater CNS exposure to each drug when OCT transporters were active, confirming their role in their direct CNS distribution from the nasal cavity to the brain. The results of this study suggest that OCT substrates might be good candidates for the delivery to the brain via the olfactory route.

## TABLE OF CONTENTS

|   |     |
|---|-----|
| LIST OF TABLES .....  | xi  |
| LIST OF FIGURES .....   | xiv |
| CHAPTER 1 INTRODUCTION .....  | 1   |
| Nasal anatomy and cellular organization.....  | 5   |
| Nose to brain delivery .....  | 8   |
| Nose to brain pathways.....   | 10  |
| Organic cation transporters (OCT).....  | 14  |
| In Vitro nasal models to study permeability.....  | 17  |
| Rat as an In Vivo animal model for nose to brain delivery.....  | 18  |
| CHAPTER 2 OBJECTIVES .....  | 21  |
| CHAPTER 3 CHARACTERIZATION OF ORGANIC CATION<br>TRANSPORTERS (OCTS) IN THE BOVINE NASAL MUCOSA .....        | 23  |
| RT-PCR (Reverse Transcriptase Polymerase Chain Reaction).....   | 24  |
| Nucleic acid purity assessment .....  | 25  |
| Western Blot / SDS PAGE.....  | 26  |
| Immunohistochemistry .....  | 28  |
| Enzyme-linked immunosorbent assay (ELISA) .....   | 29  |
| Materials .....   | 30  |
| Experimental Methods.....   | 32  |
| Preparation of nasal tissues .....  | 32  |
| RT-PCR (Reverse Transcriptase Polymerase Chain Reaction).....   | 33  |
| Western Blot .....  | 37  |
| Immunohistochemistry .....  | 39  |
| ELISA.....  | 40  |
| Results and Discussion .....  | 41  |
| Quality of RNA and cDNA.....  | 41  |
| Optimization of Mg <sup>2+</sup> concentration and number of cycles for RT-<br>PCR.....                     | 44  |
| BCA assay result.....   | 48  |
| Western blot .....  | 50  |
| Immunohistochemistry .....  | 52  |
| ELISA.....  | 56  |
| Conclusion.....   | 59  |
| CHAPTER 4 QUANTITATIVE MEASUREMENT OF OCT SUBSTRATES<br>USING LCMS IN BIOLOGICAL BUFFER(S) AND PLASMA ..... | 60  |
| Amantadine .....  | 60  |
| Cimetidine .....  | 61  |
| Materials .....   | 63  |
| Methods .....   | 63  |

|   |     |
|---|-----|
| Stock solutions and working standard .....  | 64  |
| Sample preparation for amantadine .....   | 65  |
| Sample preparation for cimetidine.....  | 65  |
| Instrumentation and operating conditions for amantadine .....   | 66  |
| Instrumentation and operating conditions for cimetidine .....   | 67  |
| Method validation .....   | 67  |
| Results and Discussion .....  | 69  |
| Amantadine .....  | 69  |
| Cimetidine .....  | 78  |
| Conclusion .....  | 85  |
| <br>  |     |
| CHAPTER 5 TRANSPORT OF AMANTADINE AND CIMETIDINE ACROSS<br>BOVINE NASAL TISSUES .....   | 86  |
| <br>  |     |
| Amantadine .....  | 86  |
| Physical properties of amantadine .....   | 86  |
| Amantadine as an OCT2 substrate .....   | 87  |
| Cimetidine .....  | 87  |
| Physical properties of cimetidine.....  | 88  |
| Cimetidine: an OCT2 substrate.....  | 88  |
| Organic cation transporter inhibitors.....  | 89  |
| L-carnitine as an OCTN2 inhibitor.....  | 90  |
| Pentamidine as an OCT2 inhibitor .....  | 91  |
| In vitro transport studies using diffusion cells .....  | 92  |
| Materials .....   | 93  |
| Experimental procedures .....   | 94  |
| Preparation of mucosal tissues.....   | 94  |
| In vitro bi-directional transport studies .....   | 94  |
| Study groups for amantadine transport studies.....  | 95  |
| Study groups for cimetidine transport .....   | 98  |
| Flux measurement and data analysis .....  | 98  |
| Results and Discussion .....  | 99  |
| Amantadine transport studies.....   | 99  |
| Amantadine transporter inhibition studies .....   | 108 |
| Cimetidine transport studies.....   | 114 |
| Cimetidine transport inhibition studies .....   | 121 |
| Conclusion .....  | 123 |
| <br>  |     |
| CHAPTER 6 THE ROLE OF ORGANIC CATION TRANSPORTERS (OCT2<br>AND OCTN2) IN THE NOSE TO BRAIN DISTRIBUTION OF<br>AMANTADINE IN RATS..... | 124 |
| <br>  |     |
| Pharmacokinetics of amantadine .....  | 124 |
| Brain penetration of amantadine .....   | 124 |
| Microdialysis as a sampling technique.....  | 125 |
| Brain partitioning ( $K_{p,brain}$ ) .....  | 131 |
| Materials .....   | 132 |
| Experimental procedures .....   | 133 |
| Animal experiments.....   | 133 |
| Anesthesia .....  | 133 |
| Probe insertion for microdialysis sampling.....   | 134 |
| Intraarterial (IA) dosing and femoral artery cannulation .....  | 137 |

|   |     |
|---|-----|
| Intranasal (IN) dosing.....   | 138 |
| Brain and plasma sampling .....   | 138 |
| Blood-brain barrier integrity test .....  | 139 |
| Euthanasia .....  | 139 |
| Microdialysis probe recovery studies.....   | 139 |
| Reuse of probes in vivo .....   | 141 |
| Determination of unbound drug ( $C_u$ ) fraction in plasma.....   | 141 |
| Study groups .....  | 142 |
| Data analysis .....   | 143 |
| Results and Discussion .....  | 144 |
| Microdialysis Recovery Results .....  | 144 |
| Drug concentrations in plasma following intra-arterial (IA) and intranasal (IN) administration .....                  | 146 |
| Brain uptake and distribution following IA and IN administration of amantadine.....                                   | 149 |
| Role of organic cation transporters in the nose to brain delivery of amantadine: transporter inhibition studies ..... | 153 |
| $C_{\text{brain}}/C_{\text{plasma}}$ ( $K_p$ ) vs. time profile as an indicator of CNS exposure .....                 | 163 |
| Conclusions .....   | 166 |
| <br>CHAPTER 7 NOSE TO BRAIN DELIVERY OF CIMETIDINE: THE ROLE OF OCT2.....   | 168 |
| Pharmacokinetics of cimetidine.....   | 168 |
| Brain penetration of cimetidine .....   | 169 |
| Materials .....   | 169 |
| Experimental methods .....  | 169 |
| Animal experiments.....   | 169 |
| Study groups .....  | 170 |
| Brain and plasma sampling .....   | 171 |
| Results and Discussion .....  | 171 |
| Microdialysis Recovery .....  | 171 |
| Drug concentrations in plasma following intra-arterial (IA) and intranasal (IN) administration .....                  | 173 |
| Brain distribution of cimetidine following IA and IN administration .....   | 175 |
| Chemical inhibition of OCT2 transport.....  | 178 |
| Conclusions .....   | 185 |
| <br>CHAPTER 8 CONCLUSION .....  | 186 |
| <br>APPENDIX .....  | 189 |
| Buffer Formulae .....   | 189 |
| <br>REFERENCES .....  | 190 |



## LIST OF TABLES

|  |     |
|--|-----|
| Table 1-1: Physiologically-relevant parameters for humans and rat implicated in the nose to brain transport of drugs . . . . .   | 19  |
| Table 1-2: A comparison of the relative mRNA expression of organic cation transporter proteins (OCTs) in the olfactory and respiratory mucosa of human and rat . . . . .             | 20  |
| Table 3-1: Base pair sequences of primers chosen for each of the organic cation transporter gene sequence used in the RT- PCR reaction . . . . .                                     | 36  |
| Table 3-2: Absorbance results of RNA samples extracted from respiratory and olfactory mucosal explants . . . . .   | 42  |
| Table 3-3: Comparison of Mg <sup>2+</sup> concentrations and amplification cycle titrations for PCR method optimization. . . . .   | 46  |
| Table 4-1: Chemical structure and physical properties of the analytes amantadine and cimetidine and their internal standards. . . . .  | 62  |
| Table 4-2: Working standard solutions of amantadine and cimetidine . . . . .   | 64  |
| Table 4- 3: Summary of calibration curves for amantadine in various matrices, aECF, rat plasma and KRB buffer . . . . .  | 72  |
| Table 4-4: Results of recovery and matrix effects for amantadine . . . . .   | 73  |
| Table 4-5: Summary of calibration curves for cimetidine in different matrix, aECF, rat plasma and KRB buffer. . . . .  | 80  |
| Table 4-6: Results of recovery and matrix effects for cimetidine. . . . .  | 81  |
| Table 5-1: Experimental design of amantadine transport studies . . . . .   | 97  |
| Table 5-2: Calculated amantadine flux across the olfactory and respiratory and thickness normalized respiratory mean flux values. . . . .  | 106 |
| Table 5-3: Kinetic parameters of the carrier-mediated transport of amantadine calculated from fitting the Michaelis-Menten equation to the flux values for each tissue type. . . . . | 107 |
| Table 5- 4: Calculated cimetidine flux across the olfactory and respiratory tissues. . . . .   | 118 |
| Table 6-1: A list of the advantages and disadvantages associated with the use of microdialysis as a technique for sampling the brain tissue ECF. . . . .                             | 126 |
| Table 6-2: The five different study groups for amantadine to compare IA vs. IN routes. . . . .   | 143 |

|   |     |
|---|-----|
| Table 6-3: Selected pharmacokinetic parameters calculated from the plasma concentration-time profiles of amantadine following intra-arterial and intranasal administration in rats .....            | 148 |
| Table 6-4: Selected pharmacokinetic parameters calculated from the olfactory bulb and striatal ECF-time profiles of amantadine following intra-arterial and intranasal administration in rats ..... | 151 |
| Table 6-5: Selected pharmacokinetic parameters calculated from plasma profiles of amantadine following intranasal administration with OCT inhibitors .....  | 155 |
| Table 6-6: Selected pharmacokinetic parameters calculated from the olfactory bulb and striatum ECF time profiles following intranasal administration with OCT inhibitors.....                       | 160 |
| Table 6-7: Rat plasma unbound fractions of amantadine .....   | 164 |
| Table 7-1: The three different study groups for amantadine to compare IA vs. IN routes. ....  | 167 |
| Table 7-2: Selected pharmacokinetic parameters calculated from the plasma concentration-time profiles of cimetidine following intra-arterial and intranasal administration in rats .....            | 171 |
| Table 7-3: Selected pharmacokinetic parameters calculated from the olfactory bulb and striatal ECF-time profiles of cimetidine following intra-arterial and intranasal administration in rats ..... | 173 |
| Table 7-4: Selected pharmacokinetic parameters calculated from plasma profiles of cimetidine following intranasal administration with OCT2 inhibitor .....  | 176 |

## LIST OF FIGURES

|  |    |
|--|----|
| Figure 1-1: Schematic representation of the section of the human nasal cavity showing the respiratory and olfactory regions of the nasal mucosa .....                        | 4  |
| Figure 1-2: Light micrographs of hematoxylin-eosin sections of bovine respiratory and olfactory mucosa.....  | 7  |
| Figure 1-3: The neuron projections from the brain to the olfactory bulb .....  | 12 |
| Figure 1-4: Schematic showing the drug transport and clearance pathways to the different regions in the brain or the systemic circulation from the nasal passages .....      | 13 |
| Figure 1-5: Protein structure of an organic cation transporter .....   | 15 |
| Figure 3-1: Agarose gel electrophoresis of extracted RNA samples .....   | 42 |
| Figure 3-2: Agarose gel electrophoresis of cDNA samples visualized using transilluminating UV light ..   | 43 |
| Figure 3-3: Agarose gel electrophoresis of PCR products showing the effect of different $Mg^{+2}$ concentrations and number of amplification cycles on DNA amplification ... | 45 |
| Figure 3-4: Agarose gel electrophoresis of RT-PCR products showing the expression of mRNAs corresponding to the organic cation transporters in bovine nasal mucosa .....     | 47 |
| Figure 3-5: Standard curve for bovine serum albumin in BCA assay for proteins.....   | 48 |
| Figure 3-6: The amount of total membrane proteins in bovine olfactory and respiratory tissue .....   | 49 |
| Figure 3-7: Western blot for OCTN2 expression in bovine olfactory and respiratory epithelia ..   | 51 |
| Figure 3-8: Immunohistochemical staining of OCTN2 in bovine respiratory epithelia ...  | 53 |
| Figure 3-9: Immunohistochemical staining of OCTN 2 in bovine olfactory mucosa. ....  | 54 |
| Figure 3-10: Immunohistochemical staining of OCTN2 in bovine respiratory epithelia and submucosa .....   | 55 |
| Figure 3-11: ELISA results showing the relative expression of OCT2 transporter protein in the olfactory and respiratory tissues.....   | 57 |

|  |    |
|--|----|
| Figure 3-12: ELISA results showing the relative expression of OCTN2 transporter protein in the olfactory and respiratory tissues .....         | 58 |
| Figure 4-1: Positive ion mass spectra of amantadine and rimantadine.....   | 70 |
| Figure 4-2: Calibration plot for amantadine :rimantadine ratio in KRB using LCMS .....   | 71 |
| Figure 4-3: Calibration plot for amantadine :rimantadine ratio in rat plasma using LCMS ..   | 71 |
| Figure 4-4: Calibration plot for amantadine :rimantadine ratio in aECF using LCMS .....  | 72 |
| Figure 4-5: Representative chromatograph of KRB buffer sample obtained from amantadine transport studies.....                                  | 73 |
| Figure 4-6: Representative chromatograph of blank rat plasma spiked with rimantadine .....   | 74 |
| Figure 4-7: Representative chromatograph of blank rat plasma spiked with amantadine and rimantadine .  | 74 |
| Figure 4-8: Representative chromatograph of plasma sample obtained from a rat, following an intranasal amantadine dose .....                   | 75 |
| Figure 4-9: Representative chromatograph of blank artificial ECF spiked with rimantadine.....  | 75 |
| Figure 4-10: Representative chromatograph of artificial ECF standard, spiked with amantadine and rimantadine .....                             | 76 |
| Figure 4-11: Representative chromatograph of an olfactory bulb ECF dialysate obtained from a rat following an intranasal amantadine dose ..... | 76 |
| Figure 4-12: Representative chromatograph of a striatum aECF dialysate obtained from a rat following an intranasal amantadine dose .....       | 77 |
| Figure 4-13: Calibration plot for cimetidine: famotidine ratio in KRB buffer using HPLC .....  | 79 |
| Figure 4-14: Calibration plot for cimetidine:famotidine ratio in rat plasma using LCMS .....   | 79 |
| Figure 4-15: Calibration plot for cimetidine:famotidine ratio in aECF using LCMS .....   | 80 |
| Figure 4-16: HPLC chromatograph cimetidine in KRB .....  | 81 |
| Figure 4-17: Representative chromatograph of rat plasma standard spiked with cimetidine and famotidine .....                                   | 82 |

|   |     |
|---|-----|
| Figure 4-18: Representative chromatograph of plasma sample obtained from a rat following an intranasal cimetidine dose .....                      | 82  |
| Figure 4-19: Representative chromatograph of aECF standard spiked with cimetidine and famotidine .....  | 83  |
| Figure 4-20: Representative chromatograph of an olfactory bulb ECF dialysate obtained from rat following an intranasal cimetidine dose .....      | 83  |
| Figure 4-21: Representative chromatograph of striatum ECF dialysate from rat dosed intranasally with cimetidine .....                             | 84  |
| Figure 5-1: Chemical structure of amantadine .....  | 87  |
| Figure 5- 2: Chemical structure of cimetidine .....   | 88  |
| Figure 5-3: Chemical structure of guanidine .....   | 90  |
| Figure 5-4: Chemical structure of L-carnitine .....   | 91  |
| Figure 5-5: Chemical structure of pentamidine isoethionate .....  | 91  |
| Figure 5-6: Representative plot of the cumulative amount of amantadine transported across the bovine respiratory mucosal explants .....           | 100 |
| Figure 5-7: Representative plot of the cumulative amount of amantadine transported across the bovine olfactory mucosal explants .....             | 101 |
| Figure 5-8: Comparison of flux values for amantadine across bovine respiratory and olfactory mucosa .....   | 103 |
| Figure 5-9: Fitting of the Michaelis-Menten equation to amantadine flux across bovine respiratory and olfactory mucosa in the m-s direction ..... | 107 |
| Figure 5-10: OCT2 inhibition of amantadine flux across bovine respiratory and olfactory mucosa in the m-s and s-m direction .....                 | 109 |
| Figure 5-11: Effect of sodium in the OCTN2 inhibition of amantadine flux across bovine respiratory tissue by L-carnitine.....                     | 112 |
| Figure 5-12: OCN2 inhibition of amnatadine flux across bovine olfactory tissue in the m-s and s-m direction .....                                 | 113 |
| Figure 5-13: Representative plots of cumulative amount of cimetidine transported across a bovine respiratory mucosa .....                         | 115 |
| Figure 5-14: Representative plots of cumulative amount of cimetidine transported across the bovine olfactory mucosa .....                         | 116 |

|  |     |
|--|-----|
| Figure 5-15: Cimetidine transport across bovine respiratory and olfactory mucosa in the m-s direction .....  | 118 |
| Figure 5-16: Comparison of thickness normalized effective permeability coefficients ( $P_e$ ) for cimetidine flux across bovine respiratory and olfactory mucosa .....               | 120 |
| Figure 5-17: Effect of OCT2 inhibitor, pentamidine on cimetidine flux across the olfactory mucosa in s-m direction .....   | 122 |
| Figure 5-18: Effect of OCT2 inhibitor, pentamidine on cimetidine flux across the respiratory mucosa in s-m direction .....   | 122 |
| Figure 6-1: A microdialysis probe showing its functional segments .....  | 128 |
| Figure 6-2: A schematic representation of the operation of the microdialysis probe .....   | 130 |
| Figure 6-3: Small animal stereotaxic used to locate the regions of interest in the rat brain .....   | 135 |
| Figure 6-4: The AP, ML and DV coordinates for striatum and olfactory bulb from the bregma .....  | 136 |
| Figure 6-5: Concentration dependence of the percentage <i>in vivo</i> recovery by loss of amantadine from the olfactory bulb and the striatum .....                                  | 145 |
| Figure 6-6: Time dependence percentage <i>in vivo</i> recovery by loss of amantadine from the olfactory bulb and the striatum probe .....  | 145 |
| Figure 6- 7: Plasma concentration time profiles of amantadine following intra-arterial and intranasal administration in rats .....   | 147 |
| Figure 6-8: Brain olfactory bulb and striatal ECF concentration- time profile of amantadine following intra-arterial and intranasal administration in rats. ....                     | 150 |
| Figure 6-9: Brain olfactory bulb and striatum ECF concentrations of amantadine following intra-arterial and intranasal administration in rats .....                                  | 152 |
| Figure 6- 10: Plasma concentration time profiles of amantadine following intranasal administration amantadine in the presence of an OCT inhibitors. ....                             | 154 |
| Figure 6-11: Brain ECF concentration-time profile of amantadine following intra-intranasal administration in the olfactory bulb and striatum in the presence of OCT inhibitors ..... | 159 |
| Figure 6-12: Brain olfactory bulb ECF concentrations of amantadine following intra-arterial and intranasal administration of amantadine in the presence of OCT inhibitors .....      | 161 |

|   |     |
|---|-----|
| Figure 6-13: Brain striatum ECF concentrations of amantadine following intra-arterial and intranasal administration of the amantadine in the presence of OCT inhibitors ..... | 162 |
| Figure 6-14: $K_{p,brain}$ vs. time profiles showing the brain : blood partition coefficient of the IA dose compared to the IN dose .....                                     | 166 |
| Figure 7-1: Concentration dependence of percentage <i>in vivo</i> recovery by loss of cimetidine from the olfactory bulb and striatal probes .....                            | 172 |
| Figure 7-2: Time dependence of percentage <i>in vivo</i> recovery by loss of cimetidine from the olfactory bulb and the striatum probes .....                                 | 172 |
| Figure 7-3: Plasma concentration time profiles of cimetidine following intra-arterial and intranasal administration in rats .....   | 173 |
| Figure 7- 4: Brain olfactory bulb and striatum ECF concentration- time profile of cimetidine following intra-arterial and intranasal administration in rats .....             | 176 |
| Figure 7-5: Brain olfactory bulb and striatum ECF concentrations of cimetidine following intra-arterial and intranasal administration in rats.....                            | 177 |
| Figure 7-6: Plasma concentration-time profiles of cimetidine following intra-nasal administration of cimetidine with OCT2 inhibitor .....                                     | 179 |
| Figure 7-7: Brain ECF concentration-time profile of cimetidine following intraarterial and intranasal administration in the olfactory bulb and striatum .....                 | 181 |
| Figure 7- 8: Olfactory bulb ECF concentrations of cimetidine following intra-arterial, intranasal and intranasal co-administration of an OCT2 inhibitor .....                 | 183 |
| Figure 7-9: Striatal ECF concentrations of cimetidine following intra-arterial, intranasal and intranasal co-administration of an OCT2 inhibitor .....                        | 184 |

## LIST OF ABBREVIATIONS

|                        |   |
|------------------------|---|
| <b>aECF</b>            | <i>artificial extracellular fluid</i>           |
| <b>APCI</b>            | <i>Atomic pressure chemical ionization</i>      |
| <b>AUC</b>             | <i>Area under the curve</i>                     |
| <b>BBB</b>             | <i>Blood brain barrier</i>                      |
| <b>BCA</b>             | <i>Bicinchoninic acid</i>                       |
| <b>BSA</b>             | <i>Bovine serum albumin</i>                     |
| <b>cDNA</b>            | <i>Complementary deoxy ribo nucleic acid</i>    |
| <b>CFTR</b>            | <i>Cystic fibrosis trans membrane regulator</i> |
| <b>C<sub>max</sub></b> | <i>Peak serum concentration of a drug</i>       |
| <b>CNS</b>             | <i>Central nervous system</i>                   |
| <b>CSF</b>             | <i>Cerebro spinal fluid</i>                     |
| <b>DAT</b>             | <i>Dopamine active transporter</i>              |
| <b>dNTP</b>            | <i>deoxyribonucleotide triphosphate</i>         |
| <b>DPBS</b>            | <i>Dulbecco's Phosphate-Buffered Saline</i>     |
| <b>ECF</b>             | <i>Extracellular fluid</i>                      |
| <b>ECL</b>             | <i>Electrogenerated chemiluminescence</i>       |
| <b>EDTA</b>            | <i>Ethylene diamine tetraacetic acid</i>        |
| <b>ELISA</b>           | <i>Enzyme linked immunosorbent assay</i>        |
| <b>HRP</b>             | <i>Horse radish peroxidase</i>                  |
| <b>IA</b>              | <i>Intra-arterial</i>                           |
| <b>IHC</b>             | <i>Immunohistochemistry</i>                     |
| <b>IN</b>              | <i>Intranasal</i>                               |
| <b>KRB</b>             | <i>Kreb's Ringer buffer</i>                     |
| <b>LCMS</b>            | <i>Liquid chromatography–mass spectrometry</i>  |
| <b>MDR1</b>            | <i>Multi-drug resistance 1 protein</i>          |



|                        |   |
|------------------------|---|
| <b>MRI</b>             | <i>Magnetic resonance imaging</i>                                 |
| <b>m-s</b>             | <i>mucosal to submucosal direction</i>                            |
| <b>NMDA</b>            | <i>N-methyl D aspartate</i>                                       |
| <b>OAT</b>             | <i>Organic anion transporter</i>                                  |
| <b>OCT1/2/3</b>        | <i>Organic cation transporter subfamily 1/2/3</i>                 |
| <b>OCTN1/2</b>         | <i>Organic cation/carnitine transporter subfamily1/2</i>          |
| <b>ORN</b>             | <i>Olfactory receptor neuron</i>                                  |
| <b>PAES</b>            | <i>Polyarylethysulfone</i>  |
| <b>PBS</b>             | <i>Phosphate buffered saline</i>                                  |
| <b>PBST</b>            | <i>Phosphate buffered saline containing 0.05% Tween 20</i>        |
| <b>PET</b>             | <i>Positron emission tomography</i>                               |
| <b>RNA</b>             | <i>Ribosnucleic acid</i>  |
| <b>RT-PCR</b>          | <i>Reverse transcriptase polymerase chain reaction</i>            |
| <b>SDS-PAGE</b>        | <i>Sodium dodecyl sulphate polyacrylamide gel electrophoresis</i> |
| <b>SLC22</b>           | <i>Solute carrier family 22</i>                                   |
| <b>SPE</b>             | <i>Solid phase extraction</i>                                     |
| <b>s-m</b>             | <i>submucosal to mucosal direction</i>                            |
| <b>TBE</b>             | <i>Tris/Borate/EDTA</i>   |
| <b>TEER</b>            | <i>Trans epithelial electrical resistance</i>                     |
| <b>TEA</b>             | <i>Tetra ethyl ammonium</i>                                       |
| <b>TFM</b>             | <i>Tissue freezing medium</i>                                     |
| <b>TMB</b>             | <i>Tetra methyl benzidine</i>                                     |
| <b>T<sub>max</sub></b> | <i>Time taken by a drug to achieve C<sub>max</sub></i>            |
| <b>T<sub>m</sub></b>   | <i>Primer melting temperature</i>                                 |
| <b>UV</b>              | <i>Ultraviolet</i>  |

## CHAPTER 1

### INTRODUCTION

The worldwide market for therapies for CNS (central nervous system) disorders is estimated at greater than \$50 billion, yet CNS therapeutic research and development is associated with considerable challenges. It takes a significantly longer time to get a CNS drug to the market (12–16 years) compared to a non-CNS drug (10–12 years), in addition to higher attrition rates for CNS drug candidates during clinical trials. Reasons for this include the complexity of brain and CNS side effects which are undetectable in preclinical and early clinical development<sup>1</sup>. One of the biggest challenges in neurotherapeutic development lies in the limited ability of many compounds intended for CNS action to cross the BBB (blood brain barrier). BBB serves to protect the brain and spinal cord from a variety of pathogens and toxic substances, but also limits the entry of many molecules for treating neurodegenerative disorders such as Alzheimer's disease, Parkinson's disease, stroke and brain tumor<sup>2-3</sup>. Although some small molecules administered by traditional routes reach the brain by crossing the BBB, usually high systemic doses are required to achieve therapeutic levels, which can lead to adverse effects throughout the body. It has been estimated that less than 2% of all small molecule drugs and virtually no large molecules can get past the BBB in appreciable amounts<sup>4-5</sup>. Drugs can be introduced directly into the CNS by intracerebroventricular or intraparenchymal injections, yet these techniques are invasive, risky, and expensive requiring surgical expertise for accurate placement<sup>6,7</sup>. Therefore, it is of great importance to identify drug delivery strategies that can bypass the BBB and directly deliver drugs to the brain. In this context, the use of the intranasal route to deliver drugs to the CNS

provides a promising alternative that has attracted considerable interest amongst the scientific community<sup>8</sup>. Recreational drugs such as nicotine (from tobacco smoke), cocaine, or amphetamines are commonly “sniffed” through the nose to achieve CNS effects<sup>9-10</sup>. Additionally, the cumulative evidence suggests that drugs are able to enter the brain directly from the nose through an olfactory or a trigeminal pathway. The olfactory or trigeminal nerve systems originate in the brain, innervate the nasal cavity and are exposed directly to the external environment outside of the BBB<sup>11</sup>. Therefore, the nasal route forms the most direct and non-invasive method of entry into the brain.

The introduction of the nasal route as a promising alternative to other conventional routes for systemic delivery of drugs is associated with a number of advantages such as convenience, easy access, rapid absorption, avoidance of intestinal and hepatic first-pass metabolism and high potential for drug transfer to the brain<sup>12-13</sup>. However, this delivery route faces challenges with respect to dose reproducibility due to two major drawbacks: (1) mucociliary clearance, which reduces the residence time of the drug in the nasal cavity and (2) nasal metabolism, where many compounds (e.g. peptides<sup>14</sup>, nitrosamines<sup>15,16</sup>, cocaine<sup>17</sup>) undergo some degree of nasal metabolism, decreasing their bioavailability following this route of administration<sup>24</sup>.

Recent developments in nasal drug delivery have suggested the potential of this route as a means to target the brain, especially for neurotherapeutics with limited blood–brain permeability<sup>18,19</sup>. To understand the feasibility of the nasal route in the direct CNS delivery of a compound, it is important to take into consideration the potential barriers between the nose and the brain. The nasal cavity can be divided into three anatomical regions, namely the vestibular, respiratory and olfactory regions of the nasal cavity

(Figure 1-1). The vestibular region is the least important of the three regions with regard to drug absorption. The respiratory region is the major site for systemic drug absorption owing to its high degree of vascularity and significant absorptive surface area. The olfactory region appears to be the most important site for direct CNS delivery, since the presence of a direct connection between the olfactory and respiratory submucosa and the brain via the olfactory and trigeminal neural pathway is well established <sup>20</sup>.

Since the olfactory region seems to play a key role in the CNS delivery of drugs via the nasal route, the membrane permeability across the olfactory mucosa, the first barrier to drug uptake and transport needs to be better understood. The nasal respiratory and olfactory mucosae express a range of both uptake and efflux transporters (CFTR, MDR1, MRP <sup>21-22</sup>, DAT <sup>23,24</sup> OAT6 <sup>25</sup>) that are implicated in the regulation of drug access to the brain via the olfactory pathway <sup>26-27</sup>. Chemturi and Donovan have reported the presence of OCT2 (organic cation transporter 2), an organic cation transporter in the bovine olfactory and respiratory nasal epithelium<sup>28</sup>. Therefore, it was proposed that the transporter-mediated increases in flux of substrates across the olfactory mucosa may increase the concentrations of these substrates in the olfactory submucosa, from where the drug can be carried into the brain <sup>29</sup>. Thus, OCT2 uptake can enhance the CNS distribution of small, charged hydrophilic substrates that will otherwise have difficulty crossing the BBB via other routes of delivery.

This research focuses on identifying and characterizing organic cation transporters in the olfactory mucosa, which can potentially target therapeutic agents to various regions of the CNS to treat neurological disorders, following intranasal administration.

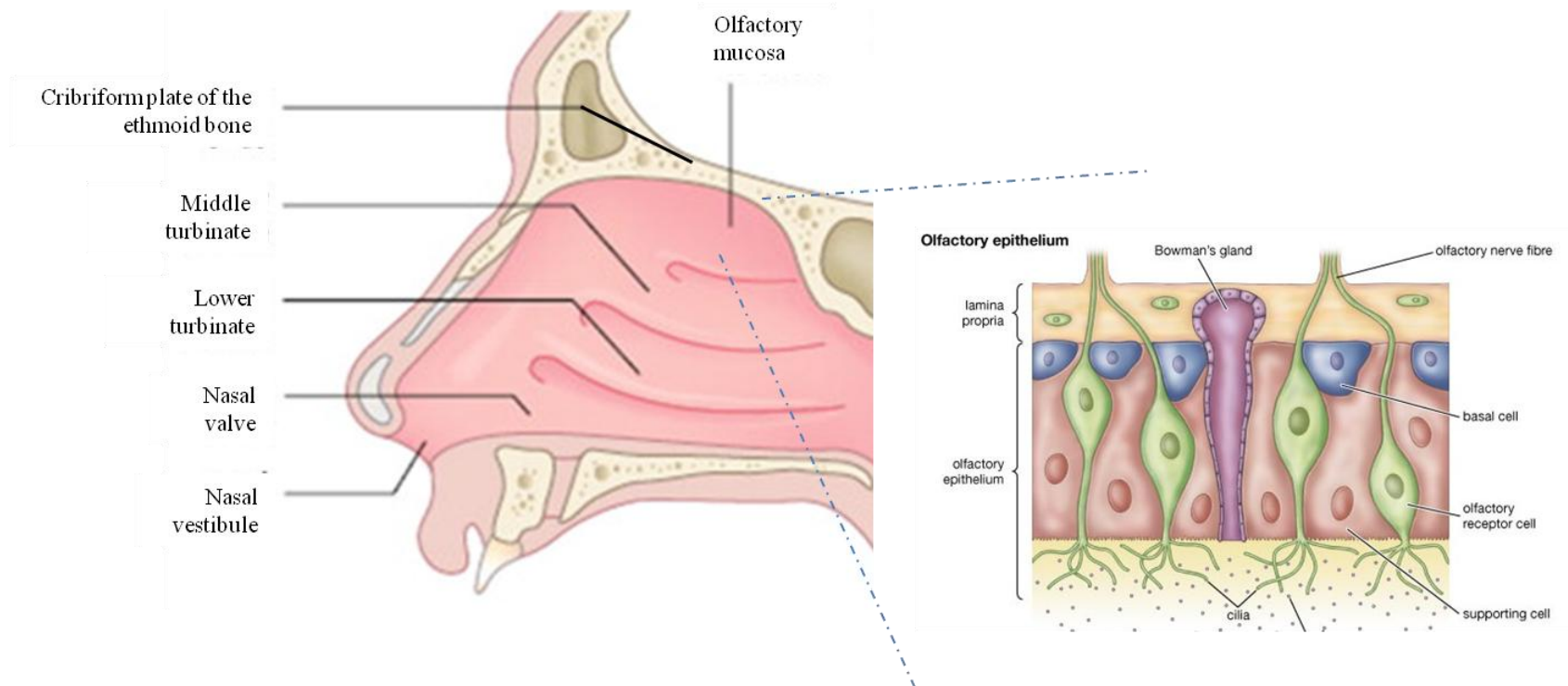


Figure 1-1: Schematic representation of the section of the human nasal cavity showing the respiratory and olfactory regions of the nasal mucosa (reproduced with permission from Elsevier<sup>30</sup> and Encyclopædia Britannica, Inc<sup>31</sup>).

Two small molecules, amantadine and cimetidine, were chosen as model drugs for this study. Both of these drugs are well established OCT2 substrates with good aqueous solubilities and both have low metabolic susceptibilities. The work described was undertaken to investigate the transport mechanisms of amantadine and cimetidine across the nasal mucosa; to further identify membrane transporters that are present in the nasal mucosa, and to explore the contribution of the transporters in the brain distribution of these drugs.

### Nasal anatomy and cellular organization

The main functions of the nose are olfaction, regulation of humidity and temperature of inhaled air, and removal of large particulates from inhaled air. The nasal cavity is divided into two halves by the nasal septum. Each nasal cavity can be divided into three regions (1) nasal vestibule, (2) the olfactory region and (3) the respiratory region (Figure 1-1). The respiratory mucosa is predominant in the lower, middle and on portions of the upper turbinate. In humans, the total surface area and the volume of the nasal cavity is  $\sim 150 \text{ cm}^2$  and 13 mL, respectively<sup>32</sup>. About 20-40 mL of mucus/day is secreted from a normal resting nasal mucosa, and together with ciliary action, these secretions provide a fundamental protective function of the nose<sup>33</sup>. Mucociliary clearance contributes to a significant loss of dosage forms administered intranasally. The olfactory epithelium covers an area of  $\sim 370 \text{ mm}^2$  in humans and is located high in the nasal cavity of humans where it partly covers the cribriform plate of the ethmoid bone and portions of the upper turbinate<sup>34</sup>. The respiratory mucosa is lined with a pseudostratified, ciliated columnar epithelium with up to 100-200 cilia/cell.

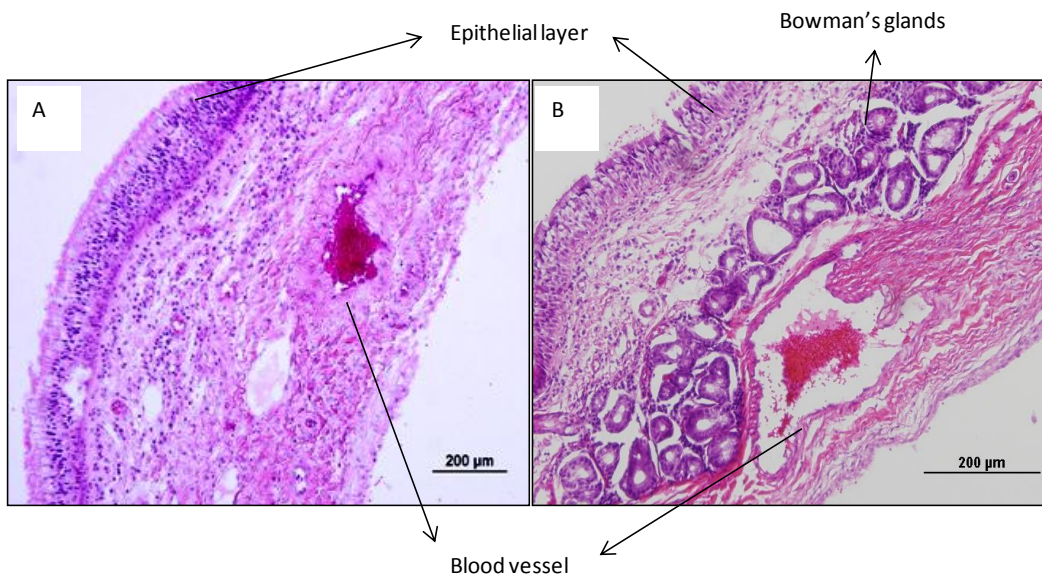


Figure 1-2: Light micrographs of hematoxylin-eosin sections of bovine (A) respiratory and (B) olfactory mucosa (reproduced with permission) <sup>35</sup>

The ethmoid bone separates the nasal and cranial cavities, and the cribriform plate is a porous bony structure that allows the passage of neuron bundles from the olfactory epithelium to the olfactory bulbs and from there to distant sites in the CNS through the subarachnoid space containing CSF (cerebrospinal fluid).

The apical surfaces of the respiratory columnar epithelium cells show the presence of microvilli which increases the surface area for absorption. The respiratory region also contains goblet cells that secrete mucus which covers the nasal mucosal surface. The olfactory region is characterized by a columnar neuroepithelium and is composed of olfactory sensory neurons that are exposed to the external environment. Sustentacular, or supporting cells, form a sheath around the neurons. The basal cells regenerate a new neuroepithelium every 40 days. The underlying lamina propria contains olfactory nerve fascicles and mucus-secreting Bowman's glands<sup>36</sup>. The olfactory receptor neurons regenerate every 3–4 weeks originating from basal cells residing in the olfactory epithelium. As a result, proteolytic enzymes and tight junction proteins present in the nasal passages are not fully functional and the nasal barrier to the CNS is therefore leaky compared to the BBB<sup>37</sup>. Light micrographs of both olfactory and respiratory mucosa are presented in Figure 1-2.

#### Nose to brain delivery

Knowledge regarding the existence of an intranasal pathway to the brain involving the olfactory epithelium and olfactory bulb dates to back to the middle of last century. Faber et al. identified the localization of poliomyelitis virus in the central nervous system after intranasal inoculation in monkeys<sup>38</sup>. The transport of a number of agents such as horseradish peroxidase, wheat germ agglutinin–horseradish peroxidase



conjugate and colloidal gold across the olfactory epithelium into the CNS in animals has also been reported by numerous investigators<sup>39-40</sup>. Similarly, a large number of studies have been performed where drugs such as estradiol, cephalexin, lidocaine and cocaine have been shown to reach the CSF, the olfactory bulb and in some cases distant parts of the brain after nasal administration<sup>10,41-42</sup>. Studies have also been directed to investigate the mechanism of transport of drugs across the olfactory epithelial membrane to identify the important physicochemical characteristics that contribute to the CNS disposition of the drug following nasal administration where the bioavailability or permeability of compounds >1 kDa, was directly correlated to the molecular weight of the compounds<sup>43-44</sup>.

Although a significant number of small molecules have been studied for potential nose to brain delivery in animal models, such as the rat and the monkey, only a handful of them have shown promise. Increasing the drug hydrophilicity, molecular weight and the degree of ionization can reduce drug transport into the CNS after intranasal administration<sup>45-46</sup>. In addition, low molecular weight drugs can be affected by the active efflux transporters at the apical membrane surface (P-gp, MDR, MRP) in the olfactory epithelium<sup>47</sup>.

Various formulation approaches have also been studied, such as microemulsions and nanoemulsions to improve drug solubility and mucoadhesive formulations to decrease mucociliary clearance. Emulsion formulations of clonazepam, sumatriptan, risperidone, zolmitriptan, or nimodipine demonstrated an increased brain uptake. For clonazepam, sumatriptan, and risperidone, the increased brain uptake was accompanied by an increased uptake into the blood<sup>48</sup>.

Successful nose to brain delivery has also been reported for neuropeptides and proteins. An olfactory mediated transfer of hexarelin has been reported in rabbits <sup>49</sup>. Vasoactive intestinal peptide, known to rapidly degrade in blood, was found in significant amounts in the trigeminal nerve pathways when administered nasally, and a glucagon-like peptide-1 antagonist was detected in high levels in the olfactory bulb, hippocampus, cerebellum and brainstem following intranasal administration <sup>50,51</sup>. Intranasally administered desferoxmine was found to have increased targeting (200-fold) to the cortex compared with intravenous delivery, and has been proposed for use in the treatment for stroke <sup>52</sup>.

Although most of the studies were performed in rodent models, a handful of studies have also been conducted in humans. No difference in CSF levels was observed for melatonin, irrespective of the route, nasal versus intravenous, indicating that the drug may be entering the CSF via the bloodstream in both cases <sup>53</sup>. Nasal administration of insulin in human volunteers were observed to give increased levels in the CSF with no associated increase in serum levels <sup>54</sup>. Phase II clinical trials of intranasal insulin, showed promising results in improving cognitive function in adults with amnesic mild cognitive impairment in Alzheimer disease <sup>55</sup>.

#### Nose to brain pathways

The exact pathways underlying the direct nose-to-brain delivery of drugs are not completely understood, but the olfactory neurons connecting the nasal passages to the brain have been postulated to play a role. In addition, pathways involving blood vessels, cerebrospinal fluid, and the lymphatic system may also play a part in the transport of molecules from the nasal cavity to the CNS.

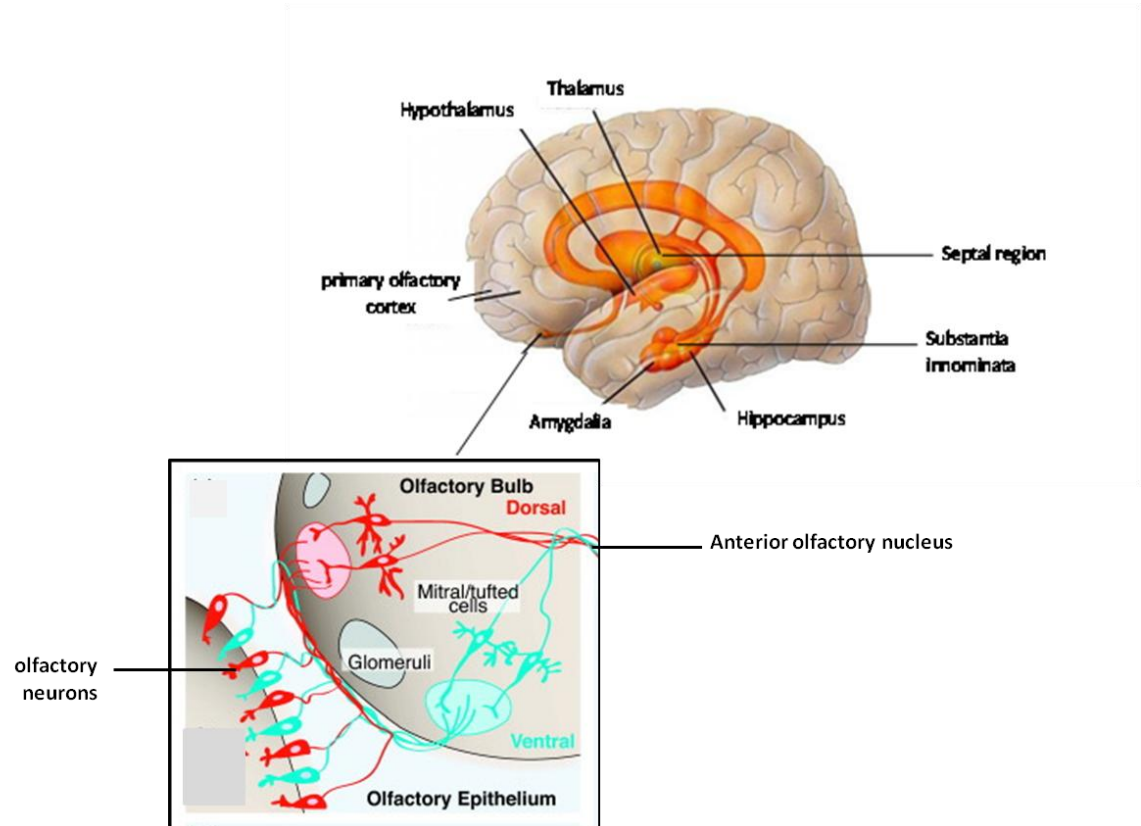


Figure 1-3: The olfactory receptor neurons (ORNs) rise in the olfactory epithelium with their axons projecting into the olfactory bulb to form synapses with the dendrites of mitral and tufted cells, giving rise to the glomeruli. The primary axons of the projection from the olfactory bulb mitral and tufted cells make connections in different parts of the brain<sup>56</sup> (reproduced with permission).

It is likely that a combination of these pathways operate, with one outweighing the other, depending on the properties of the drug, formulation and/or delivery device<sup>57,58</sup>.

The neuronal connection for the mammalian olfactory system commences as the olfactory receptor neurons (ORNs) in the olfactory epithelium. The axons from the ORNs form the olfactory nerve which projects on to the olfactory bulb and forms synapses with the apical dendrites of mitral/tufted cells, giving rise to the olfactory bulb glomeruli<sup>59</sup>. The axons of the mitral and tufted cells project directly into the primary olfactory cortex and the primary olfactory cortex projects to the hypothalamus, thalamus, hippocampus, septal region, substantia innominata and the orbitofrontal cortex<sup>60</sup> (Figure 1-3). It has been observed that large proteins and nanoparticles were transported via axons through the olfactory bulb into the olfactory cortex and from there to the cerebrum and the cerebellum<sup>61,62</sup>. Hence, all these regions form potential delivery sites for the nose-to-brain transport drugs via the olfactory epithelium. Additionally, the ophthalmic and maxillary branches of the trigeminal nerve innervate the respiratory and olfactory epithelium of the nasal passages. These two branches and the third trigeminal nerve branch, the mandibular branch, meet at the trigeminal ganglion which contains the cell bodies of these sensory nerve fibers. Afferent neurons synapse at the trigeminal ganglion to form a single incoming nerve that enters the brainstem at the level of the pons. It has been shown that these neurons can deliver the neurotrophic factor, IGF-1 (MW 7.65 kDa), to the brainstem and spinal cord areas of rats. Hence, in contrast to rostral entry of drug via the olfactory pathway, the trigeminal nerve was shown to enhance nose-to-brain delivery to caudal brain areas<sup>54</sup>.

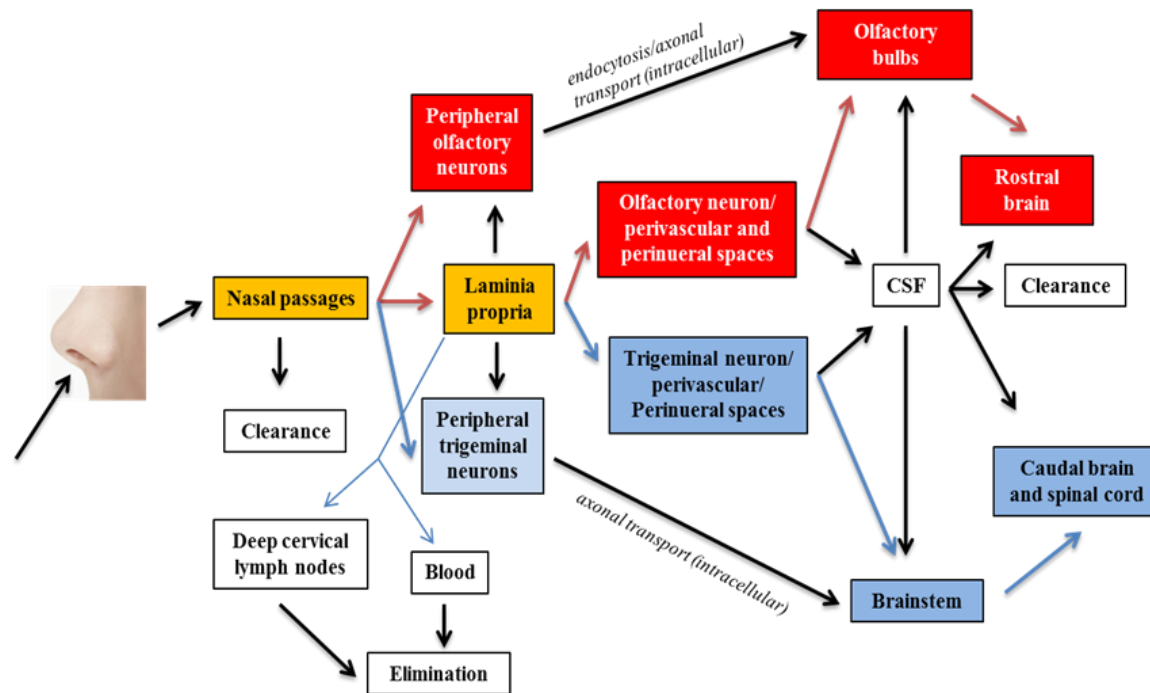


Figure 1-4: Schematic showing the drug transport and clearance pathways to the different regions in the brain or the systemic circulation from the nasal passages<sup>54</sup> (reproduced with permission). The red and blue arrows indicate the olfactory and trigeminal routes, respectively.

Since a portion of the trigeminal neural pathway, the ophthalmic nerve enters the brain through the cribriform plate alongside the olfactory neurons, it is difficult to distinguish whether intranasally administered drugs reach the olfactory bulb and other rostral brain areas via the olfactory or trigeminal pathways or both (Figure 1-4) <sup>63</sup>.

The nasal mucosa is highly vascular, with the olfactory mucosa receiving blood from small branches of the ophthalmic artery and the respiratory mucosa supplied by the capillaries of a branch of the maxillary artery. The relative density of blood vessels is greater in the respiratory mucosa compared to the olfactory mucosa making the former region an ideal site for systemic absorption of drugs <sup>64</sup>. Delivery to the CNS following absorption into the systemic circulation and subsequent transport across the BBB is possible, especially for small lipophilic drugs, which enter the bloodstream more easily and cross the BBB more readily compared to large, hydrophilic therapeutics such as peptides and proteins.

#### Organic cation transporters (OCT)

A membrane transport protein is a membrane protein involved in the movement of ions, small molecules, or macromolecules, across a biological membrane. These membrane transport proteins span the membrane across which they transport substances. The proteins may assist in the movement of substances by facilitated diffusion or active transport. Membrane transporters can be major determinants of the pharmacokinetic, safety and efficacy profiles of drugs. Numerous studies have suggested that transporters play a part in vivo in drug disposition, therapeutic efficacy and adverse drug reactions. Transporter membrane proteins present in numerous tissues including the intestine, liver,

kidney, testes, placenta, and central nervous system. For more details on various membrane transporters the reader is directed to reference <sup>78</sup>

Many drug molecules have primary, secondary, tertiary, or quaternary amines which bear a transient or permanent net positive charge, determined by the compound's  $pK_a$ . These compounds can be generally classified as "organic cations" and they typically have decreased permeabilities across biological membranes proportional to their degree of ionization. As a result, intestinal absorption, tissue distribution, renal excretion and brain uptake of these compounds depends on membrane transporters or paracellular transport for efficient uptake or elimination. Over the past 25 years, a number of transporters that translocate organic cations have been identified and their functional role in tissue/cell uptake of both endogenous substances such as hormones, neurotransmitters and exogenous substances including number of drugs have been demonstrated.

Organic cation transporters belong to solute carrier family SLC22 <sup>65</sup>. In general, organic cation transporters contain 12  $\alpha$ -helical transmembrane domains, an intracellular N-terminus, a large glycosylated, extracellular hydrophobic loop between the first and second domains, a large intracellular loop with phosphorylation sites between the sixth and seventh domains, and an intracellular C-terminus <sup>66</sup> (Figure 1-5). Within the SLC22A transporter family, OCT1/2/3 (SLC22A1/2/3) and OCTN1/2 (SLC22A4/5) mediate the transport of a variety of organic cations especially those administered as drugs. The human genes coding for OCT1, OCT2 and OCT3 are localized within a cluster on chromosome 6.q26-7 <sup>67,68</sup>, and the genes coding for OCTN1 and OCTN2 are localized in a cluster on chromosome 5q31 <sup>69,70</sup>.

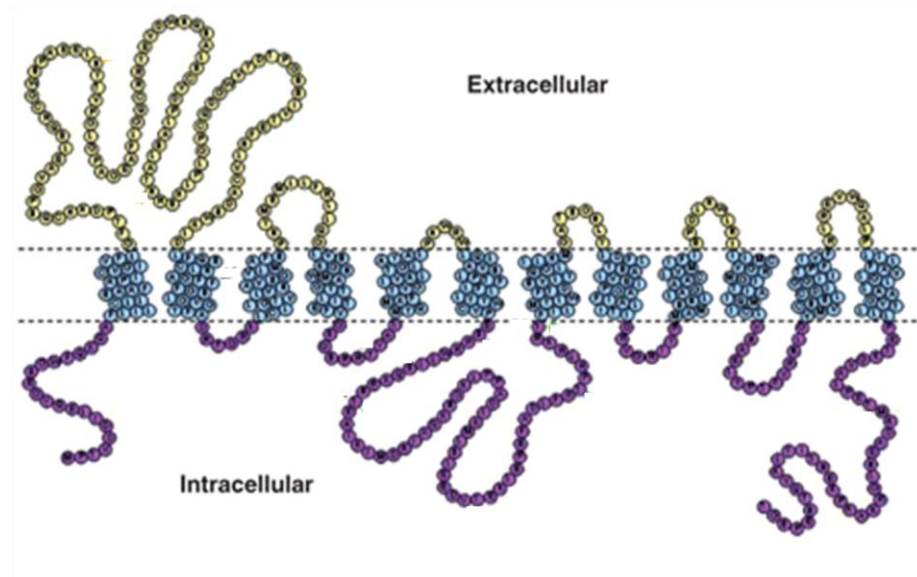


Figure 1-5: Protein structure of an organic cation transporter. The protein has 12 transmembrane domains, a large intracellular and a large extracellular loop (reproduced with permission)<sup>71</sup>.



The OCT (organic cation) and OCTN (organic cation/carnitine) transporters show broad substrate specificities and ubiquitous tissue distributions. Pharmacological and computational studies have established that hydrophobicity as a principal determinant for substrate recognition by OCTs. At least one positive charge is required for transport<sup>72-73</sup>. Few studies have focused on identifying the presence of these transporters in the nasal tissues especially in human and rodent species<sup>74,75</sup>. The results of these studies are summarised in Table 1-2. Additionally, the presence of OCT2 transporter protein was identified in the bovine respiratory and olfactory nasal tissues<sup>28</sup>. However, extensive studies have been performed to identify OCT/OCTN distribution in the lungs and brain. In humans, OCT1, OCT2, OCT3, OCTN1 and OCTN2 have been shown to be expressed in the respiratory epithelium of the trachea and bronchi, confirming expression of these transporters in some regions of the respiratory tract<sup>76,77</sup>.

The expression of OCT1, OCT2, OCT3, OCTN1 and OCTN2 have also been demonstrated in the brains of rodents and humans, and it has been proposed that their functional role at these sites is to regulate the movement of neurotransmitters such as acetylcholine, epinephrine, histamine or serotonin<sup>78</sup>. In particular, the polyspecific, electrogenic OCT2 present in human neurons has been reported to mediate the transport of monoamine neurotransmitters dopamine, norepinephrine, serotonin, histamine, and the anti-parkinsonian drugs, amantadine and memantine<sup>79</sup>.

OCT1/2/3 are known to be bi-directional, facilitative transporters, driven by the electrical potential difference (inside-negative and outside-positive) across the membrane resulting in electroneutral exchange of organic cations with other ions such as H<sup>+</sup> or Na<sup>+</sup><sup>80,81,82</sup>. The organic cation/carnitine transporter, OCTN1 (SLC22A4) shows a relatively

broad tissue distribution and was first characterized as a pH-dependent, organic cation transporter<sup>83</sup>. OCTN1 and OCTN2 substrates include verapamil and quinidine<sup>83,84</sup>. OCTN2 has been reported to transport betaine, choline, lysine, ipratropium, methionine, cephaloridine, procainamide, desipramine, clonidine and emetine<sup>85-86</sup>. OCTN2 participates predominantly in carnitine transport, whereas OCTN1 has relatively low carnitine transport activity. OCTN2 is a Na<sup>+</sup> dependent, high affinity transporter for L-carnitine and acetyl- L-carnitine, but it can also function alternatively as a polyspecific, Na<sup>+</sup> independent cation transporter<sup>84-87</sup>. It has been demonstrated that OCTN1 mediates the transport of ergothioneine, an endogenous antioxidant, suggesting that the physiological role of OCTN1 is related to biological redox reactions<sup>88</sup>. Thus OCTN1 and OCTN2 are highly specific transporters of ergothioneine and carnitine, respectively, and this substrate discrimination can assist in distinguishing their activities. Substrates transported by the OCTs exhibit mutual inhibition where the degree of inhibition by a high concentration of a given substrate may totally or partially inhibit the transport of another. The inhibition may be competitive, however, deviations from classical competitive type of inhibition have also observed for some pairs of substrates and inhibitors<sup>73,89</sup>.

#### *In Vitro* nasal models to study permeability

While animal studies are the most ideal way to study the drug delivery to the brain via the intranasal route, the mechanistic aspects of nasal absorption are better understood at the tissue or cellular level using well-controlled, *in vitro* models. Excised tissue models from non-human species form another approach to overcome the major limitations of the cellular models. The common animals used for tissues for *in vitro* nasal

permeability studies include rabbit, cow, and pigs<sup>90</sup>. These explant models possess the distinct advantage of being cost effective, easily available, reproducible and they provide a more representative organ system compared to cell culture methods. A major concern with excised animal tissues is any species differences between humans and the experimental model. Although there are some general similarities in the nasal passages of most mammalian species, there are also distinct differences that can affect the interpretation of results using a particular animal model. The human nose has been defined as being microsomatic where olfaction is a secondary function, whereas lower mammals (rats, mice, dogs and rabbits) have a complex, macrosomatic nose where olfaction is the primary function, and the upper turbinates are predominantly lined by an olfactory neuroepithelium instead of the respiratory epithelium as seen in humans<sup>91</sup>.

In the current studies, freshly excised bovine explants were used to evaluate the passive and carrier-mediated transport of the model drugs. Bovine tissue is easily obtained from local abattoirs. Morphologically, the tissues appear similar to humans, where both have 'leaky' properties (transepithelial electrical resistance (TEER) 20-150  $\Omega\text{cm}^2$  compared to  $>500 \Omega\text{cm}^2$  for typical cell cultures). Microscopic evaluations show similarities with the human respiratory epithelium, although no systematic histological studies have been reported for comparisons between these two species<sup>92,93</sup>. Light micrographs of sections from bovine respiratory and olfactory mucosa are shown in Figure 1-2. These tissue explants remain viable for ~4h following excision and both our laboratory and other researchers have shown their utility in exploring the mechanistic aspects of transport and metabolism in the nasal mucosa<sup>17,24,94</sup>. Additionally, the expression of the OCT2 transporter is well characterized in the bovine respiratory and

olfactory tissues, and previous studies in our lab have demonstrated the effectiveness of using this tissue model in understanding the role of OCT2 in the transport of dopamine<sup>28</sup>. This makes this *in vitro* model ideal for the study of transport mechanisms of small organic cation substrates across these tissues.

#### Rat as an *In Vivo* animal model for nose to brain delivery

The olfactory system in rats is far more extensive as compared to humans, with the olfactory region in rats occupying approximately 50% of the surface area of the nasal cavity as opposed to 10% in humans. The nasal cavity volume in rats is 0.26 cm<sup>3</sup>, while in humans the nasal cavity has a volume of 25 cm<sup>3</sup> where the olfactory region occupies 8% of the nasal cavity surface area (12.5 cm<sup>2</sup>)<sup>34</sup>. The CSF volume in rat is very low with high turnover rates, when compared to humans<sup>95</sup> (Table 1-1). Despite distinct anatomical differences between rodents and humans, similar pathways are available for intranasal delivery to the CNS. This was demonstrated by studies using IFN $\beta$ -1b in rats and primates, where the interferon was delivered to the CNS along the olfactory and trigeminal pathways<sup>96,97</sup>. In another study, the absence of additional uptake of melatonin in the CSF after nasal delivery compared to intravenous administration in rats was predictive of the outcome in humans, indicating that animal experiments could be predictive of the outcome in human, when studying nose to brain transport<sup>53</sup>. Translation of the nose to brain drug delivery concept into the clinic is currently underway, with clinical trials of intranasal insulin for Alzheimer's disease demonstrating success<sup>55</sup>.

Table 1-1: Physiologically-relevant parameters for humans and rat implicated in the nose to brain transport of drugs<sup>34,95</sup>.

| <i>Species</i> | <i>Nasal cavity area (cm<sup>2</sup>)</i> | <i>Olfactory region area (% of total)</i> | <i>CSF volume (mL)</i> | <i>CSF replacement (times/day)</i> |
|----------------|---|---|------------------------|------------------------------------|
| Rat            | 10  | 50%                                       | 0.090                  | ~24                                |
| Human          | 160-180                                   | 8%  | 140                    | ~5                                 |

There are also other similarities between the nasal epithelia of humans and rats especially with respect to the expression of protein transporters. The expression of organic cation transporter subtypes namely OCT1, OCT2, OCTN1 and OCTN2 in the two species were similar with respect to both the olfactory and respiratory tissues. OCT2 transporter expression in the olfactory epithelium is very high in rodents, with a magnitude almost twice the level observed in the kidneys<sup>75</sup>. Therefore, to further probe the contribution OCT2 in the uptake of drug substrates such as amantadine and cimetidine via the olfactory epithelium, rats serve as an excellent *in vivo* model.

Table 1-2: A comparison of the relative mRNA expression of organic cation transporter proteins (OCTs) in the olfactory and respiratory mucosa of human and rat<sup>74,75</sup>.

| <b>OCTs<br/>(mRNA<br/>expression)</b> | <b>Rat</b>  |           | <b>Human</b> |           |
|---------------------------------------|-------------|-----------|--------------|-----------|
|                                       | Respiratory | Olfactory | Respiratory  | Olfactory |
| <i>OCT1</i>                           | -           | -         | -            | -         |
| <i>OCT2</i>                           | +           | ++        | +            | ++        |
| <i>OCT3</i>                           | -           | -         | NK           | NK        |
| <i>OCTN1</i>                          | +           | +         | +            | +         |
| <i>OCTN2</i>                          | ++          | -         | +            | +         |

Note: (+) and (-) indicates the presence and absence of the particular mRNA. (NK) indicates information not known

## CHAPTER 2

### OBJECTIVES

Intranasal administration enables certain compounds that are otherwise unable to cross the BBB, or otherwise require very high systemic exposures to achieve therapeutic levels in the brain when administered via conventional routes, direct access to brain via the ‘olfactory pathway’. We propose that enhanced CNS bioavailability of certain drug(s) following intranasal administration can be accomplished by enhancing epithelial uptake by targeting the influx transporters present in the olfactory mucosa. The working hypothesis is that amantadine and cimetidine (well established OCT2 substrates) will show enhanced transport /uptake across the respiratory and olfactory mucosa that will result in increased drug concentrations in the brain. The primary objective of the *in vitro* transport studies conducted in bovine nasal explants is to evaluate the feasibility of targeting uptake transporters to improve CNS bioavailability of neuropharmacological agents, using the amantadine-OCT2 and cimetidine-OCT2 drug-transporter combinations, as the prototypes. The specific aims investigated to test the hypothesis about enhanced nose to brain disposition via OCT2 mediated transport include:

1. Demonstrate the expression of organic cation transporter genes and their corresponding proteins using RT-PCR and Western blotting, respectively, in the bovine olfactory and respiratory mucosa. Identify the regions of localization of these transporters in the two tissues using immunohistochemistry and compare the relative abundance of the transporters using ELISA and BCA assays.

2. Compare the flux of two OCT2 substrates, amantadine and cimetidine, across the bovine respiratory and olfactory mucosa and identify saturable mechanisms of transport.
3. Use transporter inhibitors to verify the role of specific transporters in the uptake of substrates across the nasal mucosa by characterizing the extent to which the inhibitors diminish to the permeability of these drugs across the bovine respiratory and olfactory mucosa.

The primary objective of the *in vivo* follow up experiments in rat was to investigate disposition of these drugs in both the brain and the systemic circulation following intranasal and intra-arterial administration. Specific aims include:

1. Compare two delivery routes, an intra-arterial bolus dose vs. an equivalent intranasal dose, with respect to the brain extracellular fluid (ECF) concentrations (olfactory bulb and striatum) for amantadine and cimetidine. A microdialysis technique was used to sample the brain ECF levels of these drugs in two simultaneous locations.
2. Evaluate the role of organic cation transporters in the uptake of the OCT2 and OCTN2 substrate, amantadine, and the OCT2 substrate, cimetidine, from the nasal cavity into the brain by co-administration of the transporter inhibitors, guanidine, L-carnitine and pentamidine.

CHAPTER 3  
CHARACTERIZATION OF ORGANIC CATION TRANSPORTERS  
(OCTS) IN THE BOVINE NASAL MUCOSA

In order to identify the role of organic cation transporters in the uptake of amantadine and cimetidine in the bovine nasal mucosa, it is essential to characterize the differential expression and localization of the organic cation transporter proteins in nasal tissues of *Bos taurus* (one species of cow). Extensive literature exists on the characterization of expression of the OCTs in various tissues in rats and humans, however information regarding the expression of these transporter proteins in bovine tissues, especially in the nasal region is limited to the OCT2 transporter. This transporter was shown to be present in the epithelial and submucosal regions of both the olfactory and respiratory tissues in cows<sup>28</sup>. Therefore, a combination four techniques namely, polymerase chain reaction (PCR), Western blotting, immunohistochemistry (IHC) and enzyme-linked immunosorbent assay (ELISA) were employed to evaluate the gene expression and tissue-specific localization of major organic cation transporters (OCT1, OCT2, OCTN1 and OCTN2) in the bovine olfactory and respiratory nasal mucosa. While PCR offers a cost effective method for rapidly screening for the presence of different OCT genes in the nasal tissues, Western blotting offers a method to determine specific protein expression. However, neither PCR nor Western blotting provides information about the tissue-specific cellular expression of nucleic acids, corresponding proteins, or protein activity. Therefore, immunohistochemistry was used to study the localization of the protein(s) of interest in the two tissues. Additionally, ELISA was used to obtain a semi-quantitative estimate of the relative expression of the proteins of interest in the two



tissues. Western blotting also serves as a tool to evaluate the specificity of the probe antibody chosen for ELISA and IHC, towards the protein of interest

#### *Reverse Transcriptase Polymerase Chain Reaction (RT-PCR)*

RT-PCR (Reverse transcription polymerase chain reaction) is a powerful technique where several million copies of a particular DNA sequence can be amplified from a single DNA molecule. Thermostable DNA polymerases used for basic PCR require a DNA template, and as such, the technique is limited to the analysis of DNA samples. Yet numerous instances exist in which amplification of RNA would be preferred such as detecting specific mRNA sequences corresponding to the organic cation transporters (*OCT1*, *OCT2*, *OCTN1* and *OCTN2*) in the nasal mucosa. To apply PCR to the study of RNA, the RNA sample must first be reverse transcribed to cDNA to provide the necessary DNA template for the thermostable polymerase. This process is called reverse transcription (RT), hence the name RT-PCR.

A typical PCR reaction includes target DNA, a thermostable DNA polymerase, two oligonucleotide primers, deoxynucleotide triphosphates (dNTPs), reaction buffer and magnesium. The process of PCR occurs in three steps: denaturing, annealing and extension. Each repetition of these steps constitutes one cycle and doubles the amount of DNA present in the sample. During the first step of denaturation, the double stranded DNA separates into two single strands. This is followed by an annealing step, where a pair of primers anneal (bind) to the complementary DNA sequence of interest. Primers are nucleotide sequences that mark the beginning of the DNA target sequence of interest and are complementary to each of the single DNA strands produced during the denaturation step. In the last and final step, called extension, an enzyme, *Taq* DNA

polymerase, is used to replicate the DNA strands in the presence of deoxyribonucleotide triphosphates (dNTP) and magnesium ions. *Taq* polymerase is an enzyme that begins the synthesis process at the region marked by the primers and thus results in two new double stranded DNA molecules identical to the original double stranded target DNA region. After the first few cycles the major product is a DNA fragment that is exactly equal in length to the sum of the lengths of the two primers and the target DNA and after each cycle, and the newly synthesized DNA strands can serve as template in the next cycle. These three-step cycles are repeated over and over until a sufficient amount of product is produced, where the exponential increase in PCR product is a function of cycle number. The reaction products are separated by gel electrophoresis and can be visualized directly by staining with a fluorescent nucleic acid intercalating agent such as ethidium bromide.

No single set of conditions can be applied to all PCR amplification reactions. The magnesium concentration used in the PCR mix has been shown to affect primer annealing and strand dissociation, PCR product specificity, and formation of primer-dimer artifacts. *Taq* DNA polymerase requires free magnesium as a cofactor and a typical PCR reagent mix should contain 1.5 to 2.5 mM magnesium. Additionally, the number of amplification cycles is also critical for a successful PCR. Too many cycles can increase the amount and complexity of non-specific background products and too few cycles give low product yield<sup>98,99</sup>.

#### *Nucleic acid purity assessment*

The evaluation of the purity of a nucleic acid sample is often performed by a spectral analysis of the UV absorbance of the sample. Typically a ratio of  $A_{260}/A_{280}$  is determined, where  $A_{260}$  and  $A_{280}$  are the spectrophotometric absorbances at 260 and

280 nm respectively. Although this procedure was first described by Warburg and Christian as a means to measure protein purity in the presence of nucleic acid contamination, it is most commonly used today to assess purity of nucleic acid samples<sup>100</sup>. This ratio is based on calculations using the Beer-Lambert Law (Equation 3-1), where the Absorbance (A) is the product of the extinction coefficient ( $\lambda$ ) and the concentration of the sample (C).

$$A=\lambda C \qquad \text{Equation 3-1}$$

The commonly accepted average extinction coefficients for 1 mg/ml nucleic acid solutions at 260 nm and 280 nm are 20 and 10 M<sup>-1</sup>cm<sup>-1</sup>, respectively. Using these extinction coefficients, good quality nucleic acid samples should have an A<sub>260</sub>/A<sub>280</sub> ratio greater than 1.6.

#### *Western Blot / SDS PAGE*

While PCR gives information about the mRNA expression, it is necessary to verify that this expression actually translates to the corresponding protein being produced, since there is considerable uncertainty regarding genome-wide correlation between levels of RNA and the corresponding proteins<sup>101</sup>. Western blotting is an analytical technique used to detect specific proteins by using gel electrophoresis to separate native or denatured proteins based on their sizes (length/shape of the polypeptide chain). To prepare samples for electrophoretic separation on a polyacrylamide gel, tissues are lysed to release the proteins of interest and solubilized so they can migrate individually through the separating (polyacrylamide) gel. Triton X-100, a non-ionic detergent, can solubilize membrane proteins without affecting the protein's structural

features or antigenicity, enabling the protein to be isolated in its biologically active form<sup>102</sup>. Laemmli buffer, one of the most common loading buffers used in Western blot analysis, contains an anionic denaturing detergent, sodium dodecyl sulfate (SDS), which binds to proteins in a mass ratio of 1.4:1<sup>103</sup>. Thus, SDS confers a negative charge to the polypeptide in proportion to its length and the separation of the proteins in the sample is achieved when a voltage is applied across the gel. Since all the proteins are negatively charged, the rate of migration of the proteins in the gel towards the anode will depend solely on the mass of the protein. 2-mercaptoethanol in the buffer reduces the disulphide bridges in the proteins before they adopt the random-coil configuration necessary for separation by size. To monitor the migration of proteins in the gel, a small, anionic dye molecule (bromophenol blue) is added to the loading buffer which, owing to its small size, serves as visible moving boundary in the gel during electrophoresis<sup>104</sup>. A one-dimensional electrophoresis on polyacrylamide gel is used for the separation of proteins on the basis of their molecular sizes. When separated on a polyacrylamide gel, the procedure is abbreviated as SDS-PAGE (for sodium dodecyl sulfate polyacrylamide gel electrophoresis).

Following the separation of proteins in the gel, a wet transfer technique is commonly employed, in which the proteins in the gel are transferred to a nitrocellulose membrane. Here the negatively-charged proteins travel towards a positively-charged electrode, but their path is interrupted by a membrane where the protein binds<sup>105</sup>. The transferred proteins are probed (detected) using antibodies specific to the target protein. Antibodies typically recognize a small portion of the protein of interest, commonly referred to as the epitope, and this domain may reside within the 3D conformation of the

protein. To enable access of the antibody to this region, it is necessary to unfold the protein (denature) it. Comparison of the detected bands with bands of molecular weight marker will enable the determination of the protein size and identity <sup>102</sup>.

### *Immunohistochemistry*

Immunohistochemistry (IHC) is a routine diagnostic tool that combines anatomical, immunological and biochemical techniques to visualize the localization of more than one antigens in tissue sections by the use of labeled antibody. The detecting antibody may be conjugated to another compound, such as a fluorescent dye, enzyme, radioactive element or colloidal gold. Compared to Western blotting, the greatest advantage of IHC is that it gives the spatial location of the proteins in the cell/tissue of interest <sup>106</sup>. The two major steps involved in IHC are tissue preparation and staining. Tissue preparation is the cornerstone of immunohistochemistry. To ensure the preservation of tissue architecture and cell morphology, prompt and adequate fixation is essential. Tissues of interest must be rapidly isolated and preserved to prevent the breakdown of cellular protein. This is called the fixation step where the antigens are immobilize while retaining cellular and sub cellular structure. The most common fixative is formalin, a covalent cross-linking reagent that results in formation of methylene bridges that between proteins in the tissue samples.

Most tissues prepared for immunohistochemistry are formalin-fixed and embedded in paraffin blocks. Paraffin sections produce satisfactory results for the exposure of many tissue antigens using typical antigen retrieval techniques <sup>107</sup>. For antigens which do not survive routine fixation and paraffin embedding, frozen sections

are often successfully used. The disadvantage of frozen sections however, includes poor morphology and poor resolution at higher magnifications<sup>108</sup>.

In IHC, visualization is accomplished by either direct or indirect immunofluorescence. The direct method utilizes a primary antibody labeled with a marker (such as HRP, fluorescence), but this method is not as effective as the indirect method, since the signal is not amplified. The indirect method uses an unlabeled primary antibody against target antigen in the tissue and a labeled secondary antibody that will enable detection by reaction with the primary antibody. The secondary antibody is usually raised in animal by priming the animal with IgG from the host of primary antibody. A fluorescent label enables antigen detection and visualization using confocal microscopy<sup>109</sup>. Advantages of indirect immunofluorescence include greater sensitivity, since more than one secondary antibody can attach to each primary antibody and commercially produced secondary antibodies are relatively inexpensive and are available with a variety of fluorescent labels. One major drawback of indirect immunofluorescence is the potential for cross-reactivity and the need to find highly specific primary antibodies.

#### *Enzyme-linked immunosorbent assay (ELISA)*

ELISA utilizes antibodies as specific analytic reagents to quantify the amount of a protein in a sample. In this method, an enzyme horseradish peroxidase for example which reacts with a colorless substrate to produce a colored product, is covalently linked to a specific antibody (primary or secondary for direct or indirect ELISA, respectively) that recognizes a target protein/antigen. If the antigen/protein is present, the antibody-enzyme complex will bind to it, and the enzyme component of the antibody-enzyme complex will

catalyze the follow-up reaction generating a colored product. Thus, the presence of the colored product indicates the presence of the antigen. These assays, which are rapid and convenient, can detect less than a nanogram ( $10^{-9}$  g) of a protein <sup>110</sup>.

The indirect ELISA technique is used to detect the presence of antibody and is the basis of the test for HIV infection. In this type of ELISA, the proteins are absorbed to the bottom of a well. Primary antibodies are added to the protein-coated well and allowed to bind to the antigen/protein. Finally, an enzyme-linked antibody against the primary antibody is allowed to react in the well and the unbound primary antibodies are removed by washing. A substrate is then applied which reacts with the enzyme to produce a colored product <sup>111</sup>. Indirect ELISA has the distinct advantage over direct ELISA in that the same labeled secondary antibody can be used for detection of many primary antibodies from a single species.

### Materials

RT-PCR: Trizol<sup>®</sup> for RNA extraction and ethidium bromide for nucleotide detection in agarose gels were obtained from Life Technologies<sup>™</sup> (Carlsbad, CA). The oligonucleotide primers for *OCT1*, *OCT2*, *OCTN1* and *OCTN2* genes were designed using the NCBI primer designing tool, Primer-BLAST, using bovine mRNA sequences from the NCBI database. These primers and oligo DT (deoxy-thymine nucleotides) were synthesized by Integrated DNA Technologies Inc. (Coralville, IA). The PCR reaction was carried out on a Genius Technie PCR machine (Cambridge, UK). BlueJuice<sup>™</sup> Gel Loading Buffer (containing bromophenol blue), 100 base DNA ladder and the Superscript<sup>®</sup> III reverse transcriptase enzyme for cDNA synthesis were all obtained from Invitrogen (Carlsbad, CA). The dithioerythritol was obtained from Santa Cruz Biotech

Inc. (Santa Cruz, CA), agarose from RPI International Corp. (Mount Prospect, IL) and the TBE buffer 10X (tris-borate-EDTA buffer) was from Bio-Rad (Hercules, CA) All gel electrophoresis was carried out on an Owl EasyCast B2 Mini Gel from Thermo Scientific (Asheville, NC) where the voltage was applied using Foto Force250 from Fotodyne, Inc. (Hartland, WI). The transilluminator used to visualize the agarose gel was an AlphaImager® Gel Documentation system with AlphaImager (v5.5) software from Alpha Innotech Corporation (San Leandro, CA). The centrifuge used in the PCR experiments was a Spectrafuge™16M microcentrifuge from Labnet International (Woodbridge, NJ).

IHC (Immunohistochemistry): The primary antibody, rabbit anti-mouse OCTN2; Alexa Fluor 488-conjugated goat anti-rabbit IgG, were purchased from Alpha Diagnostic International Inc. (San Antonio, TX). TFM (tissue freezing media) was obtained from Triangle Biomedical Sciences (Durham, NC); the nuclear stain ToPro3 and DPBS (Dubeccos's phosphate buffered saline) was obtained from Life Technologies, Invitrogen (Carlsbad, CA); the mounting media, Vectashield®, was from Vector Laboratories (Burlingame, CA); the snap freezing system Gentle Jane®, was from Instrumedics Inc. (St Louis, MO); and the cryostat microtome (HM550E) was manufactured by Thermo Scientific (Kalamazoo, MI) and was available in the Central Microscopy Research Facility, University of Iowa (Iowa City, IA). A Bio-Rad MRC 1024 ((Hercules, CA) confocal laser scanning microscope was used to visualize the IHC-treated sections.

Western Blot, ELISA and BCA assay: The primary antibody for OCTN2 was the same as that for IHC. The rabbit anti-rat OCT2 antibody and the secondary antibody was an HRP-conjugated, goat anti-rabbit IgG was from Alpha Diagnostic International Inc.



(San Antonio, TX). The protease inhibitor cocktail P8340 was from Sigma Aldrich Chemical (St Louis, MO). The Mini-PROTEAN<sup>®</sup>3 system, the Mini Trans-Blot<sup>®</sup> electrophoretic transfer cell and BioRad Ready Gels (10% SDS polyacrylamide gel 10% TrisHCl; 50 $\mu$ L wells, 10 well comb) and nitrocellulose membrane (0.2 $\mu$ m, 7x8.4cm) for Western blot analysis were from Bio-Rad (Hercules, CA). MagicMark<sup>™</sup> XP Western protein standards (20-120kDa) and SeeBlue Plus2<sup>®</sup> pre-stained standard (1X) were from Life Technologies and Invitrogen (Carlsbad, CA), respectively. The Micro BCA Protein Assay Kit for total protein analysis, 96-well microtiter assay-plates (Immulon<sup>™</sup> 2HB) for ELISA assay and the enhanced chemiluminescence (ECL) kit were from Thermo Scientific (Rockford, IL). The transilluminator used for gel imaging was a BioDoc-It (UVP, LLC, Upland, CA). The LabQuake shaker was from Lab Industries Inc., (Berkeley, CA). The UV spectrophotometer used for BCA and ELISA assays was SpectraMax Plus<sup>384</sup> microplate reader from Molecular Devices, LLC (Sunnyvale, CA). The centrifuge used in protein extraction and separation experiments was an Eppendorf 5804R from Eppendorf AG (Hamburg, Germany).

All others chemicals including bovine serum albumin (BSA), Triton X-100, tetramethylbenzidine (TMB) tablets, phosphoric acid and buffers salts were from Sigma Aldrich, (St Louis, MO).

The formulas for all buffers used in the experiments are detailed in the Appendix.

### Experimental Methods

#### *Preparation of nasal tissues*

Excised bovine nasal mucosa was obtained from Bud's Custom Meats Co. (Riverside, IA). Nasal turbinate mucosa was retrieved by opening the nasal cavity along

the septal midline and removing the turbinates from the lateral wall. The ethmoturbinates, covered by the olfactory mucosa, and the maxilloturbinates, covered by the respiratory mucosa were harvested and carefully stripped from the underlying cartilage. These tissues were placed in zinc formalin for IHC studies. For PCR, Western blot and ELISA the nasal tissues were immediately frozen in liquid nitrogen and stored at  $-80^{\circ}\text{C}$  until use.

*RT-PCR (Reverse Transcriptase Polymerase Chain Reaction)*

RNA extraction

Frozen respiratory and olfactory tissues were placed in separate, sterilized centrifuge tubes and the tissues were weighed. To the tubes, 1 mL of Trizol<sup>®</sup> was added and the tissues were homogenized at  $4^{\circ}\text{C}$  using a previously sterilized surgical blade to release the nucleic acids. The homogenized sample was incubated at room temperature for 5 min to permit the complete dissociation of nucleoprotein complexes. The mixture was then centrifuged at  $12,000 \times g$  for 15 min (Spectrafuge<sup>™</sup>16M microcentrifuge) at room temperature after the addition of 0.2 mL of chloroform. The mixture separates into a lower red phenol- chloroform phase, an interphase, and a colorless, upper aqueous phase. The RNA remains exclusively in the aqueous phase.

The supernatant was collected from each tube. The RNA was precipitated from the supernatant by the addition of 0.5 mL isopropanol to each tube and was separated by centrifugation at  $12,000 \times g$  for 10 min (Spectrafuge<sup>™</sup>16M microcentrifuge) at room temperature. The isopropanol layer was discarded and the RNA pellet at the bottom of the tube was washed with 70% ethanol, air dried and reconstituted in 30  $\mu\text{L}$  of RNAase free water. Aliquots of RNA solution were used to perform spectral analysis and gel electrophoresis to assess the quality of the RNA extracted. The rest of the RNA stock

was stored at  $-80^{\circ}\text{C}$  until further use. Samples of RNA were extracted individually for both olfactory and respiratory tissues from six different cows.

The isolated RNA for RT-PCR was monitored for the presence of protein and other contaminants, integrity/degradation and the concentration of RNA was determined. Each sample of the olfactory and respiratory RNA (2  $\mu\text{L}$ ) was diluted 2x times with RNAase free water and the UV absorbance of the resulting solution was measured spectrophotometrically at both 260 nm and 280 nm to determine the sample concentration and purity. Additionally, gel electrophoresis was performed by loading a volume equivalent to 1  $\mu\text{g}$  RNA along with a loading dye (bromophenol blue), on a 1% agarose gel containing 0.01% ethidium bromide. The run was carried out at 50 mA until the dye had moved a sufficient distance into the gel. The gel was then removed and visualized using an AlphaImager<sup>®</sup> Gel Documentation system.

### Synthesis of cDNA

Complementary DNA (cDNA) was synthesized from the extracted RNA by reverse transcription in a PCR thermal cycler. A volume equivalent to 2.5  $\mu\text{g}$  of the RNA extracted in the previous step and 2.5  $\mu\text{M}$  of the oligodeoxythiamine nucleotide (oligo-dT) primer were mixed in a sterilized tube and placed in the PCR instrument for a single step program for 8 min at  $70^{\circ}\text{C}$  to denature the secondary structures of RNA. A negative control tube contained an equal amount of water in the place of RNA. The tubes were removed from the instrument and quenched on ice for 2 min and a reaction mixture containing 10 mM dithioerithritol, 50 mM Tris-HCl buffer (75 mM KCl and 3 mM  $\text{MgCl}_2$ , pH 8.3). SuperScript<sup>®</sup> III (200 IU/ $\mu\text{L}$ ) reverse transcriptase enzyme and 5 mM deoxynucleotide triphosphate (dNTP) was added to it such that the final volume was

50 $\mu$ L. The resulting mixture was mixed gently by pipetting and reloaded on the PCR instrument and incubated at 42° C for 90 min. The cDNA sample was diluted 5x with RNAase free water and stored at -20° C until further use. The cDNA quality was assessed using 1% agarose gel electrophoresis.

#### Expression of organic cation transporters in bovine nasal mucosa : RT-PCR

For the detection of rat OCT 1-2 and OCTN 1-2 genes by PCR, the primers located at different exons were selected from *Bos taurus* coding sequences (Table 3-1) (NCBI). A reaction mixture was prepared such that 20  $\mu$ L of the mix contained 2 units of *Taq* polymerase, 50  $\mu$ M dNTP and 20 mM Tris-HCl buffer (25 mM KCl and 2.5 mM MgCl<sub>2</sub>, pH 8.3). The reaction mix (20  $\mu$ L) was added to tubes containing 20 pmol each of the forward and reverse primer pair for the corresponding transporter of interest along with cDNA template for respiratory or olfactory mRNA. The tubes were placed in a Genius Techne PCR System and RT-PCR reactions were performed for 35 cycles at with annealing temperature of 55° C. The PCR program followed three steps per cycle: DNA denaturation at 95° C for 30 s which renders all of the DNA in the reaction to be single stranded; primer annealing at 55° C for 30 s, during which the PCR primers bind to their complementary target sequences; and polymer extension at 72° C for 30 s where the DNA polymerase is producing a complementary copy of the target DNA strand starting from the PCR primer sequence.

For optimal amplification of the specific products, the reaction conditions were optimized at 35 cycles with a magnesium concentration of 2.5 mM. The primer annealing temperature was selected based on the T<sub>m</sub> (melting temperature) of the primers. Once the

cycles were complete, the tubes were removed and the amplified PCR products corresponding to each gene under study were visualized using gel electrophoresis.

Electrophoresis of the PCR products containing BlueJuice™ (PCR product: BlueJuice™ ratio 2:1) was carried out on a 2% agarose gel stained with ethidium bromide. The bands corresponding to the separated PCR products were visualized using transilluminating UV light.

For optimal amplification of the specific products, the reaction conditions were optimized at 35 cycles with a magnesium concentration of 2.5 mM. The primer annealing temperature was selected based on the  $T_m$  (melting temperature) of the primers. Once the cycles were complete, the tubes were removed and the amplified PCR products corresponding to each gene under study were visualized using gel electrophoresis.

Electrophoresis of the PCR products containing BlueJuice™ (PCR product: BlueJuice™ ratio 2:1) was carried out on a 2% agarose gel stained with ethidium bromide. The bands corresponding to the separated PCR products were visualized using transilluminating UV light.

The dilution of the OCT and OCTN primers were as follows: for all primers that had a label claim less than 40 nM, 100  $\mu$ L of the forward primer was mixed with 100  $\mu$ L of the reverse primer. For the primers having a label claim greater than 40 nM, 50  $\mu$ L of the forward/reverse primer was mixed with 100  $\mu$ L of the reverse/forward primer (<40nM) and 50  $\mu$ L of RNase free water. The mixed primers were stored at  $-20^{\circ}\text{C}$  and the individual primer stock was stored at  $-4^{\circ}\text{C}$  until use.

Table 3-1: Base pair sequences of primers chosen for each of the organic cation transporter gene sequence used in the RT- PCR reaction.

| Gene                                | Primers   | Primer sequence (5'-3')      | T <sub>m</sub> (°C)<br>(annealing temperature) | Product size (bp) | Accession number |
|-------------------------------------|-----------|------------------------------|--|-------------------|------------------|
| <i>OCT1</i><br>( <i>SLC22A1</i> )   | Sense     | CCC CTC ATT CAT AGA CCT GTT  | 56.4   | 160               | NM_001101098     |
|                                     | Antisense | CAG AGC GGA GTA GAG GAA GTC' | 53.9   |                   |                  |
| <i>OCT2</i><br>( <i>SLC22A2</i> )   | Sense     | GGG AGA AGC AAA AAG TCT GTC  | 54.4   | 232               | XM_599284        |
|                                     | Antisense | GAG CTG ATG CTA GAT GTT CCA' | 53.8   |                   |                  |
| <i>OCTN 1</i><br>( <i>SLC22A4</i> ) | Sense     | CAT CAA CTG GGA GAT GTT CAC' | 54.2   | 201               | NM_001206989     |
|                                     | Antisense | CGC CAG TCT CTG ATG AAG TAA  | 53.4   |                   |                  |
| <i>OCTN 2</i><br>( <i>SLC22A5</i> ) | Sense     | TCC TGT CTC CCT ACT TCG TTT  | 53.6   | 197               | NM_001046502     |
|                                     | Antisense | TTC CTT TGA CCC TTA GCA TCT  | 55.2   |                   |                  |

Note: The primers were designed using the NCBI primer designing tool, Primer-BLAST, using bovine mRNA sequences from the NCBI database.

## *Western Blot*

### Extraction of membrane proteins

The respiratory and olfactory bovine nasal tissues were cut into pieces with dimensions 1 cm x 1 cm; the tissue pieces were weighed and homogenized individually in 250  $\mu$ L of lysis buffer containing protease inhibitors (~50  $\mu$ L) (300  $\mu$ L of lysis buffer for ~ 5 mg of tissue). The homogenate was further diluted with an additional 250  $\mu$ L of lysis buffer and maintained at constant agitation for 2 hr at 4° C. The protein extract was separated from the tissue debris by centrifuging the homogenate for 20 min at 12,000 x g at 4° C in a microcentrifuge (Eppendorf 5804R). The tubes were removed, placed on ice and supernatant was stored at -80° C until use.

### Estimation of total membrane protein content in bovine nasal mucosa: BCA assay

The total amount of membrane protein extracted from the olfactory and respiratory mucosa was separately analyzed using a BCA assay kit from Pierce. This colorimetric approach is based on the use of bicinchoninic acid (BCA) as the detection reagent for  $\text{Cu}^{+1}$ , where  $\text{Cu}^{+2}$  from the kit is reduced by proteins in an alkaline environment. Sequential dilutions of the protein samples (sample volume of 150  $\mu$ L) were performed in a 96 well plate followed by the addition of 150  $\mu$ L of a working solution (25 parts of reagent A, 24 parts of reagent B and 1 part of reagent C) to each well. A set of calibration standards were prepared similarly, using bovine serum albumin (BSA) in the concentration range 0 to 30  $\mu$ g/mL, where 0  $\mu$ g/mL served as the blank. The absorbance of both the samples and standards was measured at 562 nm after incubating at 37° C for 2 hr followed by cooling to room temperature.

### SDS-PAGE

Membrane proteins were separated by SDS-PAGE electrophoresis. Membrane protein extract volumes equivalent to 100 µg of proteins for each olfactory and respiratory tissue were diluted in a ratio of 1:1 with Laemmli buffer (2x) and heated at 90°C for 5 min. The protein samples were cooled on ice and 10 µL of SeeBlue Plus® prestained standard (1x) were added to each. The samples and a set of MagicMarker™ XP (molecular weight standards (20-220 kDa)) were loaded into the wells of a 10% SDS polyacrylamide gel (BioRad Ready Gels; 10% TrisHCl; 50 µL wells, 10 well comb) and electrophoresis was performed for 35 min at a starting current of 50 mA/gel at 200 V on a Mini-PROTEAN®3 system. Separated proteins were transferred to a nitrocellulose membrane overnight at 8 mA and 30 V and 4° C using a Mini Trans-Blot® electrophoretic transfer cell.

### Immunoblotting and protein detection

The nitrocellulose membranes were treated with a blocking solution (3% BSA) for 60 min to prevent non-specific antibody binding to the membrane. The membrane was then incubated with the primary antibody (rabbit anti-mouse OCTN2 at 1:1000 dilution in blocking solution) overnight at 4° C followed by 3 washings of 15 min each with washing buffer (0.05% Tween in PBS). This was followed by incubation with a secondary antibody (horseradish peroxidase-conjugated goat, anti-rabbit IgG, at 1: 10,000 dilution in blocking solution) for 2 hr at room temperature. The immunoreactive bands were washed with the wash buffer and developed using an enhanced chemiluminescence (ECL) kit. Treated membranes were imaged using a BioDoc-It transilluminator. The protein of interest was observed as bands and the molecular weight of the observed



protein was compared to the MagicMark MW standards. Normal goat serum (10%) was used as the blocking agent.

### *Immunohistochemistry*

The tissues were placed in zinc formalin at room temperature on a LabQuake shaker for 24 hr. The tissues were then placed sequentially in 10%, 20% and 30% sucrose solutions until each tissue was completely saturated with sucrose. The tissues were cryopreserved using a Gentle Jane® snap freezing system in tissue freezing medium (TFM). Sections (10 µm) were cut from the frozen tissues using a HM50E cryostat microtome at -23° C. The sections were transferred to a slide and stored at -20° C until use. Ten sections of each olfactory and respiratory tissue were prepared.

For epitope retrieval, the sections were fixed with zinc formalin for 10 min at 4° C and washed with PBS to remove excess formalin. The sections were treated with a blocking solution (10% normal goat serum in PBS) for 20 min followed by incubation with the primary antibody solution of rabbit, anti-mouse OCTN2-IgG at 1:1000 dilution in PBS overnight at 4° C. (The dilution of the primary antibody was optimized following titrations using 1:250, 1:500, 1:1000 and 1:2000 dilutions). The slides were washed with PBS and incubated with a secondary antibody (Alexa Fluor-488 conjugated goat, anti-rabbit IgG at 1:10,000 dilution) for 30 min at room temperature. ToPro3 (nuclear stain) was used as the counterstain and Vectashield® as the mounting medium. The sections were examined using a Bio-Rad MRC1024 confocal laser scanning microscope. Sections processed in an identical manner without incubation with the primary antibody were used as the negative control.

### *ELISA*

Membrane proteins from the nasal tissues were extracted using Triton X-100 according to using the same procedure described for western blotting. Microtiter assay plates were coated with 100 $\mu$ L of sequential dilutions (1/100, 1/200, 1/400, 1/800, 1/1600 and 1/3200) of both olfactory and respiratory tissue protein extracts and were incubated overnight at 4° C in a refrigerator. Plates were washed with PBST (PBS buffer containing 0.05% Tween 20) and the wells were blocked with 400  $\mu$ L of PBS buffer containing 3% bovine serum albumin (BSA) for 2 hr, followed by four washes of PBST. Primary antibody, 100  $\mu$ L of rabbit, anti-mouse OCTN2 (rabbit anti-rat OCT2 antibody for OCT2 ELISA) at 1:5000 dilution was added to each well and incubated overnight at 4° C. The plates were washed four times with PBST and then a secondary antibody, 100 $\mu$ L of goat anti-rabbit IgG linked to HRP (1:50,000 dilution) was added to the wells and the plates were covered and incubated for 1 hr at room temperature away from direct light. After washing four times in PBST, TMB solution (tetramethylbenzidine and hydrogen peroxide in phosphate citrate buffer), an HRP substrate was added and the plates were incubated without shaking for 30 min in the dark. The reaction is stopped by the addition of stop solution, which was 50  $\mu$ L of 1M phosphoric acid and the absorbance at 450 nm was recorded within 5 min. The assays conducted were performed in duplicate and the average of the absorbance at 450 nm of duplicate wells at the same protein sample dilution for the olfactory and respiratory were plotted against the type of tissue protein sample on the same graphs with 3% BSA and empty wells serving as negative control and blank, respectively.

## Results and Discussion

### *Quality of RNA and cDNA*

Both gel electrophoresis and spectrophotometric analysis confirmed the good quality of the extracted RNA (Table 3-2).

The average ratio of the intensity of absorbance of the RNA samples at wavelengths 260 nm and 280 nm was above 1.6 for both olfactory and respiratory samples, and the corresponding concentrations of RNA stock solution were calculated by multiplying the absorbance values at 260 nm by a factor of 10 (Table 3-2) and was determined to be 1.2  $\mu\text{g}/\mu\text{L}$  for both of the respiratory and olfactory samples. Thus, it was concluded that the extracted RNA samples were sufficiently pure and free of contamination. Results from gel electrophoresis confirmed the purity of the RNA samples (Figure 3-1). Gel electrophoresis of the cDNA synthesized from the extracted RNA also showed good quality (Figure 3-2)

Table 3-2: Absorbance results of RNA samples extracted from respiratory and olfactory mucosal explants.

| <b>Sample</b> | <b>260 nm</b> | <b>280 nm</b> | <b>Ratio (260 nm/280 nm)</b> | <b>RNA conc in <math>\mu\text{g}/\mu\text{L}</math></b> |
|---------------|---------------|---------------|------------------------------|---|
| Respiratory   | 0.123         | 0.074         | 1.667                        | 1.226   |
| Respiratory   | 0.123         | 0.074         | 1.659                        | 1.233   |
| Olfactory     | 0.124         | 0.075         | 1.653                        | 1.237   |
| Olfactory     | 0.124         | 0.075         | 1.647                        | 1.237   |

Note: RNA concentration ( $\mu\text{g}/\mu\text{L}$ ) was calculated by multiplying the absorbance values at 260 nm by a factor of 10<sup>100</sup>.

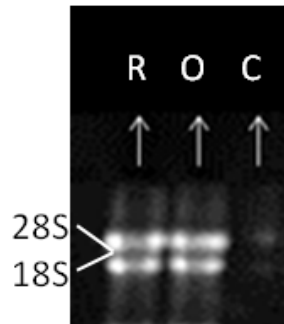


Figure 3-1: 1% agarose gel electrophoresis of extracted RNA samples (1  $\mu$ g RNA per lane) visualized using transilluminating UV light. Each lane represents RNA extracted from separate tissues. R= respiratory tissue, O= olfactory tissue and C= negative control (water), respectively. Results show 28S and 18S RNA subunits, approximately 5 kb and 2 kb in size (ladder not shown) with a 28S:18S ratio of  $\sim$ 2:1, indicating intact RNA

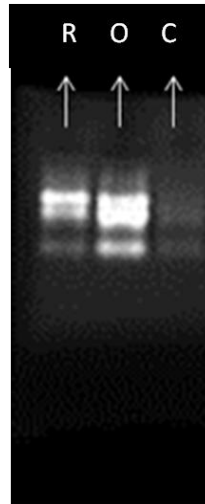


Figure 3-2: 1% agarose gel electrophoresis of cDNA samples visualized using transilluminating UV light. Lanes represent cDNA synthesized from separate tissues. R= respiratory RNA, O= olfactory RNA and C= negative control (water), respectively. The cDNA appears as a broad band or smear between 0.1–4 kb (ladder not shown).

*Optimization of Mg<sup>2+</sup> concentration and number of cycles for RT-PCR*

A series of RT-PCR reactions were carried using Mg<sup>2+</sup> concentrations of 1.5 or 2 mM at amplification cycles of 25 and 35 with primers corresponding to genes for *OCT1*, *OCT2*, *OCTN1* or *OCTN2* (Table 3-1). The optimum conditions were identified based on the conditions resulting in the highest yield of the specific PCR product and were carried out using cDNA synthesized from olfactory RNA.

The 2% gel electrophoresis showed no visible band at low Mg<sup>2+</sup> concentration (1.5 mM) at either 25 and 35 amplification cycles for any of the genes studied (Figure 3-3 and Table 3-3). As the Mg<sup>2+</sup> ion concentration was increased to 2.5 mM, bands were observed for *OCT2*, *OCTN1* and *OCTN2* genes at both 25 and 35 cycles of amplification. Even more intense bands were observed at the higher amplification cycle.

The *OCT1* gene did not show any visible bands at any of the conditions studied. Therefore, the optimum Mg<sup>2+</sup> ion concentrations and amplification cycles required for the given PCR reaction were determined to be 2.5 mM and 35 cycles. The samples containing no cDNA, (negative controls: E1, F1, G1 and H1) showed no bands, indicating the absence of contamination.

The RT-PCR results showed expression of mRNAs corresponding to the organic cation transporter genes *OCT2*, *OCTN1* and *OCTN2* in both bovine respiratory and olfactory mucosa. However, the absence of a PCR product band corresponding to *OCT1* gene suggests its absence or low expression levels in bovine nasal tissue. (Figure 3-4). These results are consistent with the studies by other researchers who have shown expression of the organic cation transporters in human and rodent nasal tissues (Table 1-2). However, *in vitro* transport studies conducted in the bovine nasal tissues

showed that OCT2 and OCTN2 played a key role in the transport of amantadine and OCT2 in cimetidine transport across the nasal tissues (Chapter 5). Since the OCT2 expression in bovine nasal tissues has already been characterized, additional characterization of the organic cation transporters in the bovine respiratory and olfactory tissues using ELISA was restricted to OCT2 and OCTN2 and Western blotting and IHC to the study of OCTN2.

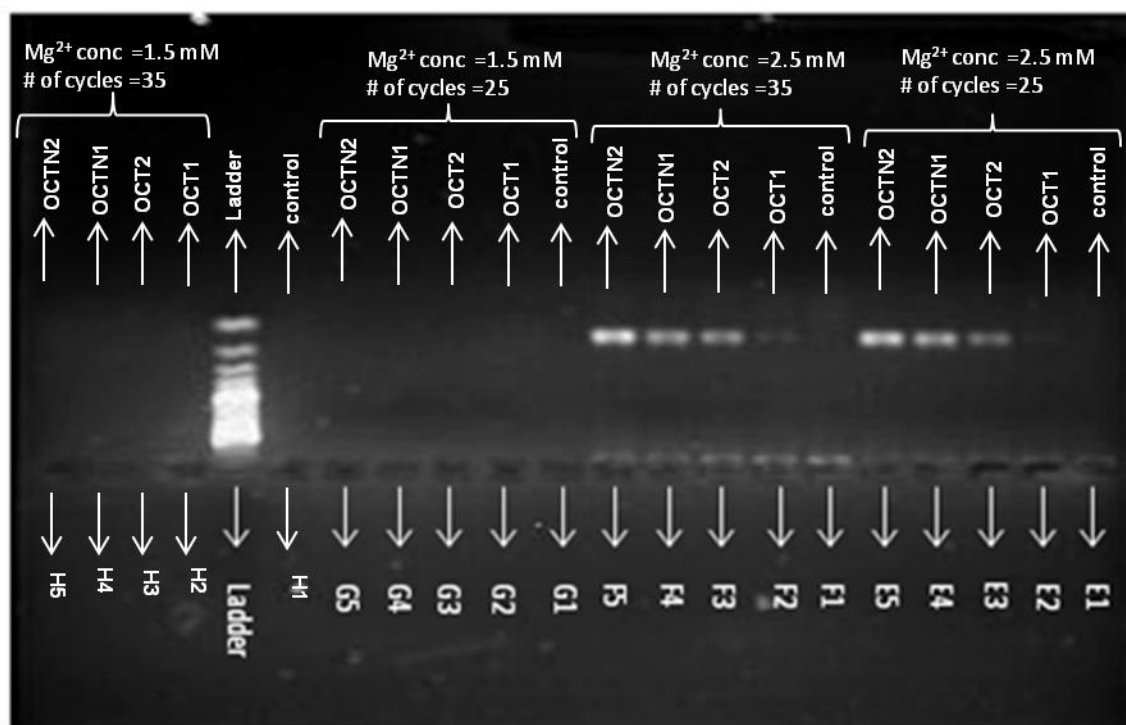


Figure 3-3: Results of 2% agarose gel electrophoresis of PCR products showing the effect of different Mg<sup>2+</sup> concentrations and number of amplification cycles on DNA amplification. All reactions were done using cDNA synthesized from olfactory RNA. Lane descriptions correspond to conditions given in Table 3-3. All samples were from a single cow.

Table 3-3: Comparison of  $Mg^{2+}$  concentrations and amplification cycle titrations for PCR method optimization.

| Sample name | Gene         | $Mg^{2+}$ | Cycles |
|-------------|--------------|-----------|--------|
|             |              | Conc (mM) |        |
| E1          | control      | 2.5       | 25     |
| E2          | <i>OCT1</i>  | 2.5       | 25     |
| E3          | <i>OCT2</i>  | 2.5       | 25     |
| E4          | <i>OCTN1</i> | 2.5       | 25     |
| E5          | <i>OCTN2</i> | 2.5       | 25     |
| F1          | control      | 2.5       | 35     |
| F2          | <i>OCT1</i>  | 2.5       | 35     |
| F3          | <i>OCT2</i>  | 2.5       | 35     |
| F4          | <i>OCTN1</i> | 2.5       | 35     |
| F5          | <i>OCTN2</i> | 2.5       | 35     |
| G1          | control      | 1.5       | 25     |
| G2          | <i>OCT1</i>  | 1.5       | 25     |
| G3          | <i>OCT2</i>  | 1.5       | 25     |
| G4          | <i>OCTN1</i> | 1.5       | 25     |
| G5          | <i>OCTN2</i> | 1.5       | 25     |
| H1          | control      | 1.5       | 35     |
| H2          | <i>OCT1</i>  | 1.5       | 35     |
| H3          | <i>OCT2</i>  | 1.5       | 35     |
| H4          | <i>OCTN1</i> | 1.5       | 35     |
| H5          | <i>OCTN2</i> | 1.5       | 35     |

Note: Samples E1, F1, G1 and H1 represent negative controls, where the RT-PCR was carried out without the cDNA.

All samples were from a single cow.

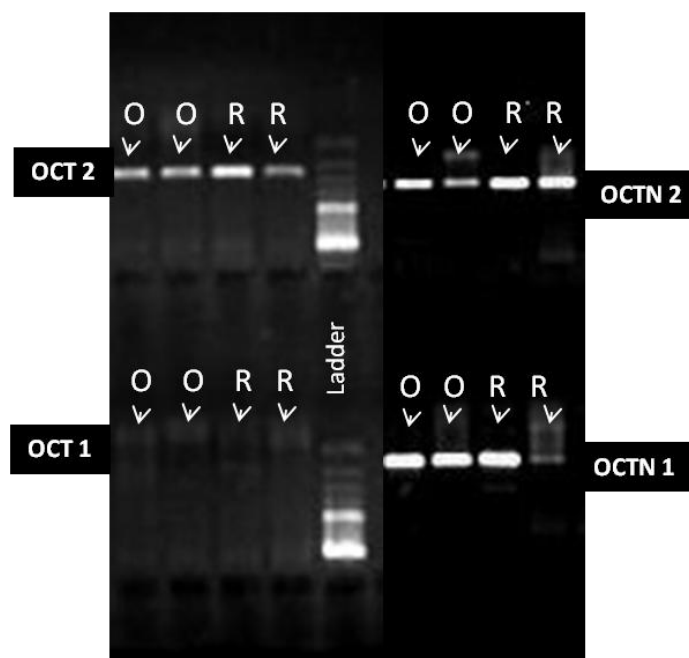


Figure 3-4: 2% agarose gel electrophoresis of RT-PCR products showing the expression of mRNAs corresponding to the organic cation transporters *OCT2*, *OCTN1* and *OCTN2* in both bovine R= respiratory and O= olfactory mucosal explants. PCR product bands corresponding to *OCT1* gene are absent. Reaction conditions: 35 amplification cycles,  $Mg^{2+}$  concentration = 2.5 mM and an annealing temperature of 55° C. Each olfactory/respiratory sample represents mRNA extracted from separate cow.



### *BCA assay result*

The total amount of membrane proteins in the respiratory and/or olfactory tissues was calculated from a calibration curve using BSA standards (Figure 3-5). The results are expressed as milligrams of protein in 500  $\mu\text{L}$  of the protein extract of each tissue which is equivalent to the amount in a  $1\text{ cm}^2$  of bovine tissue (Figure 3-6). The total amount of membrane protein was found to be significantly higher in the respiratory tissue than in the olfactory tissue ( $p < 0.05$ ).

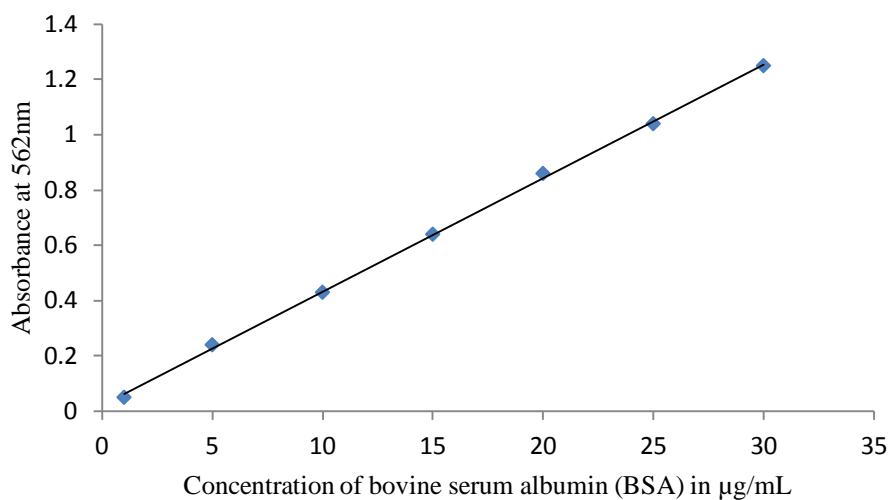


Figure 3-5: Standard curve for bovine serum albumin (BSA) in BCA assay for proteins. UV absorbance was measured at a wavelength of 562 nm and the linear range tested for quantification was 1–30  $\mu\text{g/mL}$ . Linear regression of the results gave the equation  $y = 0.0411x + 0.0223$ ,  $r^2 = 0.999$ .

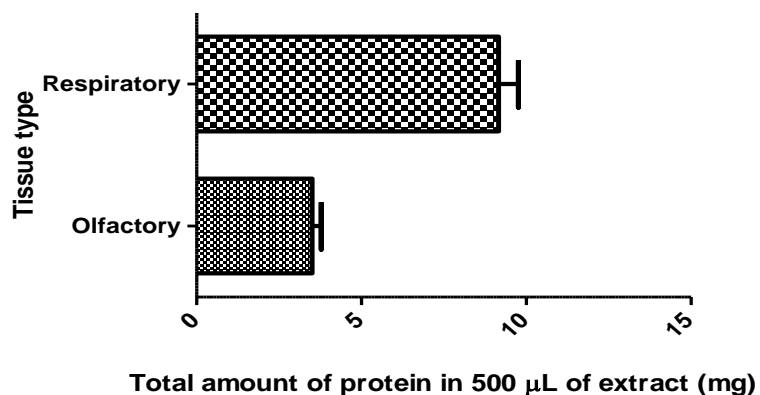


Figure 3-6: The amount of total membrane proteins extracted from a 1 cm<sup>2</sup> area of bovine respiratory and olfactory tissue using Triton X-100. The protein concentrations were calculated using the BCA assay. Results represent mean  $\pm$  standard deviation (n=3). Statistically significant differences were observed in the amount of proteins extracted from the respiratory and olfactory tissues (Student's t-test,  $p < 0.05$ ).

### *Western blot*

Previous Western blot studies in our lab have shown the presence of OCT2 transporter proteins in the bovine olfactory and respiratory mucosa<sup>28</sup>. Since bovine OCTN2 antibody was not commercially available, a rabbit anti-mouse primary antibody was used for immunoblotting. This was attempted since there is significant amino acid sequence homology for OCTN2 amongst species (~90%)<sup>112</sup>. The presence of the OCTN2 transporter protein in both the respiratory and olfactory mucosa was confirmed by the presence of a band between molecular weights of 60-70 kDa (Figure 3-7). This result is in agreement with the reported molecular weight of human OCTN2 (62.7 kDa)<sup>113</sup>. Additionally, the low background and absence of additional bands indicated that the primary antibody was specific only to OCTN2 protein. Additionally, the negative control, bovine serum albumin did not show any luminescent signal indicating absence of primary antibody binding to bovine protein. This strongly suggests that the observed band corresponds to OCTN2 presence in the nasal mucosa.

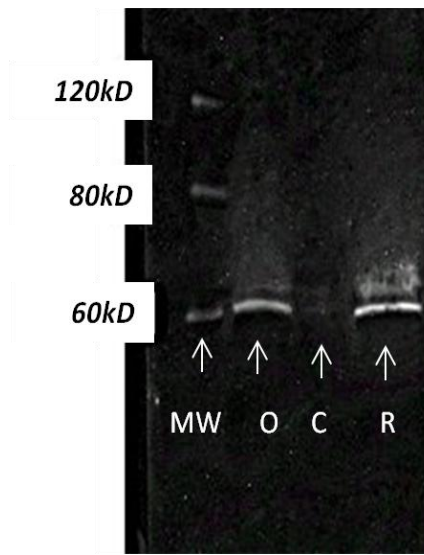


Figure 3-7: Western blot for OCTN2 expression in bovine olfactory and respiratory mucosa. Membrane proteins were extracted from olfactory and respiratory tissues using Triton X-100 and separated on polyacrylamide gels. The proteins were treated with rabbit anti-mouse OCTN2 antibody and detected using HRP conjugated goat anti-rabbit IgG secondary antibody. Bovine serum albumin was used as the negative control. Lanes represent MW= Magic Mark<sup>TM</sup> molecular weight protein standard, O= Olfactory, C= Negative control (BSA) and R = Respiratory.

### *Immunohistochemistry*

Localization of the OCTN2 transporters in the bovine respiratory and olfactory tissue explants was determined using immunohistochemistry. Positive immunoreactivity for OCTN2 protein is indicated by green fluorescence from the Alexa fluor 488-labeled secondary antibody, which has visible light excitation (495 nm) and emission (519 nm), a high quantum yield and good photostability. TroPro3 was used to counterstain the nucleus and appears as red fluorescence in the images. Significant OCTN2 expression (green fluorescence in the micrographs) was observed in the epithelial cells of both the respiratory and olfactory mucosa, compared to the negative control (Figure 3-8, 3-9). The green fluorescence appears to be present throughout the epithelial layer and suggests OCTN2 localization at both the apical and basolateral surfaces of the epithelium for both tissues. Both the olfactory and the respiratory tissues have submucosal regions rich in nasal glands and blood vessels. The submucosal region also shows positive staining for OCTN2, especially in the endothelium of the blood vessels (Figure 3-10) in the respiratory tissues. Virtually no OCTN2 signal was observed in the vasculature of the olfactory tissue, however.

The non-specific binding of the Fc fragments of the primary antibody is of concern in immunohistochemistry. Negative controls using rabbit IgG instead of the primary antibody demonstrated that the F<sub>C</sub> regions of the rabbit antibody do not bind to Fc receptors in the bovine olfactory or respiratory tissue<sup>28</sup>. Additionally, it has been shown that Fc receptors do not retain the ability to bind the Fc portion of IgG antibody for cryosections obtained from many tissues, including cow tissues fixed with formalin, as was used in our study<sup>114</sup>. In view of these reports, simple negative controls were

employed where bovine mucosal samples were prepared in the same manner but without incubation with the primary antibody. The results from the negative control demonstrate the absence of any non-specific binding by the secondary antibody (Figure 3-8, 3-9, 3-10)

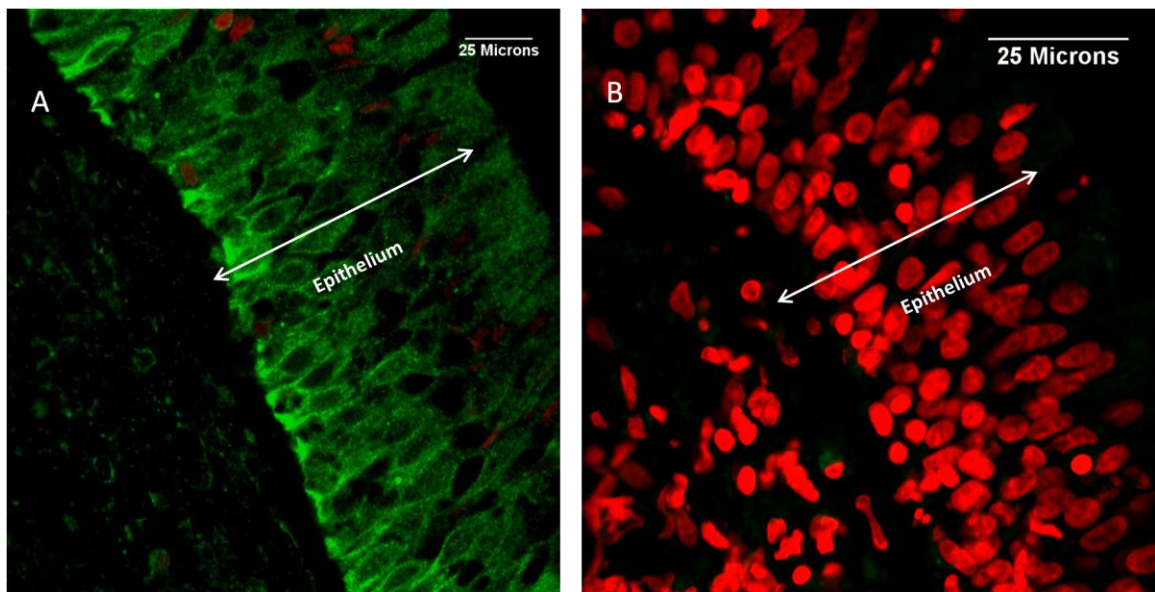


Figure 3-8: Immunohistochemical staining of OCTN2 in bovine respiratory mucosa. Immunoreactivity is indicated by green fluorescence in the micrographs and is observed in the pseudostratified columnar epithelium. The nucleus is labeled by TroPro3 and gives a red fluorescence. Scale bar is 25  $\mu\text{m}$  and section thickness is 10  $\mu\text{m}$ . (A) Respiratory tissue specimen incubated with rabbit polyclonal, anti-mouse OCTN2 (1:1000 dilution) primary antibody compared to (B) negative control without the primary antibody.

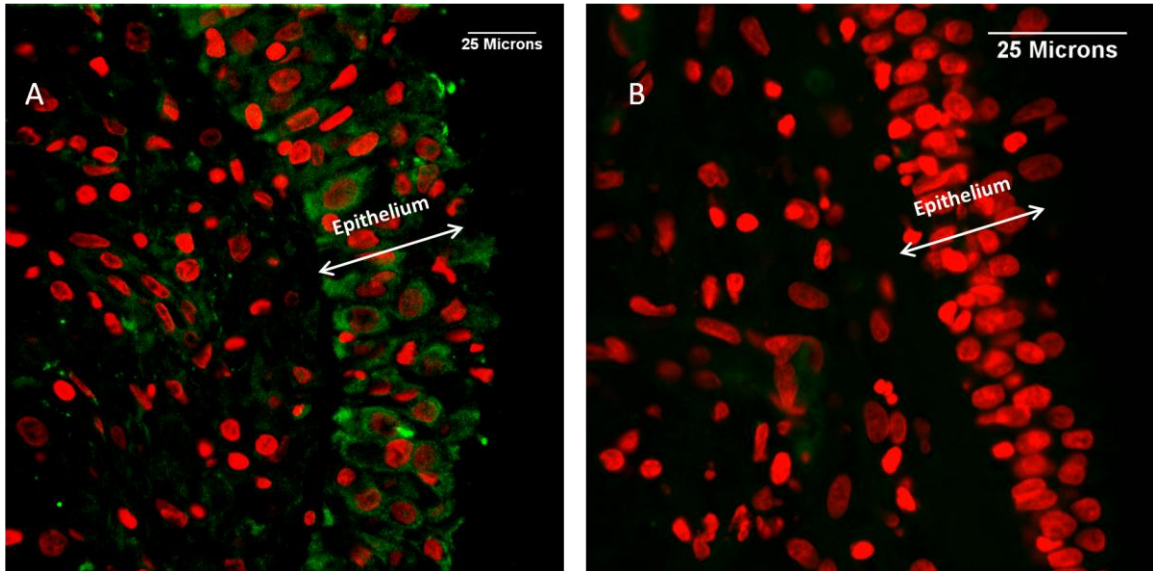


Figure 3-9: Immunohistochemical staining of OCTN 2 in bovine olfactory mucosa. Immunoreactivity is indicated by green fluorescence in the micrographs and is observed in the pseudostratified columnar epithelium. The nucleus is labeled by TroPro3 and gives a red fluorescence. Scale bar is 25  $\mu\text{m}$  and section thickness is 10  $\mu\text{m}$ . (A) Olfactory tissue specimen incubated with rabbit polyclonal, anti-mouse OCTN2 (1:1000 dilution) primary antibody compared to (B) negative control without the primary antibody.

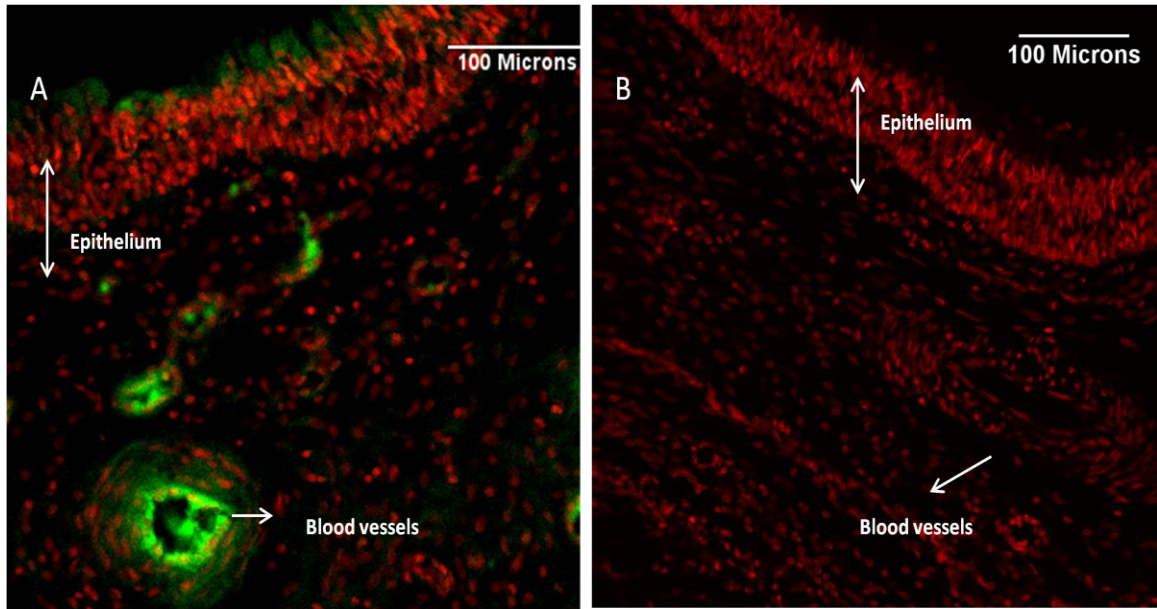


Figure 3-10: Immunohistochemical staining of OCTN2 in bovine respiratory mucosa. Immunoreactivity is indicated by green fluorescence in the micrographs and is observed in the pseudostratified columnar epithelium and the blood vessels. The nucleus is labeled by TroPro3 and gives a red fluorescence. Scale bar is 100  $\mu\text{m}$  and section thickness is 10  $\mu\text{m}$ . (A) Respiratory tissue specimen incubated with rabbit polyclonal, anti-mouse OCTN2 (1:1000 dilution) primary antibody compared to (B) negative control without the primary antibody.



### *ELISA*

A quantitative analysis of membrane proteins is not possible using Western blot, therefore, a classical indirect ELISA was successfully adapted for this purpose<sup>115</sup>. Two specific antibodies, a capture (primary) antibody (rabbit anti-mouse OCTN2 or rabbit anti-rat OCT2) and a detector (secondary) antibody (HRP conjugated goat, anti-rabbit IgG), were used to measure the relative expression of OCT2 and OCTN2 proteins in the respiratory and olfactory mucosa. Because proteins may lose antigenicity or aggregate when frozen and stored as Triton X-100 extracts, the solubilization for the studies was performed immediately before the ELISA assay.

Protein extracts probed with OCT2 antibody showed that the expression of this transporter was higher in the olfactory than the respiratory tissue (Figure 3-11). This difference is of significance since the total amount of membrane proteins in the respiratory tissue sample was 2.5 times the amount in the olfactory tissue sample, as estimated by the BCA assay (Figure 3-6). In comparison, the expression of OCTN2 was higher in the respiratory than the olfactory tissue (Figure 3-12).

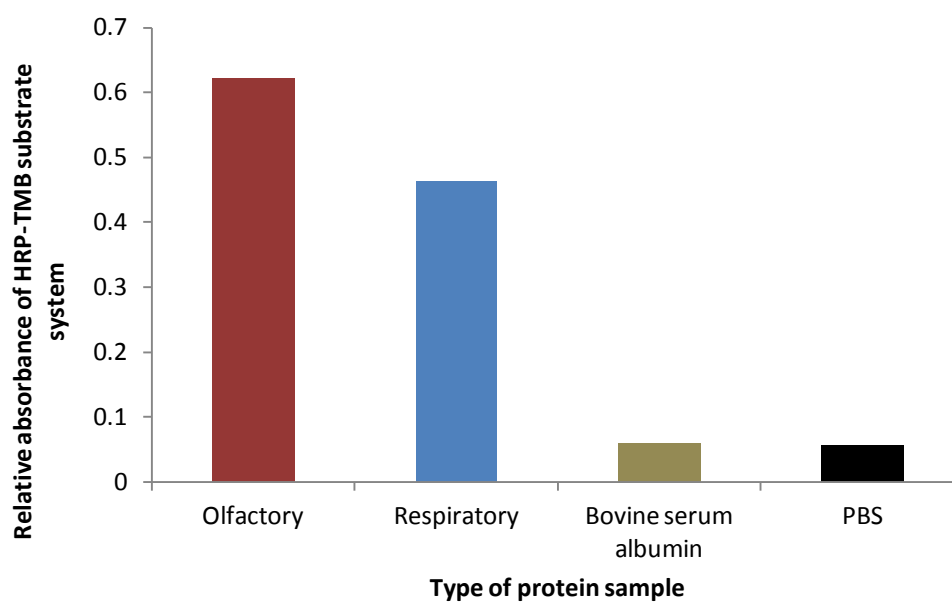


Figure 3-11: Relative expression of OCT2 transporter protein in the olfactory and respiratory tissues as indicated by the absorbance of HRP-TMB complex at 450 nm (n=2). The primary antibody was a 1:5000 dilution of rabbit anti-rat OCT2 and the secondary antibody was an Fc fragment-specific HRP conjugated goat anti-rabbit IgG at 1:50,000 dilution. BSA was used for the negative control and PBS served as the blank (n=2).

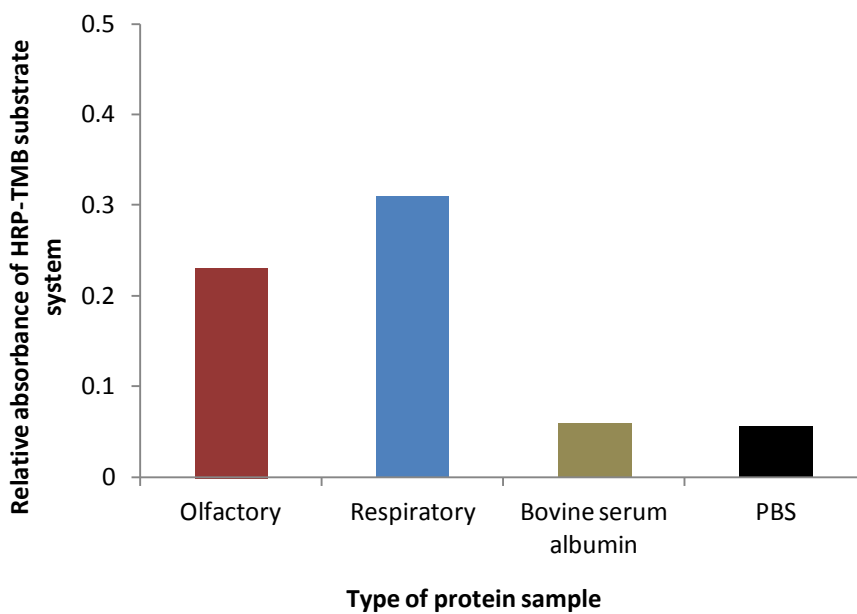


Figure 3-12: Relative expression of OCTN2 transporter protein in the olfactory and respiratory tissues as indicated by the absorbance of HRP-TMB complex at 450 nm (n=2). The primary antibody was a 1:5000 dilution of rabbit, anti-rat OCTN2 and the secondary antibody was an Fc fragment-specific HRP conjugated goat anti-rabbit IgG at 1:50,000 dilution. BSA was used as the negative control and PBS served for the blank.

### Conclusion

RT-PCR demonstrated the presence of *OCT2*, *OCTN1* and *OCTN2* genes in both bovine olfactory and respiratory tissues. Previous results from Western blotting had showed the presence of OCT2, and Western blot analysis in the current studies also indicated that OCTN2 proteins were expressed in the nasal tissues. It has been previously demonstrated that OCT2 was localized in both the epithelia and the submucosal regions of the olfactory and respiratory tissues<sup>28</sup>. Immunohistochemistry studies showed that the OCTN2 transporters are localized in the epithelial layer for both olfactory and respiratory tissues. Additionally, the OCTN2 transporter was also observed to be localized in the blood vessel endothelium in the respiratory tissues, suggesting that these transporters may have a role in the systemic absorption of substrates when administered intranasally. An evaluation of the relative expression of OCT2 and OCTN2 using ELISA revealed that OCTN2 was present in almost equal levels in the respiratory and olfactory tissues whereas, OCT2 expression was significantly higher in the olfactory tissues.

Previous investigators have reported similar qualitative expression of these transporters in the human and rodent respiratory and olfactory epithelium<sup>75,74</sup>. The similarity observed in the expression of *OCT2*, *OCTN1* and *OCTN2* genes in the bovine and human nasal tissues supports the use of bovine nasal explants as an *in vitro* model to study the role of these transporters enhanced nose to brain of uptake of organic cations for human drug therapy.

## CHAPTER 4

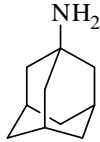
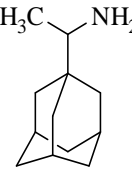
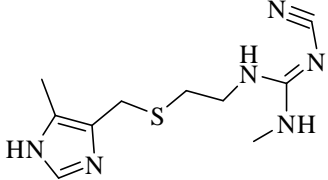
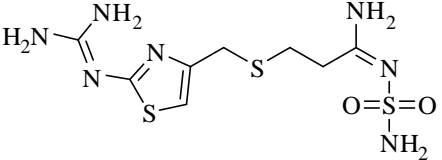
### QUANTITATIVE MEASUREMENT OF OCT SUBSTRATES USING LCMS IN BIOLOGICAL BUFFER(S) AND PLASMA

Selective and sensitive analytical methods for the quantitative evaluation of drugs are critical for the successful conduct of preclinical, biopharmaceutical and clinical studies. Bioanalytical method validation includes procedures that demonstrate that a particular method used for quantitative measurement of analytes in a given matrix is reliable and reproducible for the intended use. The fundamental parameters for this validation include accuracy, precision, selectivity, sensitivity and reproducibility. Published methods of analysis are often modified and validated to ensure suitable performance of the analytical method.

#### *Amantadine*

Amantadine is an amino-adamantane derivative that does not possess a UV chromophore, fluorescence properties or electroactive groups. Therefore, previously reported analytical methods required sample pre-treatment and chemical derivatization to achieve the desired analytical sensitivity. All these methods are associated with drawbacks including being labor-intensive with time-consuming sample preparation, the potential for incomplete derivatization, or the requirement of large volumes of plasma. Literature reports regarding the extraction and determination of amantadine from plasma using LCMS are not widespread; the only current LCMS method reported in human plasma involves sample preparation via liquid-liquid extraction (LLE). LLE decreases the mean recovery/extraction efficiency (~70%), since amantadine hydrochloride is highly water soluble and complete extraction is not easily accomplished.

Table 4-1: Chemical structure and physical properties of the analytes amantadine and cimetidine and their internal standards, rimantadine and famotidine, respectively<sup>116117118</sup>.

| Analyte or Internal standard | MW (g/mol) | pKa  | Solubility (mg/mL) | Structure   |
|------------------------------|------------|------|--------------------|---|
| Amantadine                   | 151.25     | 9.0  | ~50 (HCl salt)     |    |
| Rimantadine                  | 179.30     | 10.4 | ~50 (HCl salt)     |   |
| Cimetidine                   | 252.34     | 6.8  | 6                  |  |
| Famotidine                   | 337.43     | 6.8  | 0.67               |   |

The aim of this study was to develop a simple LCMS method for the analysis of amantadine in biologic buffer and rat plasma with faster extraction time for routine analysis, improved quantification and potential automation.

### *Cimetidine*

Several HPLC and a few LCMS methods for the determination of cimetidine in human plasma and urine have been reported<sup>119120121122123</sup>. Most methods utilized liquid-phase extraction techniques. Limitations of these methods include the requirement to extract large volumes of plasma (0.5–1.0 ml), low or inconsistent recovery in plasma and the use of an internal standard that may be not commercially available. The LCMS method developed for amantadine was modified and adapted for the assay of cimetidine in aECF (artificial extracellular fluid) and rat plasma. A validated HPLC method reported in the literature was adapted and validated for determining cimetidine concentrations in KRB buffer samples<sup>124</sup>.

### Materials

Amantadine hydrochloride, rimantadine hydrochloride, cimetidine, famotidine, analytical grade ammonium hydroxide and 0.1 N HCl were purchased from Sigma-Aldrich, (St Louis, MO). Optima HPLC grade methanol was obtained from Fisher Scientific (Fair Lawn, NJ). Deionized water was obtained from a Milli-Q<sup>®</sup> UV Plus system from Millipore (Billerica, MA). Oasis<sup>®</sup> MCX, 1cc (30 µm particle size) extraction cartridges were purchased from Waters (Milford, MA) and was used with a Cerex SPE processor (Varian) for SPE (solid phase extraction). Rat plasma (Sprague Dawley with sodium heparin as the anticoagulant) used in method validation was from Innovative Research (Novi, MI). All chemicals used in the preparation of aECF (artificial extra

cellular fluid) and KRB (Kreb's Ringer Buffer) were from Sigma Aldrich (St Louis, MO). The centrifuge used was an Eppendorf 5415D centrifuge (Eppendorf AG, Hamburg, Germany) and the concentration of the samples was carried out on a TurboVap<sup>®</sup> nitrogen evaporator (Zymark Corporation, Westborough, MA).

### Methods

A LCMS analytical method was developed and validated for amantadine using rimantadine as the internal standard. This method was modified and adapted for cimetidine analysis in rat plasma and artificial extracellular fluid (aECF), using famotidine as the internal standard. An HPLC-UV method from the literature was modified and was used in for analysis of cimetidine in KRB buffer <sup>124</sup>.

#### *Stock solutions and working standard*

Primary stock solutions of amantadine and cimetidine for the preparation of working standards and quality control (QC) samples were made from separate weighing. The primary stock solution of both analytes was prepared in methanol at a concentration of 10 µg/mL. Working standard solutions were prepared by appropriate dilution of the stock with methanol and spiking the corresponding matrix (KRB, aECF or rat plasma) to obtain concentrations shown in Table 4-2. The high medium and low quality control standards used for the evaluation of recovery and matrix effects were prepared daily by spiking the appropriate matrix to produce concentrations equivalent to 1000 (high), 400 (medium) and 25 (low) ng/mL for amantadine and 800 (high), 200 (medium) and 10 (low) ng/mL for cimetidine.

The working internal standard (IS) solutions for rimantadine hydrochloride and famotidine in methanol were 1 µg/mL and 2 µg/mL, respectively.



Table 4-2: Working standard solutions of each analyte (amantadine or cimetidine) obtained by spiking each matrix (KRB, aECF or rat plasma) with an appropriate dilution of the primary stock solution

| Matrix     | Working standard concentration (ng/mL)   |   |
|------------|--|---|
|            | Amantadine                               | Cimetidine                              |
| KRB        | 2, 8, 40, 100, 200, 400, 1000, 2000      | 500, 1000, 5000, 10,000, 20,000, 50,000 |
| rat plasma | 10, 25, 50, 100, 200, 500, 1000, 2000    | 5, 25, 75, 150, 312.5, 625, 1250        |
| aECF       | 5, 10, 20, 50, 100, 200, 500, 1000, 2000 | 1.562, 3.125, 12.5, 25, 100, 400, 800   |

#### *Sample Preparation for amantadine*

To each of the standards/samples, (200  $\mu$ L of KRB standards, 100  $\mu$ L of aECF standards or 100  $\mu$ L rat plasma), 400  $\mu$ L of methanol and 20  $\mu$ L of working IS solution (rimantadine in methanol) was added such that all samples contained 200 ng/mL of the internal standard. This was followed by the addition of 50  $\mu$ L of 0.1N HCl to keep the amantadine in the protonated form. The resulting samples were vortex-mixed and subjected to solid phase extraction (SPE) prior to LCMS analysis. For plasma standards/samples an extra centrifugation step was carried out after the vortexing step, at 16100 x g for 1 min, after which the supernatant was collected and used for SPE. Oasis MCX 30  $\mu$ m cartridges and a Cerex SPE processor were used for SPE. The cartridges were conditioned with 1 ml methanol followed by 1 mL water. The samples were loaded into the cartridges after the conditioning step, followed by two washing steps, the first with 1mL of 0.1N HCl and the second with 1 mL of methanol, 1mL each, respectively. Finally the analytes were eluted with 6% v/v NH<sub>4</sub>OH in methanol. The eluate was dried using a TurboVap<sup>®</sup> nitrogen evaporator at 35 °C for 30 min and the residue was reconstituted in 100  $\mu$ L of methanol-water (80:20 v/v) and transferred to an autosampler

vial. An aliquot (50  $\mu\text{L}$ ) was injected into the LCMS system. To protect the MS component, only fractions eluting from the column between 2 and 8 min were allowed to enter the detector.

#### *Sample preparation for cimetidine*

For the LCMS analysis of the samples from the rat studies, 300  $\mu\text{L}$  of methanol and 20  $\mu\text{L}$  of working IS solution (famotidine in methanol) were added to each of the standards (or samples) (100  $\mu\text{L}$  of aECF standards or 100  $\mu\text{L}$  rat plasma), such that all samples contained 400 ng/mL of the internal standard, famotidine. The samples were subjected to SPE process similar to that described for amantadine. The concentrated analytes were reconstituted in 100  $\mu\text{L}$  of 50:50 v/v methanol/water. An aliquot (25  $\mu\text{L}$ ) was injected into the LCMS system.

For the HPLC/UV analysis of cimetidine in KRB (*in vitro* transport studies), 200  $\mu\text{L}$  of KRB standards/samples were diluted with an equal volume of methanol followed by centrifugation in an Eppendorf 5415D centrifuge at 16100  $\times g$  for 5 min. An aliquot (25  $\mu\text{L}$ ) of the supernatant was injected into the HPLC system. No internal standard was used for cimetidine samples obtained from *in vitro* transport studies.

#### *Instrumentation and operating conditions for amantadine*

The LC system used for the analysis of amantadine was a Shimadzu LC-10AD with a SIL-10ADvp autosampler. The HPLC was coupled to a Shimadzu QP 8000 LCMS system with a single quadrupole mass spectrometer and an APCI interface. Data acquisition and processing were accomplished using Shimadzu LCMS Solution<sup>TM</sup> software. The APCI source was set in the positive ionization mode. A selected ion monitoring (SIM) setting was used with  $[\text{M} + \text{H}]^+$ ,  $m/z$  of 152.15 and 180.25 as the

detecting ions for amantadine and rimantadine, respectively. The MS operating conditions were optimized as follows: nitrogen flow rate 2.5L/min, APCI temperature 400° C, CDL temperature 250° C, and probe voltage +1.6 kV.

Chromatographic separation was carried out at room temperature on a Phenomenex Synergi Polar RP 80A (250mm × 2.0mm, 4µm) column from Phenomenex (Torrance, CA). The mobile phase consisted of methanol–water 80:20 v/v with 0.1% glacial acetic acid at a flow rate of 0.2 mL/min.

#### *Instrumentation and operating conditions for cimetidine*

The LC system used for the analysis of cimetidine (for *in vivo* studies) was a Shimadzu LC-10ADvp with a SIL-HTC autosampler. The LC was coupled to a Shimadzu LCMS 2010A single quadrupole mass spectrometer as the detector. Data acquisition and processing were accomplished using Empower 2 software. An APCI source was used and was set in the positive ionization mode. A selected ion monitoring (SIM) setting was used with  $[M + H]^+$ ,  $m/z$  of 253.35 and 259.30 as the detecting ions for cimetidine and famotidine, respectively. The MS operating conditions were optimized as follows: nitrogen flow rate 4.5 L/min, APCI temperature 400° C, CDL temperature 250° C, and probe voltage +4.5 kV

The HPLC analysis for KRB standards and samples (in vitro transport studies) was conducted on an Agilent 1100 Quaternary DAD System with Chemstation software for data analysis. The wavelength of detection was 228 nm and the injection volume was 25 µL. Chromatographic separation for both HPLC and LCMS methods was carried out at room temperature on a Phenomenex Synergi Polar RP 80A (250 mm × 2.0 mm, 4 µm)

column from Phenomenex (Torrance, CA). The mobile phase consisted of methanol–water 60:40 v/v with 0.1% glacial acetic acid at a flow rate of 0.2 mL/min.

#### *Method validation*

Method validation was carried out according to the currently accepted US Food and Drug Administration (FDA) bioanalytical method validation guidance<sup>9</sup>. The following parameters were considered.

*Specificity:* The specificity of the method was examined by screening six different batches of blank buffer (KRB or aECF) or rat plasma samples. Each blank sample was tested for interference using the proposed extraction procedure and chromatographic/spectroscopic conditions and compared with samples spiked with the analyte (amantadine or cimetidine) containing the internal standard (IS) (rimantadine or famotidine).

*Linearity:* Linearity was tested over a range of concentrations and standard calibration curves of at least seven points (non-zero standards) were used. Calibration curves were constructed by plotting the peak area ratio of analyte to the internal standard against the analyte concentration. The acceptance criterion for the correlation coefficient was 0.990 or greater; otherwise the calibration curve was rejected. Five replicate analyses were performed.

*Sensitivity:* For sensitivity determination, the lowest standard concentration in the calibration curve was considered to be the lower limit of quantification, meeting the following criteria: LLOQ response should be ten times the response of the blank and the LLOQ response should be identifiable, discrete and reproducible with a precision corresponding to a maximum 20% R.S.D.

*Recovery and Matrix Effects:* The extraction yield (or absolute recovery) was determined by comparing the analyte/IS peak area ratios obtained following the extraction procedure (SPE) to those obtained from samples which contained the same amount of analyte but where the blank matrix (aECF, KRB or rat plasma) was subjected to the extraction procedure prior to the addition of the analyte. The matrix effect on the ionization of analytes was evaluated by comparing the peak areas of analyte standards spiked in blank plasma following extraction with non-extracted standard analyte solutions at the same nominal concentration. Three different concentration levels were evaluated for both amantadine and cimetidine in each matrix, by analyzing five samples at each concentration level. If the percentage of the ratio was < 85% or >115%, an exogenous matrix effect was implied.

## Results and Discussion

### *Amantadine*

The mass spectra of amantadine and rimantadine obtained from the scan mode were characterized by a protonated molecular ion  $[M + H]^+$  as the base peak (Figure 4-1). The base peak intensity and the efficiency of ionization in APCI were higher than in the ESI mode. The acidity of the mobile phase was observed to affect the ionization of amantadine and IS and increase the sensitivity of detection of both analytes. The pKa values for amantadine and rimantadine are 9.0 and 10.4 respectively; therefore, a mobile phase consisting of 0.1% glacial acetic acid in methanol–water (80:20 v/v) was used to maximize the ionization of the compounds. Sample preparation using solid phase extraction was employed since this technique can purify and concentrate the sample while being less laborious than liquid-liquid extraction. Since amantadine and

rimantadine are weak bases, a cation exchange column was used for the sample preparation. A mixture of 6%  $\text{NH}_4\text{OH}$  in methanol was chosen as the eluting solvent.  $\text{NH}_4\text{OH}$  helps in the dissociation of amantadine and IS from the cationic column in the final elution step.

Figures 4-6 and 4-9, show chromatograms for blank aECF and rat plasma spiked with the internal standard rimantadine, indicating no endogenous peaks at the retention times of amantadine. The calibration curves for amantadine in different matrix are shown in Figure 4-3 and 4-4. Peak area ratios of amantadine to rimantadine were used for regression analysis, and a least squares regression model was fit to each standard curve. The summary of the calibration curve parameters used in method validation is listed in Table 4-3. The lower limit of quantification (LLOQ) was determined to be 2.0 ng/mL, 10.0ng/mL and 5.0 ng/mL in KRB, rat plasma and aECF, respectively. The recovery percentages are much higher than those obtained using reported liquid liquid extraction procedure<sup>5</sup>, showing very little loss of sample during the extraction process. The percentage ratios for matrix effects are within the established limits (< 85% or > 115%), therefore an exogenous matrix effect from the buffer or plasma was negligible for amantadine. The percentage recovery and matrix effects are tabulated in Table 4-4.

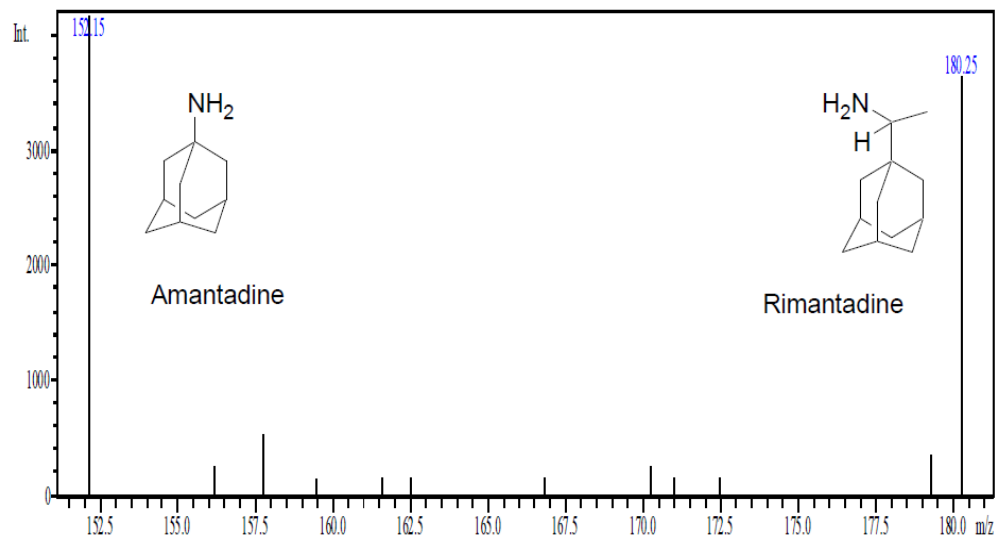


Figure 4-1: Positive ion mass spectra of amantadine ( $[M+H]^+$ , m/z 152.15) and rimantadine ( $[M+H]^+$ , m/z 180.25)

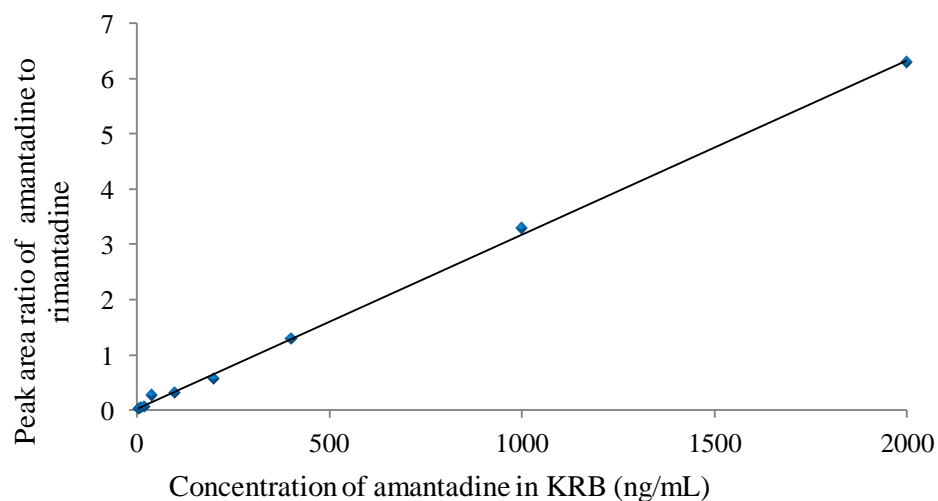


Figure 4-2: Calibration plot for amantadine:rimantadine ratio in KRB using LCMS. Linear regression of data results in the calibration curve:  $y = 0.0032x + 0.0224$ ,  $r^2 = 0.9989$ . Mobile phase: methanol–water 80:20 v/v with 0.1% glacial acetic acid; Flow rate: 0.2 ml/min; Column: Phenomenex Synergi Polar RP 80A (250 mm  $\times$  2.0 mm, 4  $\mu$ m)

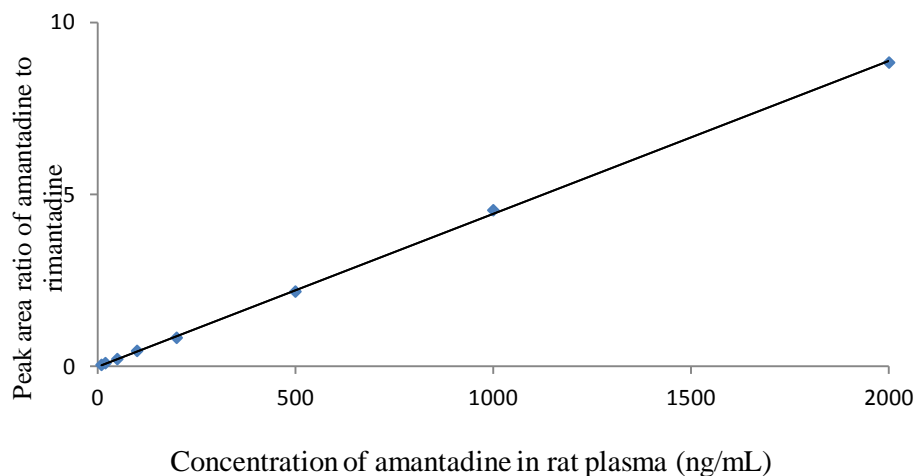


Figure 4-3: Calibration plot for amantadine: rimantadine ratio in rat plasma using LCMS. Linear regression of data results in the calibration curve:  $y = 0.0044x$ ,  $r^2 = 0.9997$ . Mobile phase: methanol–water 80:20 v/v with 0.1% glacial acetic acid; Flow rate: 0.2 ml/min; Column: Phenomenex Synergi Polar RP 80A (250mm  $\times$  2.0mm, 4 $\mu$ m)

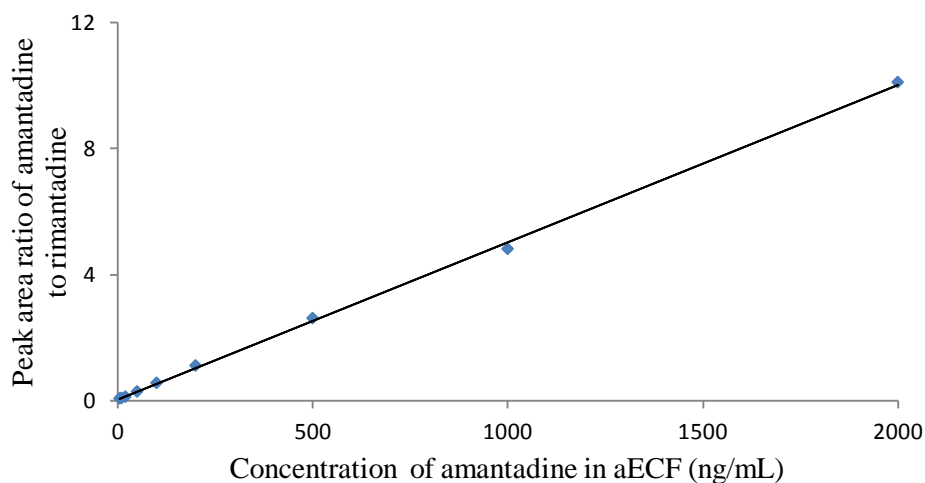


Figure 4-4: Calibration plot for amantadine: rimantadine ratio in aECF using LCMS. Linear regression of data results in the following calibration curve:  $y = 0.005x + 0.026$ ,  $r^2 = 0.9993$ . Mobile phase: methanol–water 80:20 v/v with 0.1% glacial acetic acid; Flow rate: 0.2 ml/min; Column: Phenomenex Synergi Polar RP 80A (250 mm  $\times$  2.0 mm, 4  $\mu$ m).



Table 4-3: Summary of calibration curves for amantadine in various matrices, aECF, rat plasma and KRB buffer.

| Matrix | Linear concentration range | r <sup>2</sup> | Regression equation  |
|--------|----------------------------|----------------|----------------------|
| KRB    | 2-2000 ng/mL               | 0.998          | y = 0.0032x + 0.0224 |
| Plasma | 10 – 2000 ng/ml            | 0.999          | y = 0.0044x          |
| aECF   | 5 – 2000 ng/ml             | 0.999          | y = 0.005x + 0.026   |

Note: Mobile phase: methanol:water 80:20 v/v with 0.1% glacial acetic acid; Flow rate: 0.2 ml/min; Column: Phenomenex Synergi Polar RP 80A (250 mm × 2.0 mm, 4 μm).

Table 4-4: Results of recovery and matrix effects for amantadine, n=5.

| <i>Spiked Conc (ng/mL)</i> | <i>Recovery(%)</i> |             |            | <i>Matrix effects(%)</i> |             |             |
|----------------------------|--------------------|-------------|------------|--------------------------|-------------|-------------|
|                            | <i>Plasma</i>      | <i>aECF</i> | <i>KRB</i> | <i>Plasma</i>            | <i>aECF</i> | <i>KRB</i>  |
| 1000                       | 95.5 ± 2.7         | 90.8 ± 1.4  | 96.8 ± 6.7 | 99.8 ± 2.0               | 103.2 ± 3.0 | 101.3 ± 2.8 |
| 400                        | 93.2 ± 3.2         | 89.7 ± 3.7  | 92.7 ± 4.3 | 97.5 ± 4.1               | 104.7 ± 2.2 | 102.9 ± 3.1 |
| 25                         | 91.0 ± 4.1         | 92.2 ± 3.3  | 91.3 ± 3.8 | 101.2 ± 3.8              | 100.3 ± 3.7 | 99.3 ± 5.5  |

Note: Recovery: comparison of peak area following extraction of matrix spiked with amantadine and extraction of matrix alone followed by spiking with the same concentration of analyte  
Matrix effects: comparison of peak area following the extraction of matrix which is then spiked with the analyte and an equivalent concentration of analyte in 80:20 methanol-water.

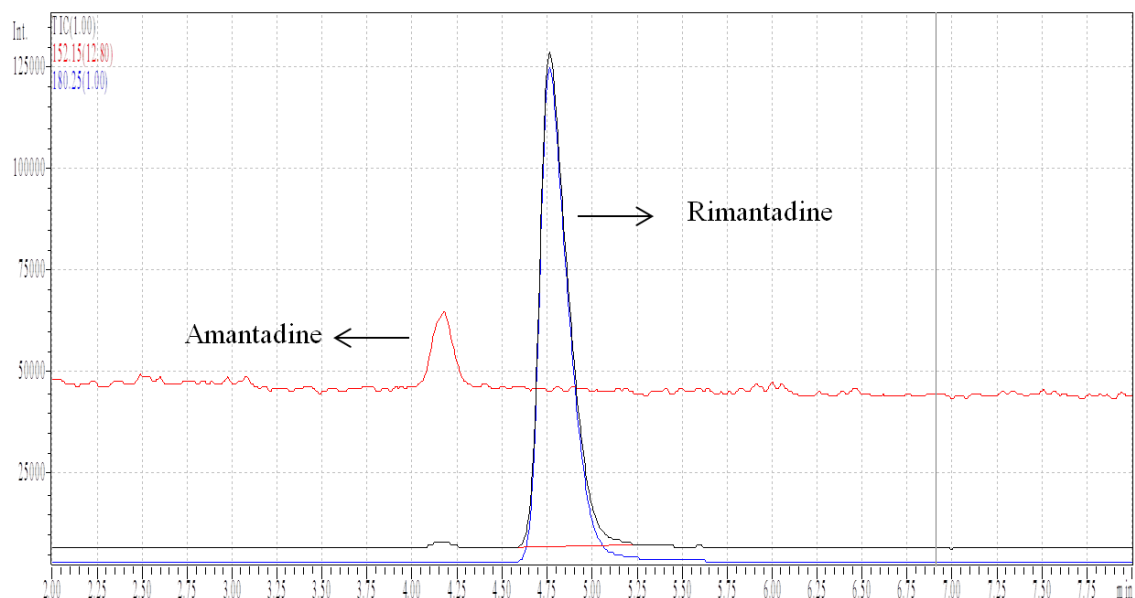


Figure 4-5: Representative chromatograph of KRB buffer sample obtained from transport studies spiked with rimantadine (200 ng/mL) as the internal standard. Mobile phase: methanol–water 80:20 v/v with 0.1% glacial acetic acid; Flow rate: 0.2 ml/min; Column: Phenomenex Synergi Polar RP 80A (250 mm × 2.0 mm, 4 $\mu$ m).

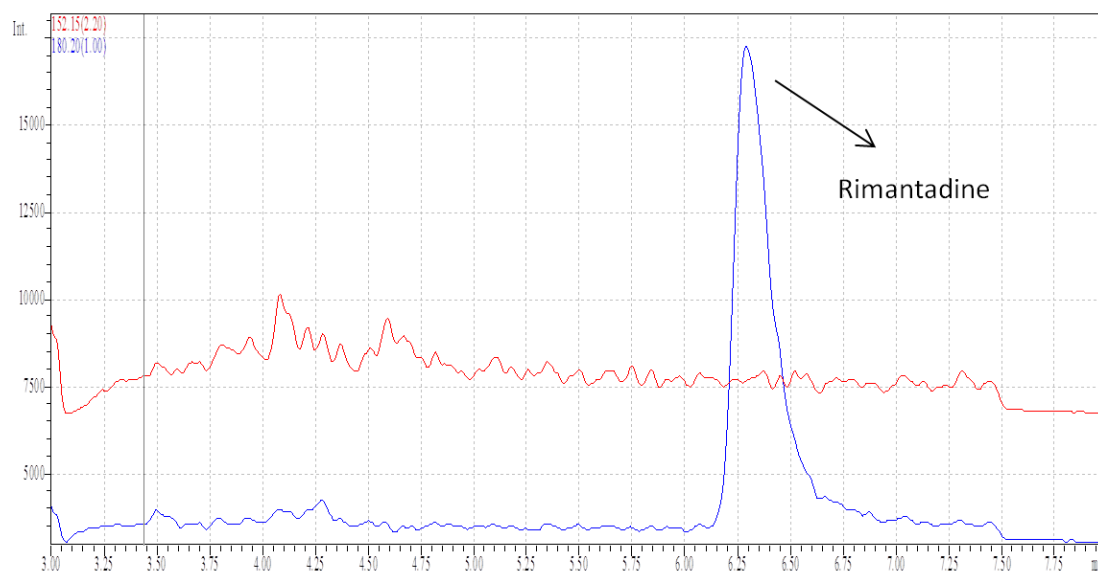


Figure 4-6: Representative chromatograph of blank rat plasma, spiked with rimantadine (200 ng/mL) as the internal standard. Mobile phase: methanol–water 80:20 v/v with 0.1% glacial acetic acid; Flow rate: 0.2 ml/min; Column: Phenomenex Synergi Polar RP 80A (250 mm × 2.0 mm, 4  $\mu$ m)

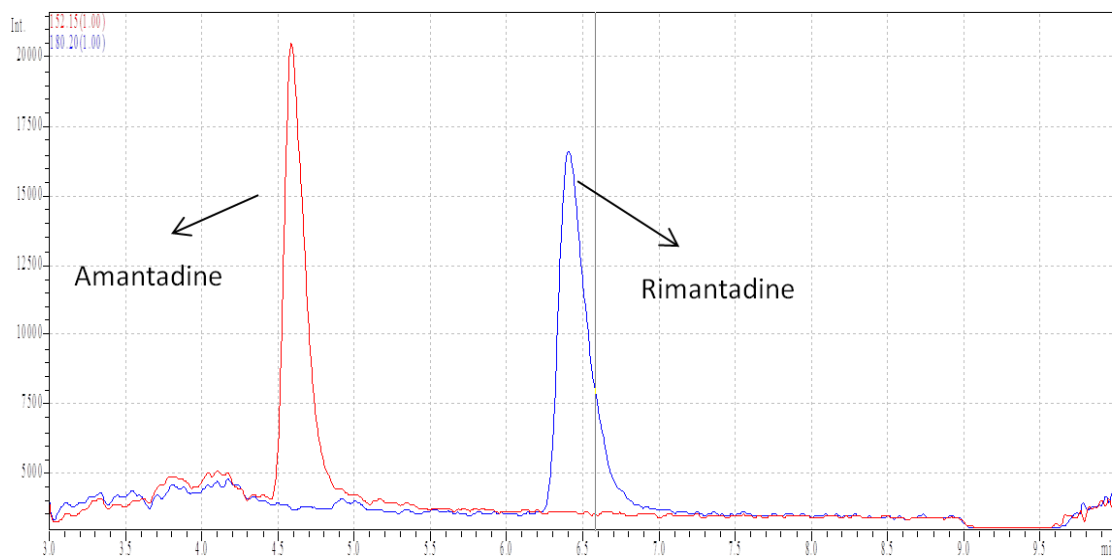


Figure 4-7: Representative chromatograph of blank rat plasma spiked with 200ng/mL of amantadine as the analyte of interest and rimantadine (200 ng/mL) as the internal standard. Mobile phase: methanol–water 80:20 v/v with 0.1% glacial acetic acid; Flow rate: 0.2 ml/min; Column: Phenomenex Synergi Polar RP 80A (250 mm × 2.0 mm, 4 μm)

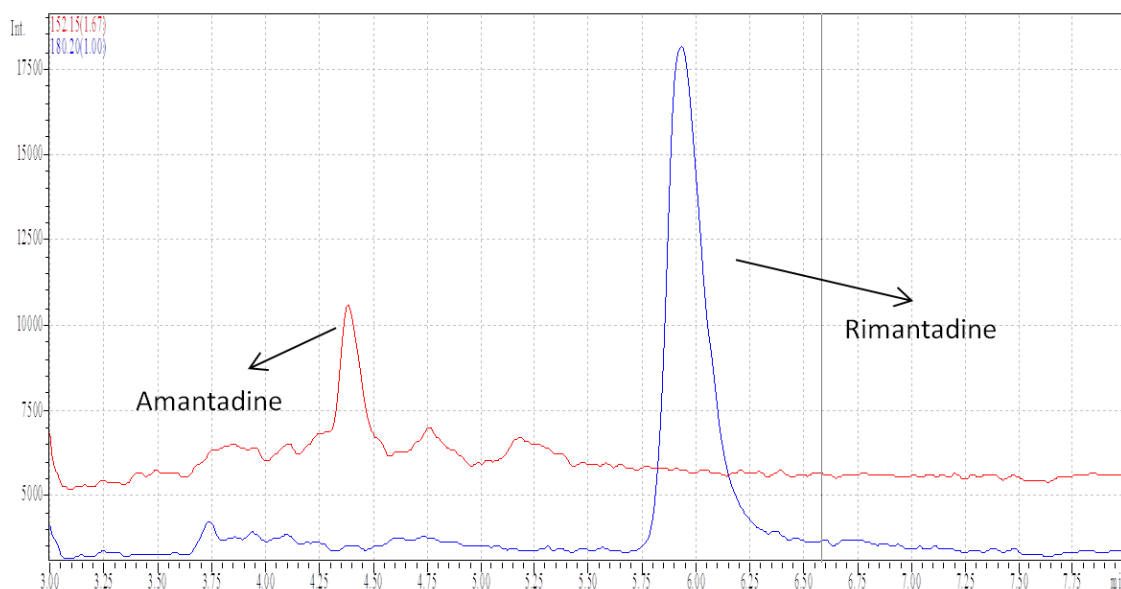


Figure 4-8: Representative chromatograph of plasma sample obtained from a rat, following an intranasal amantadine dose and spiked with rimantadine (200 ng/mL) as the internal standard. Mobile phase: methanol–water 80:20 v/v with 0.1% glacial acetic acid; Flow rate: 0.2 ml/min; Column: Phenomenex Synergi Polar RP 80A (250 mm × 2.0 mm, 4 μm)

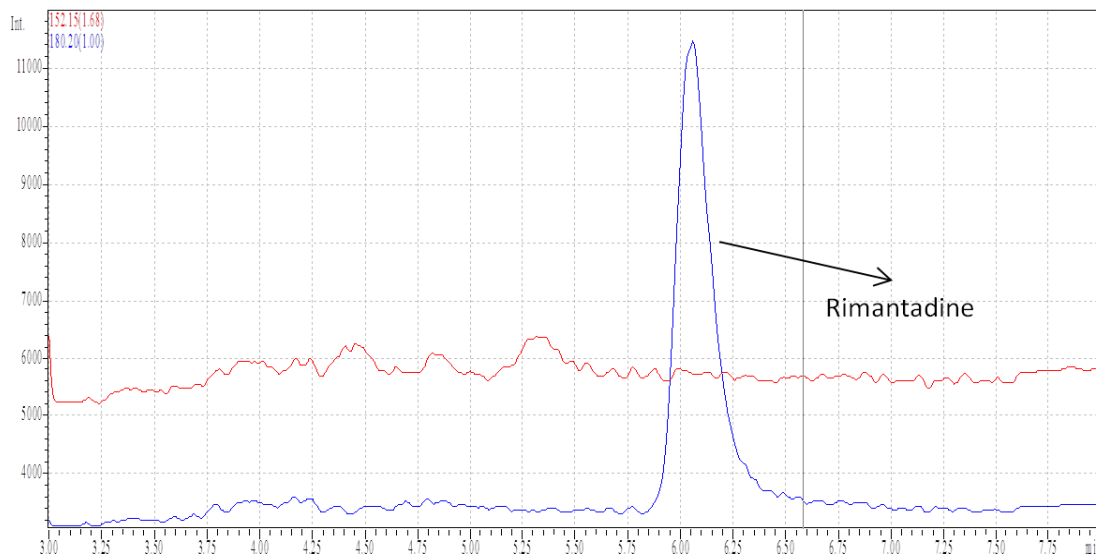


Figure 4-9: Representative chromatograph of blank artificial ECF spiked with rimantadine (200 ng/mL) as the internal standard. Mobile phase: methanol–water 80:20 v/v with 0.1% glacial acetic acid; Flow rate: 0.2 ml/min; Column: Phenomenex Synergi Polar RP 80A (250 mm × 2.0 mm, 4 μm)

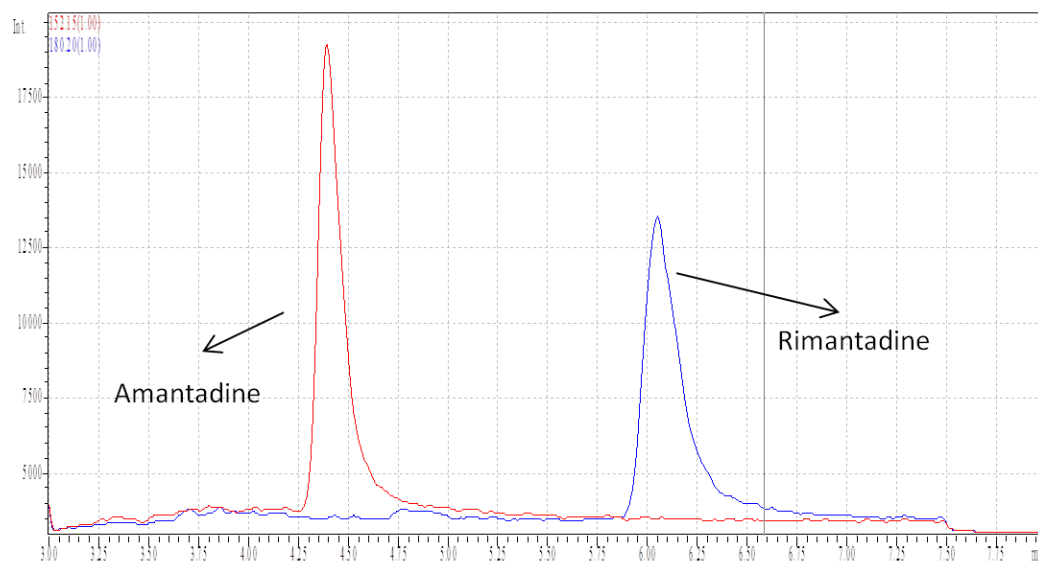


Figure 4-10: Representative chromatograph of artificial ECF standard, spiked with 200ng/mL of amantadine as the analyte of interest and rimantadine (200 ng/mL) as the internal standard. Mobile phase: methanol–water 80:20 v/v with 0.1% glacial acetic acid; Flow rate: 0.2 ml/min; Column: Phenomenex Synergi Polar RP 80A (250 mm × 2.0 mm, 4 μm)

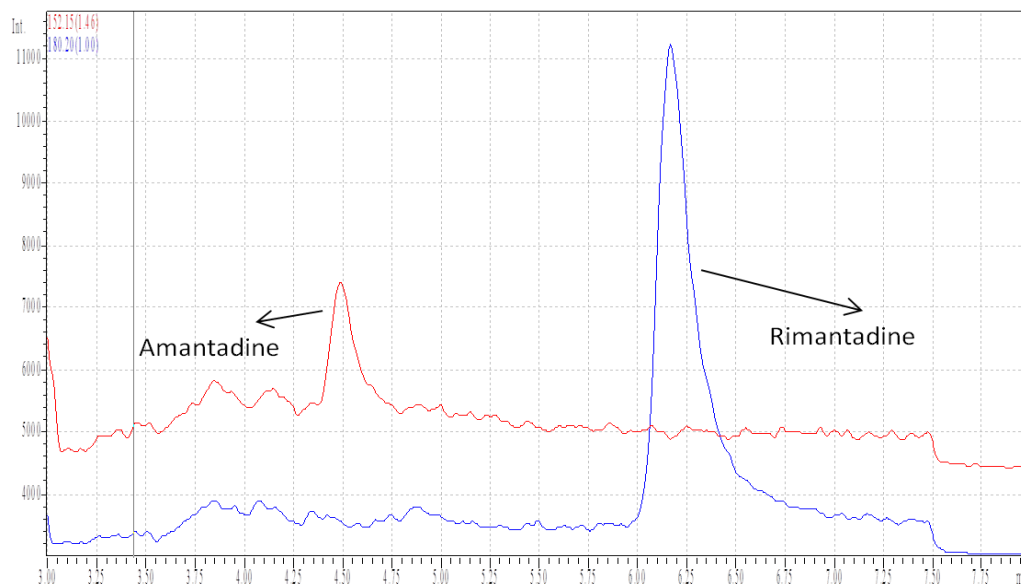


Figure 4-11: Representative chromatograph of an olfactory bulb ECF dialysate obtained from a rat following an intranasal amantadine dose and spiked with rimantadine (200 ng/mL) as the internal standard. Mobile phase: methanol–water 80:20 v/v with 0.1% glacial acetic acid; Flow rate: 0.2 ml/min; Column: Phenomenex Synergi Polar RP 80A (250 mm × 2.0 mm, 4 μm)

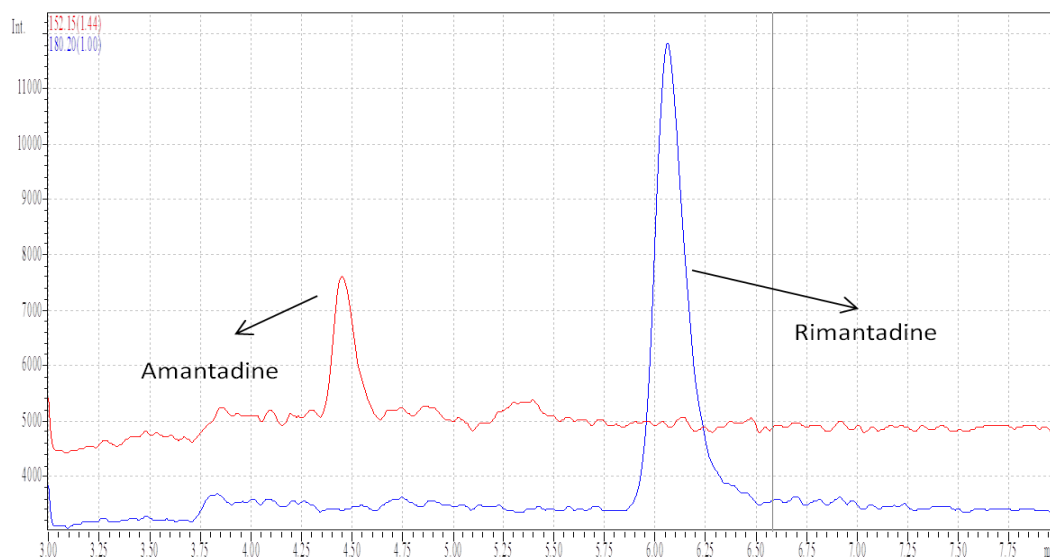


Figure 4-12: Representative chromatograph of a striatum aECF dialysate obtained from a rat following an intranasal amantadine dose and spiked with rimantadine (200 ng/mL) as the internal standard. Mobile phase: methanol–water 80:20 v/v with 0.1% glacial acetic acid; Flow rate: 0.2 ml/min; Column: Phenomenex Synergi Polar RP 80A (250 mm × 2.0 mm, 4 μm)

### *Cimetidine*

An LCMS assay was used to quantify cimetidine obtained from *in vivo* studies (aECF and rat plasma) whereas for the *in vitro* studies in KRB, an HPLC method was used.

In the LCMS method, the mass spectra of cimetidine and famotidine obtained from the scan mode were characterized by a protonated molecular ion  $[M + H]^+$  as the base peak with  $m/z$  of 253.35 and 259.30, respectively. The calibration curves for amantadine in different matrix are shown in Figure 4-1 to 4-15. Peak area ratios of amantadine to rimantadine were used for regression analysis, and a least squares regression model was fit to each standard curve. The summary of the calibration curve parameters used in method validation is listed in Table 4-5. The lower limit of quantification (LLOQ) was determined to be 500 ng/mL, 5.0 ng/mL and 1.56 ng/mL in KRB, rat plasma and aECF, respectively. Figure 4-16, 4-17 and 4-19 show chromatograms where each matrix has been spiked with cimetidine and the internal standard, famotidine. The percentage ratios for matrix effects are within the established limits (< 85% or > 115%), therefore an exogenous matrix effect from the buffer or plasma was negligible for amantadine. The percentage recovery and matrix effects are tabulated in Table 4-6.

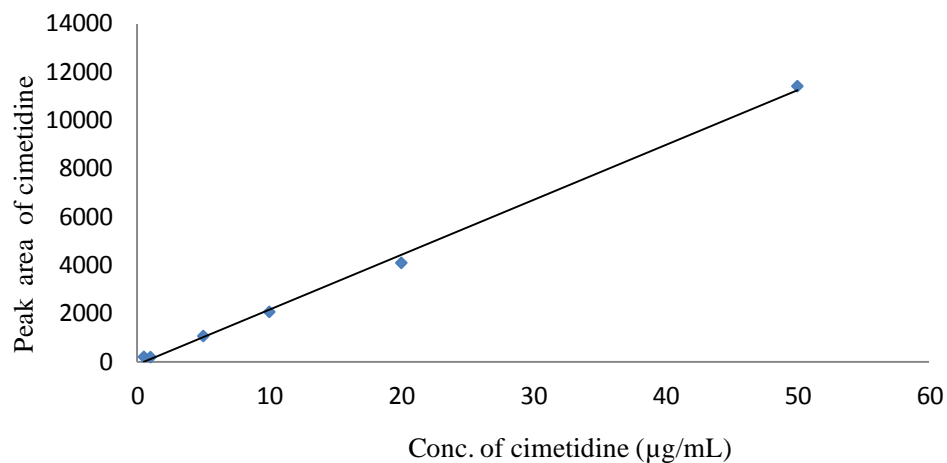


Figure 4-13: Calibration plot for cimetidine: famotidine ratio in KRB buffer using HPLC. Linear regression of data results in the calibration curve:  $y = 227.275x + 84.044$ ,  $r^2 = 0.9979$ . Mobile phase: methanol–water 60:40 v/v with 0.1% glacial acetic acid; Flow rate: 0.2 ml/min; Column: Phenomenex Synergi Polar RP 80A (250 mm × 2.0 mm, 4 µm); Wavelength: 228nm.

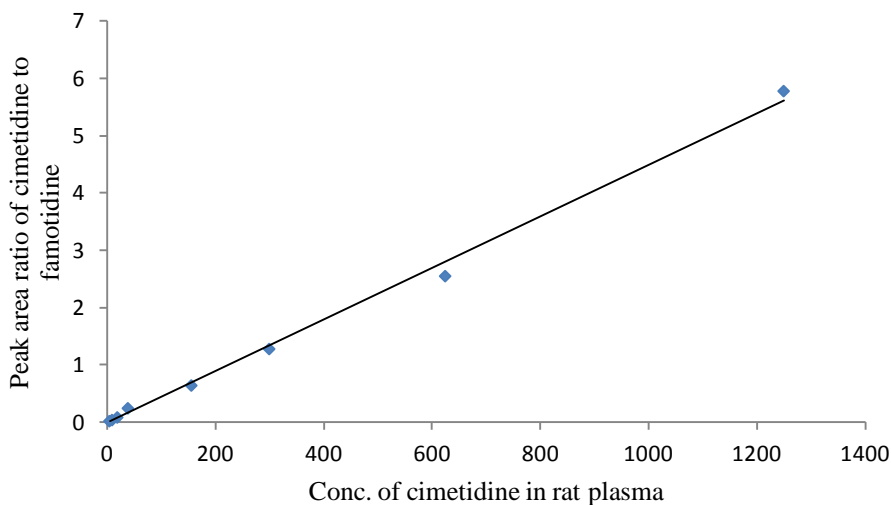


Figure 4-14: Calibration plot for cimetidine: famotidine ratio in rat plasma using LCMS. Linear regression of data results in the calibration curve:  $y = 0.0045x - 0.0419$ ,  $r^2 = 0.9964$ . Mobile phase: methanol–water 60:40 v/v with 0.1% glacial acetic acid; Flow rate: 0.2 ml/min; Column: Phenomenex Synergi Polar RP 80A (250 mm × 2.0 mm, 4 µm)

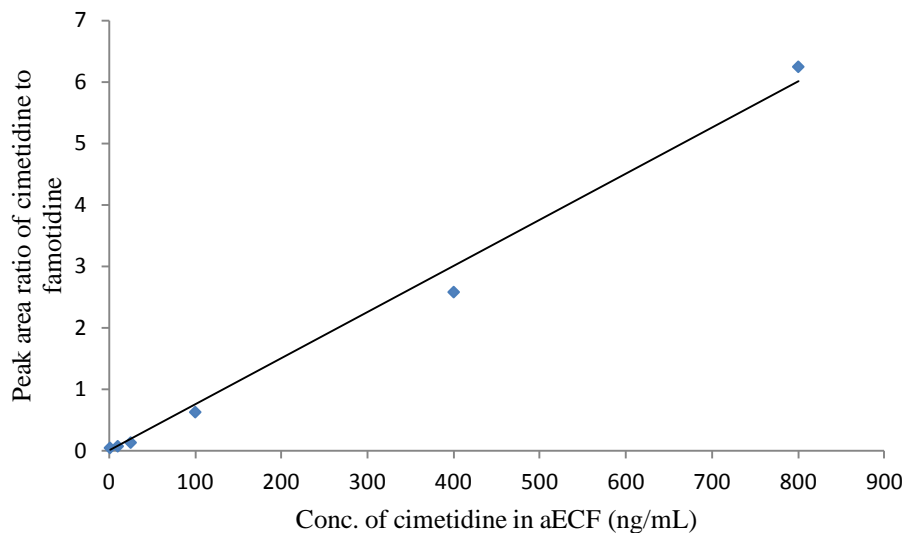


Figure 4-15: Calibration plot for cimetidine: famotidine ratio in aECF using LCMS. Linear regression of data results in the calibration curve:  $y = 0.0075x - 0.1004$ ,  $r^2 = 0.9926$ . Mobile phase: methanol–water 60:40 v/v with 0.1% glacial acetic acid; Flow rate: 0.2 ml/min; Column: Phenomenex Synergi Polar RP 80A (250 mm  $\times$  2.0 mm, 4  $\mu$ m)

Table 4-5: Summary of calibration curves for cimetidine in different matrix, aECF, rat plasma and KRB buffer.

| Matrix | Instrument | Linear concentration range | $r^2$ | Regression equation |
|--------|------------|----------------------------|-------|---------------------|
| KRB    | HPLC-UV    | 500 -50,000ng/mL           | 0.998 | $227.275x + 84.044$ |
| Plasma | LCMS       | 5 – 1250 ng/ml             | 0.996 | $0.0045x - 0.0419$  |
| aECF   | LCMS       | 1.562 – 800 ng/ml          | 0.993 | $0.0077x - 0.1004$  |

Note: Mobile phase: methanol–water 80:20 v/v with 0.1% glacial acetic acid; Flow rate: 0.2 ml/min; Column: Phenomenex Synergi Polar RP 80A (250 mm  $\times$  2.0 mm, 4  $\mu$ m).



Table 4-6: Results of recovery and matrix effects of cimetidine, n=5.

| <i>Spiked Conc (ng/mL)</i> | <i>Recovery(%)</i> |             |            | <i>Matrix effects(%)</i> |             |             |
|----------------------------|--------------------|-------------|------------|--------------------------|-------------|-------------|
|                            | <i>Plasma</i>      | <i>aECF</i> | <i>KRB</i> | <i>Plasma</i>            | <i>aECF</i> | <i>KRB</i>  |
| 800                        | 88.5 ± 3.6         | 89.2 ± 2.5  | 90.2 ± 1.9 | 105.7 ± 6.1              | 111.4 ± 6.3 | 105.3 ± 4.2 |
| 200                        | 86.4 ± 4.0         | 87.4 ± 4.2  | 92.0 ± 4.4 | 106.4 ± 5.6              | 110.5 ± 7.4 | 102.1 ± 3.5 |
| 10                         | 85.2 ± 4.5         | 88.7 ± 3.7  | 89.3 ± 3.7 | 104.1 ± 7.3              | 107.4 ± 4.9 | 106.4 ± 6.1 |

Note: Recovery: comparison of peak area following extraction of matrix spiked with cimetidine and extraction of matrix alone followed by spiking with the same concentration of analyte. Matrix effects: comparison of peak area following the extraction of matrix which is then spiked with the analyte and an equivalent concentration of analyte in 50:50 methanol-water.

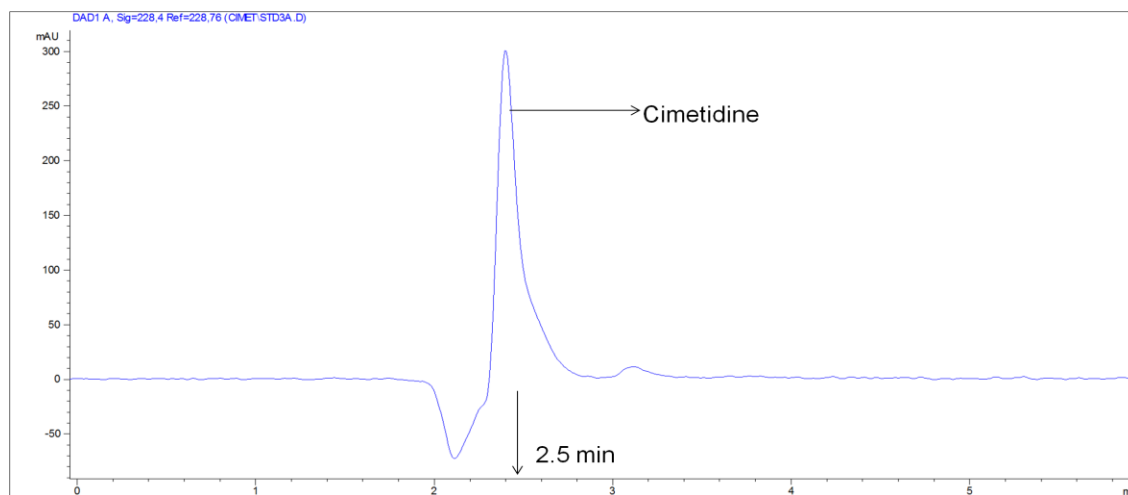


Figure 4-16: HPLC chromatograph cimetidine (5 µg/mL) in KRB (retention time: 2.5min). Mobile phase: methanol–water 60:40 v/v with 0.1% glacial acetic acid; Flow rate: 0.2 ml/min; Column: Phenomenex Synergi Polar RP 80A (250 mm × 2.0 mm, 4 µm). Wavelength: 228 nm.

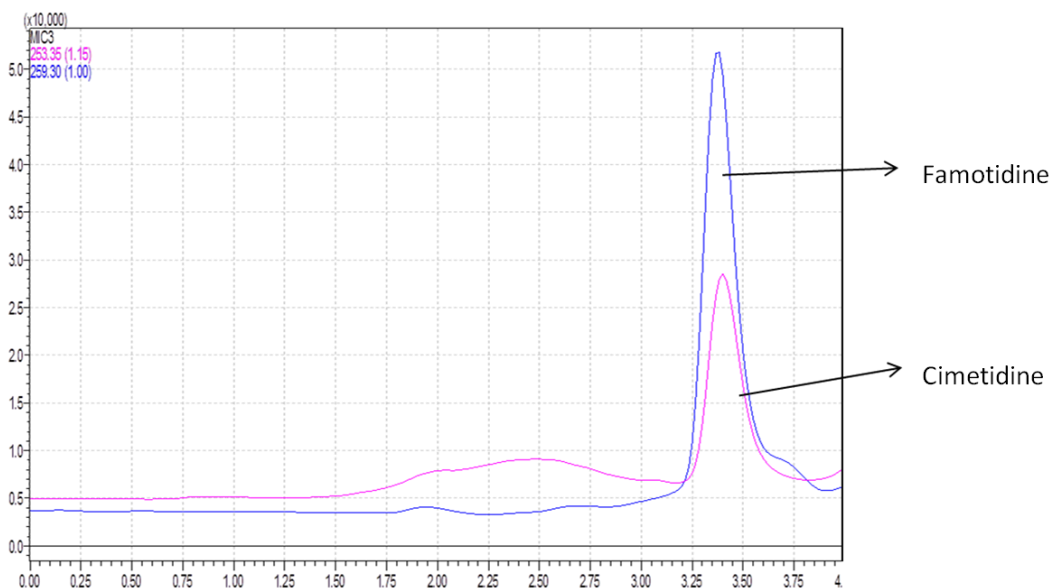


Figure 4-17: Representative chromatograph of rat plasma standard spiked with cimetidine (50 ng/mL) as the analyte of interest and famotidine (400 ng/mL) as the internal standard. Mobile phase: methanol–water 60:40 v/v with 0.1% glacial acetic acid; Flow rate: 0.2 ml/min; Column: Phenomenex Synergi Polar RP 80A (250 mm × 2.0 mm, 4 μm)

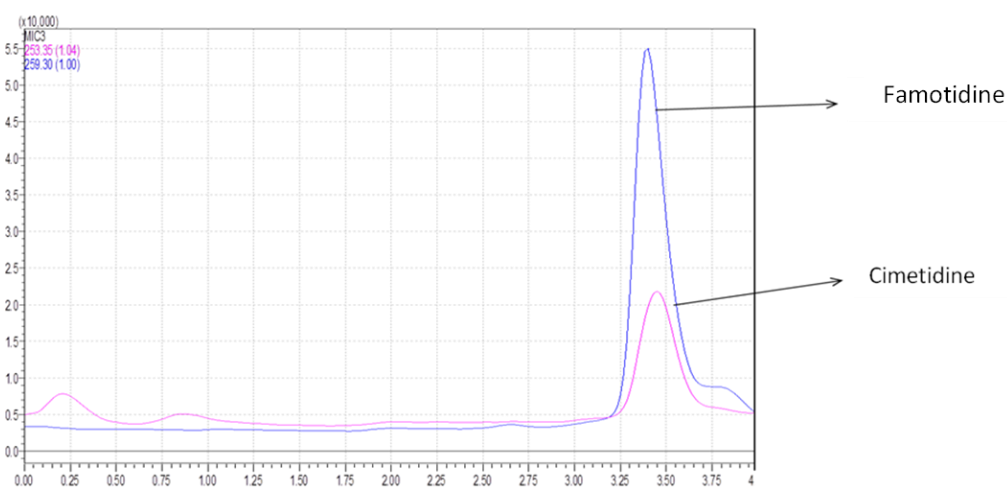


Figure 4-18: Representative chromatograph of plasma sample obtained from a rat following an intranasal cimetidine dose and spiked with famotidine (400 ng/mL) as the internal standard. Mobile phase: methanol–water 60:40 v/v with 0.1% glacial acetic acid; Flow rate: 0.2 ml/min; Column: Phenomenex Synergi Polar RP 80A (250 mm × 2.0 mm, 4 μm)

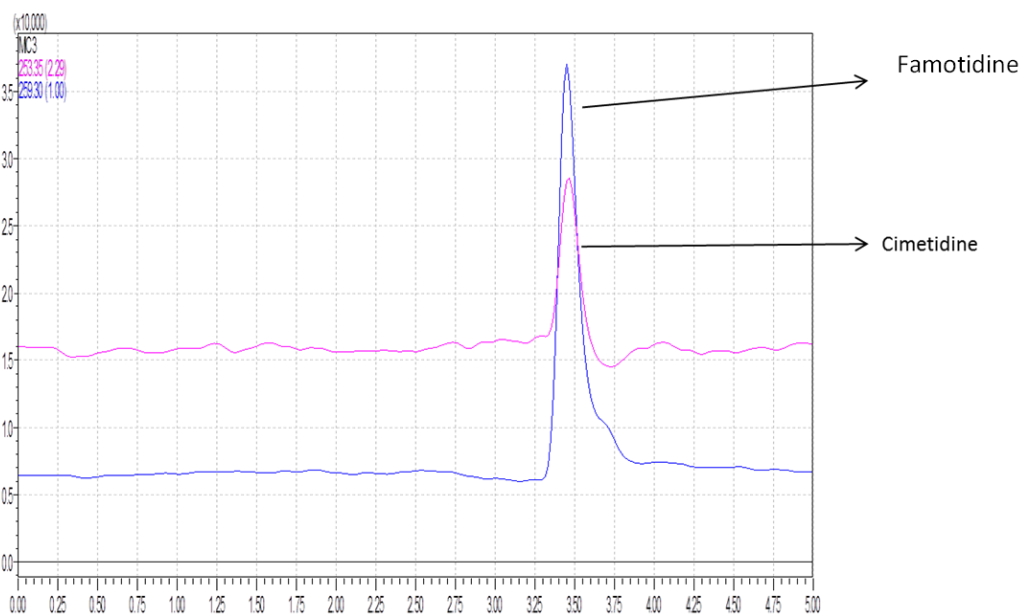


Figure 4-19: Representative chromatograph of aECF standard spiked with cimetidine (50 ng/mL) as the analyte of interest and famotidine as the internal standard. Mobile phase: methanol–water 60:40 v/v with 0.1% glacial acetic acid; Flow rate: 0.2 ml/min; Column: Phenomenex Synergi Polar RP 80A (250 mm × 2.0mm, 4 μm)

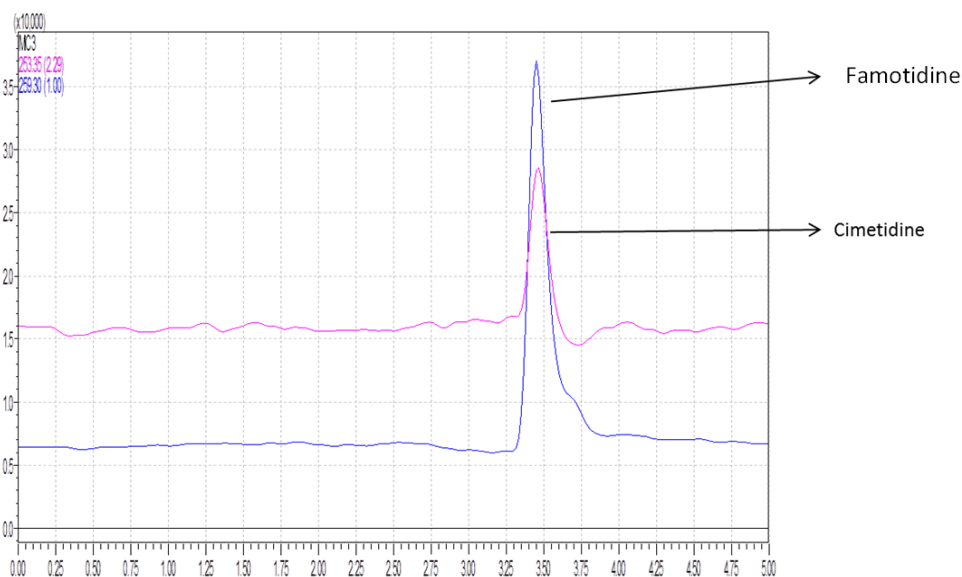


Figure 4-20: Representative chromatograph of an olfactory bulb ECF dialysate obtained from rat following an intranasal cimetidine dose and spiked with famotidine (400 ng/mL) as the internal standard. Mobile phase: methanol–water 60:40 v/v with 0.1% glacial acetic acid; Flow rate: 0.2 ml/min; Column: Phenomenex Synergi Polar RP 80A (250 mm × 2.0 mm, 4 μm)

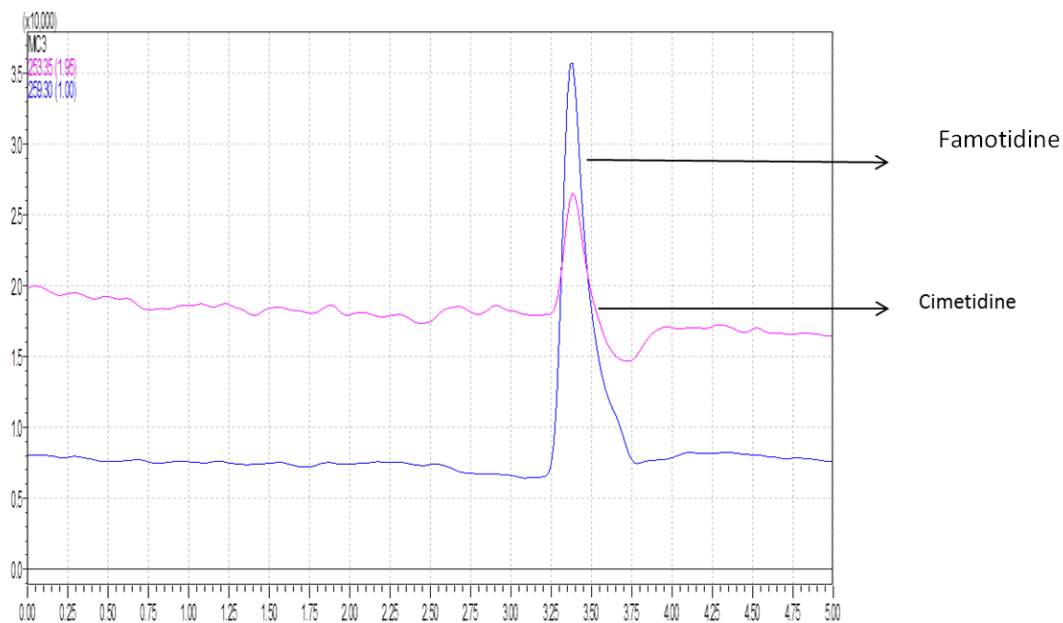


Figure 4-21: Representative chromatograph of striatum ECF dialysate from rat dosed intranasally with cimetidine and spiked with famotidine (400 ng/mL) as the internal standard. Mobile phase: methanol–water 60:40 v/v with 0.1% glacial acetic acid; Flow rate: 0.2 ml/min; Column: Phenomenex Synergi Polar RP 80A (250 mm  $\times$  2.0 mm, 4  $\mu$ m)

### Conclusion

A simple and sensitive LCMS method for the determination of amantadine and cimetidine, in different matrices such as KRB, aECF and rat plasma was developed and validated. The method exhibited good linearity in each matrix over the concentration ranges that are required for both *in vitro* transport studies and *in vivo* animal studies for both drugs. The SPE method for sample preparation ensured that the samples were free of matrix effects in addition to obtaining good analyte recovery. Isocratic elution and shorter run times (< 10 min) are helpful in carrying out the analysis rapidly. The internal standards used are commercially available and the method was successfully applied for the determination of amantadine and cimetidine in KRB obtained from the *in vitro* transport studies and also for both analysis in aECF and rat plasma obtained during the *in vivo* studies in rats.

CHAPTER 5  
TRANSPORT OF AMANTADINE AND CIMETIDINE ACROSS  
BOVINE NASAL TISSUES

*Amantadine*

Amantadine (1-aminoadamantane) is one of the oldest licensed compounds used for the prophylaxis and treatment of influenza A viral infections. Amantadine is also indicated in the treatment of extrapyramidal effects related to Parkinson's disease (PD) and was approved for this purpose by the FDA in 1973. The effect of amantadine for dyskinesia in PD was demonstrated by a multicenter, double blind, randomized, placebo-controlled, crossover trial<sup>125</sup>. Its mechanism of action is not fully understood, but it is thought to occur by enhancing dopamine release from presynaptic terminals and blockade of N-methyl-D-aspartic acid (NMDA) receptors<sup>126,127</sup>. A possible interaction with nicotinic acetylcholine receptors has also been reported<sup>128</sup>.

*Physical properties of amantadine*

Amantadine hydrochloride (Figure 5-1) is the salt of a nonchiral, symmetrical C<sub>10</sub> primary amine with a molecular weight of 151.24 g/mol. It is freely water soluble (75mg/mL at 30<sup>0</sup>C). Amantadine exists as an organic cation (97.5% ionized) at physiologic pH (pH= 7.4). It has pKa's of 9.0 and 10.1 at 25° C and 37° C respectively with a log D<sub>(7.4)</sub> of -0.6<sup>116,129</sup>. The salt is thermally stable for up to 5 years at room temperature<sup>130</sup>. The adamantane moiety of amantadine is highly lipid soluble and readily diffuses across biological membranes in its unionized form<sup>131</sup>.

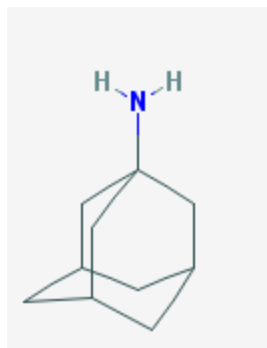


Figure 5-1: Chemical structure of amantadine (PubChem CID 2130)<sup>132</sup>

#### *Amantadine as an OCT2 substrate*

Amantadine has been shown to undergo electrogenic transport using *Xenopus laevis* oocytes expressing hOCT2. In addition, amantadine is frequently used as a probe substrate to characterize the renal tubule OCT2 systems. The  $K_m$  values for amantadine in hOCT2 expressing neuronal cells has been reported to be 27  $\mu\text{M}$ <sup>133</sup>.

#### *Cimetidine*

Cimetidine (N''-cyano-N-methyl-N'-[2-[[[(5-methyl-1H-imidazol-4-yl) methyl] thio]ethyl]-guanidine) contains an imidazole ring and is chemically related to histamine (Figure 5-2) . It is routinely used in the medical management of peptic ulcer, gastroesophageal reflux disease and Zollinger-Ellison syndrome. Cimetidine was developed by GlaxoSmithKline and was approved by the FDA for clinical use in 1979<sup>134,135</sup>. The mechanism of action of cimetidine is via the blockade of  $\text{H}_2$  receptors which are involved in the secretion of acid by the parietal cells. In addition, cimetidine has also been demonstrated to possess anti-tumor activity against colon and gastric tumors, kidney cancers and melanomas. In addition, cimetidine was also observed to be effective as an

add on therapy to temozolomide against malignant gliomas<sup>136-137</sup>. It acts as an anti-adhesive and thus serves as an anti-migratory agent for the glioma cells.

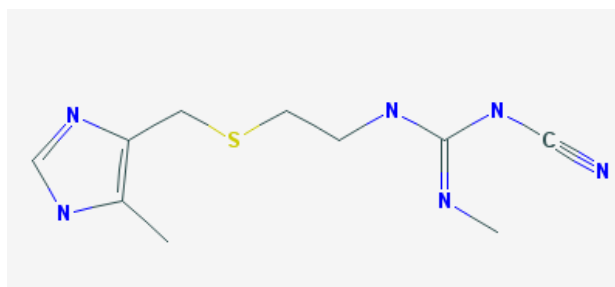


Figure 5- 2: Chemical structure of cimetidine (PubChem CID 2756)<sup>138</sup>.

#### *Physical properties of cimetidine*

Cimetidine has low intestinal permeability and has been classified as a BCS (biopharmaceutics classification system) Class III compound<sup>139</sup>. It is a weak base with pKas of 6.80 and 6.93 and log  $D_{(7.4)}$  of -0.25. Cimetidine has moderate solubility (24 mM) in the pH range 1-8<sup>117</sup>.

#### *Cimetidine: an OCT2 substrate*

Cimetidine has been demonstrated to be both a substrate ( $K_m$  for hOCT2 is  $\sim 50 \mu\text{M}$ )<sup>140</sup> and inhibitor ( $\text{IC}_{50}$  values for inhibition of OCT2-mediated  $\text{MPP}^+$  transport in HEK-OCT2 cells =  $120 \mu\text{M}$ )<sup>141</sup> for OCT2. It is one of the most commonly used probe inhibitors used in the evaluation of OCT2 activity in the tubular secretion of organic cations in the human kidney<sup>142</sup>. Cimetidine is known to reduce the renal clearance of other OCT2 substrates like metformin and procainamide, resulting in clinically significant drug-drug interactions<sup>76,143</sup>.



### *Organic cation transporter inhibitors*

#### Guanidine as and OCT2 inhibitor

Guanidine is an aminomethanamide, is an endogenous by-product of protein metabolism formed by the oxidation of guanine. Guanidine is protonated at physiological pH ( $pK_a = 13.6$ ) and its conjugate acid, the guanidinium cation  $[CH_6N_3]^+$ , is highly stable in aqueous solution due to the efficient resonance stabilization of the charge and efficient solvation by water molecules<sup>144</sup>. The maximum solubility of guanidine hydrochloride in water at room temperature is approximately 6M. The major biologic role of guanidine is in neurotransmission, where it enhances the release of acetylcholine following a nerve impulse<sup>145</sup>. Guanidine is known to be transported by OCT2 with high efficiency, and it can strongly discriminate OCT2 activity from OCT1 and OCT3, since it is neither a substrate nor inhibitor for the latter two transporters. Routinely used OCT2 inhibitors for transporter evaluation are MPP<sup>+</sup> (1-methyl 4-phenylpyridinium) and TEA (tetraethyl ammonium), but both these compounds are known to have neurotoxic effects<sup>78</sup>. Additionally they are substrates for both OCT1 and OCT2 transporters. The  $K_m$  and  $K_i$  (MPP<sup>+</sup> inhibition) value of guanidine in pcDNA3OCT2 (cDNA of rat kidney OCT2 inserted into the eucaryotic expression vector pcDNA3) transfected human embryonic kidney cells were reported to be 520–1000  $\mu$ M and 0.26–0.30mM, respectively<sup>146</sup>. Although the  $K_m$  values of guanidine for OCT2 are higher than most OCT2 substrates, the efficiency of transport of guanidine by OCT2 (comparable to the MPP<sup>+</sup> and TEA) are the result of a very high turnover number ( $k_{cat}$ )<sup>147</sup>.

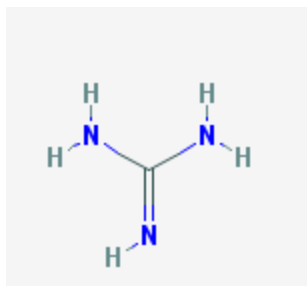


Figure 5-3: Chemical structure of guanidine (PubChem CID 5742) <sup>148</sup>

#### *L-carnitine as an OCTN2 inhibitor*

Carnitine is a quaternary ammonium compound biosynthesized from the amino acids lysine and methionine <sup>149</sup>. In living cells, it is required for the transport of fatty acids from the cytosol into the mitochondria during the breakdown of lipids for the generation of metabolic energy. It is widely available as a nutritional supplement <sup>150</sup>. Carnitine exists as two stereoisomers, with the biologically active form being L-carnitine. The sodium-dependent cation transporter, OCTN2, has been implicated in primary systemic carnitine deficiency. It has been established that Na<sup>+</sup> dependent transport of L-carnitine by OCTN2 is electrogenic and stereospecific and Na<sup>+</sup> increases the affinity of the transporter for L-carnitine <sup>151</sup>. In the uptake measurements using hOCTN2 in *Xenopus laevis* oocytes, an apparent K<sub>m</sub> for L-carnitine of 4-5 μM has been reported <sup>87</sup>. K<sub>m</sub> values of 20 μM have been reported for OCTN2 for L-carnitine in isolated enterocytes of wild-type mice (compared with (*jvs*) mice which have a hereditary deficiency of the *OCTN2* gene), and in HEK293 cells expressing mouse OCTN2 <sup>152</sup>.

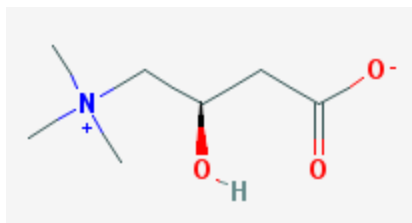


Figure 5-4: Chemical structure of L-carnitine (PubChem CID 10917) <sup>153</sup>

#### *Pentamidine as an OCT2 inhibitor*

Pentamidine has been used in the clinic since 1941, first for the treatment of African trypanosomiasis, and more recently for treatment of *Pneumocystis carinii* pneumonia (PCP) fungal infections in AIDS patients. It has also been used in antimony-resistant leishmaniasis <sup>154,155</sup>.

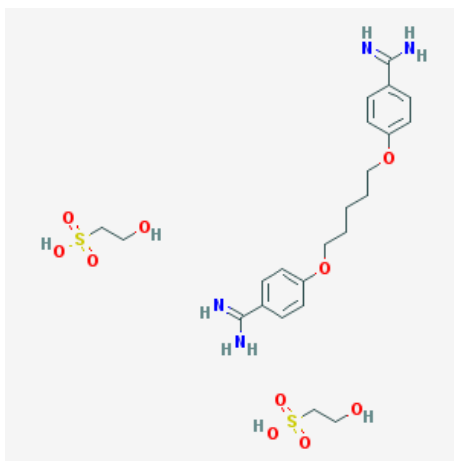


Figure 5-5: Chemical structure of pentamidine isoethionate (PubChem CID 8813) <sup>156</sup>

Pentamidine is an aromatic diamidine with pK<sub>a</sub>s of 11.5 and 12.9 and is soluble in water (100 mM as the isoethionate salt). Pentamidine has been shown to be a weak substrate for hOCT2, but it is a potent inhibitor of the transporter (IC<sub>50</sub> < 20 μM) <sup>157,158</sup>. *In vivo*, pentamidine has a long elimination half-life (> 4 days), as the compound accumulates significantly in tissues. Pentamidine undergoes extensive hepatic

metabolism, with renal excretion accounting for only a small fraction (< 10%) of the administered dose<sup>159</sup>.

*In vitro transport studies using diffusion cells*

It is well established that *in vitro*, tissue-based diffusion models are an important tool for elucidating mechanisms of biologic transport. A frequently utilized *in vitro* tissue method uses a donor-receiver chamber-type diffusion system to assess drug permeation. These *in vitro* systems provide information about permeability, transport pathways, metabolism, tissue toxicity and issues related to formulation development<sup>160</sup>. When examining transport across tissue explants in diffusion chambers (Navicyte, Harvard apparatus) Fick's second law can be modified as<sup>161</sup>

$$J = \frac{\Delta M_R}{A \Delta t} \equiv P_e \times (C_d - C_r) \quad \text{Equation 5-1}$$

$$\text{Where, } P_e = \frac{D \times K}{h}$$

$\Delta M_R / \Delta t$  = change in amount of the compound transferred to the receiver compartment over small intervals of time,  $\Delta t$ . This can be determined from the slope of a linear plot of a  $\Sigma M_R$  versus time.

J = Flux (mass transported across barrier per unit time)

K = partition coefficient

D = diffusion coefficient

h = thickness of the membrane (diffusion barrier)

A = surface area available for diffusion

$P_e$  = permeability coefficient of the solute

$C_d$  = solute concentration in the donor chamber

$C_r$  = solute concentration in the receiver chamber

$C_d - C_r$  represents the concentration gradient across the tissue

Thus, the flux is proportional to the concentration gradient, and the permeability is a proportionality factor that relates these two physical characteristics. Using (Equation 5-1), the effective permeability ( $P_e$ ) coefficient under steady state conditions can be calculated as:

$$P_e = \left( \frac{V_D}{A \Delta M_D} \right) (\Delta M_R / \Delta t) \quad \text{Equation 5-2}$$

$M_D$  = Initial amount of the drug in the donor compartment

$V_D$  = Volume of the donor compartment

Some important experimental considerations need to be addressed when carrying out *in vitro* transport studies.

- (a) The concentration gradient across the tissue should be nearly constant throughout the experiment. Normally experiments are performed under sink conditions to achieve this.
- (b) The concentration gradient should be the only gradient present across the tissue.
- (c) Unstirred water layers surrounding the barrier should be minimized.

### Materials

Amantadine HCl, cimetidine, guanidine HCl, L-carmitine HCl and pentamidine isoethionate were all purchased from Sigma Aldrich (St. Louis, MO). Navicyte<sup>®</sup> diffusion cells were obtained from Harvard Apparatus (Holliston, MA). The Lauda RM6 circulating water bath was from Brinkmann Instruments Co. (New York, NY) and the

EVOM volt-ohmmeter was from World Precision Instruments Inc, (Sarasota, FL). Kreb's Ringer's buffer (KRB) salts, HPLC solvents and all other reagents were obtained from Fisher Scientific, (Chicago, IL).

### Experimental procedures

#### *Preparation of mucosal tissues*

Excised bovine nasal mucosa was obtained from Bud's Custom Meats Co. (Riverside, IA). Nasal turbinate mucosa was retrieved by opening the nasal cavity along the septal midline and removing the turbinates from the lateral wall. The upper turbinates, covered by the olfactory mucosa, and the middle turbinates, covered by the respiratory mucosa, were harvested carefully and transported in ice-cold KRB that was previously bubbled with carbogen (95% O<sub>2</sub> + 5% CO<sub>2</sub>). Upon arrival in the lab, mucosal membranes were carefully stripped from the underlying cartilage and kept oxygenated in ice-cold KRB. Transport studies were initiated within 30 min of tissue excision.

#### *In vitro bi-directional transport studies*

Bidirectional transport studies were carried out across both olfactory and respiratory mucosae in both the mucosal to submucosal (m-s) and submucosal to mucosal (s-m) directions. Diffusion cells with a donor and receiver volume of 1 ml and diffusion cross-sectional areas of 0.64 cm<sup>2</sup> were used to measure flux across the nasal tissues. Freshly excised mucosal tissues were mounted between the donor and receiver chamber of the Navicyte<sup>®</sup> diffusion cells and equilibrated with 1 mL KRB, or KRB + inhibitor for inhibition studies, on each side at 37° C for 30 min. After the equilibration period, donor and receiver solutions were completely removed from both chambers and the donor chamber was replaced with drug solution (amantadine or cimetidine) or drug + inhibitor

solution (for inhibition studies), while the receiver chamber was replaced with the same volume of fresh KRB (KRB + inhibitor, for inhibition studies). The buffer and the drug solution or drug + inhibitor solution were always pre-warmed to 37 °C prior to transferring them to the diffusion cells. Transport studies were conducted over a range of amantadine or cimetidine donor concentrations to observe the dependence of flux on the substrate concentration. The duration of each transport study was 120 min. Aliquots (200µl) from the receiver compartment were withdrawn at 5, 15, 30, 60, 90 and 120 min. The volumes removed from the receiver compartment were replaced with an equivalent volume of fresh, pre-warmed KRB (KRB + inhibitor) after each withdrawal. The solutions in the donor and receiver compartments were aerated with carbogen (O<sub>2</sub>/CO<sub>2</sub>, 95%/5%) at a rate of 3-4 bubbles per second during equilibration and throughout the duration of the transport study. The integrity of the tissue was monitored by measuring the transepithelial electric resistance (TEER) across the tissue using an EVOM volt-ohmmeter. Resistance values lower than 100 Ω cm<sup>2</sup> were taken to be an indication of tissue damage and explants showing such low values were discarded.

#### *Study groups for amantadine transport studies*

Amantadine concentrations of 2, 20, 50 and 100µM were evaluated. The concentration range included the reported OCT2 K<sub>m</sub> value of 20 µM. All inhibition studies for both OCT2 and OCTN2 were carried out at 2 µM donor concentrations of amantadine where it was anticipated that the changes in OCT2 or OCTN2 activity would have significant effects on the total amount of amantadine transported across the tissue. The concentrations of guanidine and L-carnitine were 2 mM and 50 µM, respectively, and these were selected to be 10 times greater than the K<sub>i</sub> values reported for these

compounds and 50-100 times higher than the substrate concentration, to ensure complete inhibition of the carrier of interest<sup>162,65</sup>. The concentrations of amantadine or cimetidine in the receiver chamber was measured using a validated LCMS method (Chapter 4).

Since both OCTN1 and OCTN2 are present in the nasal mucosa, it is important to discriminate the substrate specificity of either transporter for the organic cation studied. OCTN2 is known to transport L-carnitine with high affinity in a Na<sup>+</sup>-dependent manner, and it transports other organic cations in a Na<sup>+</sup>-independent manner, whereas OCTN1 is known to interact with L-carnitine with low affinity in a Na<sup>+</sup>-independent manner<sup>87,84, 151,163,164</sup>. L-carnitine was used at concentrations high enough to impart competitive inhibition of OCTN2, and the possibility of the compound interacting with both the transporters cannot be ruled out. Therefore, these experiments were designed to distinguish between OCTN1 or OCTN2, by performing the transporter inhibition studies using L-carnitine in the presence of both sodium-containing and sodium-free KRB (Table 5-1). Sodium free KRB was prepared by replacing all the sodium equimolar amounts of potassium.



Table 5-1: Experimental design of transport studies and the buffer used. Studies for each group were performed in both the s-m and m-s directions (n= 3 per group per direction).

| Tissue type | Transporter inhibited |                        | Buffer                          |
|-------------|-----------------------|------------------------|---------------------------------|
|             | OCT2<br>(guanidine)   | OCTN2<br>(L-carnitine) |                                 |
| Respiratory | -                     | -                      | KRB                             |
|             | -                     | -                      | Na <sup>+</sup> free KRB buffer |
|             | +                     | -                      | KRB                             |
|             | -                     | +                      | KRB                             |
|             | -                     | +                      | Na <sup>+</sup> free KRB buffer |
| Olfactory   | -                     | -                      | KRB                             |
|             | +                     | -                      | KRB                             |
|             | -                     | +                      | KRB                             |

Note: Na<sup>+</sup> free buffers were used to study the effect of Na<sup>+</sup> on OCTN2 inhibition by L-carnitine. (+) and (-) indicates presence and absence of OCT2 and/or OCTN2 inhibitor.

### *Study groups for cimetidine transport*

The transport studies were carried out in the mucosal to the submucosal (m-s) direction, and the inhibition of cimetidine transport was carried out using pentamidine as the OCT2 inhibitor. The substrate concentrations of cimetidine used were 0.2, 0.8, 4 and 20 mM and all OCT2 inhibition studies were carried out at with 0.2 mM or 0.8 mM donor concentration of cimetidine and 50 mM pentamidine. The inhibitor concentration was 100 times greater than typical  $K_i$  values reported for pentamidine as an inhibitor of the OCT2 transporter. Samples from the receiver chamber were withdrawn at 5, 15, 30, 60, 90 and 120 min. The concentrations of cimetidine in KRB buffer were measured using a validated HPLC method with UV detection (Chapter 4). Typical TEER was measured during each study and only tissues with values  $> 100 \Omega\text{cm}^2$  were used.

### *Flux measurement and data analysis*

Amantadine flux in both the mucosal-to-submucosal ( $J_{m-s}$ ) and submucosal-to-mucosal ( $J_{s-m}$ ) directions was calculated by dividing the slope of the steady state portion of the cumulative amount of drug transported vs. time curve (Figure 5-6) by the tissue cross-sectional area,  $0.64 \text{ cm}^2$ . The slope was determined from the cumulative amount of the drug in the receiver compartment versus time plot using the linear regression function in Microsoft Excel 2007 (Microsoft Corp., Redwood City, WA). The experiments were performed under sink conditions.

The Student's t-test was performed to compare the mean flux and permeability values for amantadine or cimetidine at each concentration. The mean flux values were compared across different groups using ANOVA with Bonferroni corrections to evaluate

the effects on amantadine or cimetidine transport in the absence and presence of organic cation inhibitors. A value of  $p < 0.05$  was considered statistically significant.

The kinetic parameters,  $K_m$  and  $V_{max}$  were estimated for any observed saturable carrier mediated transport using the Michaelis–Menten equation (Equation 5-3) (GraphPadPrism 6.0; (GraphPad Software, Inc. La Jolla, CA) to describe the non-linear regression of the substrate concentration versus flux results<sup>165</sup>.

$$J = J_{max} C / (K_m + C) \quad \text{Equation 5-3}$$

$C$  = substrate concentration

$J_{max}$  = the maximal saturable transport rate

$K_m$  = half-saturation concentration

When  $C \ll K_m$ , flux varies linearly with concentration whereas, when  $C \gg K_m$ , the flux rates do not increase linearly with substrate concentration and reaches an asymptote ( $V_{max}$ ) as  $C$  approaches  $\infty$  (graphically). The maximal saturable transport occurs when there is no remaining free transporter available to additionally contribute to the transport.

## Results and Discussion

### *Amantadine transport studies*

The bovine nasal model has been used to study the metabolism of peptides in the nasal mucosa and more importantly in evaluating the role of transporter proteins such as DAT, OCT2 and PgP in the transport of small molecules across the respiratory and olfactory mucosae<sup>28,24,47</sup>. Typical TEER values recorded for the excised tissues were in the range of 100-200  $\Omega\text{cm}^2$  for the respiratory mucosa and 100-160  $\Omega\text{cm}^2$  for the olfactory mucosa and were in agreement with values reported in the literature. The nasal

mucosal tissues are quite leaky, which is the reason for such low levels of resistance. The amantadine concentrations in the receiver chambers were found to increase with time, but sink conditions were not maintained post 60 min. Sink conditions were assumed to be maintained when the concentration of the substrate in the receiver chamber remained less than 10% of the initial donor chamber concentration. Donor and receiver chamber concentrations were measured at the beginning and end of each experiment. If sink conditions were not maintained, only the data collected under the sink conditions were used in the calculation of flux. As a result, typically only the first three data points were utilized in the calculation of the flux (Figure 5-6, 5-7).

The amount of amantadine removed from the receiver chamber due to sampling was determined by calculating the amount of amantadine in the 200  $\mu$ L aliquot withdrawn at each time point. This amount was added to the calculated cumulative amount of drug transported into the receiver chamber at following time point to obtain the total amount of amantadine transported into the receiver chamber at each time.

The flux of amantadine across the olfactory and respiratory mucosae was observed to increase initially with increasing donor concentrations but reached limiting values at higher drug concentrations in both the m-s and s-m directions (Figure 5-8). This suggests some type of carrier was involved in the uptake of amantadine across the nasal mucosa. However, no statistically significant differences were observed when the m-s and s-m flux values were compared at each concentration for each tissue (except for flux across respiratory mucosa at 20  $\mu$ M donor concentration), ( $p$ -value < 0.05). This indicates that the carriers are likely to mediate the bidirectional transport of amantadine

across the nasal tissues. In addition, it also suggests absence of the effect of any efflux transporters on amantadine

transporters on amantadine

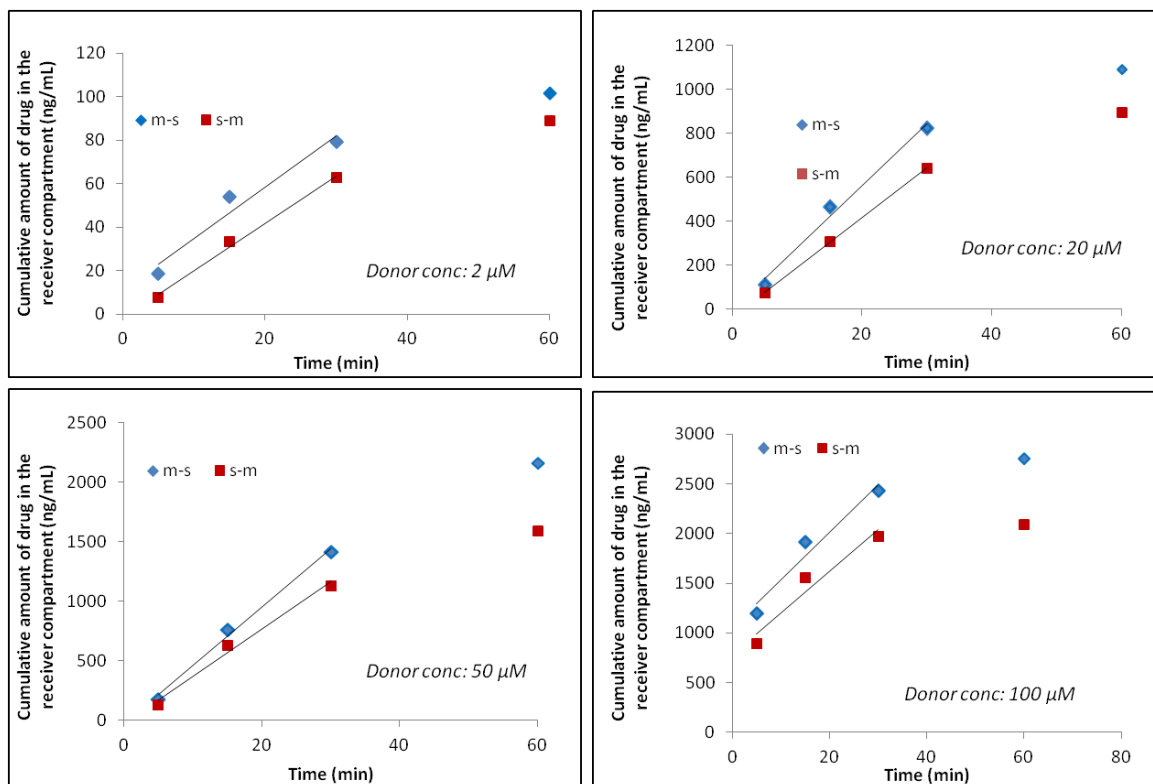


Figure 5-6: Representative plot of the cumulative amount of amantadine transported across the bovine respiratory mucosal explants as a function of time (5, 15, 30, 60 min) at 2, 20, 50 and 100 μM of amantadine donor chamber concentrations. Linear regression of the first three time points gave the equation  $y = 2.36 + 11.26x$ ,  $r^2 = 0.957$  and  $y = 2.19 - 2.20x$ ,  $r^2 = 0.994$  representing transport studies performed in m-s (mucosal to submucosal) and s-m (submucosal to mucosal) direction, respectively.

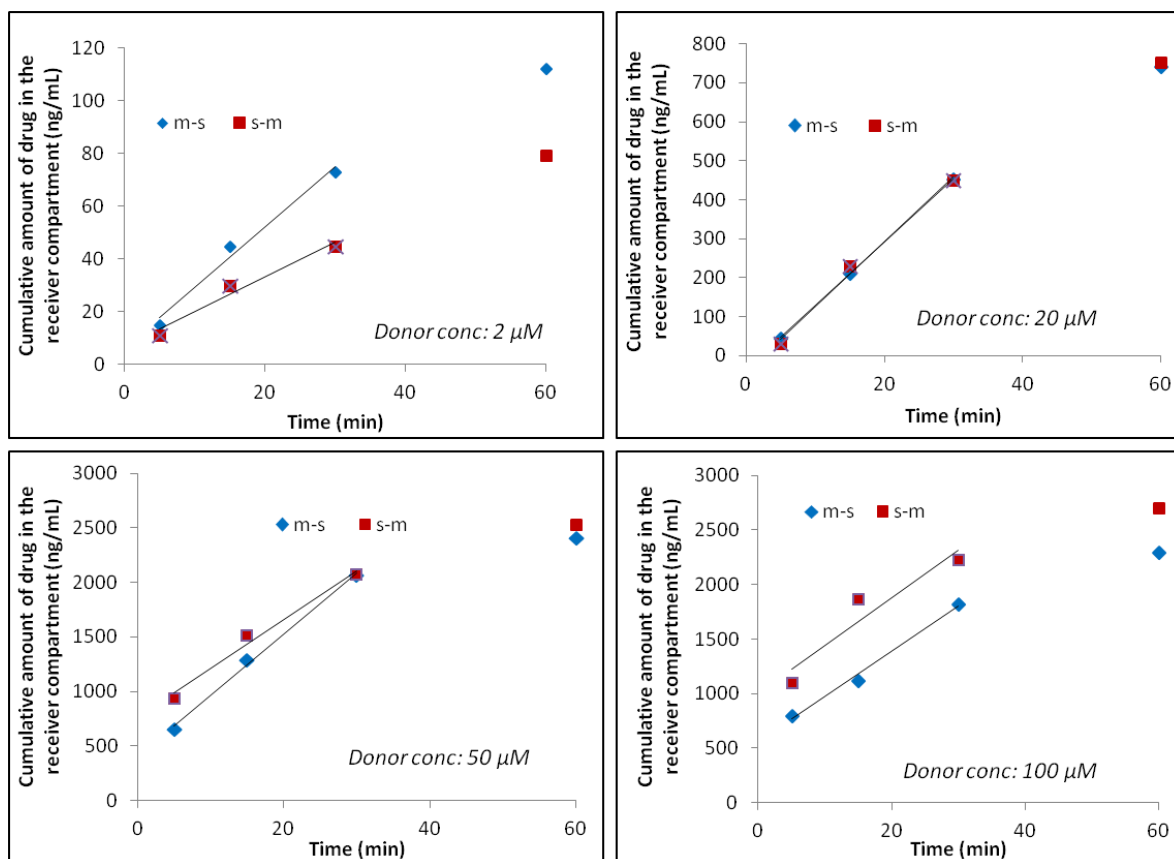


Figure 5-7: Representative plot of the cumulative amount of amantadine ( $2 \mu\text{M}=375.4 \text{ ng/mL}$ ) transported across the bovine olfactory mucosal explants as a function of time (5, 15, 30, 60 min). Linear regression of the first three time points gave the equation:  $y = 2.284 + 6.263x$ ,  $r^2 = 0.981$  and  $y = 1.193 + 8.552x$ ,  $r^2 = 0.990$  representing transport studies performed in m-s (mucosal to submucosal) and s-m (submucosal to mucosal) direction, respectively.

Since the clinically relevant direction of transport following intranasal application is in the m-s direction, the flux values at different concentrations in this direction were compared between the olfactory and respiratory tissues to give an idea regarding the relative effectiveness with which amantadine crosses these tissues. . The flux of amantadine across the respiratory mucosa was observed to be higher than across the olfactory mucosa at lower amantadine concentrations, yet at the saturating concentrations for the respiratory mucosa ( $> 50 \mu\text{M}$ ), the flux across the olfactory mucosa was higher (Figure 5-9).

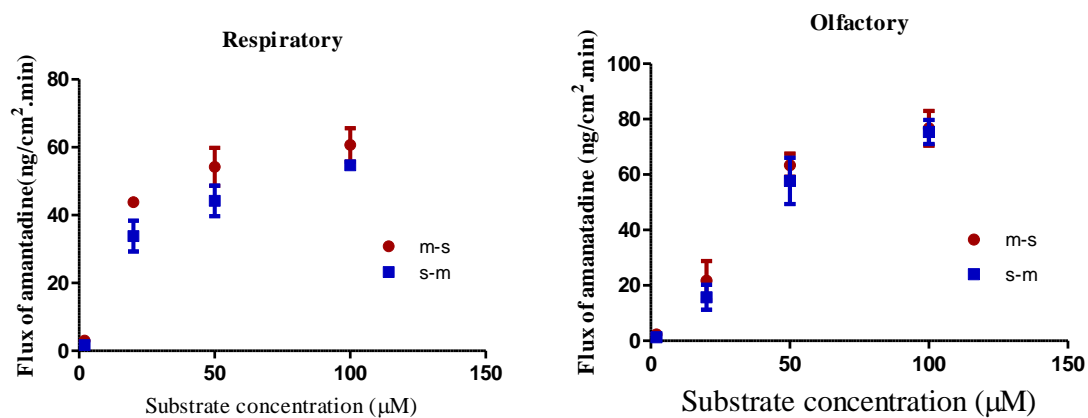


Figure 5-8: Comparison of flux values for amantadine across bovine respiratory and olfactory mucosa in the m-s and s-m direction over donor concentrations between 2-100  $\mu\text{M}$ . Results represent mean flux  $\pm$  standard deviation; n=3

Since the thickness of the respiratory mucosa is known to be greater than that of the olfactory mucosa, a correction was applied to the flux values across the respiratory mucosa by multiplying by a factor of 1.6, normalizing the flux values to an equivalent tissue thickness of olfactory tissue<sup>35</sup>. Following the correction, amantadine fluxes across the respiratory mucosa were found to be significantly higher than across the olfactory at all concentrations ( $p < 0.05$ ).

The Michaelis Menten equation was fit to the flux values in the m-s direction (with and without thickness correction) for each tissue type using GraphPad Prism 6.0 (Figure 5-10). The  $K_m$  values for the respiratory tissue ( $14.6 \pm 3.58 \mu\text{M}$ ) and the olfactory tissue ( $78.5 \pm 30.5 \mu\text{M}$ ) (Table 5-3) are in the range of the previously reported value ( $27 \mu\text{M}$ ) for the OCT2 mediated transport of amantadine<sup>133</sup>. These calculated values of  $K_m$  and  $V_{\text{max}}$  are higher than the actual values for these tissues, since the flux values have not been corrected for the passive diffusion component. The  $K_m$  and  $V_{\text{max}}$  for the thickness corrected flux values across the respiratory tissues are given in Table 5-3. These values serve as a guide to select the ideal substrate concentration for the *in vitro* organic cation transporter inhibition studies and also in determining nasal dose ranges most likely to be affected by carrier activity.



Table 5-2: Calculated amantadine flux across the olfactory and respiratory and thickness normalized respiratory mean flux values, (n=3), at 2, 20, 50 and 100 $\mu$ M donor concentrations.

| Donor concentration ( $\mu$ M) | Flux across olfactory mucosa (ng/min.cm <sup>2</sup> ) (mean $\pm$ S.D.) |                 | Flux across the respiratory mucosa (ng/min.cm <sup>2</sup> ) (mean $\pm$ S.D.) |                 | Flux across the respiratory mucosa scaled to olfactory tissue thickness (ng/min.cm <sup>2</sup> ) (mean $\pm$ S.D.) |                 |
|--------------------------------|--|-----------------|--|-----------------|---|-----------------|
|                                | $J_{m-s}$  | $J_{s-m}$       | $J_{m-s}$  | $J_{s-m}$       | $J_{m-s}$   | $J_{s-m}$       |
| 2                              | 2.30 $\pm$ 0.49  | 1.30 $\pm$ 0.22 | 3.04 $\pm$ 0.61  | 1.71 $\pm$ 0.21 | 4.87 $\pm$ 0.77   | 2.74 $\pm$ 0.34 |
| 20                             | 21.6 $\pm$ 7.1   | 15.6 $\pm$ 4.4  | 43.8 $\pm$ 1.5   | 33.8 $\pm$ 4.5  | 70.1 $\pm$ 2.4  | 54.1 $\pm$ 7.2  |
| 50                             | 63.3 $\pm$ 4.2   | 57.6 $\pm$ 8.3  | 54.2 $\pm$ 5.6   | 44.2 $\pm$ 4.4  | 86.7 $\pm$ 8.9  | 70.7 $\pm$ 7.2  |
| 100                            | 76.6 $\pm$ 6.2   | 75.3 $\pm$ 4.3  | 60.7 $\pm$ 4.9   | 54.6 $\pm$ 1.2  | 97.1 $\pm$ 7.9  | 87.5 $\pm$ 1.9  |

Note: Results are represented as mean flux  $\pm$  standard deviation (n=3).

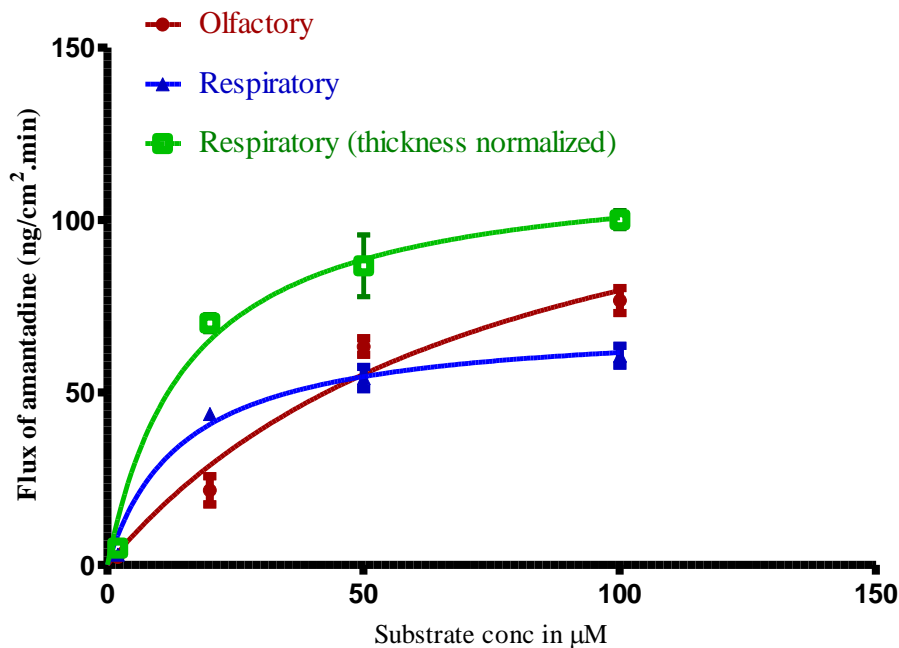


Figure 5-9: Figure represents comparison of amantadine flux across bovine respiratory and olfactory mucosa in the m-s direction. Curve represents fitting of the Michaelis-Menten equation to the respiratory, olfactory and thickness normalized respiratory mean flux values, (n=3), at 2, 20, 50 and 100µM donor concentrations. Calculated transport kinetic parameters are shown in Table 5-3. Thickness normalized respiratory flux values represent respiratory flux values normalized to an olfactory equivalent thickness by multiplying by a factor of 1.6. Results are represented as mean flux  $\pm$  standard deviation; n=3

Table 5-3: Kinetic parameters of the carrier-mediated transport of amantadine calculated from fitting the Michaelis-Menten equation to the flux values for each tissue type.

| Best-fit values                      | Olfactory        | Respiratory    | Respiratory thickness |
|--------------------------------------|------------------|----------------|-----------------------|
| $J_{\max}$ (ng/cm <sup>2</sup> .min) | 142.2 $\pm$ 29.2 | 70.6 $\pm$ 4.4 | 116.5 $\pm$ 6.6       |
| $K_m$ (µM)                           | 78.5 $\pm$ 30.3  | 14.6 $\pm$ 3.5 | 15.7 $\pm$ 3.3        |
| $r^2$                                | 0.946            | 0.961          | 0.961                 |

Note:  $J_{\max}$  and  $K_m$  values are expressed as mean  $\pm$  standard error.

*Amantadine transporter inhibition studies*

Both PCR and immunohistochemistry studies confirmed the presence of the OCT2 transporter in bovine nasal tissues. To further evaluate the activity of OCT2 in these tissues, transport studies using amantadine (2  $\mu$ M donor concentrations) were performed in the presence of an OCT2 inhibitor, guanidine (2 mM). The donor concentration was chosen such that it was below the calculated  $K_m$  values for both the respiratory and olfactory tissues. Care was taken to choose a specific inhibitor because, like substrates, inhibitor compounds are also known to be polyspecific within the organic cation transporter classes<sup>166</sup>.

A statistically significant decrease in the flux of amantadine in both the s-m and m-s direction across the olfactory mucosa was observed in the presence of 2mM guanidine ( $p < 0.05$ ), thus further confirming the role of OCT2 in the uptake of amantadine (Figure 5-10). The degree of inhibition was observed to be ~40-50%. However, guanidine was unable to affect any significant inhibition in the m-s transport of amantadine across the respiratory mucosa, although a statistically significant inhibition (~35%) was observed in the s-m direction. These results suggest that additional transporter(s) may be involved in the uptake of amantadine in the m-s direction, since saturable flux was observed in this direction with increasing donor concentrations of amantadine.

From these results, attempts were made to identify synergistic transporter(s) that may play a role in the uptake of amantadine across the respiratory tissues. PCR results identified the presence of both OCTN1 and OCTN2 as additional organic cation transporters in the bovine respiratory and olfactory tissues. However, current literature

contains no information about amantadine as a substrate for these transporters. Therefore, it was postulated that OCTN1 or OCTN2 could both be likely transporter involved in amantadine uptake.

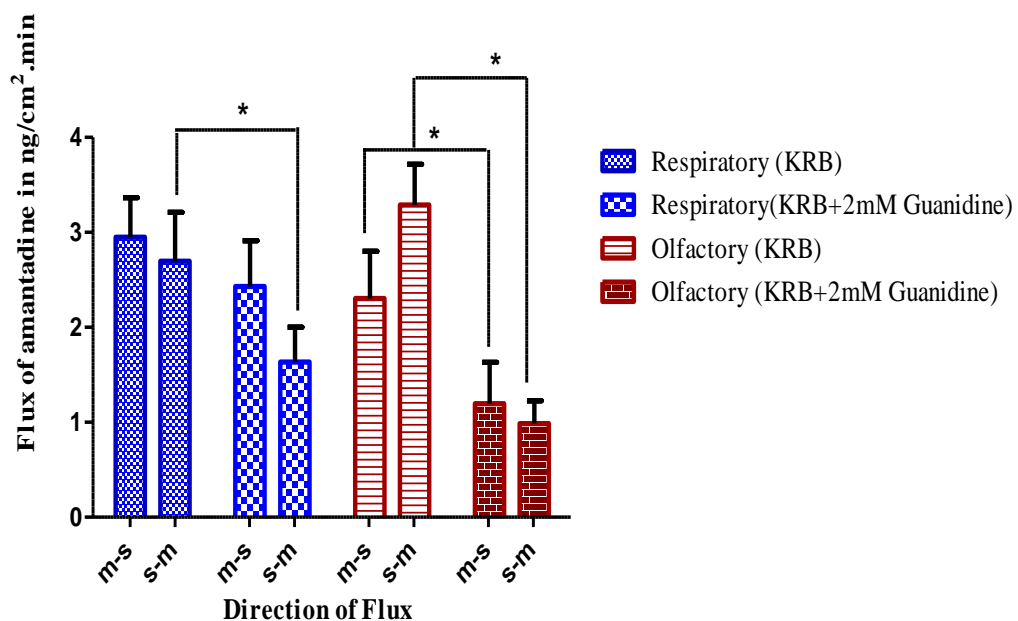


Figure 5-10: Comparison of flux values for amantadine (2  $\mu$ M) across bovine respiratory and olfactory mucosa in the m-s and s-m direction. \* indicates statistically significant decrease in flux of amantadine following OCT2 inhibition in the respiratory and olfactory tissues ( $p < 0.05$ ) Results represent mean flux  $\pm$  standard deviation;  $n=3$

Consequently, transport studies were performed across respiratory explants, using L-carnitine (50  $\mu$ M) as a competitive inhibitor for OCTN2, both in the absence and presence of sodium. No significant differences were observed in the amantadine flux values in the presence or absence of sodium, indicating that any carrier-mediated transport of amantadine across the tissue was sodium independent. Statistically significant inhibition in the transport of amantadine in the m-s and s-m directions across the respiratory mucosa was observed with L-carnitine in the presence of  $\text{Na}^+$  ( $p < 0.05$ ). A reduction in amantadine flux values across the tissues was also observed in both directions (m-s and s-m) with L-carnitine in the absence of sodium, but the differences were found to be statistically significant only in the s-m direction (Figure 5-11). Although a significant reduction in the flux of amantadine in the s-m direction was observed with L-carnitine in both the presence and absence of sodium, the degree of inhibition was significantly higher in the presence of sodium. The small reduction in amantadine flux in the s-m direction observed with L-carnitine in the absence of sodium could be the result of the action of  $\text{Na}^+/\text{K}^+$  ATPase. The  $\text{Na}^+/\text{K}^+$  ATPase actively transport three  $\text{Na}^+$  ions out of the cell in exchange for two  $\text{K}^+$  ions pumped into the cell. The sodium gradient generated by the  $\text{Na}^+/\text{K}^+$  ATPase provides the primary energy for uptake and extrusion of a variety of solutes by epithelial cells and is crucial for the efficient functioning of other  $\text{Na}^+$ -coupled transport systems<sup>167</sup>. Therefore, even though sodium is absent in the transport medium, some degree of inhibition of amantadine transport can be achieved during the time course of the experiment by L-carnitine inhibition of OCTN2 with the utilization of tissue sodium stores. These results clearly indicate that the L-carnitine inhibition of amantadine transport in the m-s direction is dependent on the availability of

sodium in the transport medium. The dependence of L-carnitine inhibition of amantadine transport on  $\text{Na}^+$  suggests that OCTN2 is an additional transporter for amantadine across the respiratory mucosa.

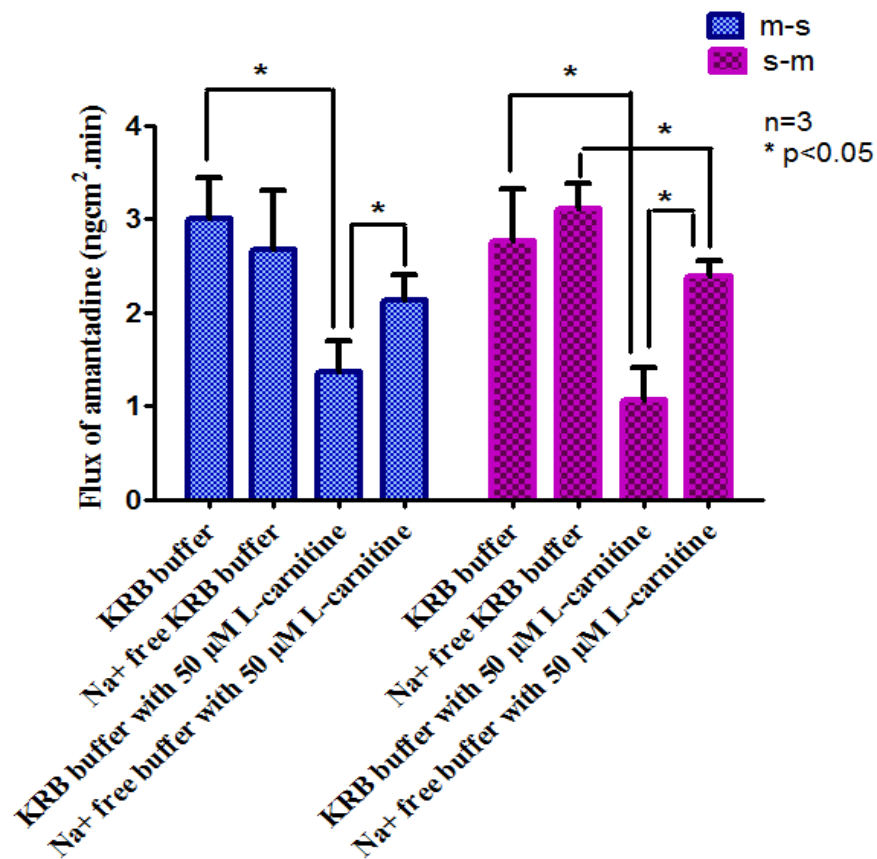


Figure 5-11: Comparison of flux values for amantadine ( $2 \mu\text{M}$ ) across bovine respiratory tissue in the m-s and s-m directions in KRB buffer and a  $\text{Na}^+$  free buffer in the presence or absence of the OCTN2 inhibitor, L-carnitine. \* indicates statistically significant difference in flux of amantadine following OCTN2 inhibition in the respiratory tissues ( $p < 0.05$ ). Results represent mean flux  $\pm$  standard deviation;  $n=3$ .

In contrast, the lack of OCTN2 inhibition in the olfactory tissues by L-carnitine indicates that amantadine flux across the olfactory tissues is relatively independent of OCTN2 activity and, instead, OCT2 play a greater role in amantadine transport in this tissue (Figure 5-12). These results indicate that the transport of amantadine across the olfactory mucosa is primarily mediated by the OCT2 transporter. On the other hand, the transport of the drug across the respiratory tissue is mediated by both OCT2 and OCTN2 transporters and the OCTN2 mediated transport of amantadine was independent of sodium.

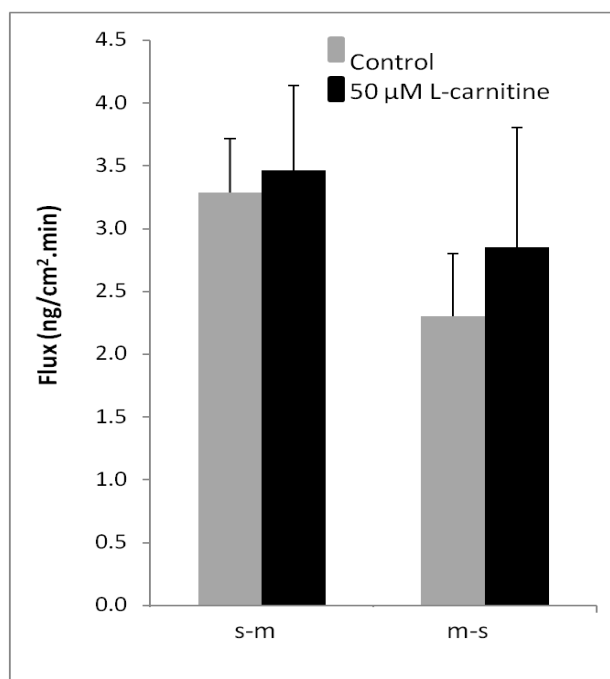


Figure 5-12: Comparison of flux values for amantadine across bovine olfactory tissue in the m-s and s-m direction in KRB buffer in the presence or absence of the OCTN2 inhibitor, L-carnitine. No statistically significant inhibition of amantadine flux across the olfactory tissue was observed. ( $p < 0.05$ ). Results represent mean flux  $\pm$  standard deviation;  $n=3$ .



### *Cimetidine transport studies*

The range of cimetidine donor concentrations (0.2-20 mM) studied was higher than the typical OCT2  $K_m$  (50-150  $\mu$ M) values for OCT2 reported in the literature<sup>140</sup>. Donor concentrations of cimetidine < 0.2mM resulted in receiver concentrations of the compound below the detection limit of the analytical method at the initial (< 60 min) time points, and studies at concentrations > 20 mM were limited by the maximum possible solubility of the compound (24 mM). At the very high donor concentrations used in the study, the concentration gradient driving passive diffusion will be very large, and, together with potential transporter saturation, the contribution of transporter-mediated uptake may not be apparent. However, the lowest donor concentration used in this study (0.2 mM) is close to the reported  $K_m$  values.

To assess whether an OCT2-mediated transport of cimetidine occurs across the nasal tissues, the effect of donor concentration on the flux of cimetidine across both the olfactory and respiratory tissues was investigated. *In vitro* transport studies across each tissue in the m-s (mucosal-submucosal) using donor concentrations of 0.2, 0.8, 4 and 20mM were carried out. The amount of cimetidine present in the receiver chamber was measured at each time point using a validated HPLC method (Chapter 4), and the cumulative amounts of cimetidine transported into the receiver chamber at each cimetidine donor concentration, as a function of time are presented in Figure 5-13, and 5-14. Sink conditions were observed to be maintained throughout the duration of the study.

Cimetidine flux values at each donor concentration were calculated from the slopes of linear regressions of the data points for the cumulative amount transported vs.

time graphs (Figure 5-14 and 5-15). The flux of cimetidine across the olfactory and respiratory mucosa was observed to increase with increasing donor concentrations and was not observed to be saturable within the range of donor concentrations studied (Figure 5-15). At the two low donor concentration studied (0.2 and 0.8 mM), the flux value of cimetidine across the respiratory and the olfactory tissue were not significantly different from each other, whereas at increasing donor concentrations (4mM and 20mM), the flux across the olfactory tissues was observed to be higher than across the respiratory tissues ( $p < 0.05$ ). It is important understand if this observed differences was the result of mechanistic differences or merely the result of thickness differences between the two tissues. The flux values of the respiratory tissue were normalized to an equivalent thickness of the olfactory tissue by multiplying by a factor of 1.6, and the results are shown in Figure 5-15. Following correction for differences in tissue thickness, cimetidine fluxes across the olfactory and respiratory tissues were equal in the m-s direction at all the donor concentrations (Table 5-4).

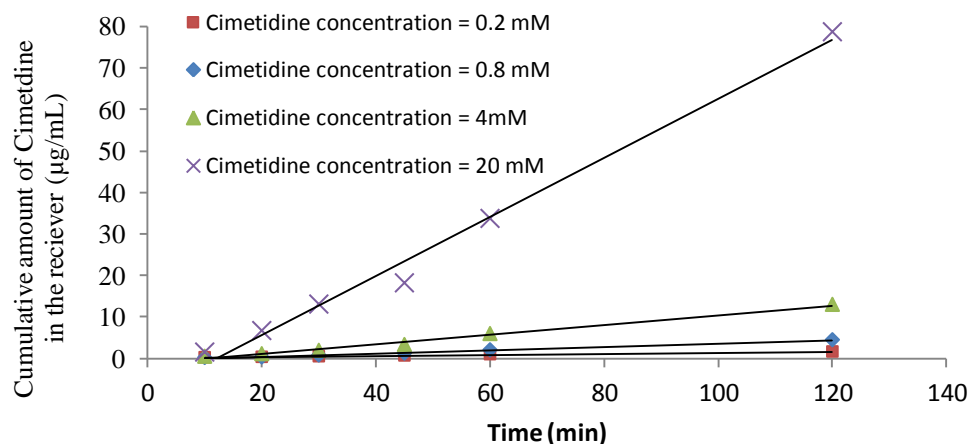


Figure 5-13: Representative plots of cumulative amount of cimetidine transported across a bovine respiratory mucosa as a function of time (5, 15, 30, 60, 90 and 120 min) in the m-s direction, at donor concentrations 0.2 and 0.8, 4 and 20 mM.

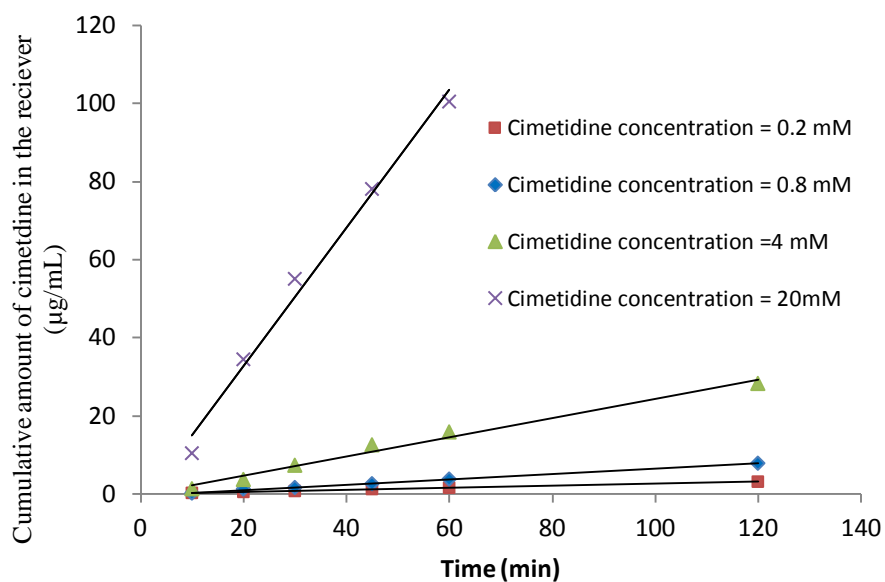


Figure 5-14: Representative plots of cumulative amount of cimetidine transported across the bovine olfactory mucosa as a function of time (5, 15, 30, 60, 90 and 120 min) in the m-s direction, at donor cimetidine concentrations 0.2 and 0.8, 4 and 20 mM.

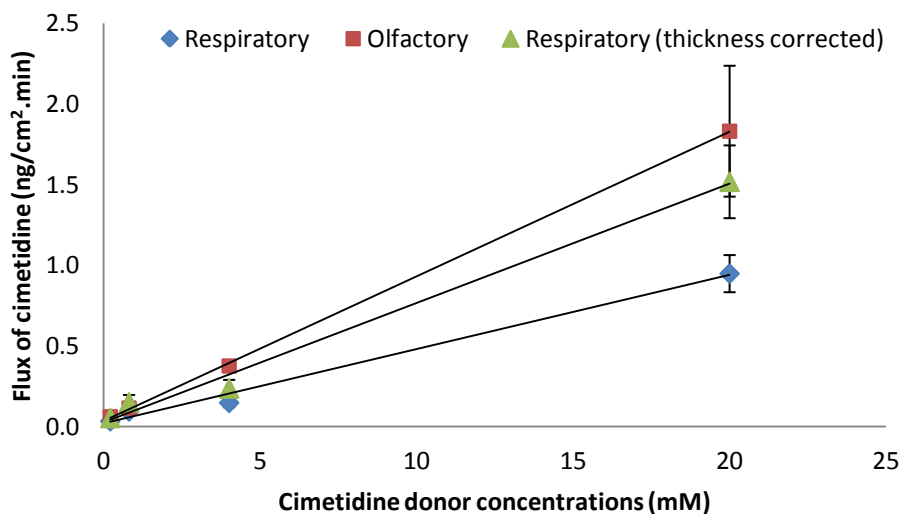


Figure 5-15: Cimetidine transport across bovine respiratory and olfactory mucosa in the m-s direction. Flux was calculated from transport studies carried out for 120 min. Linear regression of the mean flux data gave  $r^2 = 0.992$  for respiratory and 0.999 for olfactory and 0.991 for the thickness corrected respiratory. Data points represent mean flux  $\pm$  standard deviation;  $n=4$

Table 5- 4: Calculated cimetidine flux across the olfactory and respiratory tissues (n=3)

| Donor concentration (mM) | Flux across olfactory mucosa ( $\mu\text{g}/\text{min}\cdot\text{cm}^2$ ) (mean $\pm$ S.D.) | Flux across the respiratory mucosa ( $\mu\text{g}/\text{min}\cdot\text{cm}^2$ ) (mean $\pm$ S.D.) | Flux across the respiratory mucosa scaled to olfactory tissue thickness ( $\mu\text{g}/\text{min}\cdot\text{cm}^2$ ) (mean $\pm$ S.D.) |
|--------------------------|---|---|--|
|                          | $J_{m-s}$   | $J_{m-s}$   | $J_{m-s}$  |
| 0.2                      | $0.06 \pm 0.01$   | $0.03 \pm 0.06$   | $0.05 \pm 0.04$  |
| 0.8                      | $0.12 \pm 0.01$   | $0.09 \pm 0.02$   | $0.15 \pm 0.05$  |
| 4                        | $0.38 \pm 0.01$   | $0.15 \pm 0.03$   | $0.24 \pm 0.05$  |
| 20                       | $1.8 \pm 0.4$   | $0.95 \pm 0.12$   | $1.52 \pm 0.22$  |

Although, concentration was observed to have linear dependence on flux of cimetidine, the permeability coefficient ( $P_e$ ) was found to dependent on the donor concentration for both tissues. The effective permeability coefficient ( $P_e$ ) is the flux value normalized by the concentration gradient and is calculated by dividing the flux by the initial donor concentration for sink conditions (Equation 5-2). The permeability coefficient ( $P_e$ ) for passive diffusion is known to be independent of the concentration of the drug but a comparison of  $P_e$  values across the olfactory and respiratory tissues showed a decrease in their values with increasing donor concentrations of cimetidine. The  $P_e$  values reached a limiting value at the two highest donor concentrations studied. When each of the  $P_e$  values for the respiratory tissues was normalized to the equivalent thickness for the olfactory tissue (Figure 5-16), the thickness corrected  $P_e$  values for the olfactory tissue were comparable at all donor concentrations except at the lowest concentration studied (0.2 mM). The concentration dependence of  $P_e$  values indicates that passive diffusion may not be the only mechanism involved in the transport of cimetidine across the nasal mucosa, and this is particularly noticeable at low donor concentrations.

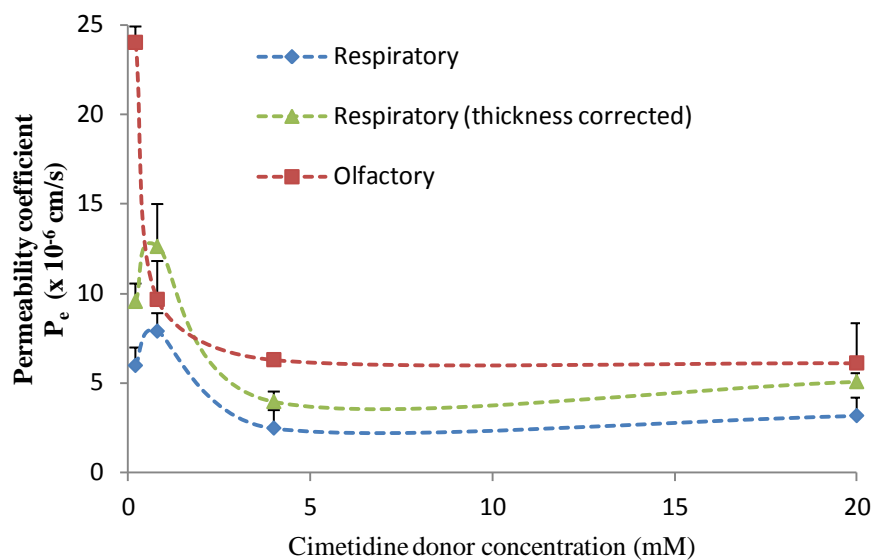


Figure 5-16: Comparison of thickness normalized effective permeability coefficients ( $P_e$ ) for cimetidine flux across bovine nasal (respiratory and olfactory) mucosa in the m-s direction at different cimetidine donor concentrations. Respiratory  $P_e$  values were normalized to the equivalent thickness of the olfactory tissue by multiplying by a factor of 1.6. Results are represented as mean  $P_e \pm$  standard error;  $n=4$ .

*Cimetidine transport inhibition studies*

As concluded in Chapter 3, both PCR and immunohistochemistry studies confirmed the presence of the OCT2 transporter in bovine nasal tissues. Additionally, cimetidine is a well established OCT2 substrate. Taking into account these results it was hypothesized that a component of the cimetidine's permeability is contributed by the OCT2 transporter.

Guanidine was successfully used to inhibit the OCT2 transport of amantadine in the nasal tissues, but guanidine did not inhibit cimetidine transport in LLCPK (pig kidney) cells which suggests that there are either independent binding site for the two compounds and/or cimetidine is a higher affinity substrate for the OCT2 transporter<sup>168</sup>. Therefore, pentamidine (50mM) was chosen rather than guanidine in these studies.

A statistically significant inhibition of the flux of cimetidine in the s-m direction across the olfactory mucosa was observed ( $p < 0.05$ ) in the presence of 50 mM pentamidine (Figure 5-17). The degree of inhibition observed was ~ 60-70% and 40-45% at 0.2 mM and 0.8 mM cimetidine donor concentrations, respectively. These results are consistent with the results of the thickness corrected  $P_e$  values, where mechanisms in addition to passive diffusion were most apparent at lower cimetidine donor concentrations with the maximum values being observed for olfactory tissues at 0.2 mM. However, pentamidine was unable to affect any significant inhibition in the m-s transport of cimetidine across the respiratory mucosa (Figure 5-18). This suggests that the expression of the transporter is lower in the respiratory than the olfactory and, as a result, the carriers get saturated at lower concentrations in the respiratory tissues.

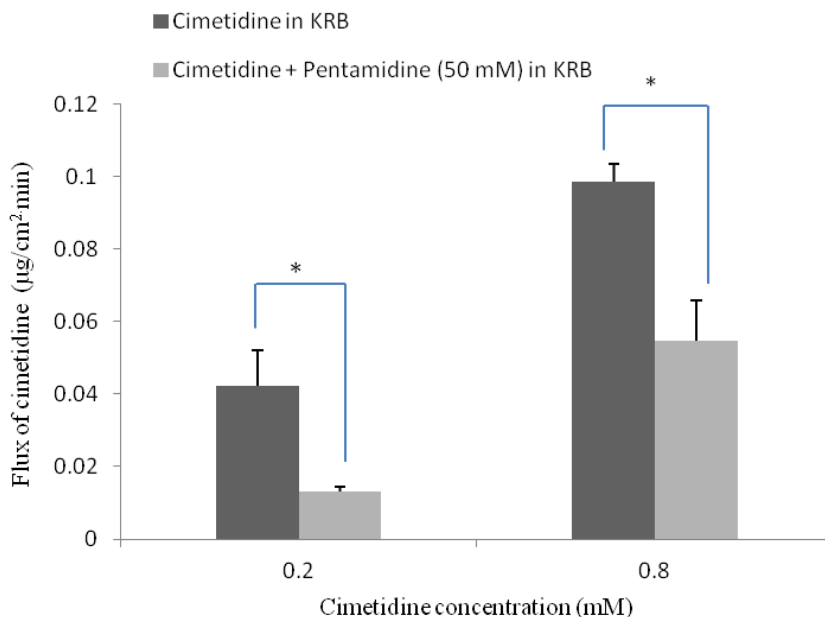


Figure 5-17: Effect of pentamidine (OCT2 inhibitor; 50 mM) on cimetidine flux across the olfactory mucosa in s-m direction. Inhibition in cimetidine flux was observed at both the concentrations. \* indicates statistically significant difference in flux of cimetidine following OCT2 inhibition ( $p < 0.05$ ). Results represent mean flux  $\pm$  standard deviation;  $n=3$ .

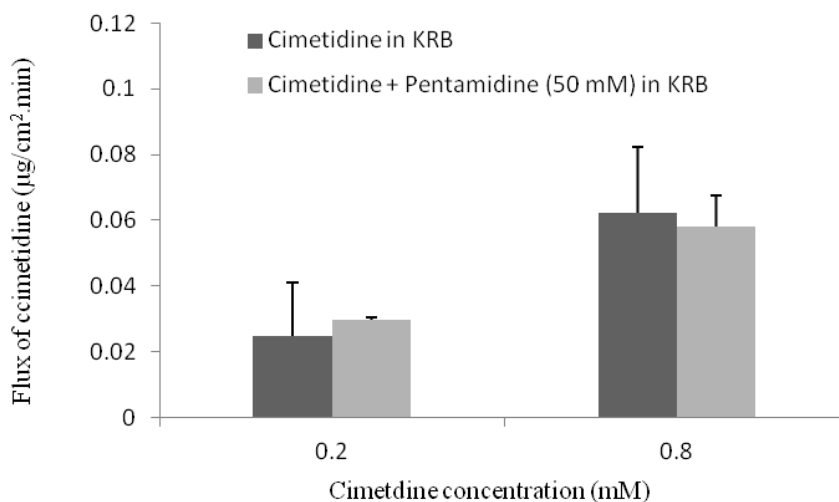


Figure 5-18: Effect of pentamidine (OCT2 inhibitor; 50 mM) on cimetidine flux across the respiratory mucosa in s-m direction. Inhibition in cimetidine flux was not observed at both the concentrations. Results represent mean flux  $\pm$  standard deviation;  $n=3$ .



### Conclusion

The *in vitro* studies conducted demonstrate that the transport of amantadine across the olfactory mucosa is mediated by OCT2 in both m-s and s-m directions, however, OCT2 does not appear to have as significant of a role in the transport of amantadine across the respiratory mucosa in the m-s direction, contrary to our expectation. Transport across the respiratory mucosa appears to be by a combination of both OCT2 and OCTN2. These results were also supported ELISA results where OCT2 expression was found to be significantly lower in the respiratory tissues when compared to the olfactory tissues. The  $K_m$  value of amantadine for OCT2 was observed to be within the range of the values previously reported in the literature, and although similar OCTN2 expression levels were observed in both the respiratory and the olfactory tissues, OCTN2 was found to significantly affect amantadine transport only across the respiratory tissues. Additionally, the transport of amantadine by OCTN2 was observed to be sodium independent.

The results from the *in vitro* transport studies of cimetidine demonstrate that the transport of the drug across the olfactory mucosa is mediated by the OCT2 transporter in the m-s direction; however OCT2 did not appear to have a role in the transport of cimetidine across the respiratory mucosa in this direction.

These *in vitro* results demonstrate that OCT2 is a key transporter for the permeation of the substrates amantadine and cimetidine across the olfactory mucosa. The enhanced transport across the olfactory mucosa may enhance the brain uptake of these drugs through the olfactory pathway following an intranasal dose.

CHAPTER 6  
THE ROLE OF ORGANIC CATION TRANSPORTERS (OCT2 AND OCTN2) IN  
THE NOSE TO BRAIN DISTRIBUTION OF AMANTADINE IN RATS

*Pharmacokinetics of amantadine*

Amantadine is well absorbed from the gastrointestinal tract and is available only as oral formulations. The drug has a large volume of distribution after i.v. and oral administration (6-10.4 L/kg) in healthy human subjects. Its plasma protein binding has been reported to be 40% and a terminal half-life of 9 to 15 hr has been determined in humans. Elimination is primarily by renal clearance by both glomerular filtration and tubular secretion<sup>169,170</sup>. Amantadine has also been measured in the nasal secretions of humans following single 200 mg oral dosing, which may explain some of the effectiveness of amantadine towards influenza A virus infections. Amantadine was found in nasal mucus at  $31 \pm 33\%$ ,  $59 \pm 61\%$  and  $95 \pm 86\%$  of the corresponding plasma amantadine concentrations at 1, 4 and 8 hours after dosing, respectively<sup>171</sup>.

*Brain penetration of amantadine*

Owing to the adamantane moiety, unionized amantadine is very lipid soluble and is able to distribute across tissues and transport across the blood brain barrier<sup>172</sup>. However, CSF measurements demonstrate the somewhat restricted entry of the drug into the brain from the blood, with only ~54% of the free drug from the plasma being detected in the CSF. Amantadine has been shown to cross the BBB using a saturable transport system in rats, which was inhibited by L-carnitine<sup>116</sup>. Additionally, polyspecific OCT2 present in human neurons has also been reported to mediate the transport of amantadine<sup>133</sup>. However, high brain tissue accumulation of the drug has been measured in

postmortem human brain in chronic users. The total brain tissue concentrations have been found to be almost 30 and 10 fold higher than that in the serum or CSF in humans and rats, respectively. The rate of clearance of the drug from the brain is very slow, with an estimated elimination half-life from brain being ~ 6.5 days; this is significantly longer than the plasma elimination half-life<sup>173</sup>. The high storage capacity of amantadine in the brain has been attributed to its lysosomotropic properties, where the drug is trapped by protonation in acidic intracellular compartments leading to its slow accumulation<sup>174</sup>. The low unbound concentrations of amantadine measured in CSF compared to free plasma concentration also suggest the presence of significant brain tissue binding<sup>175, 176</sup>.

#### *Microdialysis as a sampling technique*

The quantitative determination of brain disposition is commonly performed using one of the two methods. The first involves the direct collection of brain tissues or samples from a single animal per experimental time point to measure the total brain concentration. The second method involves the evaluation of CSF concentrations by direct lumbar puncture or via a cannula placed into the cistern magna. The former has the drawback of requiring the use of a large number of animals, and where the brain tissue samples are homogenized, the resulting concentrations in brain homogenates do not reflect the concentrations at any single site but rather reflect an average concentration of several compartments depending on how the homogenates were prepared and the method of extraction of the drug. The evaluation of CSF is associated with drawbacks such as contamination with blood and limited CSF volume available for sampling. Furthermore, CSF may or may not reflect the brain concentrations of a drug and depends on the clearance mechanism of the drug from the brain. Additionally, CSF sampling cannot

distinguish any regional concentration gradients within the brain <sup>177-178</sup>. Both these methods have significant limitations for the adequate temporal resolution to characterize drug distribution patterns in or into the brain.

Other alternate methods to measure *in vivo* drug concentrations non-invasively in the brain involve the use of analyte specific instruments, where the most popular of these include positron emission tomography (PET) and magnetic resonance imaging (MRI). PET scanning requires production of special isotopes (<sup>11</sup>C, <sup>13</sup>N, <sup>15</sup>O, <sup>18</sup>F) with extremely short half-lives. Similarly, magnetic resonance imaging uses <sup>1</sup>H or other isotopes (<sup>13</sup>C, <sup>15</sup>N, <sup>19</sup>F, <sup>31</sup>P) to create an image but require very high concentrations for detection <sup>179</sup>. Fluorescence imaging has also been used for non-invasive measurements in conjunction with near-IR tags or with enzyme substrates that become fluorescent when cleaved <sup>180</sup>. While these techniques hold significant promise for some areas of clinical medicine, such as oncology, they are quite limited with respect to the range of analytes that can be detected. Therefore, another alternate sampling technique, microdialysis, was selected for the *in vivo* studies described in this work.

Table 6-1: A list of the advantages and disadvantages associated with the use of microdialysis as a technique for sampling the brain tissue ECF (extra cellular fluid) concentrations <sup>181</sup>.

| <b>Advantages</b>                       | <b>Limitations</b>                      |
|---|---|
| continuous sampling without fluid loss  | requires sensitive analytical methods   |
| use of freely moving subjects           | tissue reactions on probe implantation  |
| direct sampling from multiple biophases | low solubility drugs cannot be analyzed |
| protein-free sample                     | probe recovery must be quantified       |

Microdialysis directly samples the unbound concentration of a drug from the extracellular fluid (ECF) surrounding the tissue of interest, without any fluid loss. Microdialysis sampling is a well-known *in vivo* collection method for low molecular weight hydrophilic analytes. The major advantage of this technique is the level of temporal and spatial resolution that can be achieved, as it allows for the monitoring of local concentrations at specific sites in the brain (or other tissues) which makes it an attractive tool for pharmacokinetic research<sup>182-183</sup>.

A microdialysis system consists of a hollow probe that is made up of a semipermeable dialysis membrane at the tip of the probe (Figure 6-1).

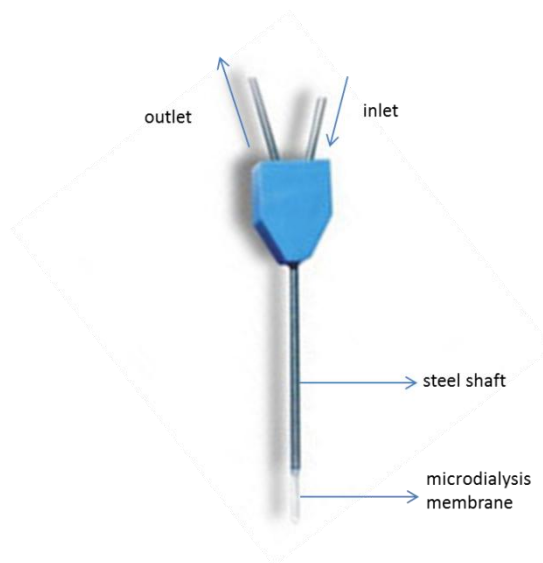


Figure 6-1: A microdialysis probe showing its functional segments.

The probe is constantly perfused at a very low flow rate, by a fluid equivalent in ionic strength, osmotic pressure and pH composition, to that of the ECF (extracellular fluid) around the tissue of interest. Free exchange of solute occurs across the semipermeable membrane along the concentration gradient.

Theoretically, when used in the sampling mode, the concentration of the analyte of interest in the dialysate exactly represents the concentration in the periprobe fluid or the tissue (Figure 6-2). Practically, this equilibrium is never achieved due to the constant flow of fresh perfusate through the probe, and therefore, only a fraction of the tissue concentration is recovered in the dialysate during its pass through the probe<sup>184</sup>. As a result, it is important to perform a calibration for the *in vivo* recovery from the probe in the range of concentrations of analyte to be recovered. This recovery can be used as a correction to the measured dialysate concentration to provide more accurate tissue concentrations following microdialysis.

The ratio between the concentration of the drug in the dialysate and the concentration in the periprobe fluid is called the relative recovery. Some of the major factors that affect the relative recovery of an analyte are the molecular weight cut-off of the dialysis membrane, dialysate flow rate, concentration gradient across the dialysis membrane and properties of the analyte<sup>185</sup>. It is a common practice in microdialysis studies for probes to be calibrated using a bulk drug solution to simulate the *in vivo* sink conditions, and to use these *in vitro* recovery values to estimate *in vivo* extracellular concentrations. However, a number of physiologic and tissue factors, such as effective diffusion of the drug through the extracellular fluid of a tissue, uptake into cells,

metabolic conversion rate, active transport across cell membranes, extent of tissue vascularization and blood flow will affect the *in vivo* recovery value<sup>186</sup>.

Microdialysis allows for the simultaneous sampling of the drug from more than one area of interest in the brain. In these studies, the estimation of the concentrations of the drug in both the olfactory bulb and another area in the brain (striatum) that is spatially resolved from the olfactory bulb but in close proximity to the CSF-containing spaces, was desired and microdialysis offered a powerful capability to obtain multiple samples over a relevant time frame for drug distribution in the brain. Brain microdialysis has been used to study distribution of compounds in different regions of the brain following intranasal administration of a number of compounds. Yang *et al.* used this sampling technique to evaluate the brain distribution of stavudine following intranasal and intravenous administration in rats<sup>187</sup>. Microdialysis was performed in freely moving rats to study the delivery of <sup>125</sup>I-cobrotoxin to the brain after intranasal administration<sup>188</sup>. Similarly, Bechgaard and co-workers used microdialysis to examine nasal drug delivery and olfactory absorption of lidocaine in rats<sup>189</sup>. Singh and co-workers used microdialysis in anesthetized rats to investigate the delivery of melatonin from a polymeric gel suspension to brain via the nasal route<sup>190</sup>. Microdialysis also finds its application in the investigation of pharmacokinetic-pharmacodynamic evaluation of CNS drugs as it can gather the unique combination of drug and biomarker levels simultaneously.

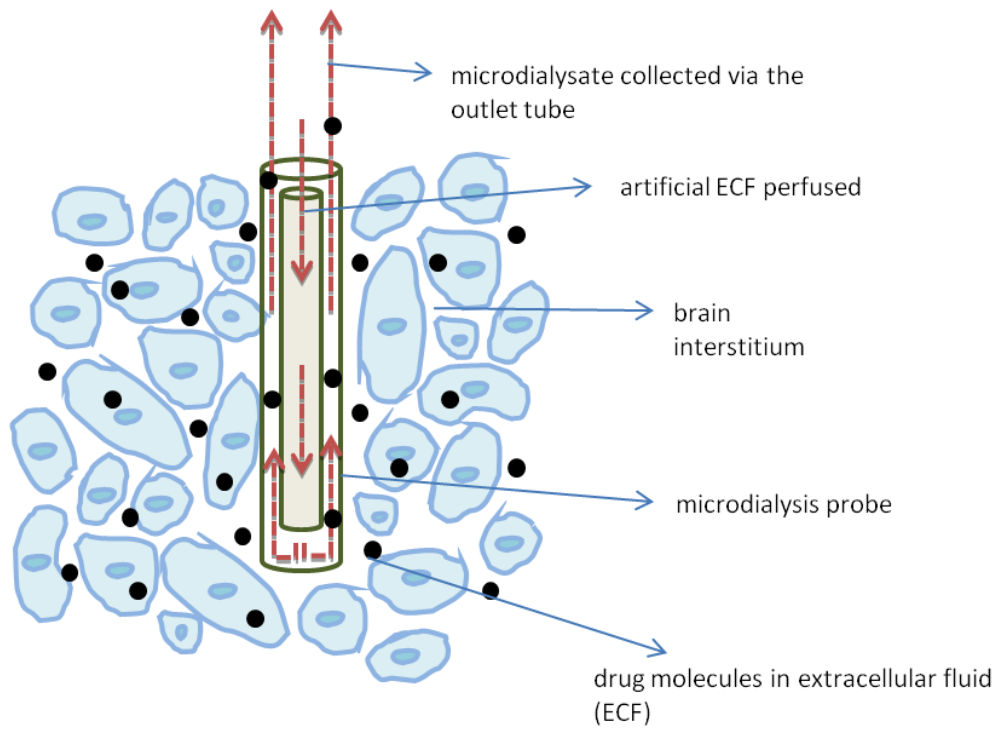


Figure 6-2: A schematic representation of the operation of the microdialysis probe, illustrating the net diffusion of the analyte of interest (black circles) into the dialysate within the probe.



*Brain partitioning coefficient ( $K_{p,brain}$ )*

The ( $K_{p,brain}$ ) provides a simple, mechanism-independent alternative for assessing the CNS exposure of the drugs.  $K_{p,brain}$  is a parameter that describes the tissue partition coefficients between brain and another compartment at the distribution equilibrium. Thus the brain/plasma ratio of unbound drug concentrations, known as  $K_{p,brain}$  provides a measure of the extent of BBB permeability, where the brain exposure has been normalized to systemic exposure<sup>195</sup>. Thus  $K_{p,brain}$  is calculated as:

$$K_{p,brain} = (AUC_{brain}/AUC_{plasma}) \quad \text{Equation 6-1}$$

*AUC<sub>brain</sub>: area under the brain concentration time curve*

*AUC<sub>plasma</sub>: area under the plasma concentration time curve*

But  $K_{p,brain}$  is inherently a time dependent parameter and using AUC values fails to take into account this time dependence. Therefore, practically  $K_{p,brain}$ , can be calculated as follows for each time point.

$$K_{p,brain} = (C_{brain}/C_{plasma}) \quad \text{Equation 6-2}$$

*C<sub>brain</sub>: concentration of free (unbound) drug in the brain.*

*C<sub>plasma</sub>: concentration of free (unbound) drug in the plasma.*

For drugs having limited BBB permeability, the entire mass of drug initially exists in the systemic circulation and the ratio,  $K_{p,brain}$ , increases from zero with time as the drug equilibrates between the two compartments. The time at which the substrate concentrations in brain and blood begin to change in parallel is referred to as the time of brain-to-blood distribution equilibrium. When brain tissue concentrations and total plasma concentrations are used in the determination of  $K_{p,brain}$ , a high brain/plasma ratio

may or may not signify high BBB permeability. It may also be the result of a high level of non-specific binding to brain tissue or low clearance of the drug from the brain. A low brain/plasma ratio can occur in the absence of non-specific binding, and neither is an indication of free drug exposure in the brain. Thus, using the free drug concentration in the brain is a more sound strategy for comparing relative CNS exposure<sup>191,192</sup>.

### Materials

Substrates and inhibitors: Amantadine hydrochloride, guanidine hydrochloride and L-carnitine hydrochloride were all purchased from Sigma Chemical (St Louis, MO).

Anesthesia: Ketaset<sup>CIII</sup> (ketamine hydrochloride USP, 100mg/mL) was from Fort Dodge animal health (Fort Dodge, IA); Anased<sup>®</sup> (Xylazine, 100mg/mL) was from Lloyd Laboratories (Shenandoah, IA); Carbocaine<sup>®</sup> (2% mepivacaine hydrochloride injection, USP) and normal saline (bacteriostatic 0.9% sodium chloride injection USP) were from Hospira (Lake Forest, IL) and heparin sodium injection USP, was manufactured by APP Pharmaceuticals LLC (Skokie, IL).

Microdialysis: A CMA 402 syringe pump with accessory kit, CMA 12 guide cannula, CMA 12 elite microdialysis with polyarylethersulphone (PAES) membrane, (MWCO 20K; membrane diameter 0.5mm, membrane length 2mm, shaft diameter 0.64 mm, shaft length 14mm), dummy probe and anchor screws were purchased from CMA Microdialysis, Inc. (North Chelmsford, MA). A stereotaxic frame for rats with probe holders and dental cement was purchased from Stoetling Co (Wood Dale IL). A drilling tool was obtained from Freedom Electric Co. (Bethel, CT) and the micro drill bits (0.25mm ad 0.5 mm) were from Cell Point Scientific (Gaithersburg, MD). Artificial tears used were Thera Tears from Akorn (Ann Arbor, MI)

The scissors, scalpel and forceps used in the surgery were from Harvard Apparatus (Holliston, MA) and the sutures (Mersilk, 2-0, 3metric) and needles were from Ethicon (San Angelo, TX). Wahl professional 8355 vibrator clipper was from Wahl® (Sterling, IL). Intramedic Clay Adams PE tubing (PE-240 and PE-20) was from Becton Dickinson and Company (Sparks, MD). The 100 µL microsyringe was from Hamilton (Reno, NV) and other syringes and BD microtainer plasma separation tubes with lithium heparin were from Becton Dickinson and Company (Franklin Lakes, NJ). All other chemicals were from Sigma Chemicals (St. Louis, MO).

### Experimental procedures

#### *Animal experiments*

Male, Sprague-Dawley rats weighing approximately 250-350 g were used; animals were provided with free access to food and water. The animal experiments adhered to the “Principles of Laboratory Animal Care” and were approved by the University of Iowa Committee on the Use and Care of Animals. All surgical instruments were cleaned with 70% ethanol solution to disinfect.

#### *Anesthesia*

Each rat was anesthetized intraperitoneally using a combination of ketamine (60 mg/kg) and xylazine (7.5 mg/kg) as preoperative agents and ketamine (36 mg/kg) with xylazine (4.5 mg/kg) as intraoperative agents. The level of anesthesia was monitored every 15 min for the duration of the experiment by checking the pedal reflex. No surgical procedure was initiated until a surgical plane of anesthesia had been reached. Supplemental anesthesia was administered intraperitoneally as needed throughout the experiment

*Probe insertion for microdialysis sampling*

Anesthetized rats were weighed and the rat was placed on a stereotaxic frame (Figure 6-3). It was ensured that the animal was breathing normally. The fur on the top of the head was shaved using a professional clipper (Wahl 8355), and 0.1 mL of 2% mepivacaine (Carbocaine<sup>®</sup>) was injected subcutaneously into the skin covering the skull. A longitudinal incision was made along the scalp to expose the surface of the skull. The eyes of the rats were refreshed with artificial tears (Thera Tears) to avoid dehydration. A minimally invasive stereotaxic surgery was performed to implant the microdialysis probes in the areas of interest based on the three dimensional coordinate system for the rat brain according to the atlas of Paxinos and Watson<sup>193</sup>. The anatomical landmarks, namely the bregma (frontal aspect) and lambda (caudal aspect), were identified, marked and checked to ensure that the bregma and lambda were aligned along the X, Y axis of the frame. The head of the rat was repositioned if necessary such that the dorso-ventral (DV) distance (Z coordinate) of bregma and lambda were equal or did not differ by more than 0.3 mm. The X, Y, and Z axis determines the medial-to-lateral (ML), the anterior-to-posterior (AP), and the dorsal-to-ventral distance (DV) from bregma, respectively, which enable precise and reproducible insertion of probes into the brain regions of interest. The coordinates for the olfactory bulb and striatum were identified relative to the bregma and are given in Figure 6-4. Two holes for probe insertion were carefully drilled through the skull using a 0.5 mm drill bit at these coordinates and a standard 25G needle was used to puncture through the meninges. Microdialysis guide cannulas fitted with dummy probes were inserted through the holes to a depth (DV) of 5 mm and 5.5 mm beneath the skull for the olfactory and striatal locations, respectively.

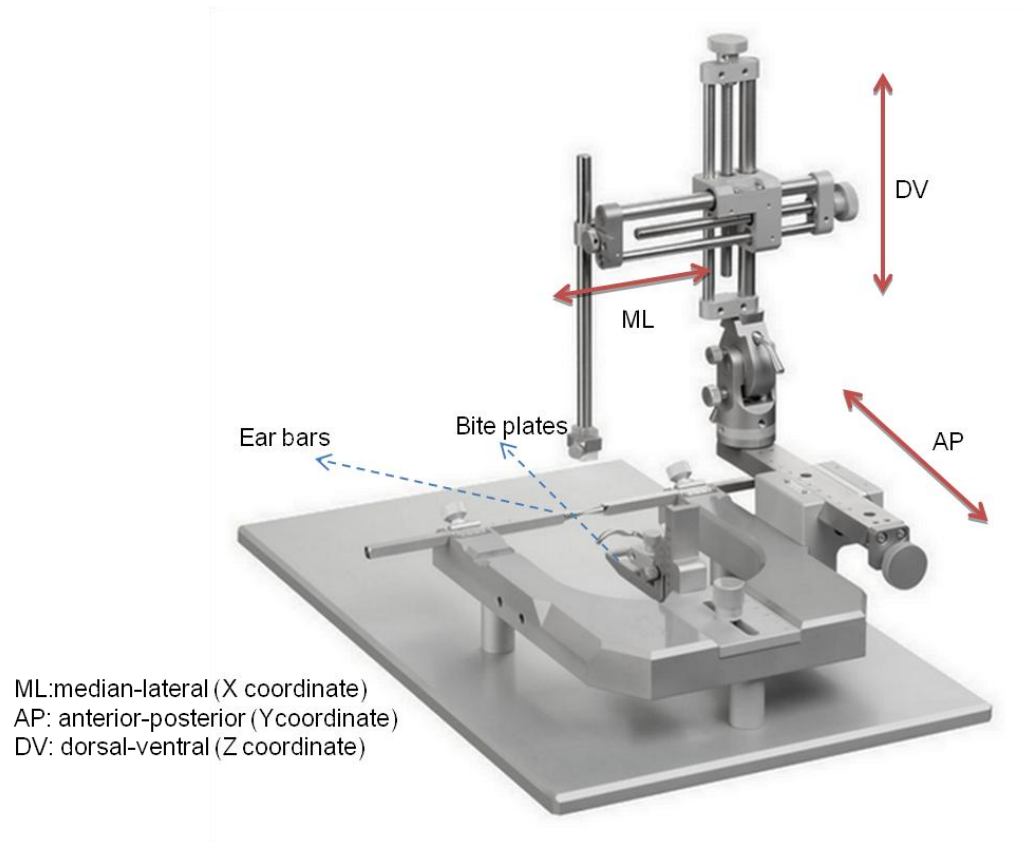


Figure 6-3: Small animal stereotaxic frame showing the ear bars, bite plates and the three dimensional micromanipulators are used to locate the regions of interest in the rat brain from coordinates available from a rat brain atlas

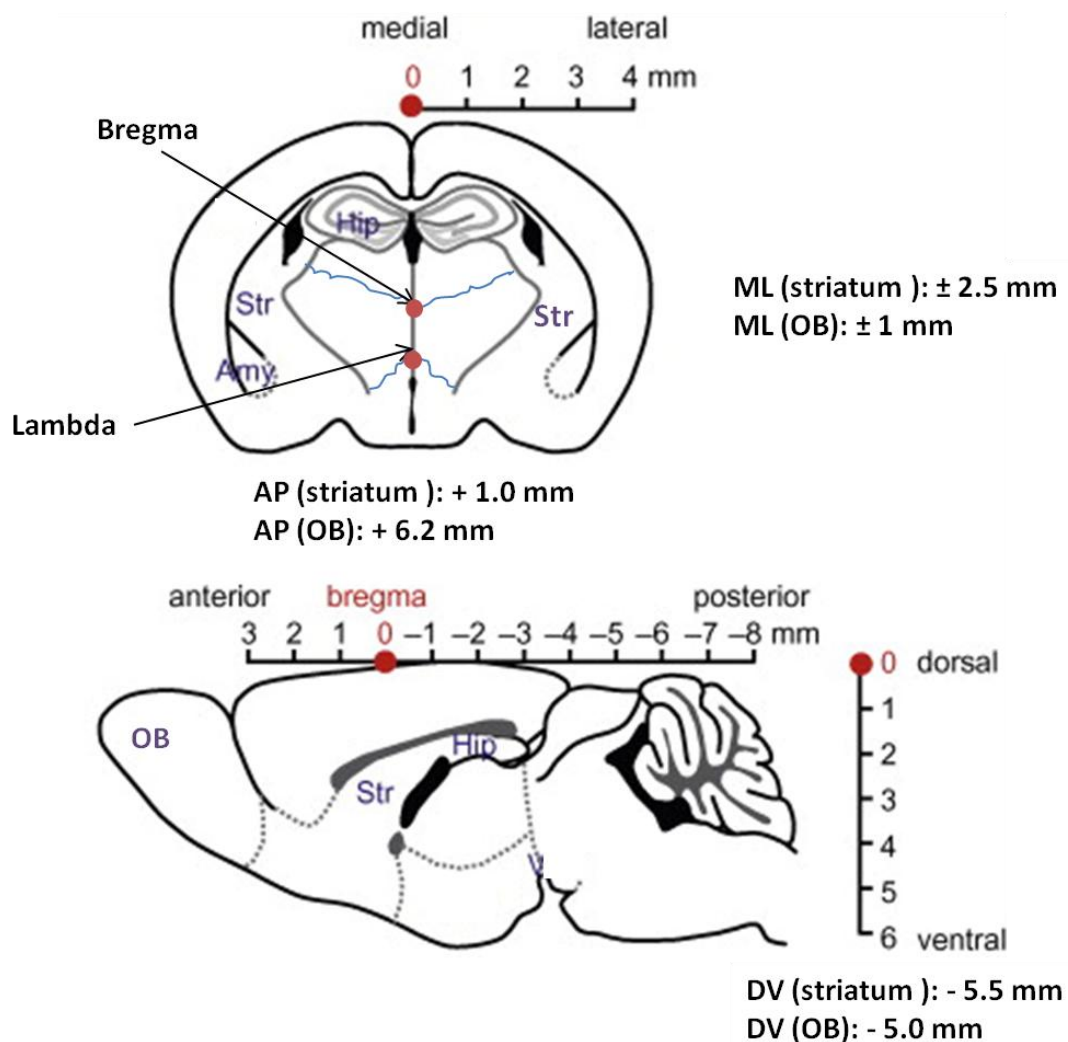


Figure 6-4: The AP, ML and DV coordinates for striatum and olfactory bulb from the bregma have been depicted in the figure. (OB=olfactory bulb; Hip=hippocampus; Str=striatum; Amy= amygdala. Filled areas (black) with black indicate CSF ventricular regions). Stereotaxic coordinates were determined from the rat brain atlas<sup>193</sup> (figure modified from<sup>194</sup>)

The cannulas were then raised from this position through a distance of 3 mm for olfactory and 3.5 mm for the striatum. This was to ensure that a 2 mm distance existed to accommodate the length of the microdialysis membrane tip when the dummy probe was replaced with the microdialysis probe. A third point was drilled in the skull contralateral to the olfactory and striatal positions, and a stainless steel anchor screw was inserted at this position. The two guide cannulas and the anchor screw were held in place using dental cement. Once the cement hardened, the dummy probes were replaced with the microdialysis probes (CMA-12) which were perfused with aECF (artificial ECF) for 30 min prior to and after the insertion of the probes into the brain. The rate of aECF perfusion during the entire study period following probe placement was 1  $\mu$ L/min. The animal was removed from the stereotaxic frame following probe placement and additional surgeries were performed, depending on the route of drug administration used in the experiment.

#### *Intraarterial (IA) dosing and femoral artery cannulation*

The femoral artery was cannulated for the purpose of sampling the blood at pre-determined time intervals and also to administer an intra-arterial dose of the drug. Incisions were made to expose the left femoral artery, and a polyethylene cannula (PE-20) was placed into the artery and held securely with sutures. The cannula was attached to a 1 mL syringe (25G needle) containing normal saline with heparin (10 U/ml). An intraarterial dose of 5 mg/kg of amantadine in 200  $\mu$ l saline was administered as a bolus into the right femoral artery. Blood (~200  $\mu$ l) was collected prior to drug administration to provide a baseline control value.

### *Intranasal (IN) dosing*

Prior to intranasal administration of the drug, the rats underwent minor surgeries to reduce the bias resulting from possible gastrointestinal or alveolar absorption of the drug. An incision was made along the neck to expose the trachea and esophagus. A tracheostomy was performed and the lower trachea was cannulated with PE-240 tubing to provide an airway and to remove secretions from the lungs. Similarly, the upper esophagus was isolated and ligated to eliminate gastrointestinal transfer of the drug. A nasal dose of 5 mg/kg of amantadine (20-25  $\mu$ L per nostril) was administered into the nasal cavity by inserting a soft polyethylene tubing (PE-10) attached to a Hamilton microsyringe. To ensure placement of as much of the dose into the olfactory region as possible, the tubing was inserted to a distance of 1.5 cm into the nasal cavity.

### *Brain and plasma sampling*

At the beginning of the blood sampling, the initial two drops of blood were discarded to eliminate dilution by the saline present in the cannula; approximately the same volume of heparinized normal saline as the total volume of blood removed was used to replace volume lost following each sample collection. Blood (200 $\mu$ L) was collected at predetermined time points (10, 15, 30, 45, 60, 75, 90, 120, 150, 180, 240, 300 and 360 min) into heparinized tubes, and the plasma was separated by centrifuging at 16,100 x g for 5 min using an Eppendorf 5415D (Hamburg, Germany). Brain dialysate fractions (30 or 60  $\mu$ L) from the olfactory bulb and striatal microdialysis probes were obtained for 30 min interval over the 6 hrs. The dialysate samples collected over 0-30, 30-60, 60-90, 90-120, 120-150, 150-180, 180-240, 240-300 and 300-360 min were



assigned time points 30, 60, 90, 120, 150, 180, 240, 300 and 360 min respectively. All samples were stored at  $-80^{\circ}\text{C}$  until analysis.

#### *Blood-brain barrier integrity test*

A major concern during the probe implantation surgery is tissue trauma and the possibility of blood-brain barrier breach during probe insertion. Any damage to the BBB was detected by the extravasation of Evans blue dye (MW 961Da), which is highly bound to serum albumin and cannot cross the barrier<sup>195</sup>. At the end of each experiment, and 30min prior to euthanizing the rat, an intraarterial dose of 2% Evans blue in saline (4 ml/kg) was administered intravenously. The brain was removed following euthanasia and visually examined for staining in regions supplied by the left internal carotid artery such as the cerebral cortex, hippocampus, thalamus and hypothalamus. The microdialysis samples were discarded if staining was observed.

#### *Euthanasia*

The animals were kept under anesthesia during the entire study period. The animals were euthanized with an intra-arterial overdose of anesthetic (ketamine and xylazine) followed by incision of the chest cavity to produce a bilateral pneumothorax. All the procedures involving rats were approved by The Institutional Animal Care and Use Committee of the University of Iowa (ACURF#1006120) and were conducted in accordance with *Guide for the Care and Use of Laboratory Animals* (National Institutes of Health Publication No.25-28, revised in 1996).

#### *Microdialysis probe recovery studies*

The term recovery describes the relation between concentration of the drug in the periprobe fluid and that in the dialysate. These concentrations will differ because of the

constant flow of the perfusate which prevents the establishment of true concentration equilibrium between the periprobe fluid and the dialysate. Reverse dialysis or retrodialysis has been used to determine probe recoveries and involves adding the drug to the perfusate and measuring the loss of drug into the tissues *in vivo*<sup>196,197</sup>. This method of probe recovery determination is based on the assumption that the *in vivo* recovery equals *in vivo* loss.

The *in vivo* recovery by loss method was used to determine amantadine recovery from the microdialysis probe at a flow rate of 1 µL/min. A flow rate of 1 µL/min was selected to allow for maximum drug recovery and adequate temporal resolution (30 min intervals) in sampling with respect to the lowest limit of quantification for the LCMS assay. Following probe insertion into the rat brain, drug free aECF (artificial extracellular fluid) was perfused through the probes for 30 min. This was followed by perfusion of drug containing aECF through the probes. Four microdialysate samples (30 µL) were collected from the probe at 30 min intervals. *In vivo* recovery calibration studies were carried out in triplicate (n=3 rats) for three different concentrations (151, 378 and 756 ng/mL) of the drug for two different regions in the brain, the olfactory bulb and striatum (n=3 rats). The samples were collected, processed and analyzed by the LCMS method.

Recovery by loss was calculated as:

$$\% \text{ Recovery by loss (RL)} = \{(C_{\text{perfusate(IN)}} - C_{\text{dialysate(OUT)}})/C_{\text{perfusate(IN)}}\} \times 100 \%$$

Equation 6-3

$C_{\text{perfusate(IN)}}$ : concentration of the drug in the perfusate (input to the probe)

$C_{\text{dialysate(OUT)}}$ : concentration of the drug in the dialysate (output from the probe)

### *Reuse of probes in vivo*

Owing to the fragility of the probes, the chance of damage to the dialysis membranes during insertion is likely. Thus the likelihood of reusing the same probes for multiple experiments was evaluated. An *in vitro* recovery by loss method (retrodialysis) was used at the end of every five *in vivo* microdialysis experiments to evaluate probe performance<sup>197</sup>. The method is similar to the *in vivo* recovery determination except that the probes are inserted into a fixed volume (10 mL) of aECF at 37°C, instead of into the rat brain. Equation 6-3 was used to determine the percentage recovery from the probe. Whenever a statistically significant reduction in probe recovery was observed compared to the calibrated probe recovery values, the results from the previous animal experiments were discarded. If no deviations were observed, the same probes were used for subsequent animal experiments.

### *Determination of unbound drug ( $C_u$ ) fraction in plasma*

Plasma unbound fractions of amantadine were determined using a centrifugal filter, Amicon Ultra-0.5 mL Ultracel 10 kDa molecular weight cut off (Millipore, Billerica, MA). Blank rat blood was collected before any dose was administered and the plasma was separated by centrifugation using BD Microtainer plasma separation tubes coated with lithium heparin. Plasma aliquots of 250  $\mu$ L were spiked with three levels of amantadine concentrations such that the final concentrations represented the high, medium and low plasma concentrations (1200, 500 and 100 ng/mL) measured in the rat studies for amantadine. The mixture was incubated for 30 min at 37°C in a VWR 1160A water bath (VWR, Denver, CO). Filtrates were obtained from the drug-spiked aliquots (n=3, for each concentration level) by transferring the sample to the Amicon filters,

centrifuging the sample using an Eppendorf 5804R (Hamburg, Germany) at 14,000 x g for 10 min at room temperature. The drug concentrations determined from plasma before and after ultrafiltration using LCMS, which gives the total and free drug concentrations respectively. The percentage of free drug was then calculated as:

$$\left( \frac{\text{Concentration in the ultrafiltrate}}{\text{Concentration in the original plasma}} \right) \times 100\%$$

Equation 6-4

This percentage was used to calculate the free drug concentrations in the plasma from the total plasma concentrations measured at each time point, and was then used in the determination of  $K_{p,\text{brain}}$  (partitioning of the unbound drug across the BBB)

#### *Study groups*

The dose of amantadine was selected after a careful evaluation of the clinical amantadine therapy literature. The reported intraperitoneal dose of amantadine, when administered to rats, is approximately 50 mg/kg for the treatment of extrapyramidal effects<sup>198</sup>. The intravenous (rat) LD<sub>50</sub> was reported to be ~90 mg/kg<sup>199</sup>. The lowest possible dose that could be used in the study was estimated to be 5 mg/kg, where doses lower than this would not give detectable levels in the brain at the initial time points from either route of administration.

Five study groups were considered, with each group ( $n = 4$  to  $5$ ) receiving amantadine (5 mg/kg) intra-arterially (IA) or intranasally (IN) with or without the OCT2 (guanidine, 50 µg/kg) or OCTN2 (L-carnitine, 2.5 µg/kg) inhibitors or both (Table 6-2). All drug and inhibitor solutions were prepared in fresh sterile saline. All inhibition studies were carried out intranasally where amantadine was co-administered with guanidine (OCT2 inhibition) or L-carnitine (OCTN2 inhibition) or both (OCT2 +

OCTN2 inhibition). The animals were prepared for IN dosing as described earlier, and the olfactory bulb and striatal free drug concentrations and plasma concentrations of amantadine were measured at time points similar to the IN and IA control groups.

#### *Data analysis*

Results were expressed as mean  $\pm$  SD (n=4 or 5) unless otherwise noted. Where appropriate, statistical comparisons using the Students t-test were performed to compare between two groups and multiple group comparisons were carried out using ANOVA with Bonferroni corrections. In all cases,  $p < 0.05$  was used as the desired level of significance. The AUCs,  $C_{\max}$  and  $T_{\max}$  were analysed using WinNonlin (v 1.0), (Pharsight, Sunnyvale, CA). All microdialysate concentrations were calculated by correcting for the probe recovery and all free drug plasma concentrations were calculated from total plasma concentrations using the free drug ratio determined experimentally. Some additional pharmacokinetic parameters were also evaluated using WinNonlin<sup>®</sup>.

Table 6-2: The five different study groups for amantadine (5 mg/kg) administration (n= 4 to 5 rats/group) used to compare IA vs. IN routes along with the inclusion of inhibitors used to evaluate the role of OCT2 and OCTN2 transporters in the brain uptake of amantadine following IN dosing.

| # | Route | OCT2 Inhibitor<br>(50 $\mu$ g/kg) | OCTN2 Inhibitor<br>(2.5 $\mu$ g/kg) |
|---|-------|-----------------------------------|-------------------------------------|
| 1 | IA    | -                                 | -                                   |
| 2 | IN    | -                                 | -                                   |
| 3 | IN    | Guanidine                         | -                                   |
| 4 | IN    | -                                 | L-carnitine                         |
| 5 | IN    | Guanidine                         | L-carnitine                         |

## Results and Discussion

### *Microdialysis Recovery Results*

A number of drugs have been known to show concentration dependent changes in the relative recovery from microdialysis probes both *in vivo* and *in vitro*. Therefore, *in vivo* recovery by loss experiments were carried out at three different concentrations of amantadine in the perfusate: 151, 378 and 756 ng/mL. These concentrations were selected to represent the typical rat brain concentrations of amantadine after systemic or intranasal administration as determined from two pilot studies. The recoveries were calculated using Equation 6-3 and the results are summarized in Figure 6-5. Recovery results demonstrated that there were no statistically significant differences in the probe recoveries of amantadine from either brain region at any of the three concentrations of amantadine studied. The olfactory bulb recovery was calculated to be  $20 \pm 1.5\%$  whereas a slightly higher recovery of  $27 \pm 2.1\%$  was observed from the probe inserted in the striatum. Recoveries have been expressed as mean  $\pm$  standard deviation of 3 observations (3 rats /concentration). The difference in the recoveries from the olfactory bulb and striatum probes shows that factors such as effective diffusion of the drug through the extracellular fluid, uptake into the cell, metabolic rates, clearance mechanisms might be different at the two sites.

Additionally, the possibility of time dependence in the *in vivo* recovery of amantadine from the olfactory and striatal probes was also investigated. For this purpose, an amantadine perfusate concentration of 378 ng/mL was used, and recoveries were estimated from dialysates collected at three time points (30, 90 and 180 min; n=3 rats) for both the olfactory bulb and striatal probes. *In vivo* recovery was found to be stable over

time for probes at both sites (Figure 6-6). Again, the striatal probe gave a slightly higher recovery as compared to the olfactory bulb probe.

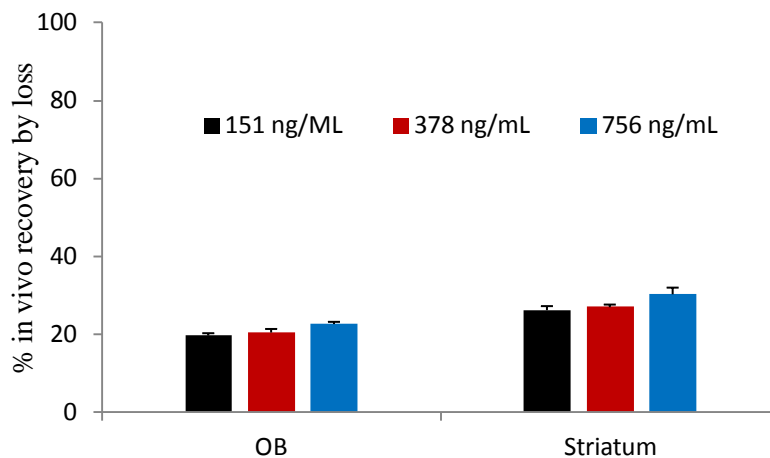


Figure 6-5: Percentage *in vivo* recovery by loss of amantadine from the olfactory bulb (OB) and the striatum probe at three different concentrations of amantadine: 151, 378 and 756 ng/mL. (mean  $\pm$  standard deviation, n=3 rats/concentration)

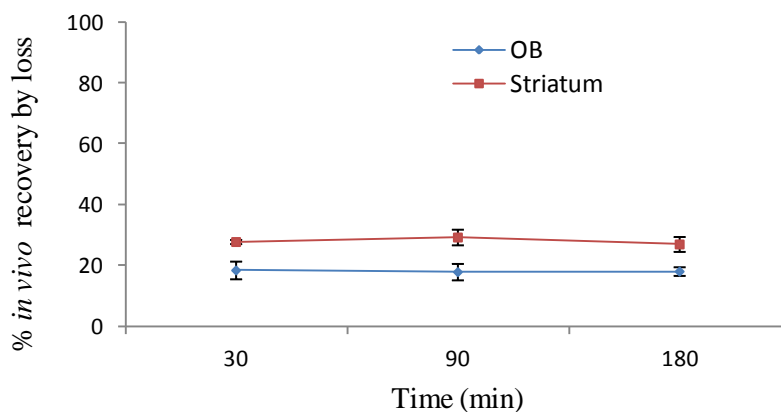


Figure 6-6: Percentage *in vivo* recovery by loss of amantadine from the olfactory bulb (OB) and the striatum probes over a 3 hour period (30, 90 and 180 min) for a perfusate concentration of 378 ng/mL. (mean  $\pm$  standard deviation, n=3 rats/time point)

As a result, average recoveries for the olfactory bulb and striatal probes were calculated as  $20 \pm 1.5\%$  and  $27 \pm 2.1\%$ , respectively and were used to calculate the actual olfactory bulb and striatal concentrations from the dialysate concentrations in the dosing experiments in rats using Equation 6-5.

$$\text{Actual concentration at the sampling site} = \{ 100 \times C_{\text{dialysate}} \} / \text{RL} \quad \text{Equation 6-5}$$

$C_{\text{dialysate}}$  : concentration in the dialysate

RL: recovery by loss

For example, if the amantadine concentration in the olfactory bulb dialysate was detected by the LCMS assay as 5 ng/mL, the actual free amantadine concentration in the olfactory bulb will be calculated and reported as:  $(100 \times 5) / 20 = 25$  ng/mL.

*Drug concentrations in plasma following  
intra-arterial (IA) and intranasal (IN)  
administration of amantadine*

The plasma concentration time course of amantadine administered in saline to rats (n=5) at a dose of 5 mg/kg (as base) following intra-arterial and intranasal administration is shown in Figure 6-7. The same dose was used for both the routes in order to compare the effectiveness of each route for amantadine delivery to the brain. Following the IA bolus dose, amantadine distribution exhibited a biexponential decline in plasma concentration. The plasma disposition of amantadine after IA administration can be described by a two compartment model; the disposition following IN administration was best described by a one-compartment model.



The disposition of amantadine is characterized by a large volume of distribution, after both routes of administration (Table 6-3). Selected pharmacokinetic parameters,  $AUC_{(0-\infty)}$ ,  $C_{max}$ ,  $T_{max}$ ,  $T_{1/2}$ ,  $V_d$ , and clearance in the central compartment are shown in Table 6-3. Following intranasal administration, appreciable systemic absorption was observed. The maximum plasma concentration of amantadine after intranasal administration was  $578.6 \pm 83.4$  ng/mL at a  $t_{max}$  of  $26.7 \pm 5.8$  min. The terminal half-life of amantadine was significantly longer and the plasma clearance was significantly lower after IN administration of the drug.

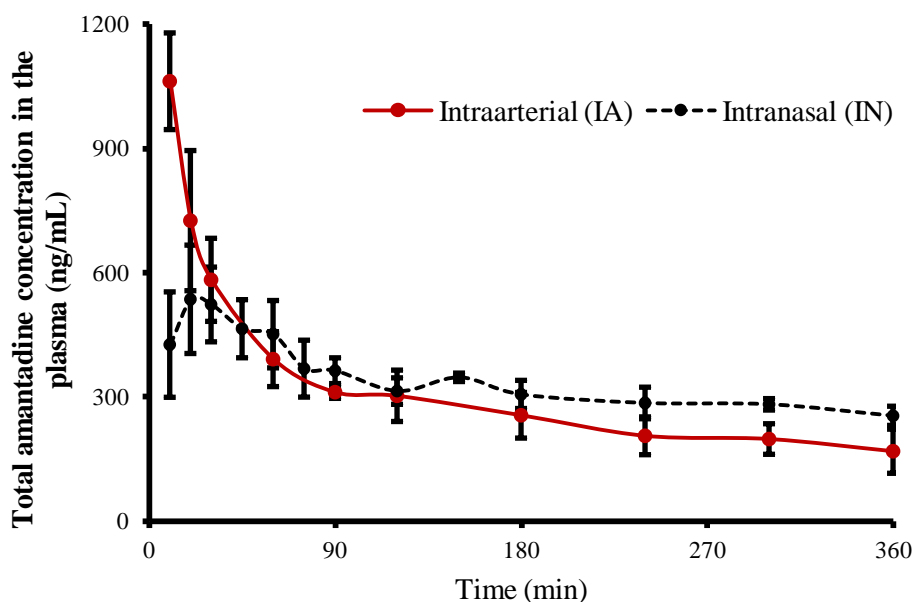


Figure 6-7: Plasma concentration time profiles of amantadine following intra-arterial (IA) and intranasal (IN) administration in rats at a dose of 5 mg/kg (mean  $\pm$  standard deviation, n=5).

An important assumption underlying the common bioavailability calculation is that the clearances after intravascular and extravascular doses are comparable, since the bioavailable dose actually corresponds to the dose eliminated from plasma. Therefore, the absolute bioavailability of IN amantadine was calculated using Equation 6-6 and was determined to be 62.1%.

$$F(\%) = \frac{AUC(IN)}{AUC(IA)} \times \frac{Clearance(IN)}{Clearance(IA)} \times 100 \quad \text{Equation 6-6}$$

The nasal respiratory tissue has a high degree of vascularity and enables the rapid absorption of drugs into the systemic circulation following nasal administration.

Table 6-3: Selected pharmacokinetic parameters calculated from the plasma concentration-time profiles of amantadine following intra-arterial (IA) and intranasal (IN) administration in rats at a dose of 5 mg/kg, determined using WinNonlin<sup>®</sup> (mean  $\pm$  standard deviation, n= 4 or 5).

| <b>PK Parameters</b>                    | <b>IA</b>          | <b>IN</b>          |
|---|--------------------|--------------------|
| $C_{max}$ (ng/mL)                       | 1644.0 $\pm$ 455.9 | 578.6 $\pm$ 83.4   |
| $T_{max}$ (min)                         | -                  | 26 $\pm$ 5.8       |
| $AUC_{(0-\infty)}$ (ng.hr/mL)           | 1916.1 $\pm$ 195.7 | 1975.9 $\pm$ 188.3 |
| Half life ( $t_{1/2}$ )(hr)             | 2.6 $\pm$ 0.4      | 6.4 $\pm$ 1.7*     |
| Clearance (ml/min/kg)                   | 32.5 $\pm$ 5.1     | 19.6 $\pm$ 2.4*    |
| Volume of distribution ( $V_d$ ) (l/kg) | 7.1 $\pm$ 1.2      | 10.1 $\pm$ 1.6     |

Note: \* represents statistically significant differences from the intraarterial (IA) administration group (p<0.05)

*Brain uptake and distribution following  
IA and IN administration of amantadine*

Our working hypothesis was that the transport of drugs into the CNS from the nasal cavity occurs via the olfactory mucosa with resulting distribution to different regions in the brain following transit via the olfactory bulb. The two regions in the rat brain which were evaluated for drug uptake were the olfactory bulb and the striatum. The olfactory bulb and striatum ECF concentration-time profiles of amantadine following intraarterial (IA) and intranasal (IN) administration are shown in Figures 6-8. A comparison of the free amantadine concentrations in the striatum and olfactory bulb following systemic and nasal administration at different time points are shown in Figure 6-9. Compared to the systemic dose, the nasal dose achieved significantly higher free drug concentration levels in the olfactory bulb post 60 min and in the striatum post 150 min ( $p < 0.05$ ), even though the plasma concentrations were comparable for both routes of administration post 60 min. This suggests the existence of a drug input into the brain in addition to that from the central compartment following nasal administration

Following IA dosing, free drug levels in the two brain regions were observed to be similar at each time point ( $p < 0.05$ ). The olfactory bulb ECF levels after IN administration of the drug were observed to be higher than the levels found in the striatum for the first 150 min post dose, but were observed to achieve similar concentrations at times  $\geq 180$  min. This observed time lag in the free drug equilibration between the striatum and olfactory bulb indicates that the drug from the additional input reaches the olfactory bulb first. The systemic input into the olfactory bulb and corpus striatum should not show regiospecificity since the local capillary density, cerebral

vascular volume, and perfusion flow rate are similar for the two regions<sup>200</sup>. Therefore, the observed differences further suggest an alternate drug input into the brain other than the systemic circulation following intranasal dosing. Furthermore, brain concentrations continues to increase following IN administration, despite ongoing clearance from the central compartment, due to continued absorption from the nasal cavity. The  $AUC_{0-6}$ ,  $C_{max}$  and  $T_{max}$  following IN and IA dose in the brain regions are given in Table 2.3.4. The  $AUC_{0-6}$ , in the olfactory bulb was significantly higher following IN dosing providing further evidence that the drug enters the brain via an olfactory pathway.

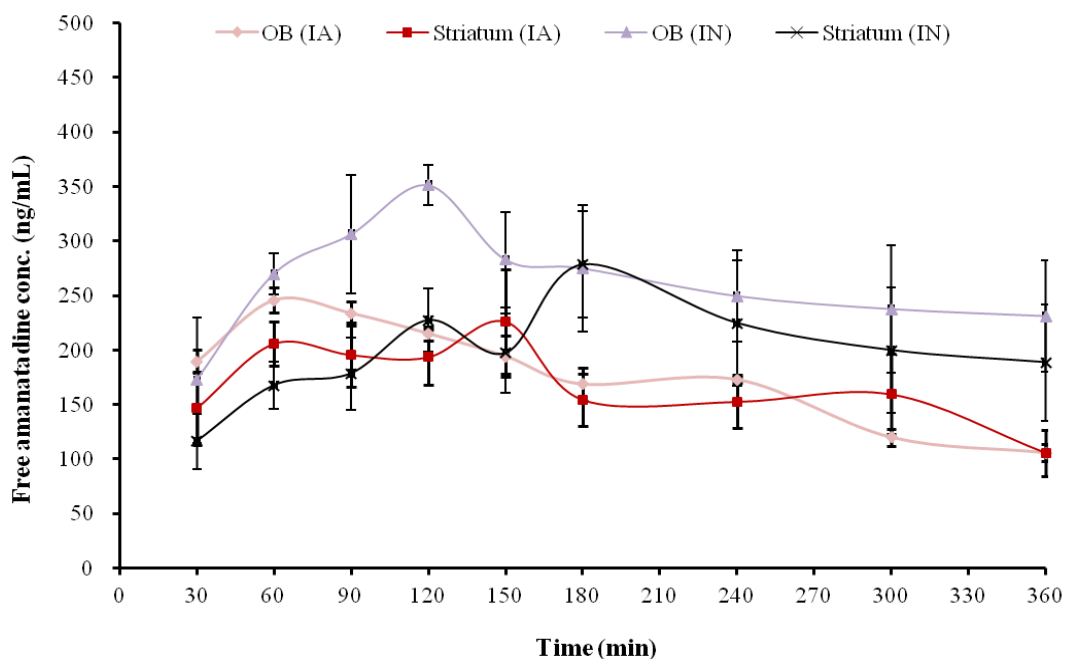


Figure 6-8: Brain (olfactory bulb and striatal) ECF concentration- time profile of amantadine following intra-arterial (IA) and intranasal (IN) administration in rats at a dose of 5 mg/kg (mean  $\pm$  standard deviation, n=5). Concentrations reported are probe recovery corrected values. Data points are connected by smooth curves. OB: Olfactory bulb.

Table 6-4: Selected pharmacokinetic parameters calculated from the olfactory bulb and striatal ECF-time profiles of amantadine following intra-arterial (IA) and intranasal (IN) administration in rats at a dose 5 mg/kg. (mean  $\pm$  standard deviation, n= 4 or 5).

| <i>Region of sampling</i> | <i>PK parameter</i>             | <i>IA</i>          | <i>IN</i>          |
|---------------------------|---------------------------------|--------------------|--------------------|
| Olfactory Bulb            | $C_{\max}$ (ng/ml)              | 233.8 $\pm$ 22.7   | 360.8 $\pm$ 3.1*   |
|                           | $T_{\max}$ (min)                | 73 $\pm$ 32        | 120.0 $\pm$ 29     |
|                           | AUC <sub>0-6h</sub> (ng.min/ml) | 61327 $\pm$ 235.6  | 92802 $\pm$ 12669* |
| Striatum                  | $C_{\max}$ (ng/ml)              | 205.0 $\pm$ 24.1   | 307.9 $\pm$ 36.3*  |
|                           | $T_{\max}$ (min)                | 65 $\pm$ 20        | 195 $\pm$ 42.4*    |
|                           | AUC <sub>0-6h</sub> (ng.min/ml) | 58765 $\pm$ 5289.6 | 71754 $\pm$ 17040  |

Note: Concentrations reported are probe recovery corrected values. \* represents statistically significant differences from the intraarterial (IA) administration group ( $p < 0.05$ )

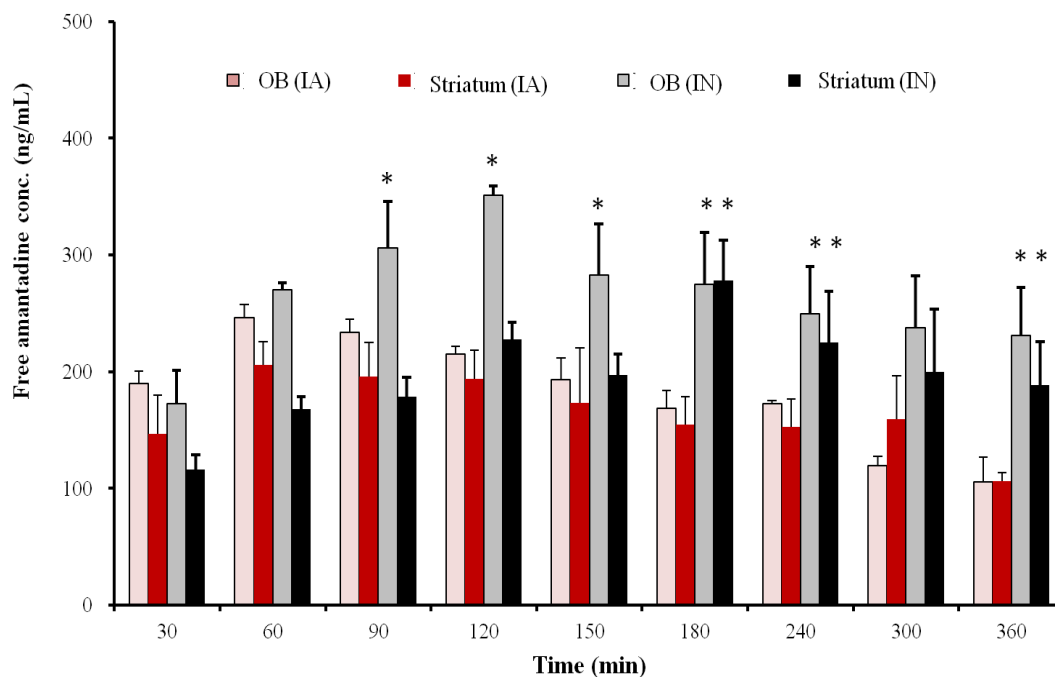


Figure 6-9: Brain (olfactory bulb and striatum) ECF concentrations of amantadine following intra-arterial (IA) and intranasal (IN) administration in rats at a dose of 5 mg/kg (mean  $\pm$  standard deviation, n=5). Concentrations reported are probe recovery corrected values. OB: Olfactory bulb, \* represents statistically significant differences compared to the IA control group ( $p < 0.05$ ).

During the first 60 min post IA and IN administration, the free drug levels in both brain regions were comparable, but it should be appreciated that the plasma concentration following IN dosing was significantly lower than after IA administration over this time interval. This suggests that additional amounts of drug enter the brain, in addition to those amounts input from the blood, within 30 min post IN dose, or even earlier, however, the sensitivity of the analytical method did not allow for accurate concentration measurements at these earlier time points. Since considerable systemic absorption is achieved following IN amantadine administration, two major inputs into the brain (nasal cavity and blood) exist, but are difficult to resolve. Therefore, the  $K_{p,brain}$  parameter was evaluated to better understand the contribution of the IN dose towards the brain levels of amantadine.

*Role of organic cation transporters in the nose to brain  
delivery of amantadine: transporter inhibition studies*

It has been observed in the *in vitro* transport studies using bovine nasal mucosa that OCT transporters play a role in the transfer of amantadine across the respiratory and olfactory tissues (Chapter 5). Owing to the similarity in the expression of these transporters in the rat and bovine nasal mucosa, it was hypothesized that these transporters increase the flux of amantadine across the olfactory mucosa and thus contribute significantly to the enhanced brain concentrations observed following IN administration to rats. As a result, competitive inhibitors of OCT2 and OCTN2, guanidine and L-carnitine, respectively, which had been used in the *in vitro* transport studies, were administered nasally along with amantadine to test their effect on the brain

uptake of amantadine. The plasma concentration-time profiles of amantadine after intranasal inhibition of OCT2, OCTN2 or both are shown in Figure 6-9.

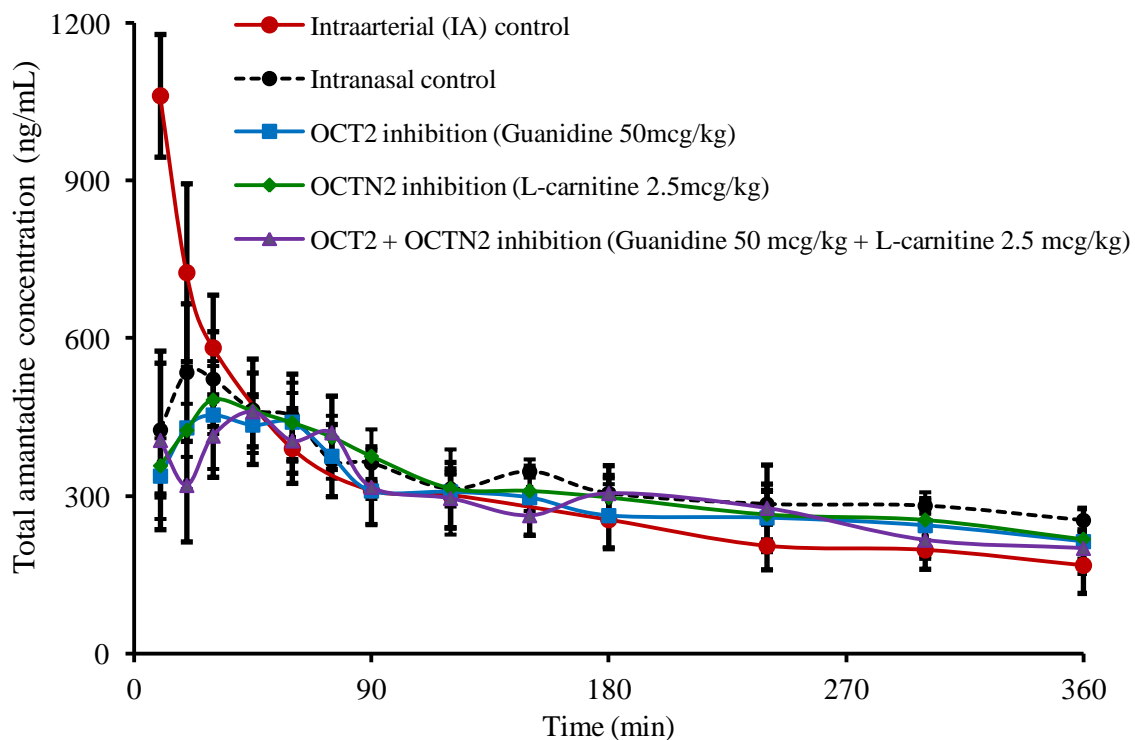


Figure 6-10: Plasma concentration time profiles of amantadine (5 mg/kg) following intranasal (IN) administration of the amantadine alone (intranasal control), in the presence of an OCT2 inhibitor (guanidine), OCTN2 inhibitor (L-carnitine) and combined OCT2 +OCTN2 inhibitors (guanidine + L-carnitine) (mean  $\pm$  standard deviation, n=5). All inhibitors were administered intranasally with amantadine.



Table 6-5: Selected pharmacokinetic parameters calculated from plasma profiles of amantadine following intranasal (IN) administration of the drug alone (intranasal control), in the presence of an OCT2 inhibitor, OCTN2 inhibitor and a combination of OCT2 + OCTN2 inhibitors (mean  $\pm$  standard deviation, n=5).

| <b>PK Parameters</b>          | <b>IN</b>          | <b>IN</b><br>(OCT2 inhibition,<br>guanidine 50<br>$\mu\text{g}/\text{kg}$ ) | <b>IN</b><br>(OCTN2 inhibition, L-<br>carnitine 2.5 $\mu\text{g}/\text{kg}$ ) | <b>IN</b><br>(OCT2 + OCTN2inhibition;<br>guanidine 50 $\mu\text{g}/\text{kg}$ +<br>carnitine 2.5 $\mu\text{g}/\text{kg}$ ) |
|-------------------------------|--------------------|---|---|--|
| $C_{max}$ (ng/mL)             | 578.6 $\pm$ 83.4   | 474.5 $\pm$ 83.0  | 467.4 $\pm$ 38.7  | 508.4 $\pm$ 73.8   |
| $T_{max}$ (min)               | 26 $\pm$ 5.8       | 38 $\pm$ 7.5  | 45 $\pm$ 12.2*  | 54 $\pm$ 13.4*   |
| $AUC_{(0-\infty)}$ (ng.hr/mL) | 1975.9 $\pm$ 188.3 | 1591.4 $\pm$ 532.3  | 1854.8 $\pm$ 227.6  | 1480.6 $\pm$ 373.1   |
| Half life ( $T_{1/2}$ )(hr)   | 6.4 $\pm$ 1.7      | 5.4 $\pm$ 2.2   | 5.7 $\pm$ 0.7   | 6.1 $\pm$ 2.6  |
| Clearance<br>(ml/min/kg)      | 19.6 $\pm$ 2.4     | 29.2 $\pm$ 12.9   | 23.2 $\pm$ 4.2  | 28.4 $\pm$ 10.6  |

Note: All inhibitors were co-administered intranasally with amantadine.\* represents statistically significant differences from the intranasal (IN) control group ( $p < 0.05$ ).

There were no statistically significant differences ( $p < 0.05$ ) between the plasma concentrations of amantadine after inhibition of either transporters or after combined inhibition when compared to the intranasal control. Furthermore, the plasma levels between groups were also not significantly different from each other (ANOVA using Bonferroni's corrections,  $p < 0.05$ ). The results indicate that OCT2 and OCTN2 have a minimal role in the systemic absorption of amantadine following nasal administration. However, the  $T_{max}$  for the OCT2 + OCTN2 inhibition group was significantly longer than all the other groups, indicating a delay in systemic absorption when both of the transporters are inhibited.

The olfactory bulb and striatum ECF concentration-time profiles of amantadine following intra- intranasal (IN) administration are shown in Figures 6-11A and 6-11B. The presence of an olfactory component in the brain uptake of amantadine from the nasal cavity is clear from the olfactory and striatal free drug levels after intranasal and intra-arterial administration. Figures 6-12 and 6-13 show the free drug levels in the olfactory bulb and striatum, in the presence of OCT2 or OCTN2 inhibition. These levels were compared to the intranasal control and also to brain concentrations after systemic administration of the drug. Inhibition of OCT2 intranasally with guanidine did not show any significant reduction in concentrations of free drug in the olfactory bulb during the first 60 min. But at times  $> 60$  min, OCT2 inhibition showed a statistically significant reduction in olfactory bulb concentrations of the drug, even though the plasma levels were similar for the guanidine group (OCT2 inhibition) and the intranasal control group ( $p < 0.05$ ). The OCT2 inhibition resulted in olfactory bulb amantadine profiles similar to those measured after the IA administration of the drug ( $p < 0.05$ ). This demonstrates that

passive diffusion alone does not account for the high levels of amantadine observed in the olfactory bulb after nasal administration. After 240 min, the effect of the OCT2 inhibition seems diminished with no significant difference being observed between the intranasal control and intranasal OCT2 inhibition group. This is possibly due to the depletion of inhibitory concentrations of guanidine from the nasal cavity or due to the clearance mechanisms for amantadine playing a greater role due to the lower concentrations at these time points. No effect of OCT2 inhibition on the striatal concentration of amantadine was observed, which could be due to the existence of a time lag in the free drug equilibration between the olfactory bulb and the striatum.

The intranasal inhibition of OCTN2 by L-carnitine did not affect the plasma, olfactory bulb or striatum concentrations of amantadine, and there were no significant differences in the concentrations of the drug among the brain regions or plasma when compared to the intranasal control group even though OCTN2 is known to be expressed to an appreciable extent in the rat respiratory and olfactory mucosa<sup>75</sup>.

It was therefore interesting to note that the combined inhibition of both OCT2 and OCTN2 resulted in a synergistic reduction in the olfactory bulb and striatal levels of amantadine following nasal administration, at time points  $\leq 90$  min, when compared to the IA, IN and OCT2 inhibition (IN) and OCTN2 inhibition(IN) groups (Figures 6-12 and 6-13). The concentration of amantadine in the brain in the combined inhibition (OCT2 + OCTN2) group at times  $< 90$  min were also significantly lower than the brain levels after systemic (IA) administration ( $p < 0.05$ ). Furthermore, the combined inhibition of the two transporters resulted in a significantly longer plasma  $t_{\max}$  compared to the intranasal control group (Table 6-6). These results indicate that the synergistic effect of combined

inhibition of OCT2 and OCTN2 decreases input into the brain from the blood and from the olfactory pathway. Post 90 min, the brain concentrations of amantadine in this group were similar to the levels observed following IA administration of the drug. Thus brain concentrations of amantadine post 90 min, following OCT2 and OCTN2 inhibition, most likely reflect the brain exposure of the drug from systemic input alone, where continued transport of the drug via the olfactory pathway into the brain has been abolished. It can also be concluded that the free drug levels in the brain during the first 60 min reflect more of the uptake from the nasal cavity than from systemic input, since this is the period where the synergistic effect of the combined inhibition group is most pronounced.

Selected pharmacokinetic parameters,  $AUC_{(0-6)}$ ,  $C_{max}$ , and  $T_{max}$ , in the olfactory bulb and striatal brain compartments following intranasal co-administration of amantadine with the inhibitors are reported in Table 6-6. A comparison of the AUC values was made to identify any differences in the total amounts of the free drug available following IN administration of amantadine in each group. The olfactory bulb  $AUC_{(0-6)}$ , was observed to be significantly lower following OCT2 inhibition or the combined inhibition of both OCT2 and OCTN2 with the total free drug exposure decreasing to 58% and 51%, respectively, compared to the intranasal control group. The simultaneous inhibition of the two transporters also resulted in a significant decrease in the striatal  $AUC_{(0-6)}$ , which was observed to be 55% of the IN control. All these results indicate the organic cation transporters, OCT2 and OCTN2, play a key role in directing amantadine to the olfactory bulb from where it appears to be subsequently transported to other regions in the brain.

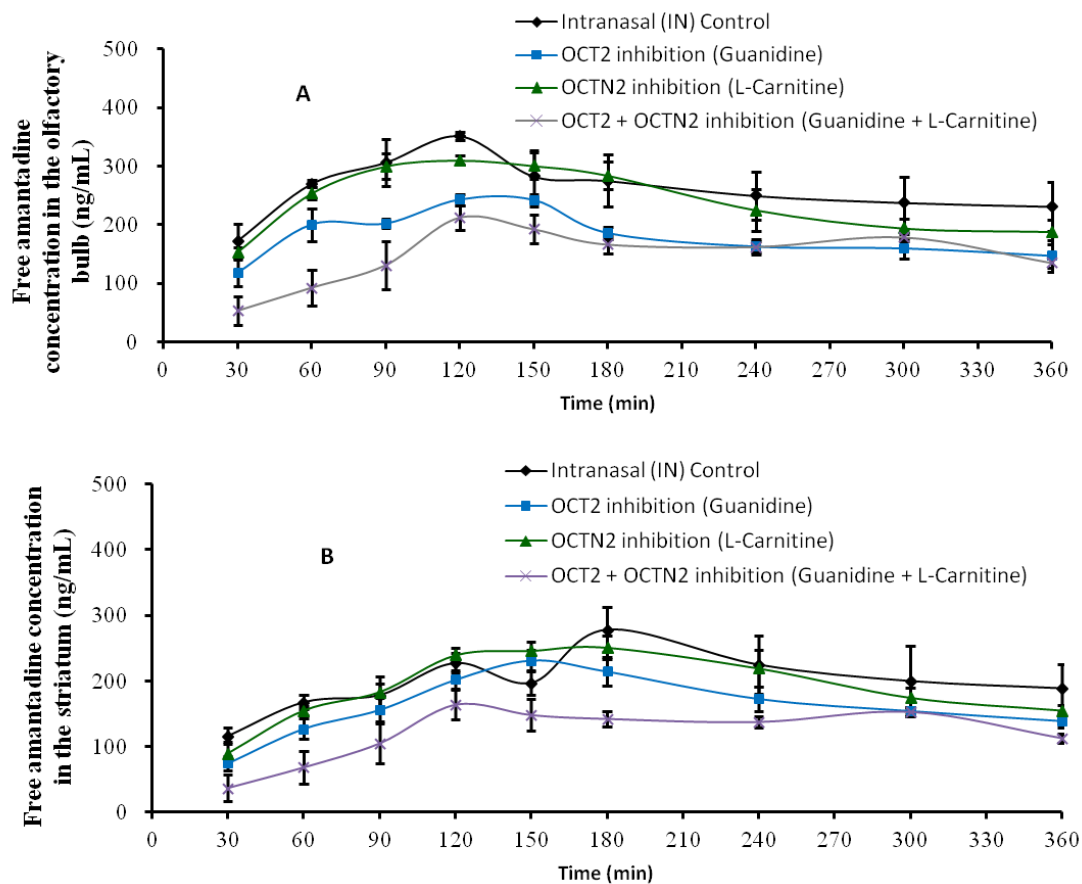


Figure 6-11: Brain ECF concentration-time profile of amantadine following intra-intranasal (IN) administration in the (A) olfactory bulb and (B) striatum. The drug was administered alone (intrasal control), in the presence of OCT2 inhibitor (guanidine), OCTN2 inhibitor (L-carnitine) and OCT2 + OCTN2 inhibitor (guanidine + L-carnitine) (mean  $\pm$  standard deviation,  $n=4$  or  $5$ ). All inhibitors were administered intranasally with amantadine. Dose of amantadine, guanidine and L-carnitine were  $5$  mg/kg,  $50$   $\mu$ g/kg and  $2.5$   $\mu$ g/kg respectively. Data points are connected by smooth curves. Concentrations reported are probe recovery corrected values.

Table 6-6: Selected pharmacokinetic parameters calculated from the olfactory bulb and striatum ECF time profiles following intranasal (IN) administration of the drug alone (intranasal control), in the presence of OCT2 inhibitor (guanidine), OCTN2 inhibitor (L-carnitine) and OCT2 +OCTN2 inhibitor (guanidine + L-carnitine) (mean  $\pm$  standard deviation, n= 4 or 5).

| Region of sampling | PK Parameter                    | IN                | IN<br>(OCT2 inhibition,<br>guanidine 50 $\mu$ g/kg) | IN<br>(OCTN2 inhibition,<br>L-carnitine 2.5 $\mu$ g/kg) | IN<br>(OCT2 + OCTN2inhibition;<br>guanidine 50 $\mu$ g/kg +<br>carnitine 2.5 $\mu$ g/kg) |
|--------------------|---------------------------------|-------------------|---|---|--|
| Olfactory Bulb     | C <sub>max</sub> (ng/ml)        | 360.8 $\pm$ 3.1   | 237.7 $\pm$ 10.2*                                   | 331.1 $\pm$ 26.2  | 231.9 $\pm$ 14.7*  |
|                    | T <sub>max</sub> (min)          | 120 $\pm$ 28.8    | 130 $\pm$ 17.3                                      | 120 $\pm$ 30.0  | 130 $\pm$ 17.3   |
|                    | AUC <sub>0-6h</sub> (ng.min/ml) | 92802 $\pm$ 12669 | 53462 $\pm$ 20499                                   | 82962 $\pm$ 3735.3                                      | 47097 $\pm$ 9029.6*  |
| Striatum           | C <sub>max</sub> (ng/ml)        | 307.9 $\pm$ 36.3  | 237.5 $\pm$ 27.9                                    | 273.8 $\pm$ 11.0  | 185.7 $\pm$ 19.8*  |
|                    | T <sub>max</sub> (min)          | 195 $\pm$ 42.4    | 171 $\pm$ 64.6                                      | 165 $\pm$ 17.3  | 172 $\pm$ 36.2   |
|                    | AUC <sub>0-6h</sub> (ng.min/ml) | 71754 $\pm$ 17040 | 58327 $\pm$ 2561.7                                  | 67641 $\pm$ 1842.7                                      | 39513 $\pm$ 7506.1*  |

Note: All inhibitors were administered intranasally with amantadine). \* represents statistically significant differences from the intraarterial administration group (p<0.05).

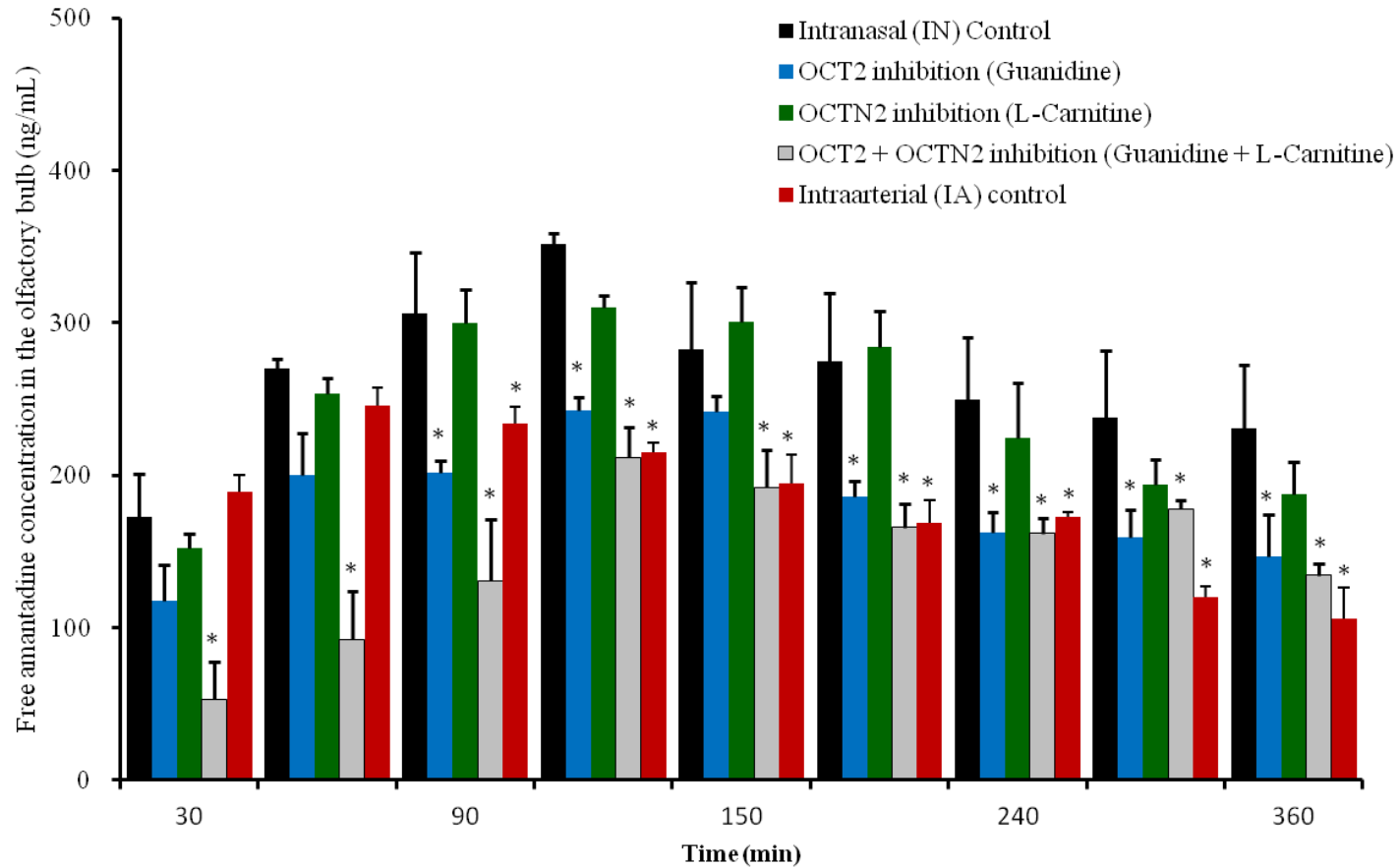


Figure 6-12: Brain olfactory bulb ECF concentrations of amantadine following intra-arterial (IA) and intranasal (IN) administration of the drug alone (intranasal control), in the presence of OCT2 inhibitor (guanidine), OCTN2 inhibitor (L-carnitine) and OCT2 + OCTN2 inhibitor (guanidine + L-carnitine) (mean  $\pm$  standard deviation,  $n = 4$  or  $5$ ). All inhibitors were administered intranasally with amantadine. Dose of amantadine, guanidine and L-carnitine were  $5 \text{ mg/kg}$ ,  $50 \text{ }\mu\text{g/kg}$  and  $2.5 \text{ }\mu\text{g/kg}$  respectively. Concentrations reported are probe recovery corrected values. \* indicates statistically significant different concentration compared to IN control ( $p < 0.05$ )

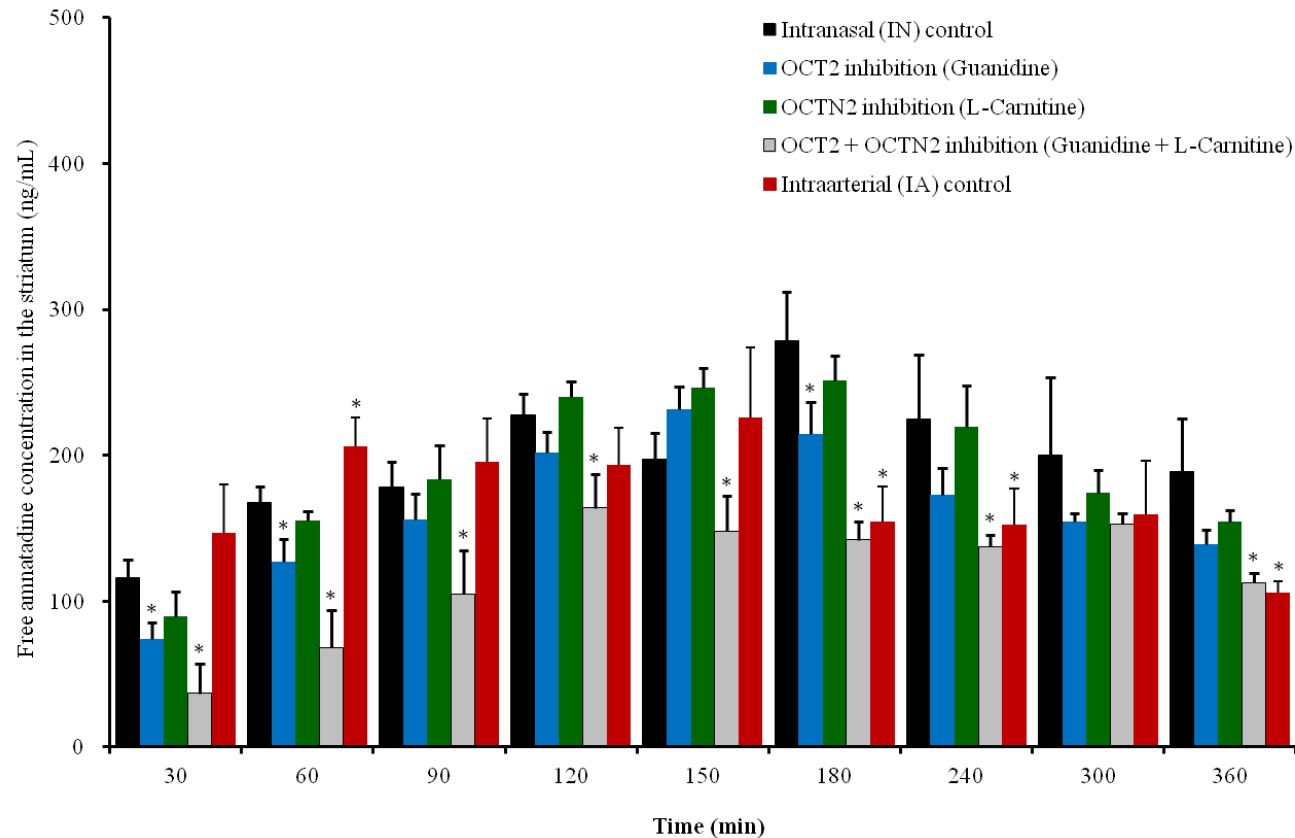


Figure 6-13: Brain striatum ECF concentrations of amantadine following intra-arterial (IA) and intranasal (IN) administration of the drug alone (intranasal control), in the presence of OCT2 inhibitor (guanidine), OCTN2 inhibitor (L-carnitine) and OCT2 + OCTN2 inhibitor (guanidine + L-carnitine) (mean  $\pm$  standard deviation,  $n = 4$  or  $5$ ). All inhibitors were administered intranasally with amantadine. Dose of amantadine, guanidine and L-carnitine were  $5 \text{ mg/kg}$ ,  $50 \mu\text{g/kg}$  and  $2.5 \mu\text{g/kg}$  respectively. Concentrations reported are probe recovery corrected values. \* indicates statistically significant different concentration compared to IN control ( $p < 0.05$ )



*C<sub>brain</sub>/C<sub>plasma</sub> (K<sub>p</sub>) vs. time profile as an indicator  
of CNS exposure*

Since amantadine shows good systemic absorption from the nasal cavity and also good BBB permeability, two major inputs exist for drug entering the brain following nasal administration: (i) from the central compartment (blood) and (ii) from the dosing site (nasal cavity). A  $K_{p,brain}$  vs. time profile can be used to determine the time for attainment of distribution equilibrium to be reached between the brain and plasma compartments. The time at which the substrate concentrations in the brain and blood begin to change in parallel is referred to as the brain-to-blood distribution equilibrium, where the  $K_{p,brain}$  remains constant over time. The  $K_{p,brain}$  values obtained at or after this distribution equilibrium point are used to compare the CNS exposure levels of drugs. The  $K_{p,brain}$  following IA administration of the drug approximates the partition coefficient across the BBB. Any increase in  $K_{p,brain}$  values for other administration routes or inhibition conditions signifies a breach in the BBB permeability or an additional input from a compartment other than the blood. Conversely, a decrease in the  $K_{p,brain}$  value post distribution equilibrium could reflect significant impairment in CNS distribution due to processes such as efflux transport or inhibition of an influx transporter.

To determine  $K_{p,brain}$ , the free drug in plasma at different time points needs to be determined. For this purpose the plasma protein binding of amantadine was determined and the results are listed in Table 6-7. The unbound plasma concentrations for all the groups were calculated from the total amantadine concentrations measured in the blood then corrected for an unbound drug fraction of 30.3%.

Table 6-7: Rat plasma unbound fractions of amantadine at three different plasma concentrations as determined by ultrafiltration (n=3/concentration)

| Total plasma amantadine conc. | % of unbound amantadine |
|-------------------------------|-------------------------|
| 100 ng/mL                     | 30.6 ± 6.0              |
| 500 ng/mL                     | 28.1 ± 5.9              |
| 1200 ng/mL                    | 33.1 ± 4.1              |

Mean: 30.3%

Model calculation of  $K_{p,brain}$  is demonstrated as follows:

The amantadine plasma and olfactory bulb ECF dialysate concentrations determined using the LCMS assay at time = 120 min was 342.2 and 72.2 ng/mL, respectively, following an IN dose of amantadine (5mg/kg).

The actual free amantadine concentration in the olfactory bulb ( $C_{brain}$ ) is then calculated by adjusting for the olfactory bulb probe recovery using Equation 6-5 as:

$$\frac{(72.2 \times 100)}{30} = 361.3 \text{ ng/mL}$$

The free amantadine concentration in plasma ( $C_{plasma}$ ) is calculated from the total amantadine plasma concentration using the results from Table 6-7 as:

$$\frac{(342.2 \times 30.3)}{100} = 103.7 \text{ ng/mL}$$

Thus, the  $K_{p,brain}$  at time = 120 min, is calculated from  $C_{brain}$  and  $C_{plasma}$  using Equation 6-7 as:

$$\frac{361.3}{103.7} = 3.5$$

The  $K_{p,brain}$  vs. time profiles for each of the experimental groups are shown in Figure 6-14. A distribution equilibrium was attained in all groups around 120 min, therefore,  $K_{p,brain}$  values after this time point were used to compare the different groups.

The IN control group and the OCTN2 inhibition group showed significantly higher  $K_{p,brain}$  values compared to the IA control group. This indicates that an additional input may be operating under these conditions. The OCT2 inhibition group showed  $K_{p,brain}$  values similar to the IA control group, indicating that the inhibition of OCT2 results in the elimination of the additional input that was observed in the IN control group. The inhibition of both OCT2 and OCTN2, on the other hand, resulted in a significant decrease in the partition coefficient ( $K_{p,brain}$ ) as compared to both IN and IA control groups. This could be the result of the absence of the nasal input and the additional inhibition of OCT2 or OCTN2 which results in a decrease in BBB permeability. OCT2 and OCTN2 are both consistently expressed at high levels in brain microvessel endothelial cells (BBB)<sup>113201</sup>; the inhibition of these transporters by guanidine and L-carnitine, respectively, seems a likely reason for the decrease in the BBB permeability of amantadine under the dual inhibition condition.

The synergistic effect of both OCT2 and OCTN2 transporters in the brain disposition of amantadine is clearly evident from these results. Some of the important factors that need to be considered in the interpretation and application of these results are the extent of brain tissue binding of amantadine and also the inhibitor :drug dose ratios. Only the unbound ECF amantadine concentrations were measured in these studies, but the total amount of the drug in the brain at any given point of time will be much higher since amantadine shows a high degree of brain tissue binding. Therefore, the ability to achieve higher therapeutic brain concentrations of the drug after an intranasal dose, compared to an equivalent intra-arterial dose, is a distinct advantage. Additionally, it should be noted that inhibitor: amantadine dose ratios were much lower than those

maintained during *in vitro* studies (Chapter 5) due to solubility limitations. Consequently, the effect of these transporters may even be more significant in the brain uptake of amantadine from the nasal cavity than what it appears in this study.

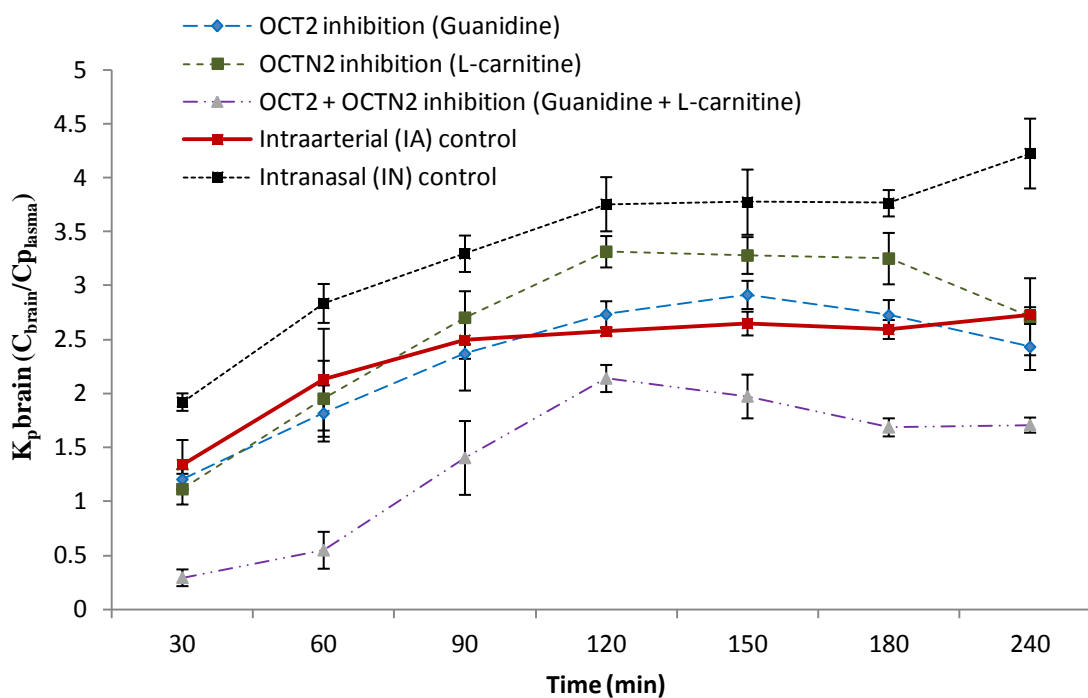


Figure 6-14:  $K_{p,brain} (C_{brain(free)}/C_{plasma(free)})$  vs. time profiles showing the brain : blood partition coefficient of the IA dose compared to the IN dose (with and without inhibition) and the attainment of distribution equilibrium at times  $\geq 120$  min, for each group (n=4 or 5).

### Conclusions

The intranasal administration of amantadine represents a promising route for delivery to the brain. ECF concentrations of the drug in the olfactory bulb and the striatum were significantly higher than those achieved by administering the same dose intra-arterially. The striatum is a site of action for amantadine and, therefore, the possibility of achieving therapeutic levels in this region without exposing the systemic circulation to high levels of the drug is a promising advantage. The results from this study also clearly demonstrate the involvement of both OCT2 and OCTN2 transporters in the disposition of amantadine into the olfactory bulb, confirming a carrier-mediated, olfactory pathway present in the nose to brain transport of amantadine.

Although both OCT2 and OCTN2 transporters seem to synergistically affect the brain disposition of amantadine following intranasal administration, only the OCT2 transporter was shown to have a significant effect when used alone. The  $K_{p,brain}$  results suggest that OCTN2 plays only a minor role in the brain uptake of amantadine via the olfactory pathway. It also appears to play a minor role in the systemic absorption and consequently the brain uptake from the central compartment. These results are consistent with the *in vitro* transport studies for amantadine using the bovine nasal explants, which only showed a significant effect for OCT2 enhancing transport across the olfactory mucosa.

CHAPTER 7  
NOSE TO BRAIN DELIVERY OF CIMETIDINE:  
THE ROLE OF OCT2

*Pharmacokinetics of Cimetidine*

Cimetidine is rapidly, but incompletely and variably, absorbed from the gastrointestinal tract. Absolute bioavailabilities following oral administration are reported to be approximately 60%<sup>202</sup>. This drug shows unusual pharmacokinetic characteristic with the appearance of two plasma concentration maxima following oral dosing<sup>203</sup>. Enterohepatic recirculation had been initially proposed to be responsible for the double peak phenomenon by Veng-Pedersen et al., but it was later observed by that biliary elimination does not significantly impact drug plasma levels<sup>204,205</sup>. Gastric motility patterns and pH have also been proposed as possible reasons behind the double peak phenomenon<sup>206,207</sup>. Following systemic administration, cimetidine shows multicompartmental characteristics in humans with extensive distribution throughout body fluids, organs and tissues. Approximately 70% of the total body content of cimetidine is found in skeletal muscle; 5-10% in the liver, GI tract and bone; 1-5% in the kidney, lung and blood; but less than 1% of it is found in the brain and CSF. The drug has low plasma protein binding (15-20%) and a high total systemic clearance (500 to 600ml/min in human), having a major renal component, with 82-96% of the dose recovered unchanged in the urine<sup>208</sup>. The elimination half-life is approximately 2 hr. Cimetidine elimination is saturable and shows non-linear kinetics<sup>209</sup>. The renal tubular secretion of cimetidine has been attributed to OCT2 in a rat model system<sup>210</sup>. Cimetidine

is also a known inhibitor of many isozymes of the cytochrome P450 system, which forms the basis for its numerous, clinically-relevant drug interactions<sup>211,212</sup>.

#### *Brain penetration of cimetidine*

Cimetidine does not cross the BBB to an appreciable extent and has been found to have limited brain exposure following oral and intravenous administration. The brain to blood ratio of cimetidine has been reported to be around 0.017 in rats. The low brain distribution of cimetidine was found not to be the result of *mdr1a* or *bcrp* efflux in mice and the low flux of cimetidine into the brain could be due to its physicochemical properties ( $\log D_{7.4}$  of  $-0.25$ ) or the result of an increased rate of clearance.

The results from investigations of olfactory drug absorption into the brain are more straightforward to interpret if the model drug does not cross the BBB to any appreciable extent. From this perspective, cimetidine serves as a good model drug owing to its limited ability to cross the BBB, thus significant brain levels following intranasal delivery can likely be attributed to the nasal input of the drug.

#### Materials

Substrates and inhibitor: Cimetidine and pentamidine isoethionate were purchased from Sigma Chemical (St Louis, MO).

All other materials used were as described in Chapter 6.

#### Experimental methods

##### *Animal experiments*

All surgical techniques and procedures for anesthesia, microdialysis probe insertion, femoral artery cannulation for systemic dosing, tracheostomy for intranasal

dosing, BBB integrity testing and euthanasia were performed as described earlier in Chapter 6.

### *Study groups*

The intravenous LD<sub>50</sub> for cimetidine in rats has been reported to be 106 mg/kg<sup>213</sup>. Intravenous and intraperitoneal doses of cimetidine which have been safely used in rats include 10 mg/kg and 25 mg/kg, exposures respectively<sup>214</sup>. Since the effect of transporter inhibition is better observed at low substrate concentrations, a dose of 750 µg/kg cimetidine was selected as the lowest possible dose that provided detectable brain dialysate concentrations following both routes (intra-arterial and intranasal) of administration. The same dose was used for both the routes.

Four study groups were considered, with each group ( $n = 4$  to  $5$ ) receiving cimetidine (750 µg/kg) intra-arterially or intranasally, with or without the OCT2 inhibitor, pentamidine (4 mg/kg) (Table 7-1). All drug and inhibitor solutions were prepared in fresh sterile saline. The animals were prepared for IN and IA dosing as described previously in Chapter 6.

Table 7-1: Study groups for cimetidine (750 µg/kg,  $n = 4$  to  $5$  rats/group) and an OCT2 inhibitor pentamidine, used evaluate the role of OCT2 transporter in the brain uptake of cimetidine following IN dosing

| # | Route<br>(Cimetidine, 750µg/kg) | OCT2 Inhibitor       |
|---|---------------------------------|----------------------|
| 1 | IV                              | -                    |
| 2 | IN                              | -                    |
| 3 | IN                              | Pentamidine (4mg/kg) |



### *Brain and plasma sampling*

At the beginning of the blood sampling, the initial two drops of blood were discarded to eliminate dilution by the saline present in the cannula. Approximately the same volume of heparinized normal saline was used to replace volume lost following each sample collection. Blood (200  $\mu$ L) was collected at predetermined time points (10, 15, 30, 45, 60, 75, 90, 120, 150, 180, 240, 300 min) into heparinized tubes, and the plasma was separated by centrifuging at 16,100 x g for 5 min using an Eppendorf 5415D centrifuge (Eppendorf AG, Hamburg, Germany). Brain dialysate fractions (30 $\mu$ L) from the microdialysis probes were collected over 30min intervals for 5hrs. The dialysate samples were collected over 0-30, 30-60, 60-90, 90-120, 120-150, 150-180, 180-240 and 240-300 min were assigned time points 30, 60, 90, 120, 150, 180, 240 and 300 min, respectively. All samples were stored at -80<sup>0</sup> C until analysis.

## Results and Discussion

### *Microdialysis Recovery*

*In vivo* recovery by loss experiments were carried out at two different concentrations (n=3 rats) of cimetidine perfusate, 25 and 250 ng/mL. These concentrations were selected to represent the typical brain concentrations following IN and IA administration of cimetidine as determined from pilot dosing studies in rats. Additionally, the time dependence of probe recovery of the drug was determined for cimetidine perfusate concentrations of 25 ng/mL where recoveries were estimated from dialysates collected at three time points (30, 90 and 180 min, n=3) for both probes. The results are shown in Figures 7-1 and 7-2. There were no statistically significant

differences ( $p < 0.05$ ) in the percentage of cimetidine recovered from the probes with respect to the concentrations of cimetidine studied or with respect to time.

The olfactory bulb and striatum recovery was calculated to be  $37.2 \pm 1.7\%$  and  $40.0 \pm 3.5\%$ , respectively. These values were used to calculate the actual olfactory bulb and striatum concentrations from the dialysate concentrations in the dosing experiments in rats. Recoveries are expressed as mean  $\pm$  standard deviation (3 rats/concentration).

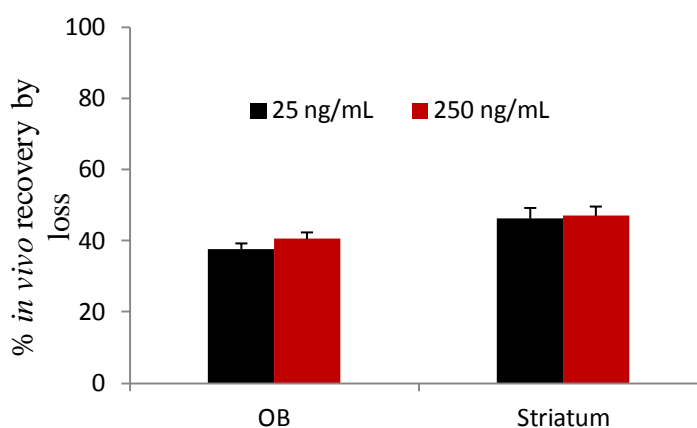


Figure 7-1: Percentage *in vivo* recovery by loss of cimetidine from the olfactory bulb (OB) and striatal probes at two different perfusate concentrations of 25 and 250 ng/mL, (n=3 rats/concentration)

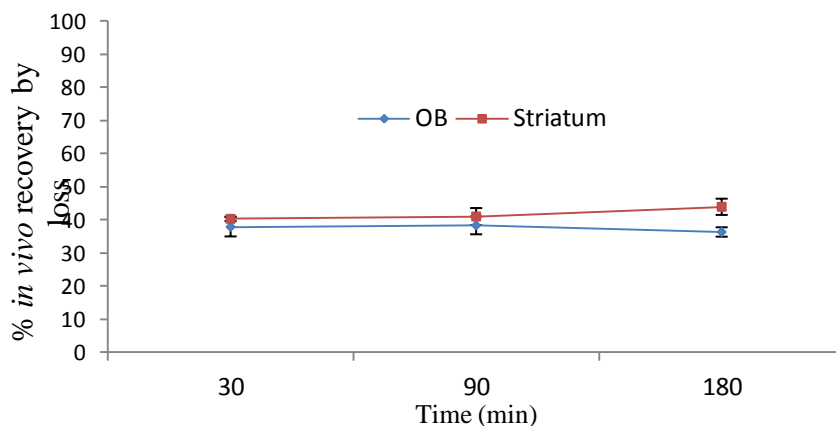


Figure 7-2: Percentage *in vivo* recovery by loss of cimetidine from the olfactory bulb (OB) and the striatum probes over a 3 hour period (30, 90 and 180 min) for a perfusate concentration of 25 ng/mL. (n=3 rats/time point)

*Drug concentrations in plasma following  
intra-arterial (IA) and intranasal (IN) administration*

The plasma concentration-time course of cimetidine (n= 4 or 5) following IA and IN administration is shown in Figure 7-3. Following the IA bolus dose, cimetidine exhibited biexponential elimination from plasma with an initial, rapidly declining distribution phase followed by a slower elimination phase. The IN dose showed an absorption phase followed by an elimination phase. Selected pharmacokinetic parameters,  $AUC_{(0-\infty)}$ ,  $C_{max}$ ,  $T_{max}$ ,  $t_{1/2}$ ,  $V_d$ , and clearance ( $Cl$ ), from the central compartment, as calculated from individual plasma concentration-time profiles following intra-arterial and intranasal dosing, are shown in Table 7-2. The total area under the drug concentration time curve ( $AUC_{0-\infty}$ ) in the plasma for IN dosing was found to be significantly lower than that for IA dosing ( $p < 0.05$ ).

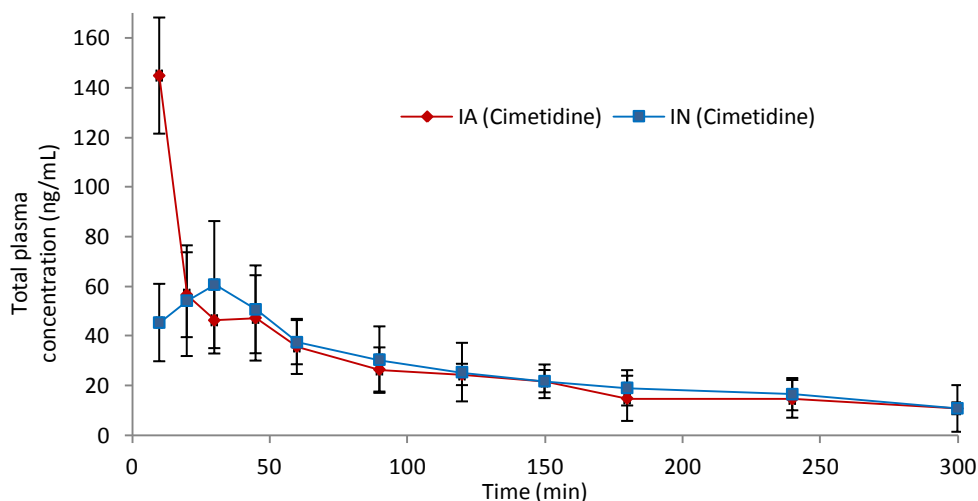


Figure 7-3: Plasma concentration time profiles of cimetidine (750 µg/kg) following intra-arterial (IA) and intranasal (IN) administration in rats (mean ± standard deviation, n=4 or 5).

Cimetidine was incompletely absorbed into the systemic circulation following intranasal administration, and a bioavailability of 43.5% was calculated using Equation 6-5. The terminal half-life and clearance from the central compartment were similar for both IN and IA dosing (Table 7-2).

Table 7-2: Selected pharmacokinetic parameters calculated from the plasma concentration-time profiles of cimetidine (750 µg/kg) following intra-arterial (IA) and intranasal (IN) administration in rats (mean ± standard deviation, n= 4 or 5).

| <b>Parameters</b>                       | <b>IA</b>    | <b>IN</b>    |
|---|--------------|--------------|
| $C_{max}$ (ng/mL)                       | 242.7 ± 33.7 | 60.5 ± 19.9* |
| $T_{max}$ (min)                         | -            | 30 ± 7.5     |
| $AUC_{(0-\infty)}$ (ng.hr/mL)           | 9729 ± 339.5 | 6020 ± 1394* |
| Half life ( $T_{1/2}$ )                 | 1.9 ± 0.3    | 1.3 ± 0.2*   |
| Clearance (l/hr/kg)                     | 4.7 ± 1.5    | 6.7 ± 2.6    |
| Volume of distribution ( $V_d$ ) (l/kg) | 1.0 ± 0.3    | 1.4 ± 0.3    |

Note: \* represents statistically significant differences from the intraarterial (IA) administration group (p < 0.05).

*Brain distribution of cimetidine following  
IA and IN administration*

The unbound cimetidine concentration-time profiles in the brain (olfactory bulb and striatum) are shown in Figure 7-4. A comparison of the unbound cimetidine concentrations in the striatum and olfactory bulb following systemic and nasal administration at different time points are shown in Figure 7-5. Following IA administration, the olfactory bulb and striatal concentrations were not significantly different ( $p < 0.05$ ). This was expected since the vascular supplies to these two regions are similar. At the early time points ( $< 20$  min), the plasma concentrations of cimetidine were much higher following the IA dose when compared to the plasma concentrations after an equivalent IN dose. The plasma profiles are comparable post-20 min. Following IN dosing, significantly higher levels of free drug were measured in both the olfactory bulb and striatum compared to the IA dose. These results indicate that, while cimetidine has poor BBB permeability, the brain concentrations achieved following IN dosing appear to indicate another source of input of drug into the brain beyond transfer from the blood.

The systemic bioavailability for cimetidine following IN administration was only 43.5 %, and, as a result, more than half of the dose may continue to be available for absorption and uptake into the brain via the olfactory pathway when the closed nasal cavity surgical model is utilized, as was done in these experiments.. The  $T_{max}$  and  $C_{max}$  of cimetidine following IN administration was found to be significantly shorter and higher, respectively, for the olfactory bulb compared to the striatum at ( $p < 0.05$ ) (Table 7-3).

This suggests that the drug reaches the olfactory bulb first indicating that a time lag exists before the drug equilibrates with areas of the brain located away from the olfactory bulb.

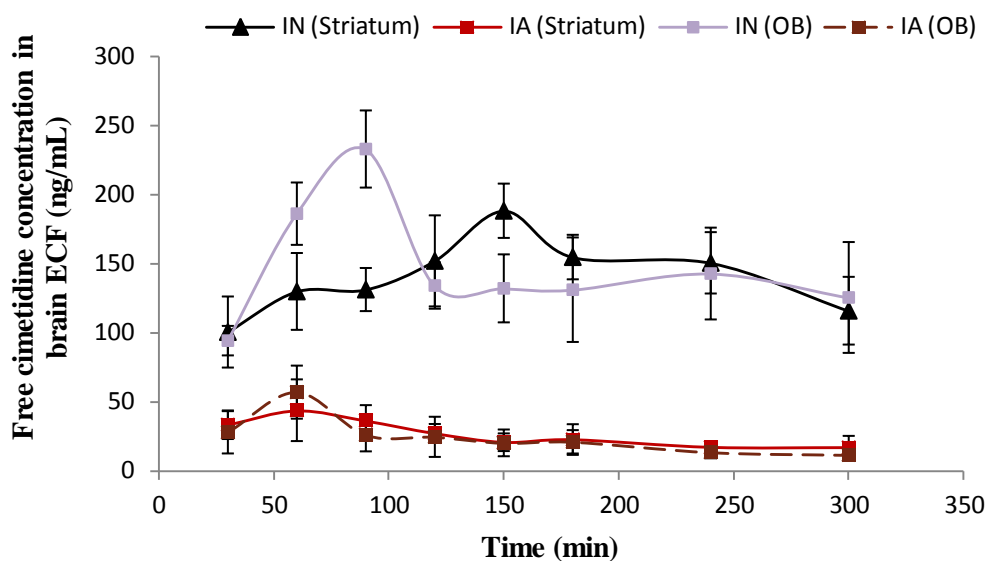


Figure 7-4: Brain (olfactory bulb and striatum) ECF concentration- time profile of cimetidine following intra-arterial (IA) and intranasal (IN) administration in rats at a dose of 750  $\mu\text{g}/\text{kg}$  (mean  $\pm$  standard deviation,  $n=5$ ). Data points are connected by smooth curves. OB: Olfactory bulb.

Table 7-3: Selected pharmacokinetic parameters calculated from the olfactory bulb and striatum ECF-time profiles of cimetidine (750  $\mu\text{g}/\text{kg}$ ) following intra-arterial (IA) and intranasal (IN) administration in rats. (mean  $\pm$  standard deviation,  $n= 4$  or 5).

| Region of sampling | Parameter                | IA             | IN                |
|--------------------|--------------------------|----------------|-------------------|
| Olfactory Bulb     | $C_{\text{max}}$ (ng/ml) | 55.8 $\pm$ 9.4 | 254.9 $\pm$ 22.1* |
|                    | $T_{\text{max}}$ (min)   | 47 $\pm$ 6.1   | 90 $\pm$ 4.7*     |
| Striatum           | $C_{\text{max}}$ (ng/ml) | 60.1 $\pm$ 7.8 | 178.1 $\pm$ 19.4* |
|                    | $T_{\text{max}}$ (min)   | 50 $\pm$ 3.7   | 155 $\pm$ 11.5*   |

Note: \* represents statistically significant differences from the intraarterial (IA) administration group ( $p<0.05$ )

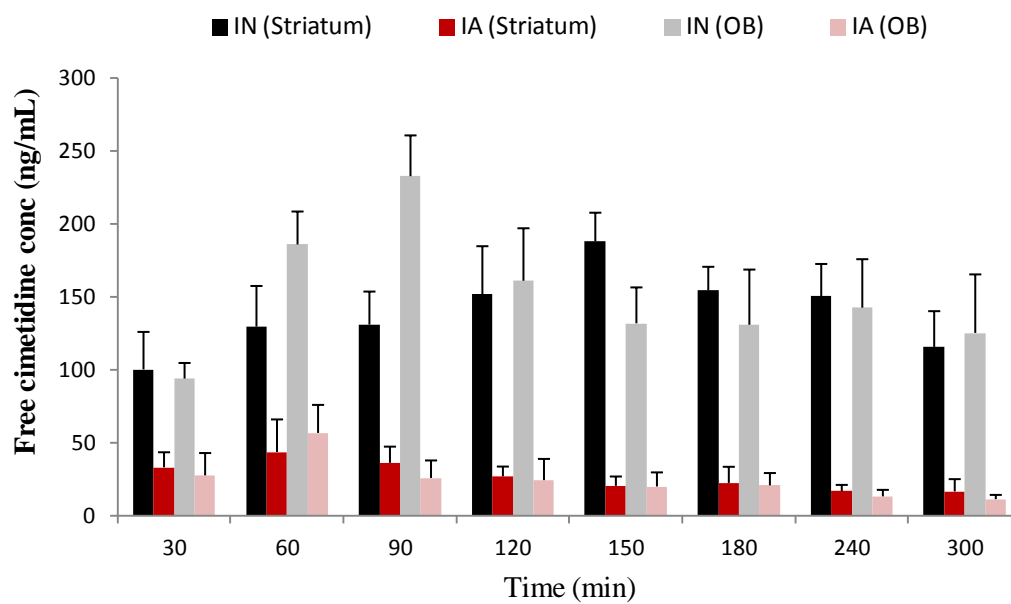


Figure 7-5: Brain (olfactory bulb and striatum) ECF concentrations of cimetidine (750  $\mu\text{g}/\text{kg}$ ) following intra-arterial (IA) and intranasal (IN) administration in rats (mean  $\pm$  standard deviation,  $n=4$ ). OB: Olfactory bulb

*Chemical inhibition of OCT2 transport*

Observations from the *in vitro* studies (Chapter 5) suggest that OCT2-mediated uptake across the olfactory mucosa may be responsible for the increased brain levels observed after an IN dose. To evaluate this hypothesis, pentamidine, an OCT2 inhibitor, at a dose of 4 mg/kg was co-administered intranasally with cimetidine. The ratio of cimetidine to pentamidine was kept high (3 mM cimetidine: 100 mM pentamidine) to achieve effective competitive inhibition.

The effect of pentamidine co-administration with cimetidine intranasally on the plasma concentrations of cimetidine was evaluated (Figure 7-6 and Table 7-4). A statistically significant increase in  $T_{max}$ ,  $t_{1/2}$  and  $AUC_{0-\infty}$  were observed in the presence of the OCT2 inhibitor ( $p < 0.05$ ). The results reveal that inhibition of OCT2 in the respiratory or olfactory tissues prolongs the absorption of cimetidine in to the systemic circulation from the nasal cavity. Furthermore, a significant reduction in the plasma clearance of cimetidine was also observed ( $p < 0.05$ ). This could be due to the effect of systemically absorbed pentamidine inhibiting the renal clearance of cimetidine. The tubular secretion of cimetidine by the kidneys is mediated by OCT2, and inhibition may result in the accumulation of cimetidine in the body resulting in higher AUC values.



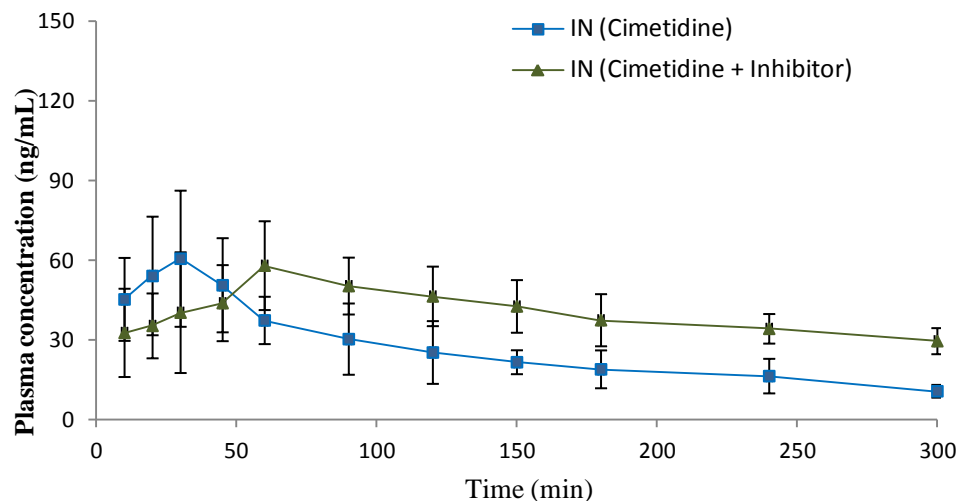


Figure 7-6: Plasma concentration-time profiles of cimetidine (750  $\mu\text{g}/\text{kg}$ ) following intra-nasal (IN) administration of cimetidine alone (IN cimetidine) and with an OCT2 inhibitor, pentamidine (4 mg/kg), (IN cimetidine + inhibitor), (mean  $\pm$  standard deviation, n=5).

Table 7-4: Selected pharmacokinetic parameters calculated from the plasma concentration-time profiles of cimetidine (750  $\mu\text{g}/\text{kg}$ ) following intra-nasal (IN) administration of cimetidine alone (IN cimetidine) and with an OCT2 inhibitor, pentamidine, (4 mg/kg), (mean  $\pm$  standard deviation, n=5).

| Parameters                    | IN<br>(Cimetidine 750<br>$\mu\text{g}/\text{kg}$ ) | IN<br>(Cimetidine 750 $\mu\text{g}/\text{kg}$ ) +<br>pentamidine 4 mg/kg ) |
|-------------------------------|--|--|
| $C_{max}$ (ng/mL)             | 60.5 $\pm$ 19.9                                    | 52.8 $\pm$ 9.4   |
| $T_{max}$ (min)               | 30 $\pm$ 8   | 70 $\pm$ 10*   |
| $AUC_{(0-\infty)}$ (ng.hr/mL) | 6020 $\pm$ 1394.7                                  | 9968 $\pm$ 1764.1*   |
| Half life ( $T_{1/2}$ )       | 1.3 $\pm$ 0.2                                      | 4.7 $\pm$ 1.7*   |
| Clearance (L/hr.kg)           | 6.7 $\pm$ 2.6                                      | 2.5 $\pm$ 0.9*   |

Note: \* represents statistically significant differences from the intranasal (IN) control group ( $p < 0.05$ )

The olfactory bulb and striatum ECF concentration-time profiles of amantadine following intra- intranasal (IN) administration are shown in Figures 7-7A and 7-7B. A comparative evaluation of the brain concentrations following IA and IN administration of cimetidine clearly shows a preferential uptake of the drug from the nasal cavity to the brain, likely via an olfactory pathway. Co-administration of pentamidine with cimetidine intranasally resulted in a significant decrease in the olfactory bulb and striatum concentrations of cimetidine (Figure 7-8 and 7-9) over the first 180 min after dosing, compared to the administration of cimetidine alone ( $p < 0.05$ ). The brain concentration of cimetidine with OCT2 inhibition was similar to that after an IA dose of the drug. At later time points ( $> 180$  min), the inhibitory effect of pentamidine on the brain uptake of cimetidine was not observed, possibly due to decreased pentamidine concentrations at the absorption site. These observations correlate well with the results from the *in vitro* studies in the bovine nasal mucosa, where significant reduction in the transport of cimetidine across the olfactory mucosa was observed in the presence of pentamidine.

Since the major input of cimetidine into the brain is from the nasal cavity following IN administration rather than from the systemic circulation, the decrease in brain concentrations following co-administration of cimetidine and an OCT2 inhibitor provides strong evidence that OCT2-mediated uptake of cimetidine in the nasal mucosa is key to the enhanced brain concentrations seen for the compound.

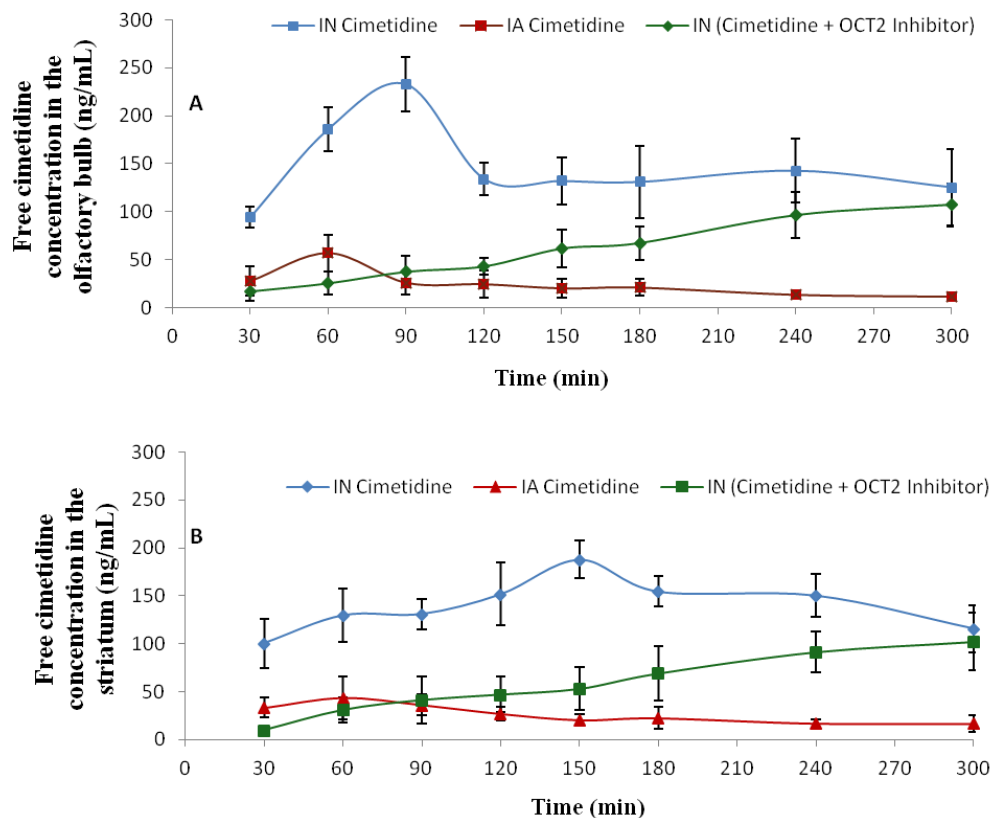


Figure 7-7: Brain ECF concentration-time profile of cimetidine (750 µg/kg) following intraarterial (IA) and intra- intranasal (IN) administration in the (A) olfactory bulb and (B) striatum. The drug was administered alone (intranasal control) and in the presence of OCT2 inhibitor, pentamidine (4 mg/kg), (mean ± standard deviation, n= 4 or 5). Data points are connected by smooth curves.

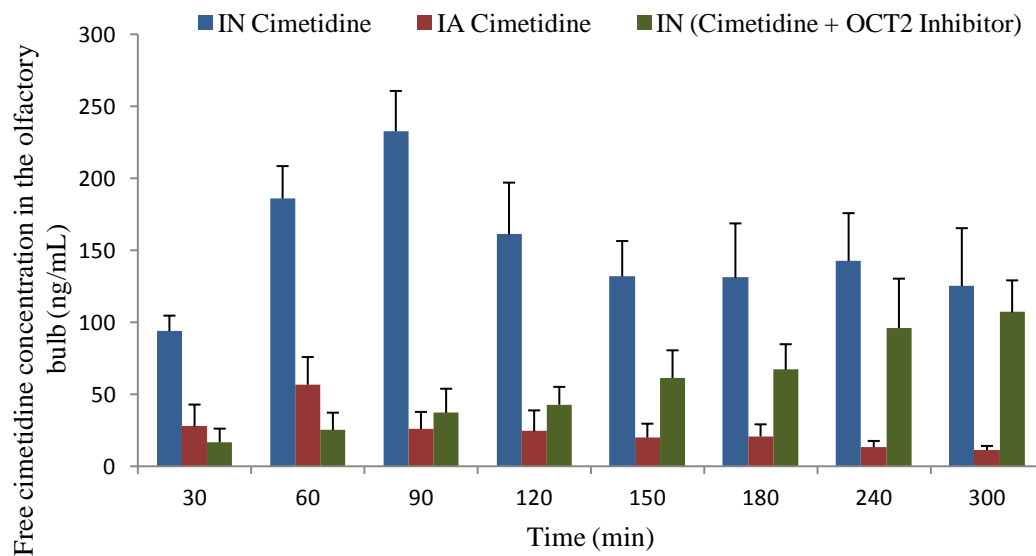


Figure 7-8: Olfactory bulb ECF concentrations of cimetidine following intra-arterial (IA), intranasal (IN) and intranasal (IN) co-administration of an OCT2 inhibitor pentamidine with cimetidine in rats (mean  $\pm$  standard deviation,  $n=4$  or  $5$ ). The doses of cimetidine and OCT2 inhibitor (pentamidine) were  $750 \mu\text{g}/\text{kg}$  and  $4 \text{ mg}/\text{kg}$  respectively.

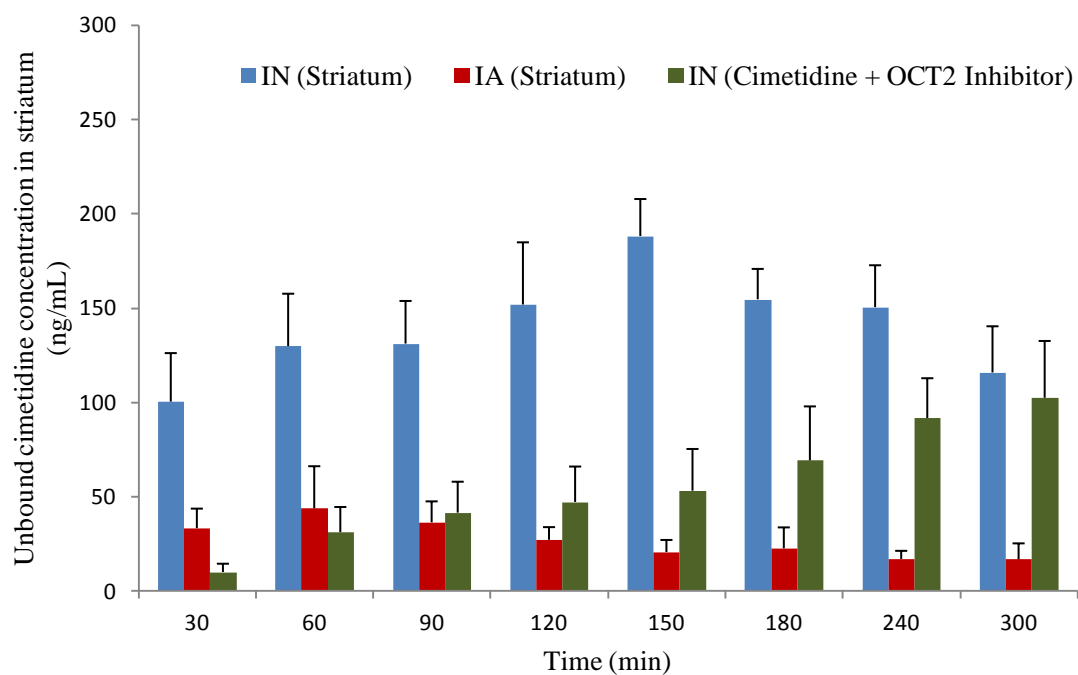


Figure 7-9: Striatal ECF concentrations of cimetidine following intra-arterial (IA), intranasal (IN) and intranasal (IN) co-administration of an OCT2 inhibitor pentamidine, with cimetidine in rats (mean  $\pm$  standard deviation,  $n=4$  or  $5$ ). The doses of cimetidine and OCT2 inhibitor (pentamidine) were  $750 \mu\text{g}/\text{kg}$  and  $4 \text{ mg}/\text{kg}$ , respectively.

### Conclusions

Cimetidine is a relatively hydrophilic drug with a low net BBB permeability following systemic administration. This study demonstrates that the nasal delivery of cimetidine in rats result in a preferential uptake into the brain (both striatum and olfactory bulb regions) compared to an equivalent intra-arterial dose of the drug. Significant inhibition of the brain uptake of cimetidine after intranasal administration was observed when pentamidine, an OCT2 inhibitor, was co-administered with cimetidine. Therefore, OCT2 was found to play a key role in the brain uptake/disposition of cimetidine after intranasal administration.

## CHAPTER 8

### CONCLUSION

The presence of anatomical connections between the nose and the brain makes the nasal route a promising alternative for the targeted delivery of small hydrophilic drug molecules that are unable to cross the BBB through commonly used routes of drug administration to reach the CNS. Many small molecules have been shown to have preferential uptake into the brain following nasal administration. Consequently, a tremendous potential exists in exploring the mechanisms controlling the brain disposition of drugs following intranasal administration. A major challenge in achieving therapeutic concentrations of drugs into the olfactory bulb and subsequently into the brain involves crossing the olfactory epithelial barrier and the olfactory submucosa. Any mechanisms that can enhance the flux of drugs across the olfactory epithelium hold promise for targeting these agents to the brain. One such mechanism involves leveraging the small molecules that are substrates of various drug transporters present in the olfactory mucosa. Thus, the main focus of these studies was to utilize the presence of organic cation transporters present in the olfactory mucosa to target small molecule, organic cation substrates into the olfactory submucosa and subsequently to enhance their brain uptake and disposition.

Amantadine and cimetidine are both small molecule drugs; both are sufficiently soluble to provide nasal doses comparable to the routine IV dose used in rodents. Furthermore, these drugs have negligible metabolic susceptibility. *In vitro* studies were used to investigate the transport systems for amantadine and cimetidine and results showed the involvement of several organic cation transporters, namely OCT2 and

OCTN2, in the transport of these drugs. OCT2 was observed to mediate the transport of both of these drugs across the olfactory tissue while a synergistic effect of both OCT2 and OCTN2 was demonstrated to mediate the transport of amantadine across the respiratory tissues.

*In vivo* studies in rats were carried out to evaluate whether the mechanisms of transport of the drugs identified in the *in vitro* studies would translate into an effective brain disposition of amantadine and cimetidine following IN administration. Both cimetidine and amantadine showed higher brain concentrations following IN administration when compared to IA administration of the equivalent dose. The inhibition of OCT2 resulted in significantly lower brain concentrations for both the drugs, demonstrating the role of the transporter in the uptake and transfer of these drugs from the nasal cavity into the brain. In the case of amantadine, the brain disposition was observed to be the result of a synergistic effect of OCT2 and OCTN2 transporters. There was a greater CNS exposure to each drug when OCT transporters were active, confirming the role in their direct CNS distribution from the nasal cavity to the brain. The results of this study suggest that OCT substrates might be good candidates for delivery to the brain via the olfactory route.

Additionally, both *in vitro* and *in vivo* approaches were introduced in this research and the correlation of results from the *in vitro* studies in bovine nasal explants and the *in vivo* studies in rats demonstrate the usefulness of the bovine nasal model for primary screening of compounds that can be targeted to the brain using the olfactory pathway. From the formulation scientist's perspective, a better understanding of permeation pathways/mechanisms is required to optimize the transfer of drugs across the mucosal



membranes and their resulting disposition to targeted anatomical sites. The results of these studies suggest one such mechanism, the use of OCT substrates as candidates for the delivery of drugs to the brain via the olfactory route. Therefore, the identification of additional transporters active in the olfactory mucosa that can improve the flux of small molecule substrates into the lamina propria may prove to be a beneficial strategy in overcoming the challenges of delivery to the brain.

Some additional challenges that need to be addressed before these results can have true clinical relevance include the efficient delivery the drug to the olfactory mucosal surfaces, a significant challenge despite easy access to the nasal cavity. Other concerns include the loss of portions of the IN dose through mucociliary clearance and the subsequent gastrointestinal absorption of the drug. However, formulation and device based approaches maybe able to solve some of these above mentioned issues.

In general, nasal delivery represents a promising route of drug administration and the utilization of drug uptake transporters in the olfactory epithelium to improve brain disposition of drugs as demonstrated with this research, offers a tremendous opportunity to bypass the blood brain barrier to efficiently deliver therapeutic treatments for CNS based diseases.

## APPENDIX

Buffer Formulae**In vitro diffusion studies**KRB buffer (pH 7.4)

|                                  |          |
|----------------------------------|----------|
| MgCl <sub>2</sub>                | 1.67 mM  |
| NaCl                             | 120 mM   |
| KCl                              | 4.56 mM  |
| Na <sub>2</sub> HPO <sub>4</sub> | 0.830 mM |
| NaH <sub>2</sub> PO <sub>4</sub> | 1.50 mM  |
| NaHCO <sub>3</sub>               | 15.0 mM  |
| CaCl <sub>2</sub>                | 1.20 mM  |
| Glucose                          | 10.0 mM  |

Na<sup>+</sup> free KRB buffer (pH 7.4)

|                                 |          |
|---------------------------------|----------|
| MgCl <sub>2</sub>               | 1.67 mM  |
| KCl                             | 124 mM   |
| K <sub>2</sub> HPO <sub>4</sub> | 0.830 mM |
| KH <sub>2</sub> PO <sub>4</sub> | 1.50 mM  |
| KHCO <sub>3</sub>               | 15.0 mM  |
| CaCl <sub>2</sub>               | 1.20 mM  |
| Glucose                         | 10.0 mM  |

**Western blot /ELISA**Lysis buffer for extraction of membrane proteins (pH 8.0)

NaCl 150 mM

TritonX 100 1.0 %

TrisHCl 50 mM

PBS 10X (pH 7.4)

NaCl 1.37 mM

KCl 26.8 mM

Na<sub>2</sub>HPO<sub>4</sub> 0.1 MKHPO<sub>4</sub> 17.6 mM

HCl (1N) To adjust pH

Running buffer (pH 8.3)

Tris base 25 mM

Glycine 190 mM

SDS 0.10 %

Transfer buffer

Tris base 25 mM

Glycine 190 mM

SDS 0.10 %

Methanol 20 %

Blocking solution (in PBS pH7.4)

BSA 3 %

Tween 20 0.05 %

PBST Wash buffer (in PBS pH7.4)

Tween 20 0.05 %

Laemmli buffer(2X) pH 6.8

|                   |         |
|-------------------|---------|
| SDS               | 4 %     |
| 2-mercaptoethanol | 10 %    |
| Glycerol          | 20 %    |
| Bromophenol blue  | 0.004 % |
| Tris HCl          | 0.125 M |

TMB (3,3',5,5'-tetramethylbenzidine) Substrate Solution

|  |           |
|--|-----------|
| TMB                                    | 1mg       |
| DMSO                                   | 1mL       |
| Hydrogen peroxide (30%)                | 2 $\mu$ L |
| Phosphate-Citrate Buffer (0.05M, pH 5) | 9mL       |

0.05 M Phosphate-Citrate Buffer

|                                 |        |
|---------------------------------|--------|
| Dibasic sodium phosphate (0.2M) | 25.7mL |
| Citric acid (0.1M)              | 24.3mL |
| Deionized waster                | 50mL   |
| Adjust to pH 5.0                |        |

**BCA assay**Reagent A (in 0.1 M NaOH)

Bicinchoninic acid (BCA)

Sodium carbonate

Sodium bicarbonate

Sodium tartrate

Reagent B

Cupric sulfate 4 %

Reagent C

BSA 2 mg/ml

Saline 0.9 %

Sodium azide 0.05%

**In vivo studies**Artificial extracellular fluid (aECF) pH

## Solution A

|                                      |        |
|--------------------------------------|--------|
| Sodium chloride                      | 8.66g  |
| Potassium chloride                   | 0.224g |
| Calcium chloride 2H <sub>2</sub> O   | 0.206g |
| Magnesium chloride 6H <sub>2</sub> O | 0.163g |
| Deionized water q.s                  | 500mL  |

## Solution B

|                             |        |
|-----------------------------|--------|
| Sodium dihydrogen phosphate | 0.027g |
| Disodium hydrogen phosphate | 0.214g |
| Deionized water q.s         | 500mL  |

Combine equal parts of solution A and solution B

## REFERENCES

1. Alavijeh, M. S., Chishty, M., Qaiser, M. Z. & Palmer, A. M. Drug metabolism and pharmacokinetics, the blood-brain barrier, and central nervous system drug discovery. *NeuroRx* **2**, 554–71 (2005).
2. Ying, W. The nose may help the brain: intranasal drug delivery for treating neurological diseases. *Future Neurology* **3**, 1–4 (2008).
3. Minn, A. *et al.* Drug transport into the mammalian brain: the nasal pathway and its specific metabolic barrier. *Journal of Drug Targeting* **10**, 285–96 (2002).
4. Pardridge, W. M. Alzheimer's disease drug development and the problem of the blood-brain barrier. *Alzheimer's & Dementia* **5**, 427–32 (2009).
5. Liu, X., Chen, C. & Smith, B. J. Progress in brain penetration evaluation in drug discovery and development. *The Journal of Pharmacology and Experimental Therapeutics* **325**, 349–56 (2008).
6. Pizzo, D. P. & Thal, L. J. Intraparenchymal nerve growth factor improves behavioral deficits while minimizing the adverse effects of intracerebroventricular delivery. *Neuroscience* **124**, 743–55 (2004).
7. Meijer, D. H., Maguire, C. A., LeRoy, S. G. & Sena-Esteves, M. Controlling brain tumor growth by intraventricular administration of an AAV vector encoding IFN-beta. *Cancer Gene Therapy* **16**, 664–71 (2009).
8. Hanson, L. R. & Frey, W. H. Intranasal delivery bypasses the blood-brain barrier to target therapeutic agents to the central nervous system and treat neurodegenerative disease. *BMC Neuroscience* **9 Suppl 3**, S5 (2008).
9. Renner, B. & Schreiber, K. Olfactory and trigeminal interaction of menthol and nicotine in humans. *Experimental Brain Research*. **219**, 13–26 (2012).
10. Chow, H. S., Chen, Z. & Matsuura, G. T. Direct transport of cocaine from the nasal cavity to the brain following intranasal cocaine administration in rats. *Journal of Pharmaceutical Sciences* **88**, 754–8 (1999).
11. Dhuria, S. V, Hanson, L. R. & Frey, W. H. Intranasal delivery to the central nervous system: mechanisms and experimental considerations. *Journal of Pharmaceutical Sciences* **99**, 1654–73 (2010).
12. Alsarra, I. A., Hamed, A. Y., Alanazi, F. K. & Maghraby, G. M. El Drug Delivery to the Central Nervous System. **45**, (2010).

13. Djupesland, P. G. Nasal drug delivery devices: characteristics and performance in a clinical perspective—a review. *Drug Delivery and Translational Research* **3**, 42–62 (2013).
14. Lee, V. H. Enzymatic barriers to peptide and protein absorption. *Critical Reviews in Therapeutic Drug Carrier Systems* **5**, 69–97 (1988).
15. Hong, J. Y. *et al.* Metabolism of carcinogenic nitrosamines by rat nasal mucosa and the effect of diallyl sulfide. *Cancer Research* **51**, 1509–14 (1991).
16. Brittebo, E. B., Castonguay, A., Furuya, K. & Hecht, S. S. Metabolism of tobacco-specific nitrosamines by cultured rat nasal mucosa. *Cancer Research* **43**, 4343–8 (1983).
17. Zhang, H., Prisinzano, T. E. & Donovan, M. D. Permeation and metabolism of cocaine in the nasal mucosa. *European Journal of Drug Metabolism and Pharmacokinetics* **37**, 255–62 (2012).
18. Illum, L. Is nose-to-brain transport of drugs in man a reality? *The Journal of Pharmacy and Pharmacology* **56**, 3–17 (2004).
19. Jogani, V., Jinturkar, K., Vyas, T. & Misra, A. Recent patents review on intranasal administration for CNS drug delivery. *Recent Patents on Drug Delivery & Formulation* **2**, 25–40 (2008).
20. Misra, A. & Kher, G. Drug delivery systems from nose to brain. *Current Pharmaceutical Biotechnology* **13**, 2355–79 (2012).
21. Wioland, M. A. *et al.* CFTR, MDR1, and MRP1 immunolocalization in normal human nasal respiratory mucosa. *The Journal of Histochemistry and Cytochemistry* **48**, 1215–22 (2000).
22. Kandimalla, K. K. & Donovan, M. D. Carrier mediated transport of chlorpheniramine and chlorcyclizine across bovine olfactory mucosa: implications on nose-to-brain transport. *Journal of Pharmaceutical Sciences* **94**, 613–24 (2005).
23. Coronas, V., Srivastava, L. K., Liang, J. J., Jourdan, F. & Moyse, E. Identification and localization of dopamine receptor subtypes in rat olfactory mucosa and bulb: a combined in situ hybridization and ligand binding radioautographic approach. *Journal of Chemical Neuroanatomy* **12**, 243–57 (1997).
24. Chemuturi, N. V., Haraldsson, J. E., Prisinzano, T. & Donovan, M. Role of dopamine transporter (DAT) in dopamine transport across the nasal mucosa. *Life Sciences* **79**, 1391–8 (2006).
25. Kaler, G. *et al.* Olfactory mucosa-expressed organic anion transporter, Oat6, manifests high affinity interactions with odorant organic anions. *Biochemical and Biophysical Research Communications* **351**, 872–6 (2006).



26. Watelet, J. B., Strolin-Benedetti, M. & Whomsley, R. Defence mechanisms of olfactory neuro-epithelium: mucosa regeneration, metabolising enzymes and transporters. *B-ENT* **5 Suppl 13**, 21–37 (2009).
27. Thiebaud, N. *et al.* Expression and differential localization of xenobiotic transporters in the rat olfactory neuro-epithelium. *Neuroscience Letters* **505**, 180–5 (2011).
28. Chemuturi, N. V & Donovan, M. D. Role of organic cation transporters in dopamine uptake across olfactory and nasal respiratory tissues. *Molecular Pharmaceutics* **4**, 936–42 (2007).
29. Lee, K.-R. *et al.* Lack of a primary physicochemical determinant in the direct transport of drugs to the brain after nasal administration in rats: potential involvement of transporters in the pathway. *Drug Metabolism and Pharmacokinetics* **25**, 430–41 (2010).
30. Dykewicz, M. S. & Hamilos, D. L. Rhinitis and sinusitis. *The Journal of Allergy and Clinical Immunology* **125**, S103–15 (2010).
31. olfactory epithelium. [Art]. Encyclopædia Britannica Online. Retrieved 10 April 2013, from <http://www.britannica.com/EBchecked/media/48235/The-olfactory-epithelium-found-within-the-nasal-cavity-contains-olfactory>.
32. Sahin-Yilmaz, A. & Naclerio, R. M. Anatomy and physiology of the upper airway. *Proceedings of the American Thoracic Society* **8**, 31–9 (2011).
33. Proctor, D. F. & Adams, G. K. Physiology and pharmacology of nasal function and mucus secretion. *Pharmacology & therapeutics. Part B: General & systematic pharmacology* **2**, 493–509 (1976).
34. Harkema, J. R., Carey, S. A. & Wagner, J. G. The nose revisited: a brief review of the comparative structure, function, and toxicologic pathology of the nasal epithelium. *Toxicologic Pathology* **34**, 252–69 (2006).
35. Zhang, H. (2009). Identification of membrane transporters to facilitate intranasal drug delivery using tissue-based pharmacokinetic approaches. (Doctoral dissertation). Division of Pharmaceutics. University of Iowa.
36. Jones, N. The nose and paranasal sinuses physiology and anatomy. *Advanced Drug Delivery Reviews* **51**, 5–19 (2001).
37. Graziadei, P. P. & Monti Graziadei, G. A. Neurogenesis and neuron regeneration in the olfactory system of mammals. III. Deafferentation and reinnervation of the olfactory bulb following section of the fila olfactoria in rat. *Journal of Neurocytology* **9**, 145–62 (1980).

38. Faber Harold The early lesions of poliomyelitis after intranasal inoculation: With comments on their relationship to the early clinical manifestations and to the nonparalytic cases. *Journal of Pediatrics* **13**, 10–37 (1938).
39. Stewart, W. B. Labelling of olfactory bulb glomeruli following horseradish peroxidase lavage of the nasal cavity. *Brain Research* **347**, 200–3 (1985).
40. Czerniawska, A. Experimental investigations on the penetration of <sup>198</sup>Au from nasal mucous membrane into cerebrospinal fluid. *Acta Otolaryngologica* **70**, 58–61 (1970).
41. Wang, X., He, H., Leng, W. & Tang, X. Evaluation of brain-targeting for the nasal delivery of estradiol by the microdialysis method. *International Journal of Pharmaceutics* **317**, 40–6 (2006).
42. Chou, K.-J. & Donovan, M. D. Lidocaine distribution into the CNS following nasal and arterial delivery: a comparison of local sampling and microdialysis techniques. *International Journal of Pharmaceutics* **171**, 53–61 (1998).
43. Huang, Y. & Donovan, M. Large molecule and particulate uptake in the nasal cavity: the effect of size on nasal absorption. *Advanced Drug Delivery Reviews* **29**, 147–155 (1998).
44. McMartin, C., Hutchinson, L. E., Hyde, R. & Peters, G. E. Analysis of structural requirements for the absorption of drugs and macromolecules from the nasal cavity. *Journal of Pharmaceutical Sciences* **76**, 535–40 (1987).
45. Sakane, T. *et al.* Direct drug transport from the rat nasal cavity to the cerebrospinal fluid: the relation to the molecular weight of drugs. *The Journal of Pharmacy and Pharmacology* **47**, 379–81 (1995).
46. Sakane, T., Akizuki, M., Yamashita, S., Sezaki, H. & Nadai, T. Direct drug transport from the rat nasal cavity to the cerebrospinal fluid: the relation to the dissociation of the drug. *The Journal of Pharmacy and Pharmacology* **46**, 378–9 (1994).
47. Kandimalla, K. K. & Donovan, M. D. Localization and differential activity of P-glycoprotein in the bovine olfactory and nasal respiratory mucosae. *Pharmaceutical Research* **22**, 1121–8 (2005).
48. Merkus, F. W. H. M. & Van den Berg, M. P. Can nasal drug delivery bypass the blood-brain barrier?: questioning the direct transport theory. *Drugs in R&D* **8**, 133–44 (2007).
49. Yu, H. & Kim, K. Direct nose-to-brain transfer of a growth hormone releasing neuropeptide, hexarelin after intranasal administration to rabbits. *International Journal of Pharmaceutics* **378**, 73–9 (2009).

50. Dufes, C. *et al.* Brain delivery of vasoactive intestinal peptide (VIP) following nasal administration to rats. *International Journal of Pharmaceutics* **255**, 87–97 (2003).
51. Banks, W. A., During, M. J. & Niehoff, M. L. Brain uptake of the glucagon-like peptide-1 antagonist exendin(9-39) after intranasal administration. *The Journal of Pharmacology and Experimental Therapeutics* **309**, 469–75 (2004).
52. Hanson, L. R. *et al.* Intranasal deferoxamine provides increased brain exposure and significant protection in rat ischemic stroke. *The Journal of Pharmacology and Experimental Therapeutics* **330**, 679–86 (2009).
53. Van den Berg, M. P., Merkus, P., Romeijn, S. G., Verhoef, J. C. & Merkus, F. W. H. M. Uptake of melatonin into the cerebrospinal fluid after nasal and intravenous delivery: studies in rats and comparison with a human study. *Pharmaceutical Research* **21**, 799–802 (2004).
54. Thorne, R. G., Pronk, G. J., Padmanabhan, V. & Frey, W. H. Delivery of insulin-like growth factor-I to the rat brain and spinal cord along olfactory and trigeminal pathways following intranasal administration. *Neuroscience* **127**, 481–96 (2004).
55. Craft, S. *et al.* Intranasal insulin therapy for Alzheimer disease and amnesic mild cognitive impairment: a pilot clinical trial. *Archives of Neurology* **69**, 29–38 (2012).
56. Leinwand, S. G. & Chalasani, S. H. Olfactory networks: from sensation to perception. *Current opinion in genetics & development* **21**, 806–11 (2011).
57. Brand, G. Olfactory/trigeminal interactions in nasal chemoreception. *Neuroscience and Biobehavioral Reviews* **30**, 908–17 (2006).
58. Wu, H., Hu, K. & Jiang, X. From nose to brain: understanding transport capacity and transport rate of drugs. *Expert Opinion on Drug Delivery* **5**, 1159–68 (2008).
59. Ranganathan, R. & Buck, L. B. Olfactory axon pathfinding: who is the pied piper? *Neuron* **35**, 599–600 (2002).
60. Brunjes, P. C. & Greer, C. A. Progress and directions in olfactory development. *Neuron* **38**, 371–4 (2003).
61. Lochhead, J. J. & Thorne, R. G. Intranasal delivery of biologics to the central nervous system. *Advanced Drug Delivery Reviews* **64**, 614–28 (2012).
62. Simkó, M. & Mattsson, M.-O. Risks from accidental exposures to engineered nanoparticles and neurological health effects: a critical review. *Particle and Fibre Toxicology* **7**, 42 (2010).

63. Johnson, N. J., Hanson, L. R. & Frey, W. H. Trigeminal pathways deliver a low molecular weight drug from the nose to the brain and orofacial structures. *Molecular Pharmaceutics* **7**, 884–93 (2010).
64. Hummel, T. & Livermore, A. Intranasal chemosensory function of the trigeminal nerve and aspects of its relation to olfaction. *International Archives of Occupational and Environmental Health* **75**, 305–13 (2002).
65. Koepsell, H. & Endou, H. The SLC22 drug transporter family. *European Journal of Physiology (Pflügers Archiv)* **447**, 666–76 (2004).
66. Koepsell, H., Lips, K. & Volk, C. Polyspecific organic cation transporters: structure, function, physiological roles, and biopharmaceutical implications. *Pharmaceutical Research* **24**, 1227–51 (2007).
67. Gründemann, D. & Schömig, E. Gene structures of the human non-neuronal monoamine transporters EMT and OCT2. *Human Genetics* **106**, 627–35 (2000).
68. Koehler, M. R., Wissinger, B., Gorboulev, V., Koepsell, H. & Schmid, M. The two human organic cation transporter genes SLC22A1 and SLC22A2 are located on chromosome 6q26. *Cytogenetics and Cell Genetics* **79**, 198–200 (1997).
69. Enomoto, A. *et al.* Molecular identification of a novel carnitine transporter specific to human testis. Insights into the mechanism of carnitine recognition. *The Journal of Biological Chemistry* **277**, 36262–71 (2002).
70. Peltekova, V. D. *et al.* Functional variants of OCTN cation transporter genes are associated with Crohn disease. *Nature Genetics* **36**, 471–5 (2004).
71. Engler, J. R., Hughes, T. P. & White, D. L. OCT-1 as a determinant of response to antileukemic treatment. *Clinical Pharmacology and Therapeutics* **89**, 608–11 (2011).
72. Ahlin, G. *et al.* Structural requirements for drug inhibition of the liver specific human organic cation transport protein 1. *Journal of Medicinal Chemistry* **51**, 5932–42 (2008).
73. Suhre, W. M., Ekins, S., Chang, C., Swaan, P. W. & Wright, S. H. Molecular determinants of substrate/inhibitor binding to the human and rabbit renal organic cation transporters hOCT2 and rbOCT2. *Molecular Pharmacology* **67**, 1067–77 (2005).
74. Agu, R. *et al.* Differential expression of organic cation transporters in normal and polyps human nasal epithelium: implications for in vitro drug delivery studies. *International journal of pharmaceutics* **406**, 49–54 (2011).

75. Genter, M. B., Krishan, M., Augustine, L. M. & Cherrington, N. J. Drug transporter expression and localization in rat nasal respiratory and olfactory mucosa and olfactory bulb. *Drug Metabolism and Disposition* **38**, 1644–7 (2010).
76. Lips, K. S. *et al.* Polyspecific cation transporters mediate luminal release of acetylcholine from bronchial epithelium. *American Journal of Respiratory Cell and Molecular Biology* **33**, 79–88 (2005).
77. Horvath, G. *et al.* Epithelial organic cation transporters ensure pH-dependent drug absorption in the airway. *American Journal of Respiratory Cell and Molecular Biology* **36**, 53–60 (2007).
78. Wu, X. *et al.* Identity of the organic cation transporter OCT3 as the extraneuronal monoamine transporter (uptake2) and evidence for the expression of the transporter in the brain. *The Journal of Biological Chemistry* **273**, 32776–86 (1998).
79. Gründemann, D. *et al.* Transport of monoamine transmitters by the organic cation transporter type 2, OCT2. *The Journal of Biological Chemistry* **273**, 30915–20 (1998).
80. Budiman, T., Bamberg, E., Koepsell, H. & Nagel, G. Mechanism of electrogenic cation transport by the cloned organic cation transporter 2 from rat. *The Journal of Biological Chemistry* **275**, 29413–20 (2000).
81. Okuda, M., Urakami, Y., Saito, H. & Inui, K. Molecular mechanisms of organic cation transport in OCT2-expressing *Xenopus* oocytes. *Biochimica Biophysica Acta* **1417**, 224–31 (1999).
82. Barendt, W. M. & Wright, S. H. The human organic cation transporter (hOCT2) recognizes the degree of substrate ionization. *The Journal of Biological Chemistry* **277**, 22491–6 (2002).
83. Yabuuchi, H. *et al.* Novel membrane transporter OCTN1 mediates multispecific, bidirectional, and pH-dependent transport of organic cations. *The Journal of Pharmacology and Experimental Therapeutics* **289**, 768–73 (1999).
84. Ohashi, R. *et al.* Na(+)-dependent carnitine transport by organic cation transporter (OCTN2): its pharmacological and toxicological relevance. *The Journal of Pharmacology and Experimental Therapeutics* **291**, 778–84 (1999).
85. Wu, X. *et al.* Functional characteristics and tissue distribution pattern of organic cation transporter 2 (OCTN2), an organic cation/carnitine transporter. *The Journal of Pharmacology and Experimental Therapeutics* **290**, 1482–92 (1999).
86. Nakamura, T. *et al.* Transport of ipratropium, an anti-chronic obstructive pulmonary disease drug, is mediated by organic cation/carnitine transporters in

- human bronchial epithelial cells: implications for carrier-mediated pulmonary absorption. *Molecular Pharmaceutics* **7**, 187–95 (2010).
87. Wagner, C. A. *et al.* Functional and pharmacological characterization of human Na(+)-carnitine cotransporter hOCTN2. *American Journal of Physiology. Renal Physiology* **279**, F584–91 (2000).
  88. Gründemann, D. *et al.* Discovery of the ergothioneine transporter. *Proceedings of the National Academy of Sciences of the United States of America* **102**, 5256–61 (2005).
  89. Volk, C., Gorboulev, V., Budiman, T., Nagel, G. & Koepsell, H. Different affinities of inhibitors to the outwardly and inwardly directed substrate binding site of organic cation transporter 2. *Molecular Pharmacology* **64**, 1037–47 (2003).
  90. Richter, T. & Keipert, S. In vitro permeation studies comparing bovine nasal mucosa, porcine cornea and artificial membrane: androstenedione in microemulsions and their components. *European Journal of Pharmaceutics and Biopharmaceutics* **58**, 137–43 (2004).
  91. Smith, T. D. & Bhatnagar, K. P. Microsmatic primates: reconsidering how and when size matters. *Anatomical Record. Part B, New Anatomist* **279**, 24–31 (2004).
  92. Adams, D. R. Transitional epithelial zone of the bovine nasal mucosa. *The American Journal of Anatomy* **176**, 159–70 (1986).
  93. Menco, B. P., Leunissen, J. L., Bannister, L. H. & Dodd, G. H. Bovine olfactory and nasal respiratory epithelium surfaces. High-voltage and scanning electron microscopy, and cryo-ultramicrotomy. *Cell and Tissue Research* **193**, 503–24 (1978).
  94. Schmidt, M. C. *et al.* Validation of excised bovine nasal mucosa as in vitro model to study drug transport and metabolic pathways in nasal epithelium. *Journal of Pharmaceutical Sciences* **89**, 396–407 (2000).
  95. Pardridge, W. M. Drug transport in brain via the cerebrospinal fluid. *Fluids and Barriers of the CNS* **8**, 7 (2011).
  96. Ross, T. M. *et al.* Intranasal administration of interferon beta bypasses the blood-brain barrier to target the central nervous system and cervical lymph nodes: a non-invasive treatment strategy for multiple sclerosis. *Journal of Neuroimmunology* **151**, 66–77 (2004).
  97. Thorne, R. G., Hanson, L. R., Ross, T. M., Tung, D. & Frey, W. H. Delivery of interferon-beta to the monkey nervous system following intranasal administration. *Neuroscience* **152**, 785–97 (2008).

98. Bustin, S. A. Quantification of mRNA using real-time reverse transcription PCR (RT-PCR): trends and problems. *Journal of Molecular Endocrinology* **29**, 23–39 (2002).
99. VanGuilder, H. D., Vrana, K. E. & Freeman, W. M. Twenty-five years of quantitative PCR for gene expression analysis. *BioTechniques* **44**, 619–26 (2008).
100. Glasel, J. A. Validity of nucleic acid purities monitored by 260nm/280nm absorbance ratios. *BioTechniques* **18**, 62–3 (1995).
101. Gry, M. *et al.* Correlations between RNA and protein expression profiles in 23 human cell lines. *BMC Genomics* **10**, 365 (2009).
102. Blancher, C. & Jones, A. SDS -PAGE and Western Blotting Techniques. *Methods in Molecular Medicine* **57**, 145–62 (2001).
103. Mahmood, T. & Yang, P Western Blot: Technique, Theory, and Trouble Shooting. *North American Journal of Medical Sciences* **4**, 429–434 (2012).
104. Burnette, W. N. Western blotting : remembrance of past things. *Methods in Molecular Biology* **536**, 5–8 (2009).
105. Trieu, E. P. & Targoff, I. N. SDS-PAGE for <sup>35</sup>S immunoprecipitation and immunoprecipitation western blotting. *Methods in Molecular Biology* **869**, 215–33 (2012).
106. Swanson, P. E. Foundations of immunohistochemistry. A practical review. *American Journal of Clinical Pathology* **90**, 333–9 (1988).
107. Shi, S.-R., Shi, Y. & Taylor, C. R. Antigen retrieval immunohistochemistry: review and future prospects in research and diagnosis over two decades. *The Journal of Histochemistry and Cytochemistry* **59**, 13–32 (2011).
108. Ramos-Vara, J. A. Technical aspects of immunohistochemistry. *Veterinary Pathology* **42**, 405–26 (2005).
109. Farr, A. G. & Nakane, P. K. Immunohistochemistry with enzyme labeled antibodies: a brief review. *Journal of Immunological Methods* **47**, 129–44 (1981).
110. Voller, A. The enzyme-linked immunosorbent assay (ELISA) (theory, technique and applications). *Ricerca Clinica Laboratorio* **8**, 289–98 (1978).
111. Hnasko, R., Lin, A., McGarvey, J. A. & Stanker, L. H. A rapid method to improve protein detection by indirect ELISA. *Biochemical and Biophysical Research Communications* **410**, 726–31 (2011).

112. Amat di San Filippo, C., Wang, Y. & Longo, N. Functional domains in the carnitine transporter OCTN2, defective in primary carnitine deficiency. *The Journal of Biological Chemistry* **278**, 47776–84 (2003).
113. Miecz, D. *et al.* Localization of organic cation/carnitine transporter (OCTN2) in cells forming the blood-brain barrier. *Journal of Neurochemistry* **104**, 113–23 (2008).
114. Buchwalow, I., Samoilova, V., Boecker, W. & Tiemann, M. Non-specific binding of antibodies in immunohistochemistry: fallacies and facts. *Scientific Reports* **1**, 28 (2011).
115. Geumann, C., Grønberg, M., Hellwig, M., Martens, H. & Jahn, R. A sandwich enzyme-linked immunosorbent assay for the quantification of insoluble membrane and scaffold proteins. *Analytical Biochemistry* **402**, 161–9 (2010).
116. Spector, R. Transport of amantadine and rimantadine through the blood-brain barrier. *The Journal of Pharmacology and Experimental Therapeutics* **244**, 516–9 (1988).
117. Jantratid, E. *et al.* Biowaiver monographs for immediate release solid oral dosage forms: cimetidine. *Journal of Pharmaceutical Sciences* **95**, 974–84 (2006).
118. Islam, M. S. & Narurkar, M. M. Solubility, stability and ionization behaviour of famotidine. *The Journal of Pharmacy and Pharmacology* **45**, 682–6 (1993).
119. Sun, X., Tian, Y., Zhang, Z. & Chen, Y. A single LC-tandem mass spectrometry method for the simultaneous determination of four H<sub>2</sub> antagonists in human plasma. *Journal of Chromatography. B, Analytical Technologies in the Biomedical and Life Sciences* **877**, 3953–9 (2009).
120. Ho, C., Huang, H. M., Hsu, S. Y., Shaw, C. Y. & Chang, B. L. Simultaneous high-performance liquid chromatographic analysis for famotidine, ranitidine HCl, cimetidine, and nizatidine in commercial products. *Drug Development and Industrial Pharmacy* **25**, 379–85 (1999).
121. Ashiru, D. A. I., Patel, R. & Basit, A. W. Simple and universal HPLC-UV method to determine cimetidine, ranitidine, famotidine and nizatidine in urine: application to the analysis of ranitidine and its metabolites in human volunteers. *Journal of Chromatography. B, Analytical Technologies in the Biomedical and Life Sciences* **860**, 235–40 (2007).
122. Zendelovska, D. & Stafilov, T. Development of an HPLC method for the determination of ranitidine and cimetidine in human plasma following SPE. *Journal of Pharmaceutical and Biomedical Analysis* **33**, 165–73 (2003).



123. Betto, P., Ciranni-Signoretti, E. & Di Fava, R. Determination of cimetidine and related impurities in pharmaceutical formulations by high-performance liquid chromatography. *Journal of Chromatography* **586**, 149–52 (1991).
124. Bartlett, J. M. & Segelman, A. B. Bioanalysis of cimetidine by high-performance liquid chromatography. *Journal of Chromatography* **255**, 239–45 (1983).
125. Snow, B. J., Macdonald, L., Mcauley, D. & Wallis, W. The effect of amantadine on levodopa-induced dyskinesias in Parkinson's disease: a double-blind, placebo-controlled study. *Clinical Neuropharmacology* **23**, 82–5 (2000).
126. Hubsher, G., Haider, M. & Okun, M. S. Amantadine: the journey from fighting flu to treating Parkinson disease. *Neurology* **78**, 1096–9 (2012).
127. Kornhuber, J. *et al.* Therapeutic brain concentration of the NMDA receptor antagonist amantadine. *Neuropharmacology* **34**, 713–21 (1995).
128. Matsubayashi, H., Swanson, K. L. & Albuquerque, E. X. Amantadine inhibits nicotinic acetylcholine receptor function in hippocampal neurons. *The Journal of Pharmacology and Experimental Therapeutics* **281**, 834–44 (1997).
129. Bleidner, W. E., Harmon, J. B., Hewes, W. E., Lynes, T. E. & Hermann, E. C. Absorption, distribution and excretion of amantadine hydrochloride. *The Journal of Pharmacology and Experimental Therapeutics* **150**, 484–90 (1965).
130. Scholtissek, C. & Webster, R. G. Long-term stability of the anti-influenza A compounds--amantadine and rimantadine. *Antiviral Research* **38**, 213–5 (1998).
131. Chew, C. F., Guy, A. & Biggin, P. C. Distribution and dynamics of adamantanes in a lipid bilayer. *Biophysical Journal* **95**, 5627–36 (2008).
132. Amantadine Compound Summary PubChem CID 2130. at [http://pubchem.ncbi.nlm.nih.gov/summary/summary.cgi?cid=64150&loc=ec\\_rcs](http://pubchem.ncbi.nlm.nih.gov/summary/summary.cgi?cid=64150&loc=ec_rcs). Retrieved 10 April 2013.
133. Busch, A. E. *et al.* Human neurons express the polyspecific cation transporter hOCT2, which translocates monoamine neurotransmitters, amantadine, and memantine. *Molecular Pharmacology* **54**, 342–52 (1998).
134. Deveney, C. W., Stein, S. & Way, L. W. Cimetidine in the treatment of Zollinger-Ellison syndrome. *American Journal of Surgery* **146**, 116–23 (1983).
135. Gudmand-Høyer, E. *et al.* Prophylactic effect of cimetidine in duodenal ulcer disease. *British Medical Journal* **1**, 1095–7 (1978).
136. Lefranc, F., Yeaton, P., Brotchi, J. & Kiss, R. Cimetidine, an unexpected anti-tumor agent, and its potential for the treatment of glioblastoma (review). *International Journal of Oncology* **28**, 1021–30 (2006).

137. Lefranc, F. *et al.* Combined cimetidine and temozolomide, compared with temozolomide alone: significant increases in survival in nude mice bearing U373 human glioblastoma multiforme orthotopic xenografts. *Journal of Neurosurgery* **102**, 706–14 (2005).
138. Van der Ven, L. T. *et al.* Growth of cultured human glioma tumour cells can be regulated with histamine and histamine antagonists. *British Journal of Cancer* **68**, 475–83 (1993).
139. Cimetidine Compound Summary PubChem CID 2756. at [http://pubchem.ncbi.nlm.nih.gov/summary/summary.cgi?cid=2756&loc=ec\\_rcs#x281](http://pubchem.ncbi.nlm.nih.gov/summary/summary.cgi?cid=2756&loc=ec_rcs#x281). Retrieved 10 April 2013.
140. Shugarts, S. & Benet, L. Z. The role of transporters in the pharmacokinetics of orally administered drugs. *Pharmaceutical Research* **26**, 2039–54 (2009).
141. Tahara, H. *et al.* A species difference in the transport activities of H2 receptor antagonists by rat and human renal organic anion and cation transporters. *The Journal of Pharmacology and Experimental Therapeutics* **315**, 337–45 (2005).
142. Zolk, O., Solbach, T. F., König, J. & Fromm, M. F. Structural determinants of inhibitor interaction with the human organic cation transporter OCT2 (SLC22A2). *Naunyn-Schmiedeberg's Archives of Pharmacology* **379**, 337–48 (2009).
143. Umehara, K.-I., Iwatsubo, T., Noguchi, K. & Kamimura, H. Functional involvement of the organic cation transporter 2 (rOct2) in the renal uptake of organic cations in rats. *The Journal of International Medical Research* **36**, 123–36 (2008).
144. Giacomini, K. M. *et al.* Membrane transporters in drug development. *Nature Reviews. Drug Discovery* **9**, 215–36 (2010).
145. Yamada, T., Liu, X., Englert, U., Yamane, H. & Dronskowski, R. Solid-state structure of free base guanidine achieved at last. *Chemistry* **15**, 5651–5 (2009).
146. Kaplan, J. E., Davis, L. E., Narayan, V., Koster, J. & Katzenstein, D. Botulism, type A, and treatment with guanidine. *Annals of Neurology* **6**, 69–71 (1979).
147. Gründemann, D., Liebich, G., Kiefer, N., Köster, S. & Schömig, E. Selective substrates for non-neuronal monoamine transporters. *Molecular Pharmacology* **56**, 1–10 (1999).
148. Kimura, N., Masuda, S., Katsura, T. & Inui, K. Transport of guanidine compounds by human organic cation transporters, hOCT1 and hOCT2. *Biochemical Pharmacology* **77**, 1429–36 (2009).

149. Guanidine Compound Summary PubChem CID 5742. at [http://pubchem.ncbi.nlm.nih.gov/summary/summary.cgi?cid=5742&loc=ec\\_rcs](http://pubchem.ncbi.nlm.nih.gov/summary/summary.cgi?cid=5742&loc=ec_rcs). Retrieved 10 April 2013.
150. Krajcovicová-Kudlácková, M., Simoncic, R., Béderová, A., Babinská, K. & Béder, I. Correlation of carnitine levels to methionine and lysine intake. *Physiological Research* **49**, 399–402 (2000).
151. Pekala, J. *et al.* L-carnitine--metabolic functions and meaning in humans life. *Current Drug Metabolism* **12**, 667–78 (2011).
152. Ohashi, R. *et al.* Molecular and physiological evidence for multifunctionality of carnitine/organic cation transporter OCTN2. *Molecular Pharmacology* **59**, 358–66 (2001).
153. Kato, Y. *et al.* Organic cation/carnitine transporter OCTN2 (Slc22a5) is responsible for carnitine transport across apical membranes of small intestinal epithelial cells in mouse. *Molecular Pharmacology* **70**, 829–37 (2006).
154. Carnitine Compound Summary PubChem CID 10917. at [http://pubchem.ncbi.nlm.nih.gov/summary/summary.cgi?cid=10917&loc=ec\\_rcs](http://pubchem.ncbi.nlm.nih.gov/summary/summary.cgi?cid=10917&loc=ec_rcs). Retrieved 10 April 2013.
155. De Jong, M. D., Lange, J. M., Smits, N. J. & Reiss, P. Pneumocystis carinii infection during prophylaxis with nebulized pentamidine in a patient with AIDS. *Nederlands Tijdschrift Geneeskunde* **135**, 424–7 (1991).
156. Baker, N., De Koning, H. P., Mäser, P. & Horn, D. Drug resistance in African trypanosomiasis: the melarsoprol and pentamidine story. *Trends in parasitology* **29**, 110–8 (2013).
157. Pentamidine Compound Summary PubChem CID 8813. at [http://pubchem.ncbi.nlm.nih.gov/summary/summary.cgi?cid=8813&loc=ec\\_rcs](http://pubchem.ncbi.nlm.nih.gov/summary/summary.cgi?cid=8813&loc=ec_rcs). Retrieved 10 April 2013.
158. Ming, X. *et al.* Transport of dicationic drugs pentamidine and furamidine by human organic cation transporters. *Drug Metabolism and Disposition* **37**, 424–30 (2009).
159. Kido, Y., Matsson, P. & Giacomini, K. M. Profiling of a prescription drug library for potential renal drug-drug interactions mediated by the organic cation transporter 2. *Journal of Medicinal Chemistry* **54**, 4548–58 (2011).
160. Poola, N. R., Kalis, M., Plakogiannis, F. M. & Taft, D. R. Characterization of pentamidine excretion in the isolated perfused rat kidney. *The Journal of Antimicrobial Chemotherapy* **52**, 397–404 (2003).

161. Merkle, H., Ditzinger, G., Lang, S., Peter, H. & Schmidt, M. In vitro cell models to study nasal mucosal permeability and metabolism. *Advanced Drug Delivery Reviews* **29**, 51–79 (1998).
162. Youdim, K. A., Avdeef, A. & Abbott, N. J. In vitro trans-monolayer permeability calculations: often forgotten assumptions. *Drug Discovery Today* **8**, 997–1003 (2003).
163. Koepsell, H., Schmitt, B. M. & Gorboulev, V. Organic cation transporters. *Reviews of physiology, biochemistry and pharmacology* **150**, 36–90 (2003).
164. Lahjouji, K., Mitchell, G. A. & Qureshi, I. A. Carnitine transport by organic cation transporters and systemic carnitine deficiency. *Molecular Genetics and Metabolism* **73**, 287–97 (2001).
165. Xu, S. *et al.* Transport of L-carnitine in human corneal and conjunctival epithelial cells. *Molecular Vision* **16**, 1823–31 (2010).
166. Runge, S. W., Hill, B. J. F., Moran, W. M. & Turrens, J. F. A simple classroom teaching technique to help students understand Michaelis-Menten kinetics. *CBE Life Sciences Education* **5**, 348–52 (2006).
167. Urakami, Y. Molecular diversity of organic cation transporter (OCT) mediating renal excretion of drugs. *Yakugaku zasshi : Journal of the Pharmaceutical Society of Japan* **122**, 957–65 (2002).
168. Kaplan, J. H. Biochemistry of Na,K-ATPase. *Annual Review of Biochemistry* **71**, 511–35 (2002).
169. Sasaya, M., Hatakeyama, Y., Saitoh, H. & Takada, M. Stereoselective permeation of new fluorinated quinolone derivatives across LLC-PK1 cell monolayers. *Biological & pharmaceutical bulletin* **22**, 707–12 (1999).
170. Aoki, F. Y. & Sitar, D. S. Clinical pharmacokinetics of amantadine hydrochloride. *Clinical Pharmacokinetics* **14**, 35–51 (1988).
171. Pacifici, G. M. *et al.* Effect of amantadine on drug-induced parkinsonism: relationship between plasma levels and effect. *British Journal of Clinical Pharmacology* **3**, 883–9 (1976).
172. Hayden, F. G., Minocha, A., Spyker, D. A. & Hoffman, H. E. Comparative single-dose pharmacokinetics of amantadine hydrochloride and rimantadine hydrochloride in young and elderly adults. *Antimicrobial Agents and Chemotherapy* **28**, 216–21 (1985).
173. Wanka, L., Iqbal, K. & Schreiner, P. R. The Lipophilic Bullet Hits the Targets: Medicinal Chemistry of Adamantane Derivatives. *Chemical reviews* (2013).

174. Kornhuber, J. *et al.* Pharmacokinetic characterization of amantadine in human brain tissue. *Therapeutic Drug Monitoring* **28**, 693–5 (2006).
175. Kornhuber, J., Retz, W. & Riederer, P. Slow accumulation of psychotropic substances in the human brain. Relationship to therapeutic latency of neuroleptic and antidepressant drugs? *Journal of Neural Transmission. Supplementum* **46**, 315–23 (1995).
176. Hesselink, M. B., De Boer, B. G., Breimer, D. D. & Danysz, W. Brain penetration and in vivo recovery of NMDA receptor antagonists amantadine and memantine: a quantitative microdialysis study. *Pharmaceutical Research* **16**, 637–42 (1999).
177. Kornhuber, J. *et al.* Therapeutic brain concentration of the NMDA receptor antagonist amantadine. *Neuropharmacology* **34**, 713–21 (1995).
178. De Lange, E. C. M. & Danhof, M. Considerations in the use of cerebrospinal fluid pharmacokinetics to predict brain target concentrations in the clinical setting: implications of the barriers between blood and brain. *Clinical Pharmacokinetics* **41**, 691–703 (2002).
179. Liu, X. *et al.* Evaluation of cerebrospinal fluid concentration and plasma free concentration as a surrogate measurement for brain free concentration. *Drug Metabolism and Disposition* **34**, 1443–7 (2006).
180. Lin, J. H. CSF as a surrogate for assessing CNS exposure: an industrial perspective. *Current Drug Metabolism* **9**, 46–59 (2008).
181. Shen, D. D., Artru, A. A. & Adkison, K. K. Principles and applicability of CSF sampling for the assessment of CNS drug delivery and pharmacodynamics. *Advanced Drug Delivery Reviews* **56**, 1825–57 (2004).
182. Summerfield, S. G. *et al.* Toward an improved prediction of human in vivo brain penetration. *Xenobiotica* **38**, 1518–35 (2008).
183. Barretto, R. P. J. *et al.* Time-lapse imaging of disease progression in deep brain areas using fluorescence microendoscopy. *Nature Medicine* **17**, 223–8 (2011).
184. Plock, N. & Kloft, C. Microdialysis--theoretical background and recent implementation in applied life-sciences. *European Journal of Pharmaceutical Sciences* **25**, 1–24 (2005).
185. Chaurasia, C. S. *et al.* AAPS-FDA workshop white paper: microdialysis principles, application and regulatory perspectives. *Pharmaceutical Research* **24**, 1014–25 (2007).
186. Darvesh, A. S. *et al.* In vivo brain microdialysis: advances in neuropsychopharmacology and drug discovery. *Expert Opinion on Drug Discovery* **6**, 109–127 (2011).

187. Li, Y., Peris, J., Zhong, L. & Derendorf, H. Microdialysis as a tool in local pharmacodynamics. *The AAPS Journal* **8**, E222–35 (2006).
188. Höcht, C., Opezzo, J. A. W. & Taira, C. A. Applicability of reverse microdialysis in pharmacological and toxicological studies. *Journal of pharmacological and toxicological methods* **55**, 3–15 (2007).
189. Tang, A., Bungay, P. M. & Gonzales, R. A. Characterization of probe and tissue factors that influence interpretation of quantitative microdialysis experiments for dopamine. *Journal of Neuroscience Methods* **126**, 1–11 (2003).
190. Le Quellec, A. *et al.* Microdialysis probes calibration: gradient and tissue dependent changes in no net flux and reverse dialysis methods. *Journal of Pharmacological and Toxicological Methods* **33**, 11–6 (1995).
191. Yang, Z., Huang, Y., Gan, G. & Sawchuk, R. J. Microdialysis evaluation of the brain distribution of stavudine following intranasal and intravenous administration to rats. *Journal of Pharmaceutical Sciences* **94**, 1577–88 (2005).
192. Li, F., Feng, J., Cheng, Q., Zhu, W. & Jin, Y. Delivery of 125I-cobrotoxin after intranasal administration to the brain: a microdialysis study in freely moving rats. *International Journal of Pharmaceutics* **328**, 161–7 (2007).
193. Bagger, M. & Bechgaard, E. A microdialysis model to examine nasal drug delivery and olfactory absorption in rats using lidocaine hydrochloride as a model drug. *International Journal of Pharmaceutics* **269**, 311–322 (2004).
194. Jayachandra Babu, R., Dayal, P. P., Pawar, K. & Singh, M. Nose-to-brain transport of melatonin from polymer gel suspensions: a microdialysis study in rats. *Journal of Drug Targeting* **19**, 731–40 (2011).
195. Ohtsuki, S. & Terasaki, T. Contribution of carrier-mediated transport systems to the blood-brain barrier as a supporting and protecting interface for the brain; importance for CNS drug discovery and development. *Pharmaceutical Research* **24**, 1745–58 (2007).
196. Maurer, T. S., Debartolo, D. B., Tess, D. A. & Scott, D. O. Relationship between exposure and nonspecific binding of thirty-three central nervous system drugs in mice. *Drug Metabolism and Disposition* **33**, 175–81 (2005).
197. Paxinos, George and Watson, C. *The Rat Brain Stereotaxic coordinates*. (Academic Press, MA ).
198. Seshadri, A. J. & Hayashi-Takagi, A. Gene manipulation with stereotaxic viral infection for psychiatric research: spatiotemporal components for schizophrenia. *Progress in Brain Research* **179**, 17–27 (2009).

199. Kaya, M. & Ahishali, B. Assessment of permeability in barrier type of endothelium in brain using tracers: Evans blue, sodium fluorescein, and horseradish peroxidase. *Methods in Molecular Biology* **763**, 369–82 (2011).
200. Wang, Y., Wong, S. L. & Sawchuk, R. J. Microdialysis calibration using retrodialysis and zero-net flux: application to a study of the distribution of zidovudine to rabbit cerebrospinal fluid and thalamus. *Pharmaceutical Research* **10**, 1411–9 (1993).
201. Clément, R. *et al.* In vitro and in vivo microdialysis calibration using retrodialysis for the study of the cerebrospinal distribution of bupivacaine. *Journal of Pharmaceutical and Biomedical Analysis* **17**, 665–70 (1998).
202. Brown, F., Davies, J. A. & Redfern, P. H. The mechanism of the hypothermic effect of amantadine in rats and mice. *The Journal of Pharmacy and Pharmacology* **30**, 287–90 (1978).
203. Vernier, V. G. *et al.* The toxicologic and pharmacologic properties of amantadine hydrochloride. *Toxicology and Applied Pharmacology* **15**, 642–65 (1969).
204. Zhao, R. & Pollack, G. M. Regional differences in capillary density, perfusion rate, and P-glycoprotein activity: a quantitative analysis of regional drug exposure in the brain. *Biochemical Pharmacology* **78**, 1052–9 (2009).
205. Lin, C.-J. *et al.* Cellular localization of the organic cation transporters, OCT1 and OCT2, in brain microvessel endothelial cells and its implication for MPTP transport across the blood-brain barrier and MPTP-induced dopaminergic toxicity in rodents. *Journal of Neurochemistry* **114**, 717–27 (2010).
206. Somogyi, A., Rohner, H. G. & Gugler, R. Pharmacokinetics and bioavailability of cimetidine in gastric and duodenal ulcer patients. *Clinical pharmacokinetics* **5**, 84–94 (1980).
207. Pedersen, P. V & Miller, R. Pharmacokinetics and bioavailability of cimetidine in humans. *Journal of Pharmaceutical Sciences* **69**, 394–8 (1980).
208. Veng Pedersen, P. Pharmacokinetic analysis by linear system approach I: cimetidine bioavailability and second peak phenomenon. *Journal of Pharmaceutical Sciences* **70**, 32–8 (1981).
209. Kaneniwa, N., Funaki, T., Furuta, S. & Watari, N. Study of the absorption site of cimetidine. *Journal of Pharmacobio-dynamics* **9**, 321–6 (1986).
210. Oberle, R. L. & Amidon, G. L. The influence of variable gastric emptying and intestinal transit rates on the plasma level curve of cimetidine; an explanation for the double peak phenomenon. *Journal of Pharmacokinetics and Biopharmaceutics* **15**, 529–44 (1987).

211. Kaneniwa, N., Funaki, T., Furuta, S. & Watari, N. Influence of gastric emptying rate on the absorption of cimetidine in rats. *Journal of the Pharmaceutical Society of Japan* **105**, 966–72 (1985).
212. Somogyi, A. & Gugler, R. Clinical pharmacokinetics of cimetidine. *Clinical pharmacokinetics* **8**, 463–95 (1983).
213. Guay, D. R., Matzke, G. R., Bockbrader, H. N. & Dancik, J. Comparison of bioavailability and pharmacokinetics of cimetidine in subjects with normal and impaired renal function. *Clinical Pharmacy* **2**, 157–62 (1983).
214. Ji, L., Masuda, S., Saito, H. & Inui, K. Down-regulation of rat organic cation transporter rOCT2 by 5/6 nephrectomy. *Kidney International* **62**, 514–24 (2002).
215. Knodell, R. G., Browne, D. G., Gwozdz, G. P., Brian, W. R. & Guengerich, F. P. Differential inhibition of individual human liver cytochromes P-450 by cimetidine. *Gastroenterology* **101**, 1680–91 (1991).
216. Levine, M. & Bellward, G. D. Effect of cimetidine on hepatic cytochrome P450: evidence for formation of a metabolite-intermediate complex. *Drug Metabolism and Disposition* **23**, 1407–11 (1995).
217. Brimblecombe, R. W., Leslie, G. B. & Walker, T. F. Toxicology of cimetidine. *Human Toxicology* **4**, 13–25 (1985).
218. Eto, K. *et al.* Influences of cigarette smoke inhalation on pharmacokinetics of cimetidine in rats. *Drug Metabolism and Drug Interactions* **9**, 103–14 (1991).